AN EVAPORATRANSPIRATION-INTERCEPTION MODEL FOR URBAN AREAS

By

CHRISTINE SUSAN BETHAM GRIMMOND

BSc. (Hons.) University of Otago, 1980
MSc. University of British Columbia, 1984

A THESIS SUBMITTED IN PARTIAL FULFILLMENT OF

THE REQUIREMENTS FOR THE DEGREE OF

DOCTOR OF PHILOSOPHY

in

THE FACULTY OF GRADUATE STUDIES

(Department of Geography)

We accept this thesis as conforming

to the required standard

THE UNIVERSITY OF BRITISH COLUMBIA

November 1988

© CHRISTINE SUSAN BETHAM GRIMMOND, 1988

In presenting this thesis in partial fulfilment of the requirements for an advanced degree at the University of British Columbia, I agree that the Library shall make it freely available for reference and study. I further agree that permission for extensive copying of this thesis for scholarly purposes may be granted by the head of my department or by his or her representatives. It is understood that copying or publication of this thesis for financial gain shall not be allowed without my written permission.

Department of Geography

The University of British Columbia
Vancouver, Canada

Date 4 November 1988

ABSTRACT

This study presents a model to calculate evapotranspiration from urban areas for use over a wide range of meteorological conditions. The evapotranspiration-interception model is a modified version of those attributable to Penman-Monteith (1965), Rutter et al. (1971) and Shuttleworth (1978).

Sub-models to calculate anthropogenic heat flux, storage heat flux, aerodynamic resistance, surface resistance and drainage are developed. The model and its sub-components, where possible, are tested against measured data from a suburban site in Vancouver, B.C. This is the first extended set of winter/spring time energy balance measurements for a city. It shows that the latent heat flux can be the most important output flux of the energy balance in wintertime. The spring energy balance is similar in form to that in summer.

Construction of valid energy balances for spatially-non-uniform surfaces such as cities requires that all component fluxes represent identical source areas. Given that the radiative field is relatively uniform in space it is appropriate to match all fluxes to the source areas for the turbulent fluxes since these are very variable. A scheme to match areas is developed using the Schmid (1988) model for the turbulent source areas and a geographic information system containing the surface characteristics necessary to calculate the spatially-corresponding anthropogenic and storage fluxes.

The anthropogenic heat flux at a point is more variable in space than time. Therefore the calculated flux is strongly influenced by the method used to identify the source area. A test of storage heat flux models concludes that the objective hysteresis model of Cleugh (1988) performs well, especially during the daytime. The model introduces an appropriate temporal asymmetry in

the storage flux.

The surface resistance model developed for the city is a modified version of that suggested by Jarvis (1976). The performance of the model is good and resembles that obtained for similar models applied to forests.

Comparison of modelled and measured evapotranspiration using the complete model shows this to be a promising method which is capable of providing realistic hourly and daily estimates of the areally-averaged latent heat flux and surface water state in urban areas.

TABLE OF CONTENTS

	Page
ABSTRACT	ii
TABLE OF CONTENTS	iv
LIST OF TABLES	viii
LIST OF FIGURES	xi
LIST OF SYMBOLS & ABBREVIATIONS	xiv
ACKNOWLEDGEMENTS	xxi

PART I INTRODUCTION

CHAPTER 1 INTRODUCTION

1.1	Rationale	1
1.2	The approach taken to model seasonal evapotranspiration	5
1.3	Penman-Monteith-Rutter evapotranspiration-interception model	6
1.4	Approach to problem solution and structure of the thesis	10

CHAPTER 2 OBSERVATION PROGRAMME

2.1	Physical setting	11
2.2	General climatology of Vancouver and the measurement period	11
2.3	Measurement considerations	14
2.4	The instruments	17

PART II DEVELOPMENT AND TESTING OF SUBMODELS

CHAPTER 3 SURFACE DESCRIPTION

3.1	Introduction	26
3.2	Boundary selection for surface description	31
3.2.1	Radiant fluxes	33
3.2.2	Turbulent fluxes	35

3.3 Surface database 44

3.4 Summary 50

CHAPTER 4 ANTHROPOGENIC HEAT FLUX

4.1 Introduction 52

4.2 Methods of calculation 52

4.2.1 Anthropogenic heat produced by combustion of vehicle fuels 52

4.2.2 Anthropogenic heat produced by combustion from stationary sources 53

4.2.3 Anthropogenic heat produced by metabolism 55

4.3 Modelled values of anthropogenic heat flux 56

4.5 Incorporation of anthropogenic heat flux into the energy balance 63

CHAPTER 5 STORAGE HEAT FLUX

5.1 Introduction 66

5.2 Methods of calculation 67

5.2.1 Objective linear regression model 67

5.2.2 Hysteresis model 68

5.2.3 Objective hysteresis model 69

5.3 'Measured' storage heat flux 1987 72

5.4 Comparison of storage heat flux models with 'measured' storage heat flux 76

5.4.1 The different models 82

5.4.2 Influence of landuse description 85

5.5 Discussion 86

CHAPTER 6 ENERGY BALANCE

6.1 Introduction 86

6.2 Determination of hourly energy balances 86

6.3 Measured hourly energy balance, 1987 88

CHAPTER 7 RESISTANCES, DRAINAGE AND STORAGE CAPACITY

7.1 Introduction 99

7.2 Aerodynamic resistance 99

7.3 Surface resistance 104

7.4 Drainage 112

7.5 Storage capacity 116

PART III MODEL PERFORMANCE AND CONCLUSIONS

CHAPTER 8 PERFORMANCE OF THE EVAPOTRANSPIRATION-INTERCEPTION MODEL

8.1 Introduction 120

8.2 Structure of the model 120

8.3 Performance of the model 126

8.3.1 Methods used to compare the performance of the model 126

8.3.2 Base run of the model 128

8.4 Sensitivity analysis of the model 141

8.4.1 Rutter 142

8.4.2 Time step 142

8.4.3 Aerodynamic resistance 147

8.4.4 Surface resistance 151

8.4.5 Storage capacities 156

8.4.6 Drainage functions 167

8.5 Discussion 174

CHAPTER 9 CONCLUSIONS

9.1 Summary of conclusions 179

9.2 Future research 182

REFERENCES CITED 183

APPENDIX I Julian day calender for the measurement period, 1987 193

APPENDIX II Equations used in calculations

II.1 Temperature difference 194

II.2 Slope of the saturation vapour pressure curve 194

II.3 Psychrometric constant 194

II.4 Latent heat of vaporization 195

II.5 Mixing Ratio 195

II.6 Vapour pressure 195

II.7 Saturation vapour pressure 195

II.8 Specific heat of air at constant pressure 195

II.9 Density of moist air 196

II.10 Adjusted virtual temperature 196

II.11 Relative humidity 196

II.12 Vapour pressure deficit 196

II.13 Specific humidity deficit 196

APPENDIX III Error analysis for the RTDMS and fluxes calculated from it 197

APPENDIX IV Calculation of stability and friction velocity 199

APPENDIX V Procedure for accessing different geometries from the database

V.1 Circles and quadrants 204

V.2 Ellipses 204

V.3 Sectors 205

V.4 Discussion 206

LIST OF TABLES

Table		Page
2.1	Normal (1951-1980) and 1987 measurements of climatic variables for Vancouver International Airport	15
2.2	Instrumentation	21
3.1	Framework for urban climate classification proposed by Oke (1984)	28
3.2	Mean length of plumes for use with the sectors model	42
3.3	Information contained within the surface database for each grid square	46
4.1	Fuel consumption, density and net heat combustion	54
5.1	Percentage of surface type in the Sunset study area for use with the objective hysteresis model for storage heat flux density	70
5.2	Surface coefficients for the objective hysteresis storage heat flux density model	71
5.3	Coefficients resulting from a fit of the measured 1987 ΔQ_S and Q* data to the hysteresis ΔQ_S model	75
5.4	Monthly variation in hysteresis equation coefficients	77
5.5	Statistical results of comparison between measured and modelled ΔQ_S	78
6.1	Comparison of Q_{HS} and $Q_{H\beta}$ with varying errors in ß	90
6.2	Mean daily energy budget components for 1987	91
6.3	Daytime energy balance fluxes and ratios for measurement period and by month, 1987	93
6.4	Mean daily Q* and ΔQ_S by month for Kerrisdale, Vancouver	96
7.1	Surface resistance model fitted parameters and test statistics	110
7.2	Values of drainage function parameters	115
7.3	Values of storage capacities for paved surfaces & roofs	118
7.4	Values of storage capacities for vegetation	119

8.1	Initial data requirements for the model	123
8.2	Hourly data requirements for the model	125
8.3	Output from the evapotranspiration-interception model	127
8.4	Values assigned to parameters for base run of the model	129
8.5	Statistics for base model values of Q_E	131
8.6	Statistics of model performance for Q_E when Rutter transition equations are used	143
8.7	Statistics of model performance for Q_E when computational time step changed	146
8.8	Statistics of model performance for Q_E when the r_a equation is changed	149
8.9	Statistics of model performance for Q_E when r_S maximum is changed	152
8.10	Statistics of model performance for Q_E when r_S parameters are changed	154
8.11	Statistics of model performance for Q_E when the value of S is changed for pavement	157
8.12	Statistics of model performance for Q_E when the value of S is changed for buildings	159
8.13	Statistics of model performance for Q_E when the value of S is changed for coniferous vegetation	160
8.14	Statistics of model performance for Q_E when S is changed for deciduous vegetation and the timing of the transition period is altered	161
8.15	Statistics of model performance for Q_E when S is changed for irrigated and unirrigated grass	162
8.16	Statistics of model performance for Q_E when S capacity is changed for all surface types	165
8.17	Statistics of model performance for Q_E when drainage functions are changed and S = 0.5 mm	168
8.18	Statistics of model performance for Q_E when drainage functions are changed and S = 1.0 mm	169
8.19	Statistics of model performance for Q_E when drainage functions are changed and S = 2.0 mm	170

8.20	Comparison of the performance of two models to calculate evapotranspiration in urbanized terrain	177
II.1	Coefficients for use with the Lowe (1977) polynomials	194
III.1	RTDMS thermopile calibration values	197
IV.1	Comparison between measured and modelled values of u* and z/L	203

LIST OF FIGURES

Figure		Page
1.1	Urban energy and water balances	2
1.2	Conceptual framework of the modified Penman-Monteith-Rutter Shuttleworth evapotranspiration-interception model	2
2.1	The location of the Sunset site in the Vancouver area and surrounding land use	12
2.2	View looking southwest from the tower	13
2.3	Idealised arrangement of boundary layer structures over a city (after Oke, 1984)	16
2.4	Schematic of the Sunset tower and instrument locations	19
2.5	Photographic view of the top part of Sunset tower	20
3.1	Aerial photograph of area to the northwest of the tower	29
3.2	Schematic of the influence of the location of the boundaries for surface description	30
3.3	Wind direction frequency (%) for the Sunset site JD 21-179, 1987	32
3.4	Dimensions of the source area for turbulent flux measurements	36
3.5	Source area for one hour with the 9 weighted bands using the plume model	39
3.6	Examples of different source areas with changing meteorological conditions	41
3.7	Examples of 'sectors'	43
3.8	Map of grid squares which contain major roads in the area covered by the database	45
3.9	Maps of surface type	48
3.10	Influence of changing source area on percentage of land use characteristics influencing measurements	51
4.1	Mean profiles of traffic counts for major and minor roads	54
4.2	Anthropogenic heat flux for JD 22, 1987	57

4.3	Map of anthropogenic heat flux for 900 LAT, JD 22, 1987 centred on the Sunset site	58
4.4	Anthropogenic heat flux with increasing radius from the tower for JD 22, 1987	59
4.5	Hourly anthropogenic heat flux modelled using plumes & a 2 km radius circle as the basis for assigning values for surface parameters	61
4.6	Wind direction frequency plot for: a) all hours b) hours when Q_F plumes > Q_F 2 km radius circle c) hours when Q_F plumes < Q_F 2 km radius circle	62
4.7	Plot of hourly Q_F calculated using plumes & sectors for assigning values for surface parameters	64
5.1	Plots of hourly ensemble averages of storage heat flux residual for hours with varying errors in ß	73
5.2	Residuals versus modelled storage heat flux densities using the objective hysteresis model	80
5.3	Modelled versus measured storage heat flux densities with error in ß < 20%	81
5.4	Maps of storage heat flux for: (a) ensemble 800 LAT (b) ensemble 1200 LAT	84
6.1	Comparison of Q_H determined using eddy correlation (SAT) & calculated from ß - energy balance method	89
6.2	Ensemble average energy balance plots	92
7.1	Aerodynamic resistance calculated for hours when it was possible to calculate stability with direct measurements of sensible heat flux	101
7.2	Diurnal trend of ensemble mean and standard deviation of measured surface conductance	107
7.3	Comparison between hourly measured and modelled surface conductance	111
7.4	Ensemble mean of hourly measured and modelled surface conductance	113
8.1	Basic structure of the evapotranspiration-interception model for urban areas	121

8.2	Comparison of hourly measured and modelled QE for the 'base' model run	132
8.3	Comparison of daily measured and modelled QE for the 'base' model run	133
8.4	Cumulative plot of measured and modelled 'base' run E	134
8.5	Time series of hourly measured and modelled Q_E ('base')	135
8.6	Ensemble plots of measured and modelled 'base' run Q_E	137
8.7	Plots of precipitation, water use, surface wetness and modelled surface water state	139
8.8	Influence of using the Rutter and Shuttleworth transition equations on the cumulated E	144
8.9	Influence of changing the time step on cumulated E	145
8.10	Influence of using a 3600 s time step on cumulated E	148
8.11	Influence of equation used to calculate aerodynamic resistance on cumulated E	150
8.12	Influence of the maximum value assigned to r_S on cumulated E	153
8.13	Influence of parameters used for calculating r_S on cumulated E	155
8.14	Influence of the value assigned to surface storage capacity of grass on cumulated E	163
8.15	Influence of changing all the surface storage capacities on cumulated E	166
8.16	Influence of changing drainage functions and coefficients on cumulated E when S = 0.5 mm for all surfaces	171
8.17	Influence of changing drainage functions and coefficients on cumulated E when S = 1.0 mm for all surfaces	172
8.18	Influence of changing drainage functions and coefficients on cumulated E when S = 0.5 mm for all surfaces	173
8.19	Comparison of daily measured and modelled evaporation using the Grimmond et al. (1986) advection-aridity model and the 1987 Sunset data	178
IV.1	Measured versus modelled u*	201
IV.2	Measured versus modelled z/L	202

LIST OF SYMBOLS AND ABBREVIATIONS

Some symbols are relevant for one equation and are not listed here

A	source area (m^2)
A_I	area irrigated
A_U	area unirrigated
AE	available energy ($W\ m^{-2}$)
a	plume model dimension - distance to upwind edge of plume (m)
a_i	empirical coefficient used in objective linear storage heat flux density parameterization.
a_1 a_2 a_3	empirical coefficients used in hysteresis type storage heat flux density determination
a_0 - a_6	coefficients used to calculate s and e_S
b	empirical coefficient in drainage function
b + c	plume model dimension - length of plume (m)
b_i	empirical coefficient used in objective linear storage heat flux density parameterization
C	state of surface water store (mm)
C_A	compressibility factor of moist air
C_i	mean consumption (of electricity Watts; gas Joules) for an individual consumer by premise class (i)
ΔC	change in surface water status (mm)
c_f	intercept of linear functional relationship
c_P	specific heat of air at constant pressure ($J\ Kg^{-1}\ K^{-1}$)
D	drainage ($mm\ h^{-1}$)
D_0	drainage rate when C=S ($mm\ h^{-1}$)
d	zero-plane displacement length (m)
d	Wilmott & Wicks (1980) index of agreement
d	plume model dimension - half width of plume (m)

E	evapotranspiration (mm)
E_{PM}	evapotranspiration determined from Penman-Monteith equation (mm)
EV	energy used by vehicles (J m^{-1})
e_a	vapour pressure (Pa)
e_S	saturation vapour pressure (Pa)
F	water released due to anthropogenic activities (mm)
GEF	gas efficiency (0.675)
GR	grid consumption (E electricity (W), G gas(J))
g	acceleration due to gravity (m s^{-2})
g_a	aerodynamic conductance (mm s^{-1})
g_S	surface conductance (mm s^{-1})
g_{ST}	stomatal conductance (mm s^{-1})
I	piped water supply (mm)
JD	Julian day
K*	net shortwave radiation (W m^{-2})
k	von Kármán's constant
L, LAI	leaf area index (m m^{-1})
L	Monin-Obukhov stability length (m)
L↑	long-wave radiation emitted from the surface (W m^{-2})
L↓	long-wave radiation received at the surface (W m^{-2})
Lm	maximum leaf area index (m m^{-1})
L_V	latent heat of vaporization (J kg^{-1})
M	metabolic rate (subscript a animals, p humans) (W)
MAE	mean absolute error
m_f	slope of linear functional relationship
m_o	slope of linear regression forced through the origin

N&S	Nash & Sutcliffe (1970) 'goodness of fit'
NHC	net heat consumption by fuel type (J Kg^{-1})
n	number of hours or data points
nv_i	number of vehicles in contributing area by road type (i)
P	precipitation (mm)
PX	water arriving at the surface (mm)
P_1	fitted parameter for surface resistance model (mm s^{-1})
P_2	fitted parameter for surface resistance model (W m^{-2})
P_3	fitted parameter for surface resistance model (kg m^{-1})
P_4	fitted parameter for surface resistance model (g kg^{-1})
P_5	fitted parameter for surface resistance model (°C)
P_6	fitted parameter for surface resistance model (mm^{-1})
p	atmospheric pressure (Pa)
Q*	net all-wave radiation (W m^{-2})
ΔQ_A	net heat advection (W m^{-2})
Q_E	latent heat flux (W m^{-2})
Q_{ER}	Q_E calculated as a residual from the energy balance (W m^{-2})
Q_{ES}	Q_E calculated using sonic anemometer thermometer - sensible heat flux & Bowen ratio (W m^{-2})
$Q_{E\beta}$	Q_E calculated using the Bowen ratio - energy balance (W m^{-2})
Q_F	anthropogenic heat flux (W m^{-2})
Q_{FH}	anthropogenic heat produced by combustion from stationary sources (W m^{-2})
Q_{FM}	anthropogenic heat produced by human/animal metabolism (W m^{-2})
Q_{FV}	anthropogenic heat produced by combustion of vehicle fuels (W m^{-2})
Q_H	sensible heat flux (W m^{-2})
$Q_{H\beta}$	sensible heat flux determined from Bowen ratio (W m^{-2})

Q_M	maximum hourly net all-wave radiation (W m^{-2})
ΔQ_S	storage heat flux (W m^{-2})
ΔQ_{SR}	storage heat flux determined as a residual (W m^{-2})
R	gas constant for dry air (J kg^{-1} K^{-1})
R	parameter in Shuttleworth (1988) surface resistance equation
RH	relative humidity (%)
RMSE	root mean square error
$RMSE_S$	systematic root mean square error
$RMSE_U$	unsystematic root mean square error
RTDMS	reversing temperature difference measuring system
Δr	runoff (mm)
r	mixing ratio (kg kg^{-1})
r^2	coefficient of determination
r_a	aerodynamic resistance (s m^{-1})
r_b	boundary layer resistance (s m^{-1})
r_H	sensible heat flux resistance (s m^{-1})
r_S	surface resistance (s m^{-1})
r_{SS}	Shuttleworth surface resistance used in transition between wet and dry surface water state (s m^{-1})
r_{ST}	stomatal resistance (s m^{-1})
r_V	latent heat flux resistance (s m^{-1})
S	surface water capacity (mm)
SAT	sonic anemometer-thermometer system
S_{ds}	summer water storage capacity for deciduous trees (mm)
S_{dst}	daily increment in storage capacity for deciduous trees during growing season (mm)
S_{ws}	winter water storage capacity for deciduous trees (mm)

S_1, S_2	fitted parameters in surface conductance model (mm)
ΔS	change in water storage (mm)
s	slope of the saturation vapour pressure versus temperature curve (Pa C^{-1})
sd	standard deviation
S.E.	standard error
T	temperature ($^{\circ}C$)
T_F	throughfall (mm)
T_d	dry bulb temperature ($^{\circ}C$)
T_L	minimum temperature limit in surface conductance model ($^{\circ}C$)
T_M	maximum temperature limit in surface conductance model ($^{\circ}C$)
T_S	stemflow (mm) (Chapter 1)
T_S	surface temperature ($^{\circ}C$) (Chapter 4)
T'_V	adjusted virtual temperature (K)
T_W	wet bulb temperature ($^{\circ}C$)
ΔT	temperature difference ($^{\circ}C$)
t	time
t_b	Julian day that the winter to summer transition for deciduous vegetation storage capacity begins
t_e	Julian day the summer storage capacity for deciduous vegetation is reached
u	mean wind speed (m s^{-1})
u_*	friction velocity (m s^{-1})
V	vapour pressure deficit (Pa)
W	parameter in Shuttleworth (1978) surface resistance equation
WFS_i	weighting of fuel sales by fuel type (i)
w_s	surface wetness
wu	external water use (mm)

$\overline{w'T'}$	kinematic sensible heat flux density (W m^{-2})
X	fraction of water on the canopy
X_P	sensed concentration or effect level in source area model
z	measurement height (m)
z_i	mixed layer depth (m)
z_S	height of sensor (m)
z_0	momentum roughness length (m)
z_{0V}	water vapour roughness length (m)
z_1	measurement height of bottom cart of RTDMS (m)
z_2	measurement height of top cart of RTDMS (m)
z_3	measurement height of wind speed (m)
α	albedo
α_i	fraction of area covered by ith surface type used in the linear objective storage heat flux density parameterization.
ß	Bowen ratio (Q_H/Q_E)
δq	specific humidity deficit (g kg^{-1})
$\delta\theta$	soil moisture deficit (mm)
ϵ	ratio of the molecular weight of water vapour to dry air (Appendix II)
ϵ	emissivity (Chapters 3 & 4)
γ	psychrometric constant (Pa C^{-1})
Γ	dry adiabatic lapse rate (K m^{-1})
ρ	density of air (kg m^{-3})
ρ_i	density of fuel types (i) (kg m^{-3})
τ	averaging time (s)
$\theta*$	temperature scale for turbulent heat transfer (K)
$\Delta\theta$	potential temperature difference (K)

σ_φ	standard deviation of the wind direction ($^\circ$ or rad)
σ	Stefan-Boltzman constant (W m^{-2} K^{-4})
φ	mean wind direction ($^\circ$ or rad)
ψ_H	stability function for heat
ψ_M	stability function for momentum exchange
ψ_V	stability function for water vapour exchange

ACKNOWLEDGEMENTS

Dr. Tim Oke, my supervisor, provided academic stimulation and guidance throughout my graduate studies. His advice, encouragement and humour have been much appreciated. I would like to express my appreciation of my supervisory committee: Dr. M. Church, Dr. D.G. Steyn and Dr. S.O. Russell, for their comments at all stages of my studies and their prompt reading of my thesis.

Jeff Joyce, Gabor Friska, Rene Kondratsky and John Butcher provided help in the field. My fellow climatology graduate students Jamie Voogt, Matthias Roth and Peter Jackson provided useful discussion. HaPe Schmid contributed through many hours of discussion and assistance in the field.

The following organizations generously provided data: B.C.Hydro, City of Vancouver Water Works and Traffic Departments, Vancouver School Board, and Vancouver Parks Board. B.C. Hydro provided the site for the tower in their Mainwaring substation. Funding for this research has been provided to Dr. T.R. Oke by Natural Sciences Engineering Research Council of Canada and Atmospheric Environment Service of Environment Canada. Personal funding was provided through University of British Columbia Graduate Fellowships and Teaching and Research Assistantships in the Department of Geography.

In particular I would like to thank Helen Cleugh for many hours of discussion on all topics and invaluable help in the field, no matter what the weather; and Catherine Souch for her assistance in all aspects of this work and above all for her support and encouragement.

CHAPTER 1 INTRODUCTION

1.1 Rationale

Evaporation (E), the mass equivalent of the latent heat energy flux (Q_E), is the term that links the energy and the water balances. In the urban environment the water balance is written:

$$P + I + F = E + \Delta r + \Delta S + \Delta A \quad (1.1)$$

where P - precipitation (mm);
I - piped water supply (mm);
F - water released due to anthropogenic activities (mm);
Δr - runoff (mm);
ΔS - change in water storage (mm) for the period of interest; and
ΔA - net moisture advection (mm)

and the urban energy balance as:

$$Q^* + Q_F = Q_E + Q_H + \Delta Q_S + \Delta Q_A \quad (1.2)$$

where Q^* - net all-wave radiation (W m^{-2});
Q_F - energy released due to anthropogenic activities (W m^{-2});
Q_H - sensible heat flux (W m^{-2});
ΔQ_S - storage heat flux (W m^{-2}); and
ΔQ_A - net heat advection (W m^{-2}).

These balances apply to the top of a volume which extends to sufficient depth that vertical heat and water exchange is negligible (Fig. 1.1). Fluxes are determined per unit area of the top of the volume. A fuller explanation of this concept is given by Oke (1988). Traditionally evaporation in an urban environment has been assumed to be considerably less than that from neighbouring rural areas because of the supposed contrast between the hydrologic properties of building materials and vegetation-covered soils (Chandler, 1976). However this expectation has not been widely tested and urban evaporation has received little attention in the fields of both urban climatology and urban hydrology. Very few, if any comprehensive, reliable observations of natural water loss to the air by evaporation and evapotranspiration in urban areas exist (Atkinson, 1985). Indeed it hardly

Figure 1.1 Urban energy and water balances (after Oke, 1988).

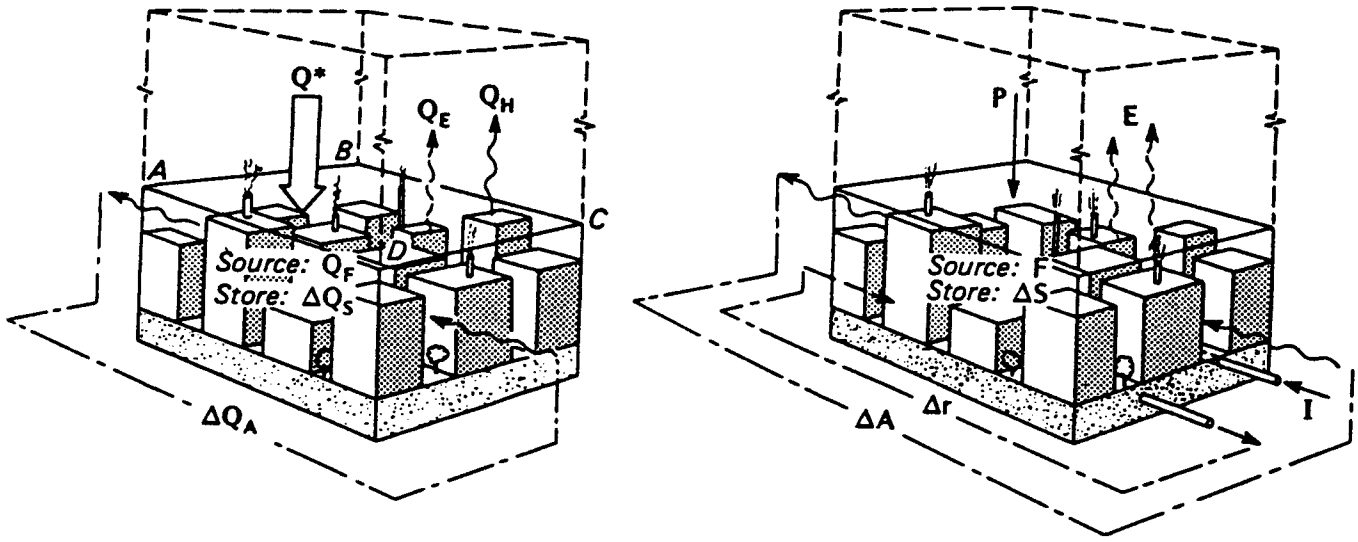

Figure 1.2 Conceptual framework of the Penman-Monteith-Rutter-Shuttleworth evapotranspiration-interception model adapted for urban areas. 'Floating plane' is equivalent to ABCD in Fig. 1.1.

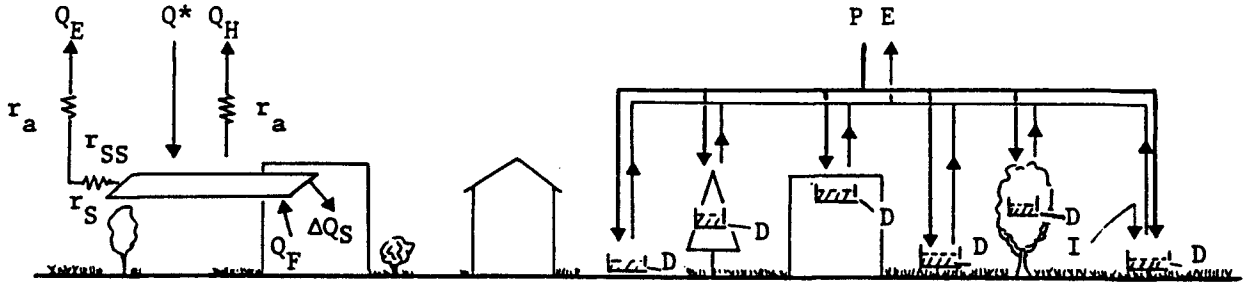

Q* - net all-wave radiation density
Q_H - sensible heat flux density
Q_E - latent heat flux density
Q_F - anthropogenic heat flux density
ΔQ_S - storage heat flux density
r_a - aerodynamic resistance
r_S - surface resistance
r_{SS} - surface resistance (Shuttleworth, 1978)
P - rainfall
E - evapotranspiration
D - drainage
I - external water use

rates mention in textbooks on the subject (e.g. Lazaro, 1979; Landsberg, 1981; Hall, 1984). Interestingly, recent work by Kalanda et al. (1980) and Grimmond and Oke (1986) shows that evaporation has a larger magnitude than originally thought, for example, in a temperate city (Vancouver, B.C.) it has been shown to constitute 37% of the losses of the annual external water balance.

A recent trend in urban runoff work is towards continuous simulation, rather than modelling the runoff from individual rainfall events. Between-event simulation makes it necessary to account not only for the runoff but also for the other components of the water balance. Currently evapotranspiration is either ignored or dealt with via evaporation pan data (e.g. Alley et al., 1980; Wenzell and Voorhees, 1980; Sman et al., 1988) so that van den Ven (1988) concludes that the weakest point in the urban water balance remains the estimation of evapotranspiration.

A model for use in conjunction with available runoff models to determine continuous hourly evapotranspiration would be useful for the modelling of water quantity, water quality and urban climate. In the water quantity modelling it is of interest to be able to predict the surface water storage status, and for water quality modelling it is valuable to know the volumes of water present both during and between storms (low flows) in order to calculate pollutant concentrations. In the field of urban climatology there is a more ready awareness of the evaporative term. However there has still only been a limited number of urban energy balance studies, and their emphasis has been to study dry summertime conditions. This is largely due to the difficulty of conducting micrometeorological measurements at the local scale (see Chapter 3 for discussion of scales) in urban areas, and especially in non-dry conditions. The few studies conducted under non-summertime conditions have not separated the turbulent terms (Q_H, Q_E) of the energy balance (e.g. Kerschgens and Drauschke,

1986).

Models to determine the evapotranspiration from urban areas can be divided into two groups (Oke et al., 1988). Firstly, there are those which consider evapotranspiration as one flux in the total surface energy balance These are one-, two- and quasi-three-dimensional numerical boundary layer models. The convective fluxes are often partitioned using a static moisture availability factor or an assumed Bowen ratio. Ross and Oke (1988) conclude that the latent heat flux is the poorest part of three urban climate models they validated against measured energy balance fluxes (dry summertime). The second group includes simple statistical algorithms and physically-based models utilising hydro-meteorological data as input. Currently none is capable of modelling evapotranspiration for urban areas over a range of seasonal conditions.

The objective of this thesis is to develop a model to estimate hourly, and longer-time period, evapotranspiration for urban areas, that is useful across a wide range of meterological conditions. It should be noted that the case of snow on the surface is not included. Within the Oke (1984) framework of urban climate classification the model to be developed is relevant to the "local" scale. This means that the model should simulate the processes associated with urban units of the size of city-blocks to land use zones.

1.2 The approach taken to model seasonal evapotranspiration

If evapotranspiration is to be calculated under diverse meteorological conditions it is necessary to have a model that can cope with changing water availability on the surface during and following rainfall. It is therefore deemed appropriate to take an evapotranspiration-interception approach.

The physical structure of the city has been compared in form to that of a forest (Oke, 1976, 1989) through the existence of an urban canopy layer below

the urban boundary layer. The urban canopy layer consists of the air contained between the roughness elements (buildings and trees) which are equivalent to the trees in a forest. It is therefore proposed that an appropriate model framework is the Penman-Monteith-Rutter-Shuttleworth evapotranspiration-interception model (Monteith, 1965; Rutter et al., 1971) originally developed for forests. The conceptual framework of this model adapted for urban areas is shown diagrammatically in Figure 1.2. This model is the most successful, rigorous, robust physically-based evapotranspiration-interception model currently available (Gash, 1979; Shuttleworth, 1983, 1988a).

In essence the model is used to calculate a running water balance of the 'canopy' and 'trunks'. It requires inputs of hourly rainfall and the meteorological parameters necessary to estimate evaporation, and provides outputs of throughfall, stemflow and evaporation of intercepted water. The evaporation is calculated from the Penman-Monteith equation. The model allows for a continuous treatment of surface resistance for the transition between wet and dry surfaces. The following section outlines the Penman-Monteith-Rutter-Shuttleworth evapotranspiration-interception model and the adaptations incorporated so that it can be applied to urban areas.

1.3 Penman-Monteith-Rutter-Shuttleworth evapotranspiration-interception model

The process of evapotranspiration from surfaces which have some vegetative cover can be considered to consist of three phases:

1) evaporation from a totally wet surface;

2) evapotranspiration from a partially wet surface; and

3) transpiration from a dry surface (water loss from vegetation whose outer surfaces are dry).

In the first phase, the water that is evaporated is intercepted water. The

amount of intercepted water at any particular time is controlled not only by evaporation but also by the amount of precipitation, and the 'canopy' morphology which influences surface storage and drainage. In an urban area an array of surfaces (buildings, roads, vegetation) create the 'canopy'.

If it is assumed that the components of the 'canopy' are exposed to the same local scale climate then a single-source (layer) model can be used to determine the latent heat flux (Q_E). The best tested approach is the physically-based Monteith (1965) version of the Penman equation (Stewart, 1984; Dolman et al., 1988):

$$Q_E = \frac{s(Q^* - \Delta Q_S) + (\rho\ c_p\ V)/r_H}{s + \gamma\ (r_V + r_S)/r_H} \qquad (1.3)$$

where s - slope of the saturation vapour pressure versus temperature curve (Pa $^{\circ}C^{-1}$);
Q^* - net all wave radiation (W m^{-2});
ΔQ_S - storage heat flux (W m^{-2});
γ - psychrometric 'constant'(Pa $^{\circ}C^{-1}$);
ρ - density of air (kg m^{-3});
c_p - specific heat of air (J kg^{-1} $^{\circ}C^{-1}$);
V - vapour pressure deficit of the air (Pa);
r_H - sensible heat flux resistance (s m^{-1});
r_V - latent heat flux resistance (s m^{-1}); and
r_S - surface resistance (s m^{-1}).

All of the terms in this equation are influenced by the urban environment and it is also necessary to include an additional term, the anthropogenic heat flux (Q_F), so:

$$Q_E = \frac{s(Q^* + Q_F - \Delta Q_S) + (\rho\ c_p\ V)/r_H}{s + \gamma\ (r_V + r_S)/r_H} \qquad (1.4)$$

Equation 1.4 is applicable to dry surfaces (phase 3 outlined above). In applying 1.4 it is commonly assumed that r_H and r_V are equal and related to r_M, the equivalent resistance for momentum (this is often called the aerodynamic resistance, r_a). Equation 1.4 can thus be re-written:

$$Q_E = \frac{s\ (Q^* + Q_F - \Delta Q_S) + (\rho\ c_p\ V)/r_a}{s + \gamma\ (1 + r_S/r_a)} \qquad (1.5)$$

When the surface is completely wet (phase 1) the r_S term of equation 1.5 is

zero. Therefore equation 1.5 becomes:

$$Q_E = \frac{s\ (Q^*+Q_F-\Delta Q_S) + (\rho\ c_p\ V)/r_a}{s + \gamma} \qquad (1.6)$$

The transition between evaporation of intercepted water (phase 1) and transpiration (phase 3) for forested areas has been modelled by Rutter et al. (1971, 1975). The Rutter model calculates evaporation using equation 1.6 when the surface is wet (phases 1 & 2) adjusted by a function (X) of current canopy water storage (C) and canopy storage capacity (S):

$X=1$ when $C \geq S$

$X=C/S$ when $C<S$. (1.7)

S is defined as the amount of water left on the canopy when rainfall and throughfall have ceased. It corresponds to the storage capacity of Zinke (1967) following Horton (1919), or canopy saturation value of Leyton et al. (1967). It is comparable to field capacity of a soil (Rutter et al., 1971).

The overlap between the evaporation of intercepted water and transpiration is poorly defined in the Rutter model (Shuttleworth, 1983). To unify the two processes correctly, a physically continuous transition between wet and dry canopies is required. Equation 1.3 forms the basis of the unified model proposed by Shuttleworth (1978), in which r_S is replaced by a redefined surface resistance, r_{SS}, equal to r_S in dry conditions and to zero in wet conditions, with a smooth transition between the two depending on the fractional surface wetness. Shuttleworth's theoretical analysis has been tested over tall vegetation (Shuttleworth, 1978) and takes the form:

$$r_{SS} = \left[\frac{W}{r_b(s/\gamma + 1)}\right] + \left[\frac{(1-W)}{r_S + r_b(s/\gamma + 1)}\right]^{-1} - r_b(s/\gamma + 1) \qquad (1.8)$$

where $W = 1$ when $C \geq S$ (1.9)

$$W = \frac{R-1}{R-S/C} \quad \text{when } C<S \qquad (1.10)$$

$$R = \frac{(r_S/r_a)(r_a-r_b)}{r_S + (s/\gamma + 1)\ r_b} \qquad (1.11)$$

where r_b - mean boundary layer resistance (s m^{-1}), defined by Shuttleworth (1983) as:

$$r_b = 1.1u*^{-1} + 5.6u*^{1/3} \quad (1.12)$$

where u* - friction velocity (m s^{-1}).

Both Rutter and Shuttleworth use equation 1.5 when the surface is completely dry (phase 3).

The Rutter model can be used to calculate a continuous or running water balance, summarised by the continuity equation:

$$\frac{dC}{dt} = P(1-T_F-T_S) - D - E_{PM} \quad (1.13)$$

where t - time (h);
P - precipitation (mm);
T_F - throughfall or proportion of rain falling directly to the ground through the gaps in the canopy;
T_S - proportion of rain diverted to the 'trunks';
D - drainage (mm h^{-1}); and
E_{PM} - evapotranspiration (mm).

This model represents the canopy as a single-layer store of moisture which is filled by incoming rainfall; is capable of holding a pre-set amount of water, S; and drains at a rate, D, expressed as an empirical function in proportion to the amount of water in the store. The throughfall (T_F) represents water not available for evaporation from the canopy. Subsidiary evaporation may arise from trunks wetted by stemflow (T_S). Rutter et al. (1971) estimate this via a sub-model involving a secondary water store whose mathematical behaviour mimics that of the canopy. Multi-layer models also have been developed (e.g. Sellers and Lockwood, 1981). Shuttleworth (1988a) considers, the treatment of the whole canopy as a single moisture store the simplest, and therefore the most robust and general model of evapotranspiration-interception. In this study, which is a first attempt to use the evapotranspiration-interception approach in the urban environment, the canopy is treated as a single-layer moisture store, but with

parallel stores which allow consideration of the different surface types within the urban area.

As a first approximation the urban system consists of two surface types: built/impervious and vegetated. The canopy can be considered sparse with no closed, elevated layer above the ground, unlike a forest. The trees usually have vegetation (grass) below, therefore when water falls between them it may be caught by the vegetation below. The near surface vegetation has the same local climate as the large vegetation. There is little relevance to the concept of throughfall from impervious surfaces (buildings; paved road, paths) therefore this term can be set to zero or a very small number for both the vegetated and built surface types.

In urban areas the subsidiary loss, due to 'stemflow', from wetted 'trunks' can be interpreted as that from walls of buildings and from trunks of the tall vegetation. It is generally not possible for walls to be wetted by 'stemflow' from the roof due to roof guttering, although it is possible for the walls to be wetted directly during rainfall. However walls tend not to be extensively wetted under normal rain (Lacy, 1977). The surface area of trunks in the urban system is not large (see Chapter 3), hence the amount of water being stored can be regarded as negligible. It is therefore proposed that urban stemflow also be set to zero.

In urban areas there is an additional source of water for wetting the canopy, the piped water supply (I).

Thus, neglecting throughfall and stemflow and adding irrigation the model can be re-formulated for urban areas as:

$$\frac{dC}{dt} = (P + I) - D - E_{PM} \qquad (1.14)$$

C can now be considered to be the surface storage state.

The specific nature of the urban surface resistance and drainage functions are

presented in Chapter 7.

1.4 Approach to problem solution and structure of the thesis

To develop and test the model outlined above measurements were conducted over a wide range of meteorological conditions. They were conducted from January to June, 1987 in a suburb of Vancouver, B.C. The evaporative flux was determined using the energy balance framework and micrometeorological measurements. A description of the methods and measurements is contained in Chapter 2. Although the energy balance itself is not the focus of this study these are amongst the first energy balance measurements conducted in winter and spring, so discussion of the fluxes is included in Chapter 6.

Development of the urban evapotranspiration-interception model involved the need for other sub-models to calculate anthropogenic heat flux, storage heat flux, aerodynamic resistance, surface resistance and drainage. A common requirement of these sub-models and the overall model is knowledge of the 'surface'. There is no clear cut methodology to determine what the 'surface' is or what area should be considered for description. This issue is addressed in Chapter 3. The results of this are used in the development of the models of anthropogenic heat flux (Chapter 4); storage heat flux (Chapter 5); and surface resistance and drainage (Chapter 7). The full evapotranspiration-interception model is tested against the measured latent heat fluxes in Chapter 8 together with sensitivity analyses of the model.

CHAPTER 2 OBSERVATION PROGRAMME

2.1 Physical Setting

Vancouver, B.C. (49° 15'N, 123° 18'W) is located on the west coast of North America, but is climatically isolated from the continental interior by a series of mountain chains parallelling the coastline. The city is sheltered from the Pacific Ocean by Vancouver Island. The city is situated at the west end of the Lower Fraser Valley and has low to moderate relief.

Observations for this study were conducted in the Sunset suburb, Vancouver (Fig. 2.1). This site has been used for a number of climatological studies. Sunset has predominantly one- and two-storey single family dwellings (Fig. 2.2). The area has a slight southwestward slope towards the Fraser River.

2.2 General climatology of Vancouver and the measurement period

The general climatology of Vancouver is described in Hay and Oke (1976), the following is a brief description. The large scale upper level flow is generally from the westerly quarter, from the Pacific. Embedded in this flow are disturbances (cyclones) which are best developed and most frequent in winter. High-pressure (anti-cyclonic) regimes have a relatively low frequency in the winter months, normally being unable to withstand the invasion of a vigorous cyclonic disturbance. Summer brings an extension of the Pacific anticyclone regime into the mid-latitudes, resulting in the predominance of high-pressure conditions and generally clear, warm weather. Several physical features of the landscape combine to produce local climate variations. Chief among these are the influences of topography, proximity to the ocean, and urbanization.

The setting of Vancouver leads to the occurrence of land/sea and mountain/valley circulations. The effect of the land/sea breeze is to cause

Figure 2.1 The location of the Sunset site in the Vancouver area and surrounding landuses.

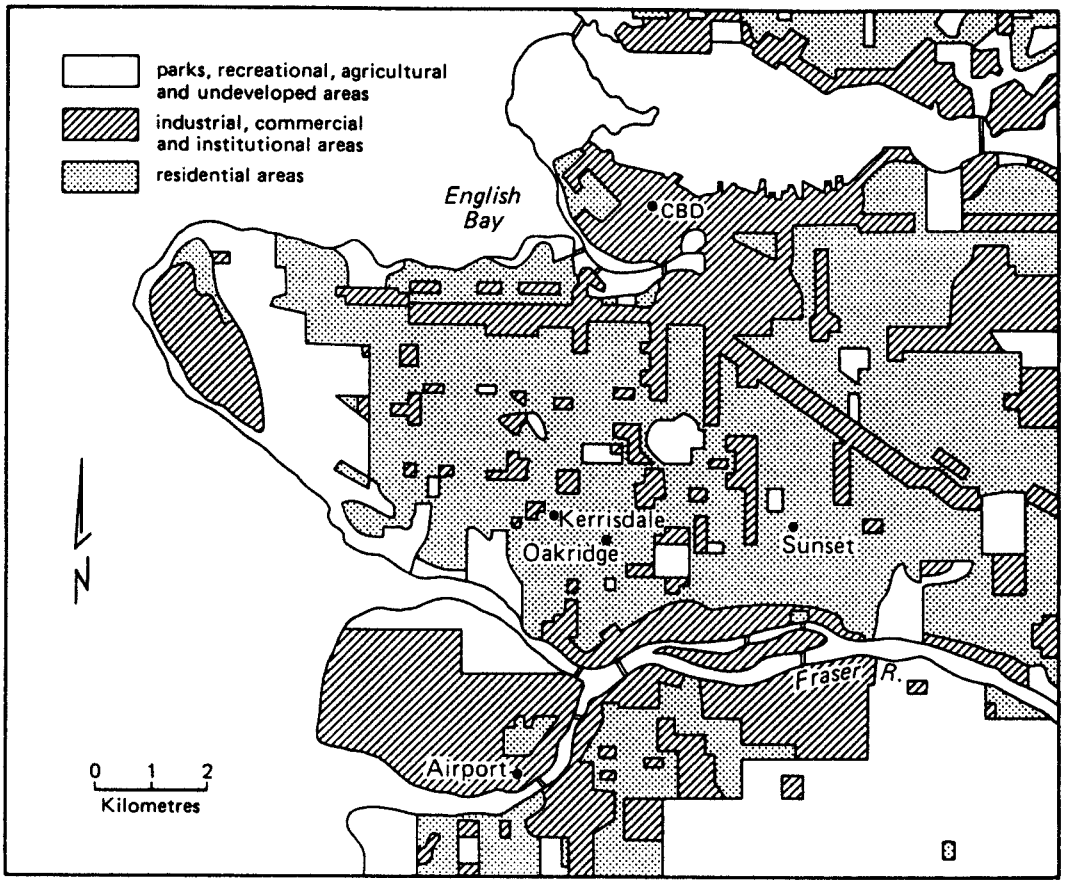

Sunset - site of tower for present study
Kerrisdale - site of tower for Grimmond (1983) study
Oakridge - site of water use meter
Airport - AES climate station

Figure 2.2 View looking southwest from the tower

predominantly westerly winds during daytime and weaker easterly flow during the night. The land/sea breeze has a higher frequency during the summertime (Steyn and Faulkner, 1986). Due to the sea breeze and the associated advection of marine air, the height of the planetary boundary layer is typically reduced to only 500 m (Steyn and Oke, 1982; Cleugh, 1988; Steyn and McKendry, 1988).

In this study measurements were conducted from Julian Day (JD) 21 (January 21) to 179 (June 28) 1987 (see Appendix I for JD calendar). Table 2.1 provides monthly average climate statistics to enable a comparison of the climatic status of 1987 with the 'normal'. It is based on data collected by the Atmospheric Environment Service (AES) at the Vancouver International Airport Climate Station (Fig. 2.1). In general, the measurement period was warmer than normal, had a greater number of sunshine hours, but had almost normal precipitation (more as rain and less as snow than normal).

2.3 Measurement considerations

The objective of this research was to determine fluxes from an area of suburban land use; i.e. at the local scale (Oke, 1984), rather than from individual surfaces such as lawn or pavement. Therefore measurements must be made well above the height of the roughness elements to ensure observations are conducted in the surface layer (Fig. 2.3), so that they represent the integrated effects of the surface types which characterise the land use. Cleugh and Oke (1986) note that "due to the presence of relatively tall roughness elements and the great spatial variability of surface materials which characterise suburban terrain, the choice of the sensor height and averaging time (τ), is not a simple task".

Roth (1988) reports a study of the turbulence spectra of temperature, the vertical and longitudinal wind components as well as the cospectra of the

Table 2.1 Normal (N) (1951-1980) and 1987 measurements of climatic variables for Vancouver International Airport (Canada, Dept. of Environment, A.E.S., 1987; Hay & Oke, 1976)

Month	Precipitation (mm)		Mean Air Temperature (°C)		Bright Sunshine (hours)		Mean Relative Humidity (%)		Mean Wind Speed (km h^{-1})	
	N	1987	N	1987	N	1987	N	1987	N	1987
JANUARY	146.8	130.7	2.5	4.4	53.5	59.5	87	83	12.2	12.3
FEBRUARY	114.7	78.0	4.6	6.5	87.2	80.1	85	77	12.4	10.7
MARCH	101.0	142.9	5.8	8.0	129.3	126.1	82	80	13.5	11.6
APRIL	59.3	63.2	8.8	10.4	180.5	174.7	75	73	13.3	12.6
MAY	51.6	85.8	12.2	13.0	246.1	267.3	74	73	11.8	13.7
JUNE	45.2	17.8	15.1	16.0	238.4	296.7	76	73	11.5	12.1
JAN-JUNE	525.9	534.7	8.2	9.7	935.0	1004.4				

NOTES:

January - Mild temperatures prevailed during the month with low snowfall totals, while in other respects the month was very near normal

February - In general the month was dull, warmer than expected, with rainfall falling frequently but below the normal total for the month

March - Warm and wet. Mean temperature for the month was more than 2 degrees above normal and precipitation was more than 50% higher than normal

April - Mild conditions dominated the month with precipitation near normal and predominantly falling in the first half of the month

May - Considerably sunnier and warmer than normal, but rain fell on more than the normal number of days and the amount was more than 60% greater than normal

June - Well below normal precipitation amounts and much higher than normal sunshine

Figure 2.3 Idealised arrangement of boundary layer structures over a city (after Oke, 1984).

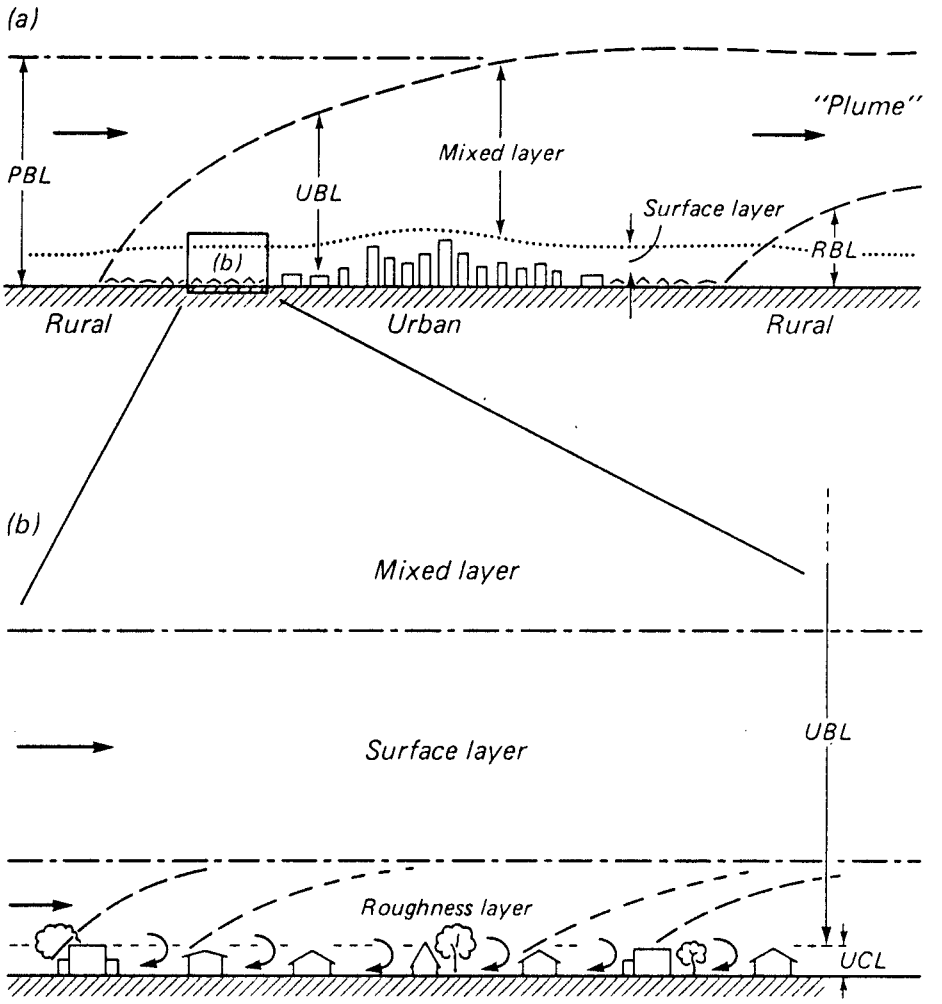

fluxes of sensible heat and momentum at the Sunset site, including an assessment of whether the measurement height used is above the 'roughness sub-layer' (Raupach, 1979) or 'transition layer' (Garratt, 1980). Roth concluded that, although the sensor height of 20-21 m above zero plane displacement, is at, or below, recommended values for the top of the roughness sub-layer, the height is suitable for turbulence measurements.

Cleugh and Oke (1986) use Wyngaard's (1973) analysis to yield τ for this measurement height at the Sunset site. In unstable conditions ($z/L = -1$) they find τ between 80 and 130 minutes for a sensible heat flux measured with 10% uncertainty, and 36 to 60 mins for 15% uncertainty. In neutral stability τ should be about 67% greater. Roth (1988) compared averaging times for heat flux covariances computed over 60 min with the mean of those over four 15 min periods and found no significant under- or over-estimation over the range 5 to 300 W m^{-2}. Similar conclusions arise from qualitative assessment of the spectra; i.e the averaging time for turbulent fluxes can be relaxed.

In accord with these findings a sensor height of >20 m above zero plane displacement, and an averaging time of 60 minutes were selected for the present study. The displacement length was determined for the Sunset site by Steyn (1980), using the techniques of Kutzbach (1961) and Nicholson (1975), to be 3.5 m. Steyn (1980) calculated the roughness length, via Lettau's (1969) method, to be 0.52 m.

2.4 The Instruments

The instruments were mounted on a 29 m triangular section steel lattice free standing tower located within the Mainwaring substation of B.C. Hydro. The base of the tower is 5 m below the level of the surrounding embankment. The maximum effective height of the tower is 20.5 m (height of instrument

minus zero plane displacement and embankment).

The environmental variables measured were: net radiation flux density (Q*), sensible heat flux density (Q_H), wind speed (u) and direction (φ), wet (T_W) and dry (T_d) bulb air temperature, relative humidity (RH), surface wetness (w_S), precipitation (P) and soil moisture deficit ($\delta\theta$). Details of the instrumentation and their positions on the tower are provided in Figures 2.4 and 2.5 and Table 2.2. The signals were logged on two Campbell Scientific Inc CR21X data loggers. The data were written to cassette tapes and read on to the UBC mainframe computer using a Campbell Scientific Inc C20 Audiosphere Interface. All times referred to are local apparent time (LAT).

The sonic anemometer-thermometer system (SAT) used for measuring sensible heat flux density (Q_H), utilises the eddy correlation approach. The vertical velocity is sensed as a phase shift in the sound wave, and the air temperature by a fine wire thermocouple (diameter 12.7μm). The wind speed and temperature were sampled at 10 Hz and covariances determined for 15 min periods. The hourly Q_H was obtained from the average of the four 15 min values.

It is difficult to assess the actual measurement error associated with eddy correlation estimates of Q_H (Cleugh, 1988). The results of Roth (1988) indicate that the sonic anemometer-thermometer measures $\overline{w'T'}$ cospectra "adequately". An inter comparison of hourly fluxes from two instruments obtained a RMSE of 12 W m^{-2} (Cleugh, 1988; Schmid, 1988). Tanner (Campbell Scientific, pers. comm., 1987) suggests that the measurement error is less than 10%.

The reversing temperature difference measurement system (RTDMS), used to determine Bowen ratios ($\beta=Q_H/Q_E$), was similar to that described by McCaughey et al. (1987). The wet and dry bulb thermocouples (10 junction copper/ constantan thermopiles) were mounted within shields on two carts which move up

Figure 2.4 Schematic of the Sunset tower and instrument locations. Instruments include: net pyrradiometer, sonic anemometer/ thermometer (level 4, SW); relative humidity probe, Met-101 wind vane, Met-101 cup anemometer (level 3, NE); Bowen Ratio system (levels 1 and 2). (Adapted from Cleugh, 1988; Roth, 1988).

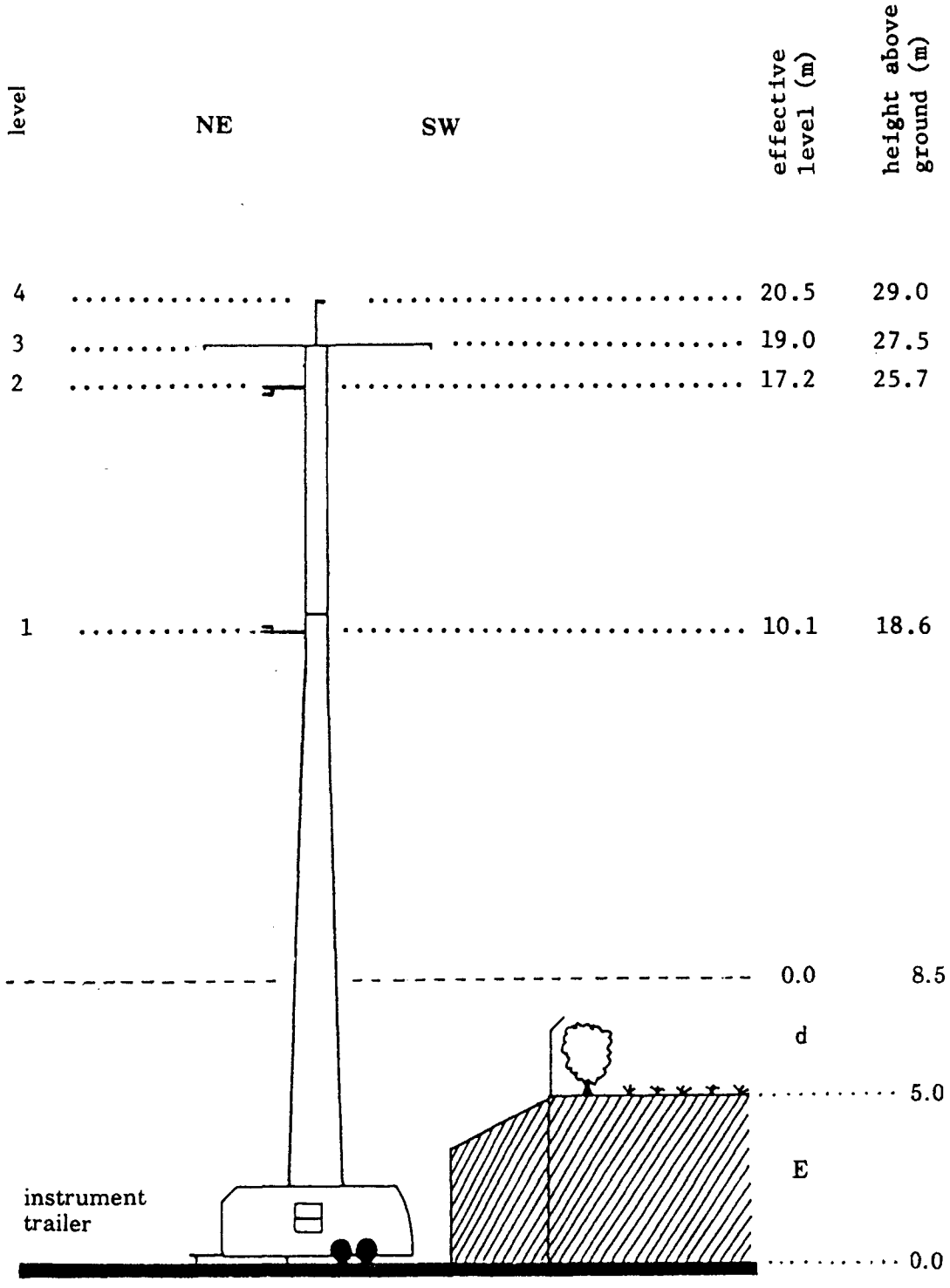

Figure 2.5 Photographic view of top part of Sunset tower.

Table 2.2 Instrumentation

Variable	Instruments (Manufacturer model)	Effective[a] Height (m)	Sampling Time (s)	Recording Interval (min)
Q*	Net pyrradiometer (Swissteco S1)	20.5	1	5
Q_H	Sonic anemometers thermometer (Campbell Scientific CA27)	20.5	0.1	15
u	Cup anemometer (Met-One 012A)	19	1	5
φ	Wind vane (Met-One 024A)	19	1	5
RH & T	Humidity & temperature probe (Rotronics Instrument Corp MP-100)	19	1	5
T_d & T_W	McCaughey RTDMS			
	upper cart	17.2	1	10
	lower cart	10.1		
w_s	Surface wetness sensor Weiss	-	1	5
P	Raingauge (Meteorological Research Inc 382B)	-	1	5

a Height above ground minus embankment height and zero plane displacement

and down on a trackway. The carts, separated by 7.1 m, are reversed twice each hour. A ten minute period allows for travelling (less than 4 mins) and equilibration at the new level. The remaining 20 minutes at each level allowed for two 10 minute averages. ß was calculated:

$$ß = \frac{\gamma\ (\Delta T_d + \Gamma\ \Delta z)}{(s + \gamma)\ \Delta T_W - \gamma\ \Delta T_d} \qquad (2.1)$$

where ΔT_d - dry bulb temperature difference ($^{\circ}C$);
ΔT_W - wet bulb temperature difference ($^{\circ}C$);
Γ - dry adiabatic lapse rate ($^{\circ}C\ m^{-1}$);
s - slope of the saturation vapour pressure curve at T_W (Pa $^{\circ}C^{-1}$);
γ - psychometric constant (Pa $^{\circ}C^{-1}$); and
Δz - sensor separation (m).

See Appendix II for the methods used to determine the individual terms.

Q_H can be determined from ß using the energy balance:

$$Q_{Hß} = [ß\ (Q^* + Q_F - \Delta Q_S)]\ /\ (1 + ß) \qquad (2.2)$$

where Q_F - anthropogenic heat flux (see Chapter 4); and
ΔQ_S - storage heat flux (see Chapter 5).

Similarly the latent heat flux (Q_E) can be determined:

$$QE_ß = (Q^* + Q_F - \Delta Q_S)\ /\ (1 + ß) \qquad (2.3)$$

Alternatively, Q_E can be calculated using ß and the Q_H measured with the SAT:

$$Q_{ES}=Q_H/ß \qquad (2.4)$$

See Chapter 6 for discussion of the methods used to determine energy balance fluxes.

The error analysis used to determine the precision of the reversing temperature difference measurement system (RTDMS) follows the procedure of Kalanda (1979) who conducted an error analysis of a reversing temperature system following the method of Cook and Rabinowicz (1963) (Appendix III). Using this method errors were determined for the temperature differences, absolute temperatures, ß, $Q_{Hß}$ and $Q_{Eß}$. The errors calculated for each hour were used to stratify the data to decide whether it was of use to test the submodels (see Chapter 5) and for the determination of 'measured' Q_E (see

Chapter 6).

Net all-wave radiation was measured with a net pyrradiometer. The polythene domes were kept inflated and free of internal condensation by air pumped through granulated silica desiccant. Typical measurement errors for net pyrradiometers are 3-4% on instantaneous measurements (Latimer, 1972). For hourly values an error of 5% is generally used (Cleugh and Oke, 1986).

The relative humidity and temperature probe was housed in a reflective shield which allowed air flow around the sensor but protected the sensor from solar radiation and precipitation. The relative humidity is measured with a C-80 HYGROMER sensor which is connected to a capacitive bridge. The unit senses temperature with a precision Pt 100 RTD which forms part of a measuring bridge. The output from the bridge feeds an amplification and linearization circuit. The instrument has a nominal accuracy of $\pm$ 1.5% RH at 25°C and $\pm$ 2.5% over the temperature range of -50 to +150°C (manufacturer's specifications). The nominal accuracy of the temperature over the range -20 to + 50°C is $\pm$ 0.35°C (manufacturer's specifications). The instrument repeatability is 0.5% for RH and 0.1°C for temperature, or better (manufacturer).

An unshielded tipping bucket rain gauge was mounted with the 200 mm orifice approximately level with the top of the embankment. It tipped with the accumulation of 0.2 mm in a collection bucket. A reed switch is actuated by a magnet on the tipping bucket. The tipping bucket mechanism has a nominal accuracy of $\pm$ 1% for up to 76.2 mm h^{-1} and $\pm$ 5% up to 254 mm h^{-1} (manufacturer specifications). There is no means of measuring the 'true' precipitation (i.e. the amount of water which would have reached the ground had the gauge not been present, hence all measurements are relative). Measurement errors for daily totals can be assumed to be $\pm$ 7% based on research conducted by Hutchinson (1969), Mandeville and Rodda (1970), Finkelstein (1971), Rapier and Grant

(1971), Waugh (1971) and Aldridge (1976). The random errors for shorter time periods will be greater. Hutchinson (1969) reports errors of 12.5%, at the 95% confidence limits, for individual storms.

The wind speed sensor was a 3-cup anemometer with a magnetic-reed switch assembly which produced a series of contact closures, the frequency of which was proportional to the wind speed. The starting speed of the anemometer is 0.5 m s^{-1} and the nominal accuracy over the calibrated range of 0 to 50 m s^{-1} is $\pm$1.5% (manufacturer specifications). The wind direction sensor uses a light weight, air-foil vane and a potentiometer to produce an output that varies in proportion to wind direction. The vane has a 0.5 m s^{-1} threshold and a $\pm 5^{\circ}$ nominal accuracy (manufacturer specifications). The atmospheric pressure data used in this study were collected at the Vancouver International Airport Climate Station (see Fig. 2.1).

Three surface wetness sensors were built following the general design of Weiss and Lukens (1981) (Weiss, pers. comm.). The sensors consist of a frame (0.1 m x 0.1 m) with 30 AWG wire threaded across the centre with muslin material weaved through the wire. The wire has a 2 V AC voltage passing through it and the output voltage, which varies depending on the wetness of the material (a surrogate for the surface), is logged on the CR21X. The output does not give a numerical value of degree of wetness but an indication of whether the surface is wet or dry. Two sensors were located on grass and a third in a coniferous hedge just outside the Mainwaring substation site. Vandalism prevented more extensive use of this type of instrumentation. Visual observations of the drying of different surface types were made on numerous occasions through the measurement period.

Gravimetric soil moisture samples were taken approximately three times a week from two sites near the tower. From mid May (JD 133) samples were

gathered at an additional three sites, both irrigated and non-irrigated, around the tower area. The average dry weight moisture content (Gardner, 1965) for the profile from the surface to a depth of 200 mm was determined. These data were used with dry bulk density measurements (Hillel, 1971) to determine soil moisture deficit ($\delta\theta$).

Water use was monitored by the Engineering Department, City of Vancouver from May 19, 1987 (JD 139) in the residential area of Oakridge (Fig. 2.1). The water use for the 21 ha catchment was recorded at 15 min intervals with a resolution of 2.832 m^3. The volume used externally for irrigation was separated from the total based on previous work in the same catchment (Grimmond, 1983). It was assumed that the same depth of water was applied to the irrigated area in the Sunset suburb as was applied in the Oakridge catchment. From visual surveys at both sites it was determined that different proportions of the residential vegetation were irrigated (Oakridge 95%; Sunset 60%). The external water use data set was extended back to JD 121, selected as the day of the onset of irrigation (based on observations and Grimmond, 1983), using a multiple regression equation developed from the hourly 1987 data set incorporating time of day, hours since rain, available energy, temperature and vapour pressure deficit.

PART II DEVELOPMENT AND TESTING OF SUBMODELS

CHAPTER 3 SURFACE DESCRIPTION

3.1 Introduction

A fundamental methodological problem in urban hydroclimatological research is the definition of the location, and other characteristics, of the urban 'surface'. The active surface of any system is one of its most important climatic determinants because it is the primary site of energy, mass and momentum transfer and transformation. The urban-atmosphere interface is extremely complex thereby defying simple description (Oke, 1984). Measurement and modelling both require the surface datum to be defined and described: to characterise the site where measurements have been conducted; and if the objective of a study is to validate a model it is obviously important that the model surface description/inputs and outputs are for the same surface as that for which the measurements were conducted.

The surface definition utilized is dependent upon the process(es) being studied and the spatial and temporal scale of the study. Different hydroclimatic fluxes are influenced by different characteristics of the surface. Therefore the first step in any investigation is to identify the characteristics of importance to the process(es). For example, studies of net radiation require albedo and emissivity to describe the surface; turbulence work may need the roughness length, displacement length, roughness element separation, height of roughness elements; and storage heat flux studies need thermal admittance, percentage of green and built space.

The scale of the study determines what is regarded as being homogeneous and what is heterogeneous. At any scale, temporal or spatial, which is regarded as homogeneous for the entity under study there is sub-scale heterogeneity. This study is concerned with determination of fluxes at the local scale, as defined

by Oke (1984), in an urban area (Table 3.1); i.e. scale II-4 with sub-scales I-1 to I-4. The suburban surface is extremely non-homogeneous at the subscale. For example, around the measurement site there are parks, small areas of commercial buildings, schools, churches etc in addition to housing areas (see Fig. 3.1). Within each of these types of properties there are sub-scale heterogeneities: concrete, grass, deciduous and coniferous trees etc.

Once the scale and the appropriate parameters for the surface description have been identified, there remains the practical decision of where to draw boundaries. Because of sub-scale heterogeneity the choice of boundaries may unknowingly or purposefully change the apparent site description. This can be demonstrated with a very simple example. If circle 'a' (Fig. 3.2) indicates the site description boundaries rather than circle 'b', then the value assigned to the surface parameter "number of trees" changes from 0 to 21. If this is an important parameter (e.g. modelling surface resistance for evapo-transpiration) then the site description obviously is very different depending on the location of the boundaries.

Often the site has been described in a static sense. One description of the surface has been used for all periods of measurements or modelling, and does not vary with wind direction or meteorological conditions (e.g. stability). Typically this description is based on a mean parameter for a circle around the measurement site. A circle has been used by a number of researchers working at the Sunset site (Kalanda, 1979; Steyn, 1980; Oke et al., 1981; Loudon, 1984), elsewhere in Vancouver (Yap,1973), in St Louis (Ching et al., 1983), and Worcester (Yersel and Goble, 1986). Although some of these researchers have divided the circle up into equal size sectors (e.g. 16 - 22.5° sectors).

The choice of radius for the circle is often based on calculated fetch

Table 3.1 Framework for urban climate classification proposed by Oke (1984)

a) **Turbulent Boundary Layers**

Layer	Flow characteristics	Dimensions[a]	Scale
I. Urban canopy buildings (UCL)	Highly turbulent, controlled by roughness elements	Same as H[b] typically 10 m	Micro
Roughness sub layer	Highly turbulent wakes and plumes, transition zone	2D - 3D[b] typically 20-40 m	Micro
II. Urban boundary layer (UBL)	Turbulent, includes surface & mixed layers	Depends on surface fluxes of heat and momentum, typically day 1 km, night 0.2 km	Local & Meso

b) **Urban Morphology**

Urban units	Urban features	Urban climate phenomena	Dimensions H	W	L	Scale
1. Building	Single building, tree or garden	Wake, plume or shadow	10m	10m	10m	Micro
2. Canyon	Urban street & bordering buildings or trees	Canyon shelter, circulation, shade, bioclimate	10m	30m	300m	
3. Block	City block, park, factory complex	Climates of parks, building clusters, cumulus mini-breezes		0.5km	0.5km	
4. Land-use zones	Residential commercial industrial etc.	Local climates incl. winds, cloud modification		5km	5km	Local
5. City	Urban area	Heat island, urban circulation urban effects in general		25km	25km	Meso

a Dimensions of boundary layers are depths of affected atmosphere; dimensions of morphological units are those of urban structures or plan area.

b H - building height, D - building spacing

Figure 3.1 Aerial photograph of area to the northwest of the tower. Note that the area includes a park as well as housing.

Figure 3.2 Schematic of the influence of the location of the boundaries for surface description. See text for further explanation.

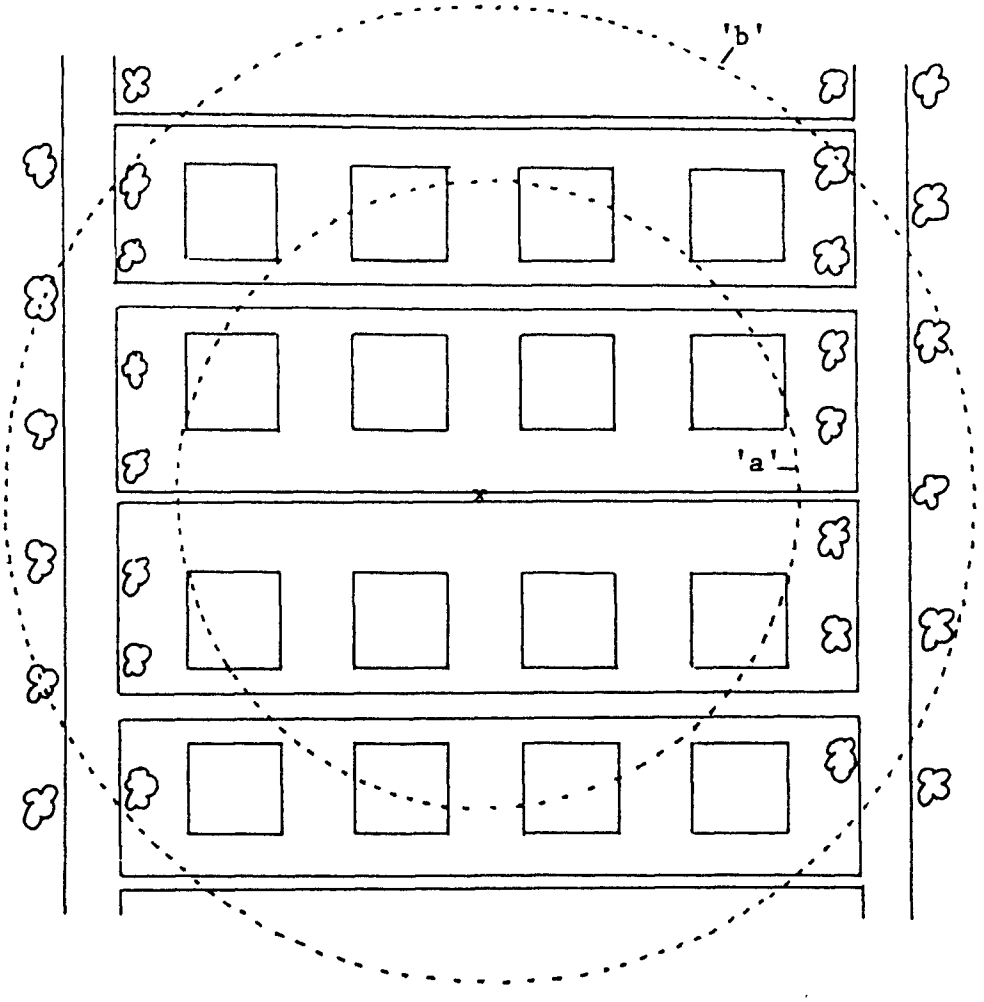

requirements. For example, Steyn (1980) calculated the fetch requirements for the Sunset site to be 1485 m using the relation presented by Munro and Oke (1975). The 2 km radius used provides an extra 500 m to ensure adequate fetch. Yap (1973) working elsewhere in Vancouver, also calculated the required fetch to be approximately 1.5 km, and chose a circle of 2 km radius. There does not appear to be an objective means to decide on the size of the radius.

The circle approach assumes either that the surface is spatially homogeneous and/or, that over time the variation of wind direction will create spatial averaging. In reality there are preferred wind directions. This can be seen from the wind frequency rose for the measurement period JD 22-179, 1987 (Fig. 3.3). The surface contributing to a turbulent flux at a point is constantly changing. This suggests that a dynamic approach may be more appropriate (i.e. where the surface characteristics and changing meteorological conditions, including wind direction, are taken into account).

This chapter is concerned with methods to describe the surface which are dynamic and the development of a database of surface characteristics for use with these methods. The methods and database outlined in this chapter are used subsequently to calculate anthropogenic and storage heat flux so as to arrive at a spatially-consistent energy balance when combining measured and calculated terms. They are also used to model latent heat flux densities which are consistent with measured values.

3.2 Boundary Selection for Surface Description

As stated in Chapter 1, the objective of this research is to develop and test an evapotranspiration model at the local scale. To test the model it is necessary to have latent heat flux (Q_E) measurements. These were determined within an energy balance framework, in which it is necessary to have values of

Figure 3.3 Wind direction frequency (%) for the Sunset site (JD 21-179, 1987)

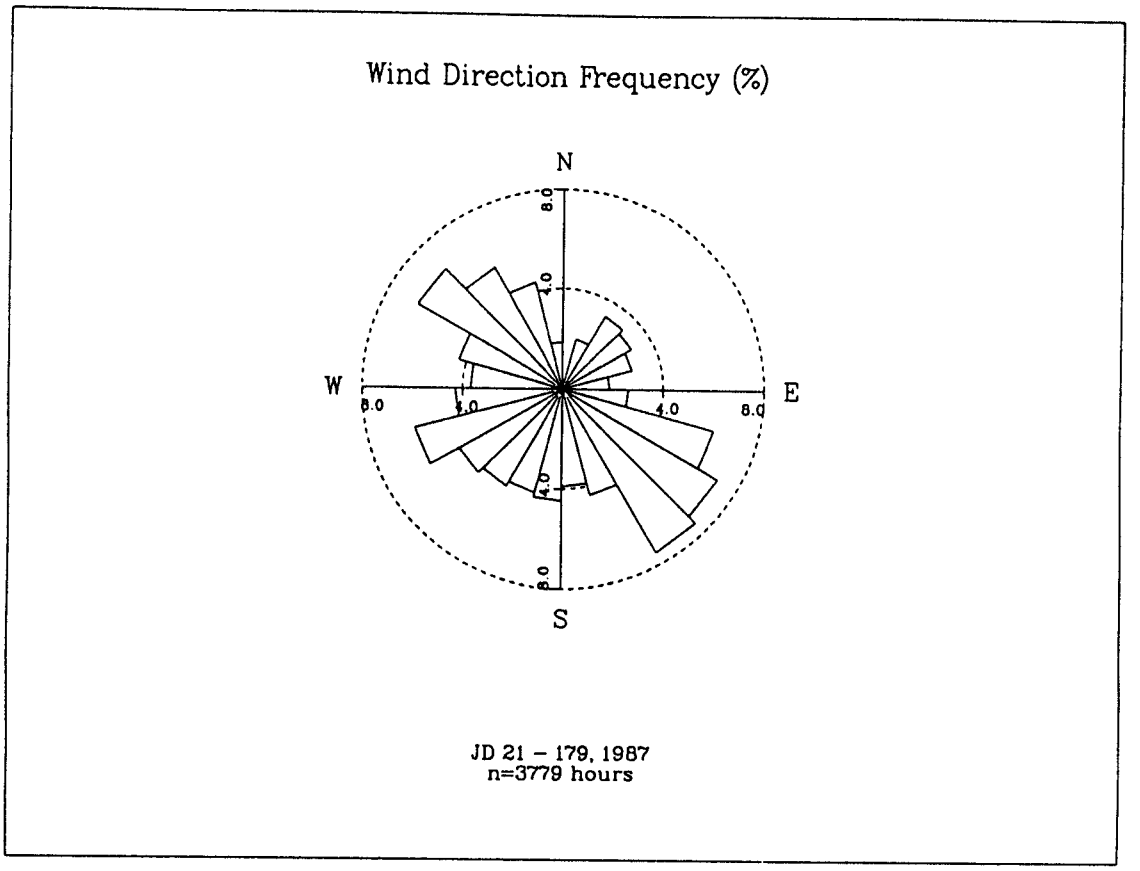

the anthropogenic heat flux (Q_F) and storage heat flux (ΔQ_S). To model these fluxes (Q_E, Q_F, ΔQ_S) it is necessary to input certain surface characteristics (see Chapters 7, 4,and 5 respectively for details). Therefore there needs to be a basis for locating the boundaries for the areas used to determine surface parameters. In this section it is intended to consider what shapes (areas) should be used to describe the site for modelling purposes so that it will be consistent with the source areas of the measurements, and therefore a spatially consistent energy balance computed.

In this study, net radiation (Q^*), sensible heat flux (Q_H), and the Bowen ratio ($\beta=Q_H/Q_E$) were measured directly (see Chapter 2). In order to consider the areas that contribute to their measurement, at a point on the tower, these can be divided into measurements of radiant (Q^*) and turbulent (Q_H and Q_E) energy flux densities.

3.2.1 Radiant Fluxes

Albedo, emissivity and surface temperature are the surface parameters normally used to describe a site when considering radiant fluxes. Albedo influences the net short-wave radiation; and emissivity and surface temperature influence the net long-wave radiation. Oke (1987) reviewed the "available evidence regarding spatially representative values of the surface albedo of cities". He noted "remarkable convergence of opinion, considering the geographical diversity of the cities represented" and suggested a value of 0.14 for urban centres and 0.15 for suburbs. It is not possible to measure an areal average for emissivity. Arnfield (1982) tabulated emissivities for a range of surfaces to use with his geometric urban radiation model. The values he calculated for eight urban land use zones in Columbus, Ohio show a relatively small range from 0.937 to 0.961 in snow-free conditions. Schmid

(1988) conducted a study on the spatial variance of remotely-sensed surface temperature for an area around the Sunset tower. He showed that the spatial distribution of surface temperature has a dominant component of a highly regular pattern and a minor component of breaks in this regularity caused by parks, school grounds etc. He concluded, based on strong consistency of spectral variance distributions between different areas and domain sizes that there is an overall homogeneity to the spatial surface temperature distribution.

Q*, when measured with a net pyrradiometer, is based upon a circular view from the tower. The radius of the "seen area" with a view factor of 0.95, calculated using Reifsnyder (1967), is 108 m when the net pyrradiometer is mounted at a height of 24 m. This is considerably smaller than the 2 km radius circle used for surface description in previous studies. However, Grimmond (1983) and Cleugh (1988) have demonstrated that within a 5 km radius circle of the Sunset tower there is very little variability of Q* under clear conditions. The measured variability of 0.5-4.5% is of the same order as typical measurement errors (Latimer, 1972). Under cloudy conditions there is a slightly greater variability (6%) between sites (Grimmond, 1983). It is greatest under partly cloudy conditions when it is possible for cloud to affect one site but not another.

It is concluded that net radiation is conservative with respect to variability of surface types within urban land uses, and therefore an area larger than the view of the net pyrradiometer is allowable for surface description. The area probably should not be smaller otherwise it may not sample a sufficiently representative range of surface types.

3.2.2 Turbulent fluxes

The area influencing the measurement of turbulent fluxes at a point is upwind in the prevailing wind direction. The collection of surface elements which influence the air parcels that are sampled as they pass the sensor is termed the 'source area'. The upwind, downwind and lateral boundaries of the source area are dependent on the characteristics of the flow and on the boundary layer development in the atmospheric layer between the surface and the sensor level (Schmid, 1988).

Pasquill (1972) developed a model to determine the dimensions of the source areas dominantly affecting point measurements. The dimensions of the elliptically-shaped source areas (Fig. 3.4a) are a fairly sensitive function of sensor height, and are further affected by stability and roughness, in that order of importance. Pasquill demonstrated that all of the dimensions of the source area increase as the stability changes from unstable to neutral to stable conditions.

The model allows for the patchiness of the surface at a variety of scales which affect the boundary layer structure. The surface is regarded as an array of elementary 'sources' from which a property is emitted, or 'sinks' in the case of momentum. The scalar (heat, water vapour etc.) produced by any given source, and sampled at a given height, rises to a maximum at a distance downwind and then declines continuously at greater distances. Pasquill used Smith's (1957) reciprocal theorem, which states that the concentration at ground level downwind of a point- or line-source at sensor height z_S is identical to the concentration at the x and y but at the height z_S, due to an exactly similar source at the ground. This can be visualised using Figure 3.4b. Instead of calculating the dispersion from a point (e.g. a smoke stack) to an area, the 'reciprocal' is calculated, i.e. the area influencing that

Figure 3.4 Dimensions of the source area for turbulent flux measurements:
(a) plan view
(b) side view

(a)

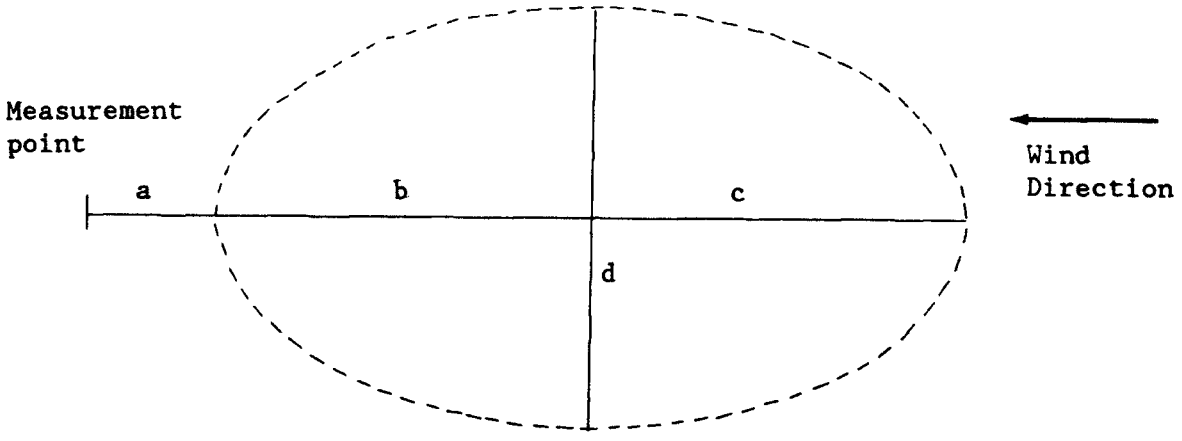

a - distance to upwind edge of source area

b + c - length of source area

d - half the width of source area

(b)

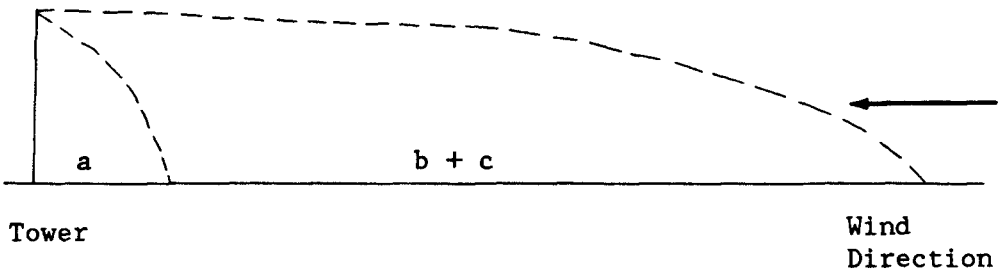

point.

The functional form of the source areas is precisely that contained in the theoretical ground-level distribution from an elevated source if the reciprocal relation between the distributions from ground and elevated sources is adopted. Pasquill used a Gaussian form of vertical distribution and assumed complete reflection of the plume. From the reciprocal relation the contour defining the source or sink area will be identical with the isopleth for a given concentration. He chose the area bounded by the $X_{max}/2$ i.e. the area in which the concentration from an elementary unit point source is greater than one half of the maximum concentration from such a source, as sensed at the same height.

Schmid (1988) has updated Pasquill's approach in view of some recent developments in diffusion theory. The model was developed to identify the source area of measured turbulent fluxes and their representativeness. Schmid uses his model in urban and non-urban areas to identify the source areas of turbulent sensible heat flux measurements and to assess the representativeness of observation sites.

A short range plume model forms the core of the Schmid source area model. Schmid follows Weil's (1985) applied diffusion modelling recommendations and utilizes the probability density function (p.d.f.) plume dispersion model developed by Gryning et al. (1987). Whereas Pasquill assumed Gaussian diffusion for both the horizontal and vertical distributions. Schmid incorporates Weil's (1985) conclusion that while plume diffusion is Gaussian in the horizontal, it is not so in the vertical. The implication is that, with skewed vertical diffusion, the symmetry assumption in Smith (1957) is invalid and the concept of reciprocity should be modified or replaced. Schmid used a slightly different concept of reciprocity which is not constrained by any

particular form of vertical or horizontal diffusion. The total effect experienced by the sensor is determined by the weighted contributions of all sources upwind, and the resulting two-dimensional source weight distribution function has its maximum at the maximum source location. The geometric location of all point sources, whose effect level at the sensor location equals an arbitrary criterion 'P', which defines a sensed concentration or effect level (X_P), forms a closed curve, which is the boundary of the P-source area. Schmid uses the fraction of the total effect which is contributed by the P-source area as the criterion for 'P'. The P-source area is defined in a similar fashion to the F-percentage effective fetch by Gash (1986). The model identifies nine weighted source area levels. Schmid's model was developed for unstable conditions. In the current work it was extended, using Gryning et al. (1987), to incorporate stable conditions. For unstable conditions, the stability functions used in the model were changed in this study from those of Dyer and Bradley (1982) to those of Dyer (1974) based on the comparison with measured u_* and z/L (see Appendix IV). For stable conditions the relations of Dyer (1974) and van Ulden and Holtslag (1985) were used (see Appendix IV).

The inputs necessary to determine the weighted source areas from the model are: the site conditions (roughness (z_0) and zero-plane displacement (d)); and meteorological scaling parameters (Monin-Obukhov stability length (L), friction velocity (u_*), and either the standard deviation of wind direction (σ_φ) and mean wind speed (u), or the mixed layer depth (z_i)). The output of the model consists of nine source area ellipses for each hour (Fig. 3.5). The area between each ellipse has equal weight; i.e. the area labelled 'a' contributes the same amount to the measured flux as that labelled 'b'.

It is proposed here that the weighted source areas, identified via the Schmid model, are the most appropriate means for assigning boundaries to

Figure 3.5 Source area for one hour with the nine weighted bands. The area labelled 'a' contributes the same amount to the measured flux as that labelled 'b'. Inner circle 2 km radius, outer 5 km.

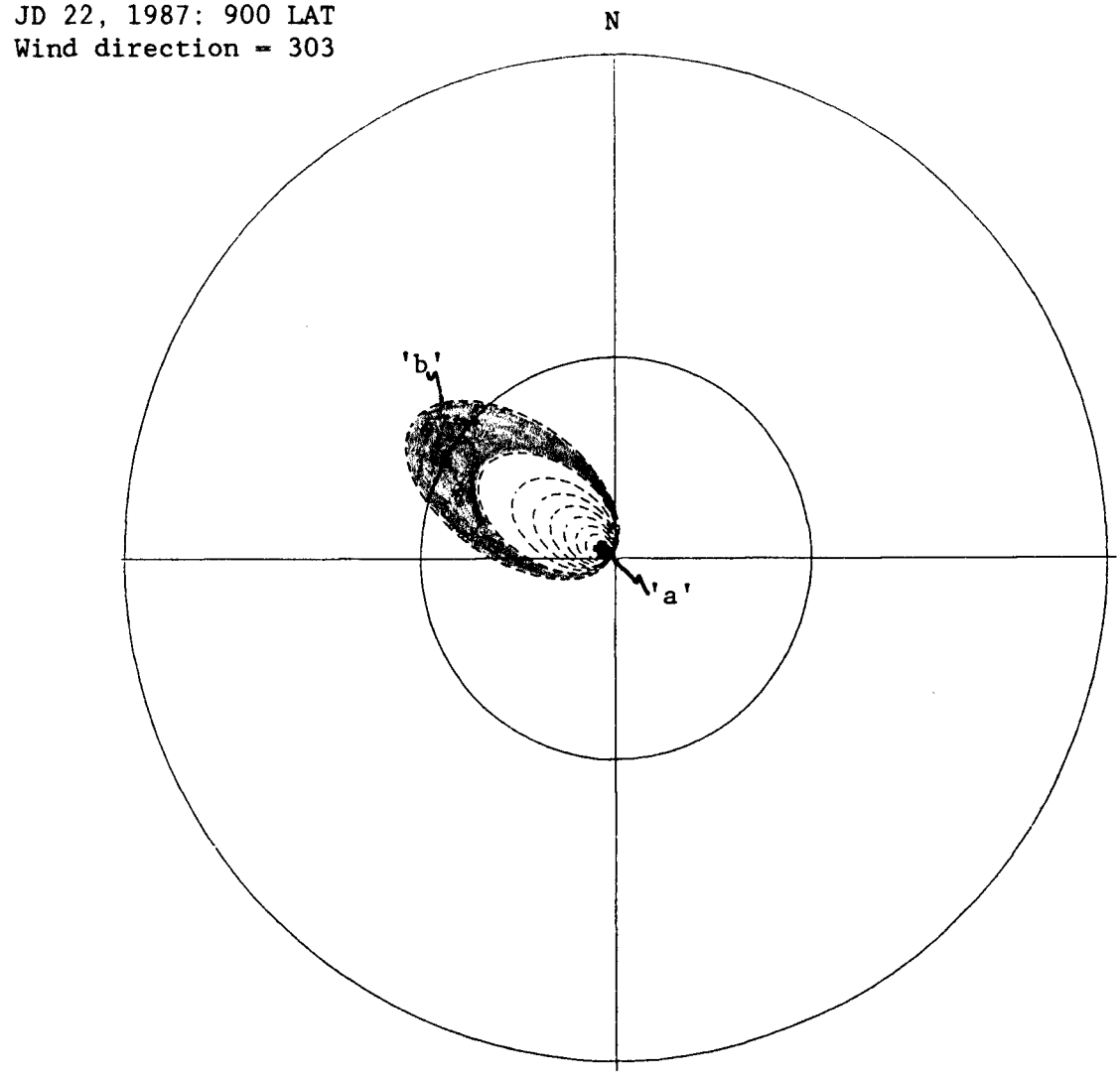

determine values of surface parameters, for modelling energy balance fluxes, to obtain a consistent energy balance with the measured terms. Use of the Schmid source area model leads to a dynamic assessment of surface parameters because, unlike the fixed circle of influence approach, the location of the boundaries change with meterological conditions. Figure 3.6 shows the location and shape of the source area for four different hours during a 24 h period. The first three (Fig. 3.6a,b,c) are consecutive hours which have increasing convective activity, and the fourth (Fig. 3.6d) is under stable conditions. It can be seen that the source area size decreases as conditions become more unstable.

Table 3.2 gives the mean, standard deviation, minimum, and maximum of the plume dimensions by stability class for all hours used in this study.

Calculation of the hourly source areas requires hourly values of L and u_*, which in turn require measured values of the sensible heat flux density (see Appendix IV). This is not always available so a very simple scheme, termed here 'sectors', is also proposed for comparison. This scheme takes into account several features: the source area is aligned along the mean wind direction (φ), the lateral dispersion is influenced by σ_φ, and areas closer to the measurement point contribute more than areas further away. The 'sectors' are aligned along φ and have a width of $2\sigma_\varphi$ (Fig. 3.7). The length of the 'sectors' and the location of the weighted boundaries were determined from the mean dimensions for stable and unstable 'plumes' for the hours when Q_H data were available (Table 3.2a,b). For the unstable case the mean b+c dimensions were used for the sectors (Table 3.2a). For the stable case the Table 3.2b values were increased so that concentration level 9 was equal to 5000 m and the other levels were increased by the same percentage (101.9%) (Table 3.2c). The reason is that the Schmid model cuts off at 5000 m and therefore biases

Figure 3.6 Examples of different source area with changing meteorological conditions. Inner circle 2 km radius, outer 5 km.

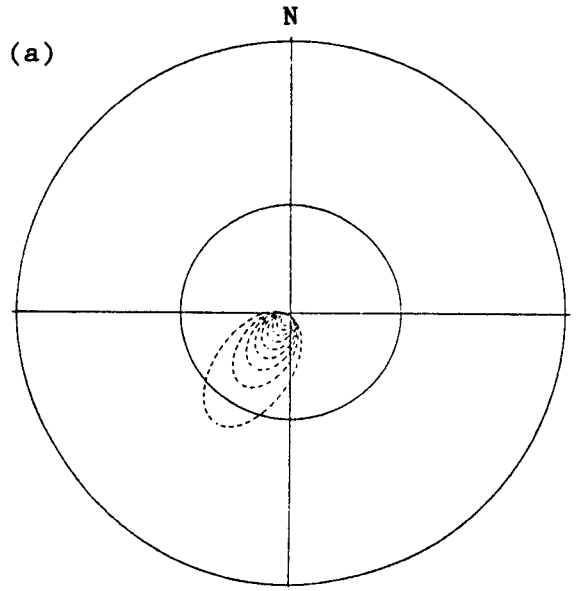

JD 22, 1987: 900 LAT
Wind direction = 303
L = -1433
u* = 0.19

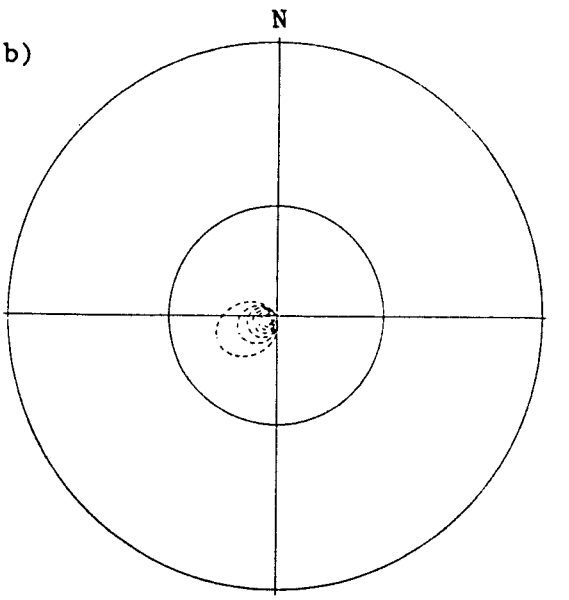

JD 22, 1987: 1000 LAT
Wind direction = 246
L = -44
u* = 0.17

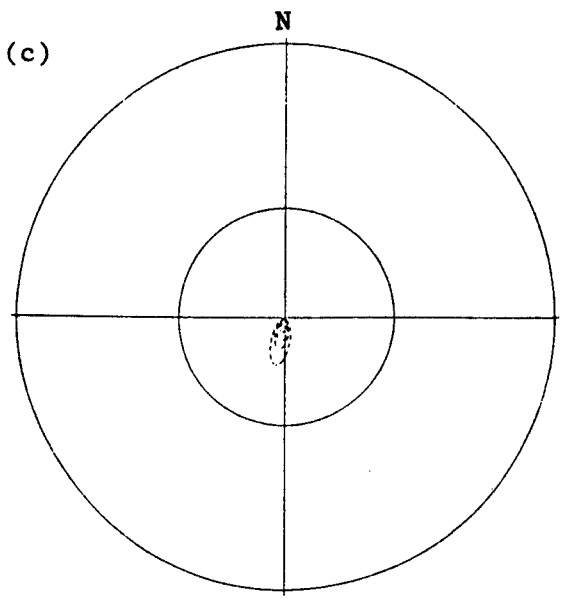

JD 22, 1987: 1100 LAT
Wind direction = 191
L = -23
u* = 0.21

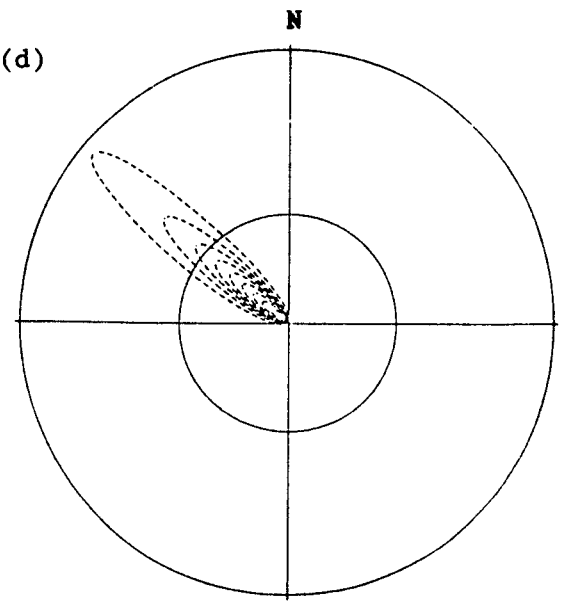

JD 23, 1987: 0300 LAT
Wind direction = 310
L = 462
u* = 0.37

Table 3.2 Mean length of plumes (calculated from the modified Schmid (1988) model) for use with the sectors. Calculated from 1476 unstable hours and 241 stable hours. All dimensions are in metres. Figure 3.3 shows the position of the a, b+c and d dimensions.

Conc. Level	a				b+c				d			
	Mean	s.d.	Max	Min	Mean	s.d.	Max	Min	Mean	s.d.	Max	Min
(a) Unstable												
1	42.4	14.0	60.8	6.5	113.2	47.5	200.0	14.0	32.4	14.2	188.3	4.0
2	35.8	11.7	50.8	5.6	178.5	75.8	320.2	21.8	47.9	21.2	282.0	5.8
3	31.8	10.3	44.9	5.1	247.8	106.5	451.7	29.7	62.7	28.1	370.3	7.5
4	28.9	9.3	40.7	4.7	330.2	142.6	607.2	39.0	79.0	35.7	470.3	9.3
5	26.7	8.5	37.6	4.4	427.6	183.5	784.6	50.1	97.0	44.0	579.7	11.3
6	25.0	8.0	35.2	4.1	538.7	229.2	985.4	62.5	116.3	52.9	696.9	13.5
7	23.5	7.4	33.1	3.9	681.8	288.7	1251.1	76.6	139.8	63.9	840.6	16.4
8	22.0	6.9	30.8	3.7	909.0	382.7	1676.6	95.0	175.0	80.3	1053.1	20.6
9	20.1	6.2	28.0	3.6	1405.0	591.8	2610.0	118.9	247.5	112.9	1481.3	29.8
(b) Stable												
1	87.4	1.7	91.0	83.8	319.7	16.4	350.9	286.0	39.6	21.4	197.7	11.1
2	72.3	1.3	75.1	69.6	512.1	27.8	565.1	454.9	60.6	32.8	302.3	17.0
3	63.4	1.1	65.7	61.1	723.9	41.4	802.8	638.9	82.3	44.5	407.8	22.9
4	57.1	1.0	59.2	55.0	972.5	56.9	1080.8	858.2	106.2	57.5	526.6	29.8
5	52.6	0.9	54.6	50.5	1252.2	73.7	1392.2	1106.0	131.9	71.3	653.1	36.8
6	49.1	0.9	51.0	47.2	1569.1	93.6	1746.6	1381.6	159.8	86.3	790.6	44.7
7	45.9	0.8	47.6	44.1	1999.4	124.5	2234.8	1747.4	196.0	106.1	971.9	54.9
8	42.5	0.8	44.1	40.9	2702.3	179.6	3041.0	2335.4	252.5	136.6	1246.9	70.1
9	38.2	0.7	39.6	36.8	4301.9	322.4	4906.6	3636.1	371.5	201.0	1818.8	102.7

(c) Stable/Neutral - values used for 'sectors' length.

1	372
2	595
3	841
4	1130
5	1455
6	1824
7	2324
8	3141
9	5000

Figure 3.7 Examples of 'sectors'. Inner circle 2 km radius, outer 5 km.

(a) JD 22, 1987: 1000 LAT Unstable
Wind direction = 246
s.d. = 36

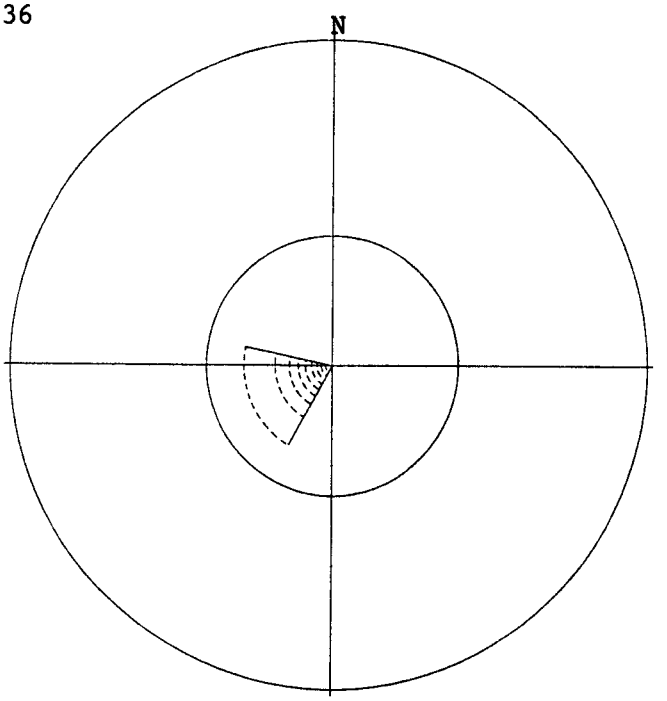

(b) JD 21, 1987: 600 LAT Stable
Wind direction = 298
s.d. = 14

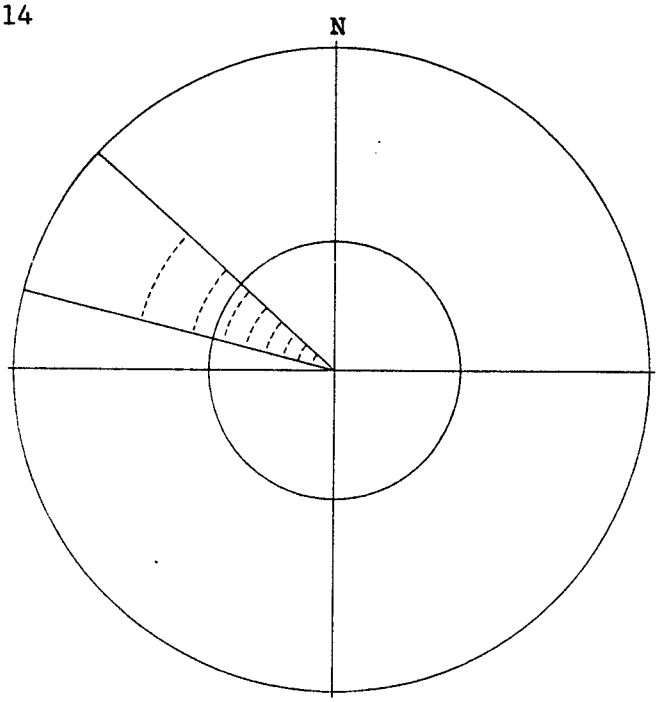

the mean to less than 5000 m. From Pasquill (1972) it seems appropriate to increase them and put all non-unstable hours into one set.

3.3 Surface Database

To calculate the surface parameter values it was necessary to create a computerised database and accessing system which would allow a parameter to be assessed in response to different source area shapes as conditions and scenarios changed.

The requirements of the database were that the individual grid squares of information would allow the influence of small differences in location of the area boundaries to be identified, but not so small that the effort required to gather the necessary information was unrealistic. These requirements were deemed met using 100 m x 100 m squares, and data were collected for a 5 km radius circle centred on the tower (i.e. approximately 8000 squares). The choice of a 5 km circle was based on the areal limits permitted by the Schmid (1988) model. Each square was assigned an X and Y co-ordinate between -50 and +50 (no zero). As an example, Figure 3.8, is a map of the grid squares which contain a major road.

The Greater Vancouver Regional District (GVRD) 1:2500 land use maps, which have the land use for individual properties, for Municipalities of Burnaby (1980) and Richmond (1980) and the City of Vancouver (1983) were used as the initial data source. For each grid square the data listed in Table 3.3 were obtained. Additional information was gathered from Statistics Canada (1987) for the 1986 census, aerial photographs (Vancouver City Planning Dept., 1985, scale 1:2500), and visual inspection. The areal extent of surface types within a property were determined from City of Vancouver By-Laws (1987); facilities within each park from Vancouver Board of Parks and Recreation (1986) and

Figure 3.8 Map of grid squares which contain major roads in the area covered by the database. Each point is a 100 x 100 m square. The grid extends from -50 to -1 and 1 to 50 along the longest axes (N - S and E - W). Inner circle 2 km radius, outer 5 km

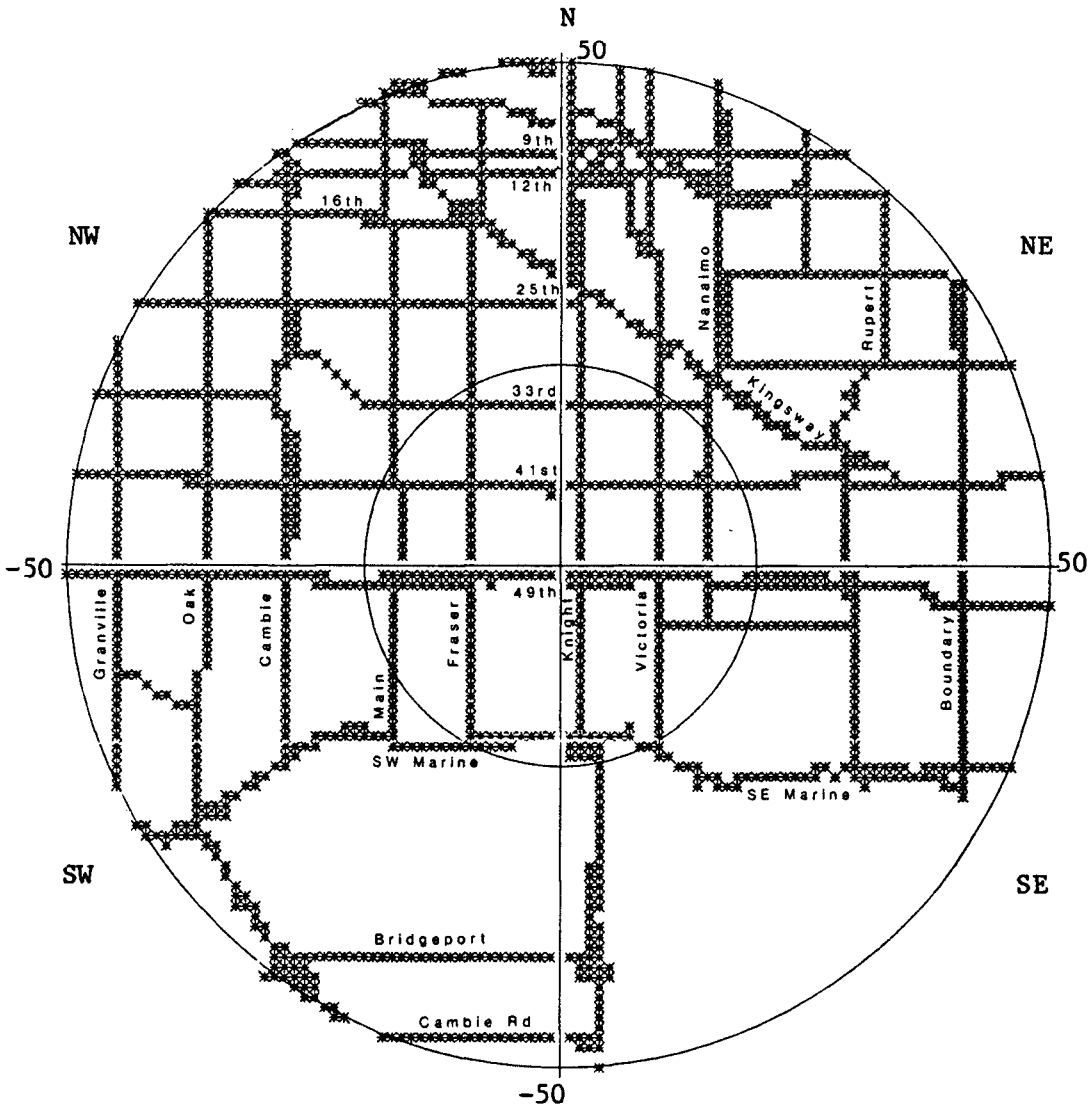

Table 3.3 Information contained within the surface database for each grid square

	Information	Source
1	X co-ordinate	
2	Y co-ordinate	
	Single family dwellings	
3	Number	GVRD landuse maps
4	Area	GVRD landuse maps
	Apartments	
5	Number of lots	GVRD landuse maps
6	Number of units	GVRD landuse maps
7	Area	GVRD landuse maps
	Apartments above commercial	
8	Number of lots	GVRD landuse maps
9	Number of units	GVRD landuse maps
10	Area	GVRD landuse maps
	Commercial	
11	Number	GVRD landuse maps
12	Area	GVRD landuse maps
	Industrial	
13	Number	GVRD landuse maps
14	Area	GVRD landuse maps
	"Institutional"[a]	
15	Number	GVRD landuse maps
16	Area	GVRD landuse maps
17	Code	GVRD landuse maps
	Parks[b]	
18	Area	GVRD landuse maps
19	Code	GVRD landuse maps
	Roads[c]	
20	Back alley length	GVRD landuse maps
21	Minor length	GVRD landuse maps
22	Major length	GVRD landuse maps
	Population	
23	Population/dwelling	Stat Canada 1986 Census by census tract
24	Population	From database

a "Institutional" - for example schools, church, hospital railway yards
- three "blocks" of space were assigned to this
- Code refers to the type of institution

b Parks - Code refers to individual park

c Roads - widths assigned based on GVRD land use maps and visual inspection

Hickok (1977); data for schools from Vancouver School Board (1982); and aerial photographs (Vancouver City Planning Department, 1985). Further information was calculated and added for the modelling of individual fluxes; i.e. sub-databases were generated for the calculation of specific fluxes (see subsequent chapters).

The database was compared with a previous detailed surface description conducted by Grimmond (1983) for the Hudson Catchment; a 21 ha area approximately 4.5 km west of the Sunset Tower. The surface characteristics were found to agree very closely. The population calculated from the database also corresponded very closely to that for individual census tracts.

A second more detailed surface survey was conducted of 10 blocks near the tower. For each 1 m x 1 m square the surface type and height were determined. The information included: vegetation type; vegetation type beneath; shape of vegetation; building type; roof type; and paved surface materials. The information was gathered from visual surveys and aerial photographs (Vancouver City Planning Dept., 1985, scale 1:2500).

To conduct the comparison between different boundary location scenarios different geometric shapes (circles, quadrants, ellipses and sectors) had to be accessed from the database. Appendix V outlines the procedures used to determine which co-ordinates should be accessed for the different geometries. Once the grid co-ordinates are identified the required information from the database can be accessed and the value of the surface parameter calculated.

With the use of the database it is possible to produce maps of surface types contained within each grid square. Figure 3.9a-h shows the plan area of particular surface types in 1000 m^2 classes within each grid square (a square contains 10000 m^2). If a particular surface type does not occur in a square then it will appear blank (e.g. much of Fig. 3.9d). In order to illustrate the

Figure 3.9 Maps of surface type:

° < 1000 m2
· < 2000
– < 3000
Y < 4000
+ < 5000
× < 6000
⋈ < 7000
△ < 8000
≡ < 9000
□ < 10000
✱ 10000

(a) Buildings

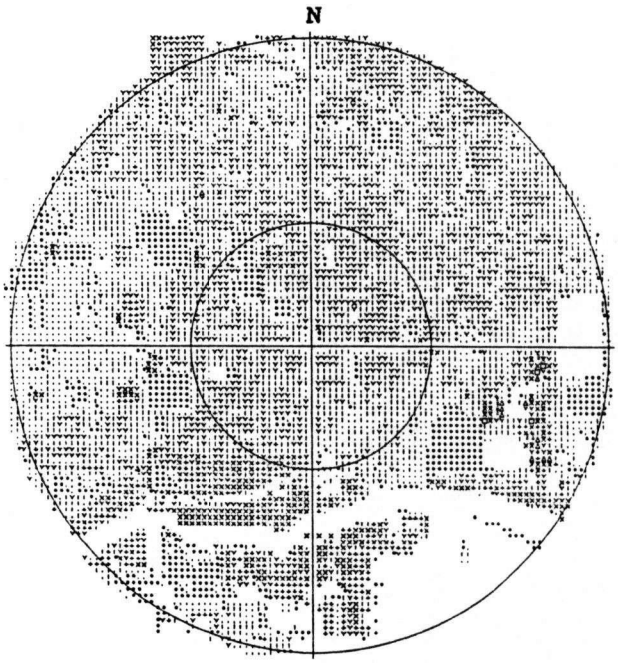

(b) Pavement

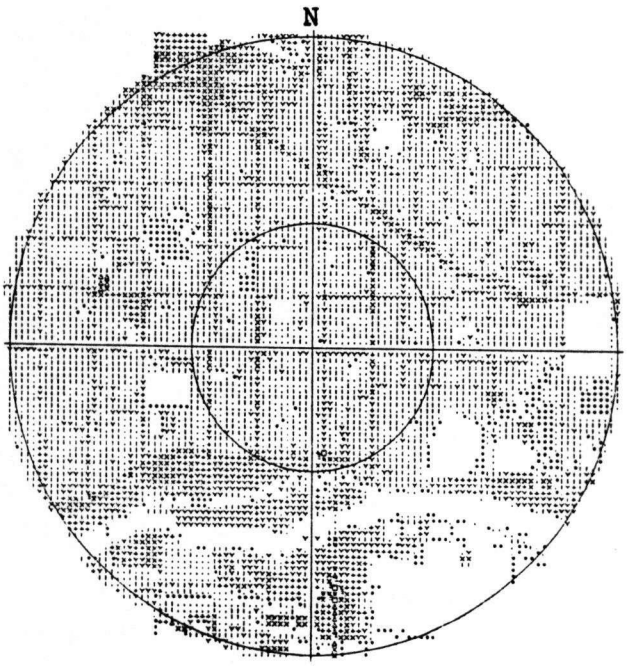

(c) Gravel

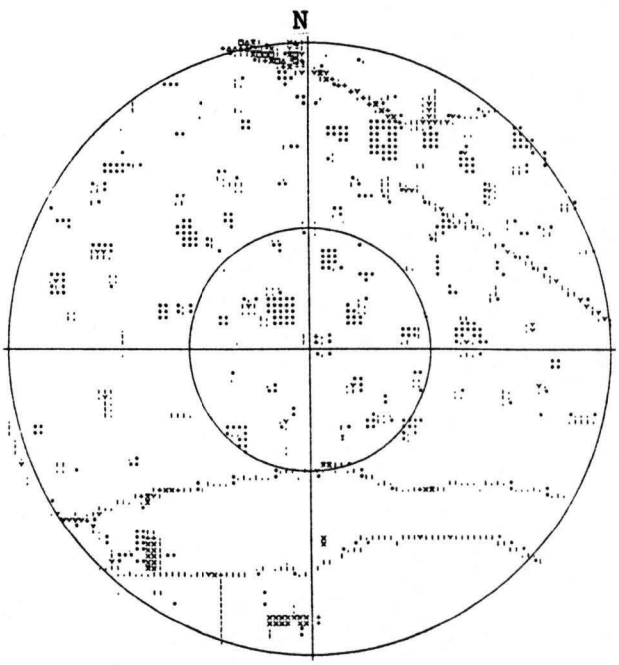

(d) Water

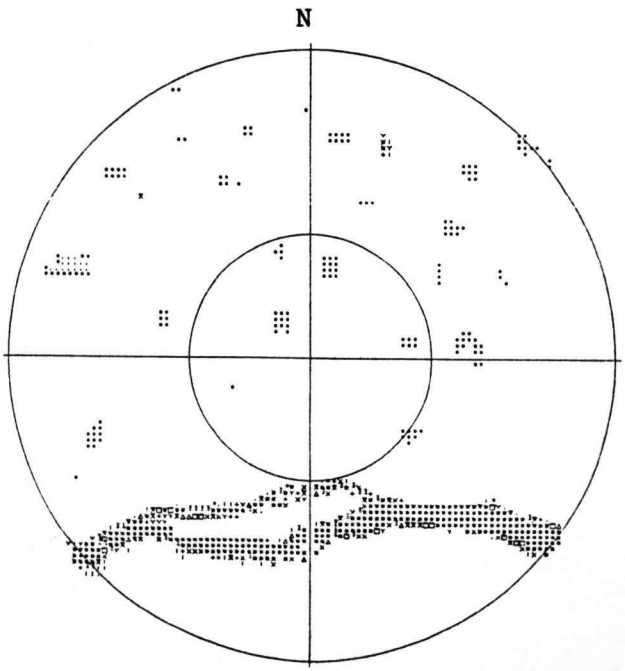

Figure 3.9 Maps of surface types (cont.):

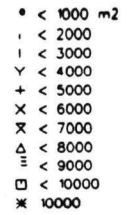

(e) Grass

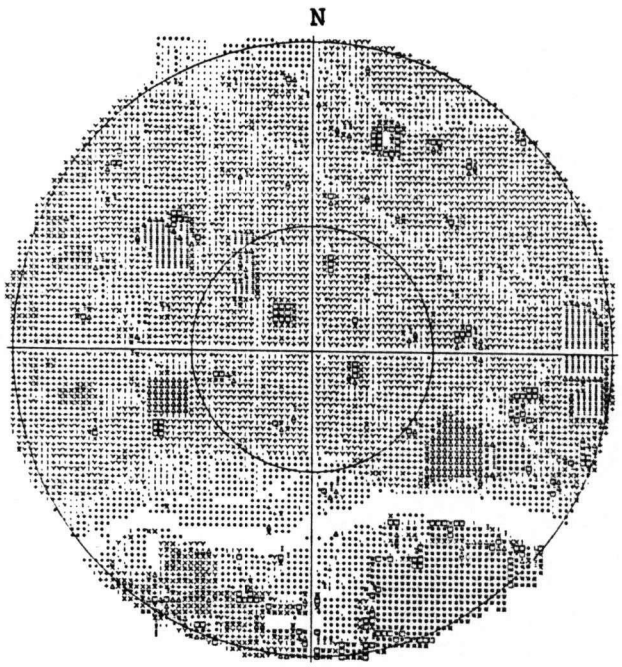

(f) Coniferous trees

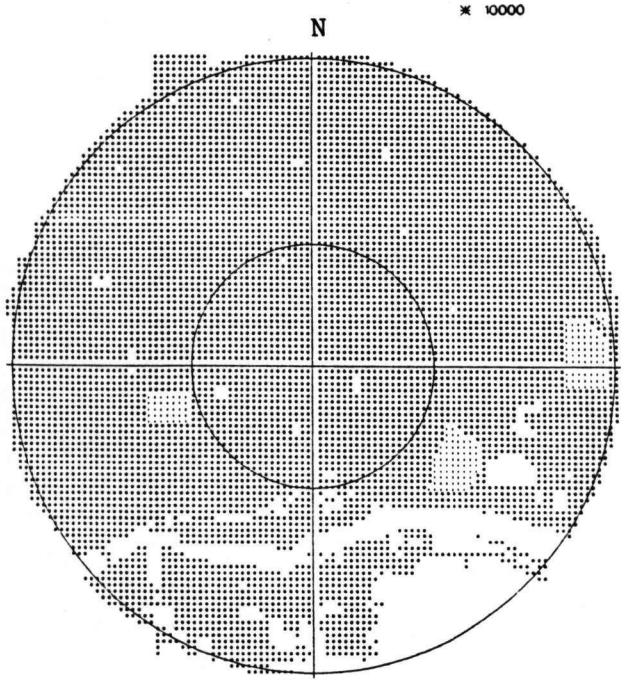

(g) Deciduous trees

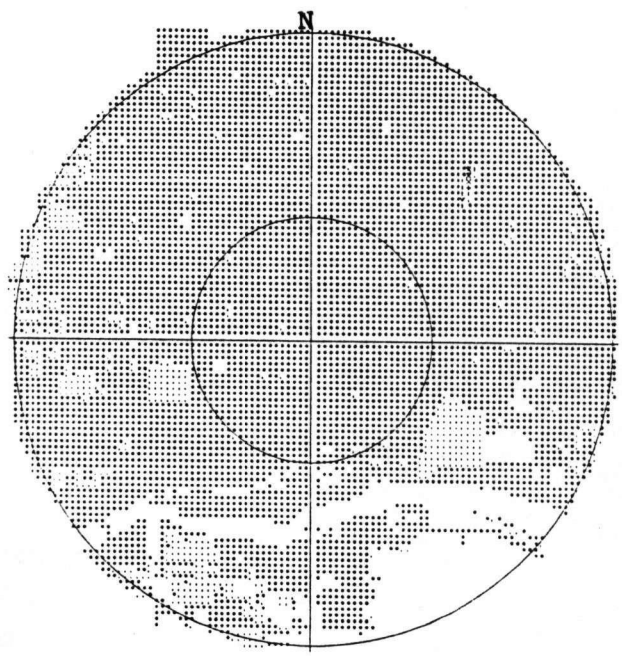

(h) Total vegetation

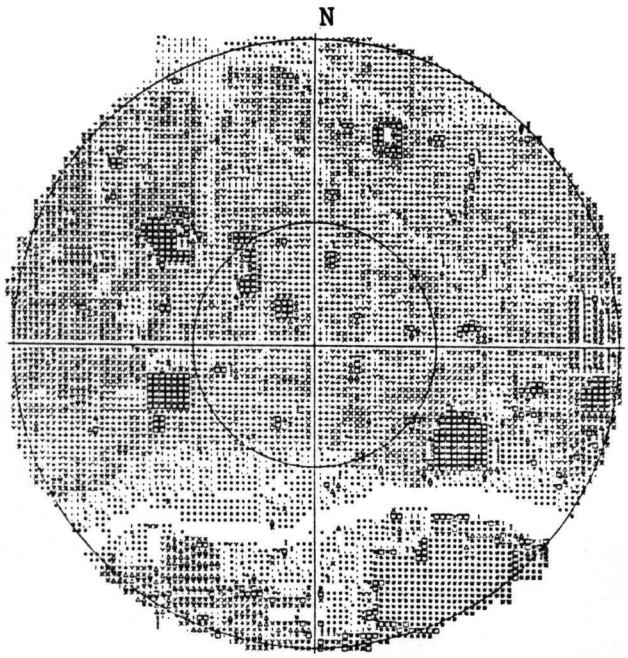

temporal variability introduced by this dynamic modelling approach Figure 3.10a,b,c shows the variation in proportion of three of the more important surface types through time, for those hours of the study period when the source area could be calculated using plumes. The significance of these changes are discussed in subsequent chapters.

3.4 Summary

In this chapter an objective means of locating the boundaries to assign values to surface parameters has been proposed, termed 'plumes'. This takes into account the area actually contributing to a turbulent flux measurement at a point and how this changes with meteorological conditions. It is assumed that fluxes modelled using plumes for the assignment of boundaries and derivation of surface parameters are closest to the 'true' values. In subsequent chapters fluxes modelled using the plume method are compared with the other methods outlined in this chapter. This is achieved with the aid of the 100 m x 100 m grid squares database described here.

Figure 3.10 Influence of the changing source areas on percentage of land use characteristics influencing measurements. Source areas are plumes. Note vertical scales are different.

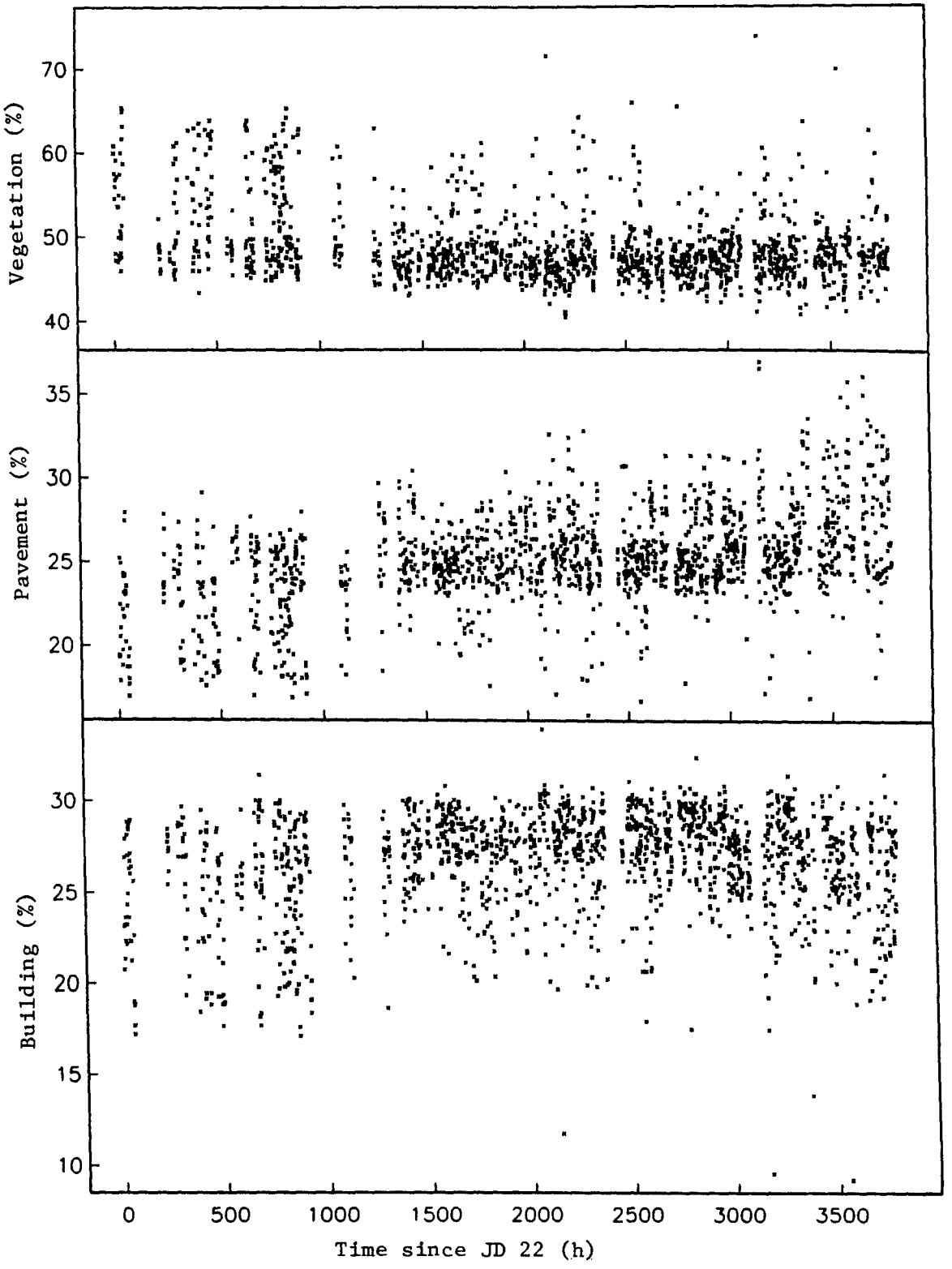

CHAPTER 4 ANTHROPOGENIC HEAT FLUX

4.1 Introduction

Anthropogenic heat flux (Q_F), the energy released due to human activities, is often regarded as negligible or is ignored in urban energy balance studies. This is due to two factors, both of which are related to the fact that most of these studies have been conducted under summer conditions. Firstly, in many urban areas the absolute size of Q_F is smaller in summer than in winter. Secondly, even if this was not the case in the summertime the magnitude of the other fluxes are larger and therefore the relative importance of Q_F is smaller. Its magnitude may only be of the order of the error of measurement. Thus not only its proportional significance, but also its absolute magnitude is larger under non-summer time conditions in a temperate city such as Vancouver. Therefore Q_F must be considered in seasonal energy budgets.

Q_F can be subdivided into three components:

$$Q_F = Q_{FV} + Q_{FH} + Q_{FM} \qquad (4.1)$$

where Q_{FV} - heat produced by combustion of vehicle fuels (W m^{-2});
Q_{FH} - from "stationary sources" (primarily within buildings)(W m^{-2}); and
Q_{FM} - heat released by metabolism (W m^{-2}), generally this is negligible compared to the other two components but for completeness was incorporated in this study.

Q_F can not be measured directly. This chapter outlines the methods used to determine Q_F on an hourly basis; and considers the influence of surface description on its estimation.

4.2 Methods of calculation

4.2.1 Anthropogenic heat produced by combustion of vehicle fuels

Q_{FV} is defined as the energy produced by the combustion of vehicle fuels within the source area. This is a function of the amount of gasoline used and its energy content, which can be related to the number of vehicles travelling

within the source area, the distance they travel, the type of gasoline used, and their fuel efficiency (distance travelled per unit of gasoline).

Q_{FV} was calculated for each hour (t) using the source area (A) surface description:

$$Q_{FV} = [(n_{Vi}(t)\ D_{Vi})\ EV]/[A\ 3600] \quad (4.2)$$

where n_{Vi} - number of vehicles by road type (major or minor) in the source area;
D_{Vi} - distance of road within the contributing area by road type (m);
EV - energy used by a vehicle (J m^{-1}):

$$EV = (NHC_i\ \rho_i\ WFS_i)/FE \quad (4.3)$$

where NHC_i - net heat combustion by fuel type (J kg^{-1});
ρ_i - density of fuel by fuel type (kg l^{-1});
WFS_i - weighting of fuel sales by fuel type; and
FE - average fuel economy (m l^{-1}).

In British Columbia three types of fuel are commonly used. Table 4.1 lists the values used for NHC and ρ_i for these fuel types. The fuel sales, WFS, were used to weight the relative proportions of these fuel types for the Q_{FV} calculations. An average value of 11.2531 x 10^3 m l^{-1} was used for the fuel economy (Whitford, 1984). This represents an average for all vehicle types driving in a city, to account for the variety which travel within the study area. Figure 4.1 illustrates the n_V profiles for the study area for the major and minor roads. The data were obtained from traffic counts conducted by Vancouver City Traffic Department. D_V was determined based on the area of roads within the source area each hour from the surface database (see Chapter 3).

4.2.2 Anthropogenic heat flux produced by combustion from stationary sources

In the study area, the two fuels which contribute to Q_{FH} are electricity and gas; other fuels were regarded as being negligible and were ignored. Two scales of data were available to enable the calculation of Q_{FH}. Firstly, data

Table 4.1 Fuel consumption, density and net heat combustion (sources: Oilweek, Sept 21, 1987; Shell Canada Ltd. personal communication, 1988)

Fuel Type	Consumption in BC Jan-June, 1987 (Ml)	Consumption (%)	Density Range[a] (kg m^{-3})	Net Heat Combustion (J kg^{-1})
Premium unleaded	185.8	11.03	740-770 (755)	44,332,985
Regular unleaded	621.1	36.86	720-740 (730)	44,862,959
Regular leaded	878.1	52.11	710-730 (720)	45,072,159

a Gasoline density varies with fuel mix and season - the midpoint value (in brackets) was used

Figure 4.1 Mean profiles of traffic counts for major and minor roads in the study area

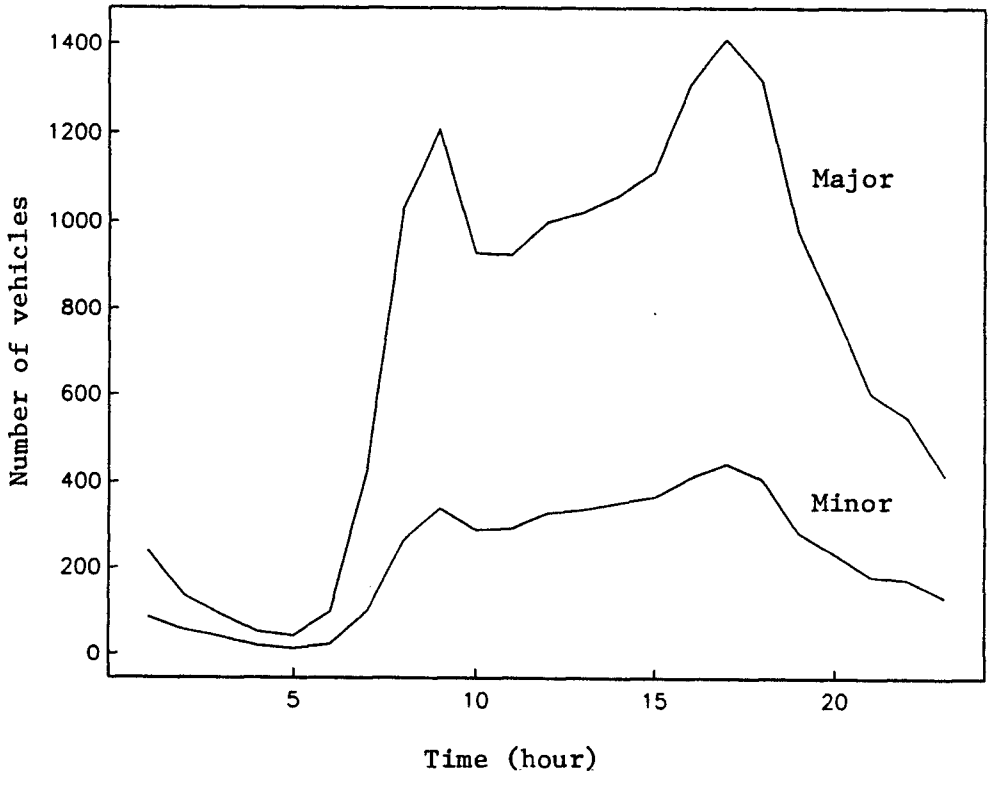

at the individual property (consumer) scale were available for 600 consumers within close proximity of the measurement tower. The data were stratified by premise class: single family dwelling, apartments, institutional (further subdivided into schools, churches, hospitals etc), industrial etc. These data were available in variable two monthly billing period intervals with no indication of hourly variability of use. Secondly, the only available information showing hourly differences in consumption, was at the scale of the "Integrated System for BC" for electricity, and the "Lower Mainland" for gas. The approach taken was to apportion the local scale premise class data using the grid fluctuations.

For each hour Q_{FH} was calculated using :

$$Q_{FH} = [(GR_E(t)\ \Sigma(n_{Ei}\ C_{Ei})) + ((GR_G(t)\ \Sigma(n_{Gi}\ C_{Gi})\ GEF)/3600)]/A \quad (4.4)$$

where GR(t) - hour (t) grid consumption (gr(t)) as a proportion of the total grid consumption for the study time period (Σgr(t)):

$$GR(t) = gr(t)/\Sigma gr(t) \quad (4.5)$$

subscript E and G - electricity and gas respectively;
n - number of consumers by premise class (i);
C - total mean consumption for an individual consumer by premise class (Watts electricity, Joules gas);
GEF - gas efficiency (0.675); note electricity = 1.00; and
A - source area (m^2).

BC Hydro provided the gas and electricity data at the two scales (grid and consumer). The number of consumers for each hour for each premise class was determined from the surface database (see Chapter 3).

4.2.3 Anthropogenic heat produced by metabolism

Q_{FM} is calculated using:

$$Q_{FM}\ (t) = [(n_P\ M_P\ (t)) + (n_A\ M_A\ (t))]/A \quad (4.6)$$

where n - number of people (subscript P) or animals (subscript A);
M(t) - metabolic rate (W) at time t; and
A - contributing area (m^2).

The day was subdivided into two time periods: "active" (0700 - 2300 hours) and

"sleep" (2300 - 0700 hours). Metabolic rates from Oke (1978) were used for the people, and the number of people contributing for each hour estimated using the database. Following Bach (1970) M_A was set to approximately 25% of Mp. The number of animals was assumed to be 10% of the people.

4.3 Modelled values of anthropogenic heat flux

Figure 4.2 shows the temporal trend of the three Q_F components and their combined total for JD 22, 1987, using the 2 km radius circle to determine the required mean surface parameters. The influence of the morning and afternoon rush hours are apparent in the Q_{FV} and Q_F profiles, and the slightly out of phase peaks in Q_{FH}. Q_{FM} is relatively small and shows a step transition between the 'sleep' and 'active' periods of the day. In the summer time Q_{FH} is reduced but Q_{FV} remains approximately the same.

Using the database it is possible to calculate the size of the anthropogenic heat flux density for each grid square for any hour. Fig. 4.3 is a map of Q_F for the hour 900 LAT, JD 22, 1987. Q_F ranged from 0 W m^{-2}, for the Fraser river and some farm land in Richmond (see Fig. 2.1), to approximately 80 W m^{-2}, where two major roads and high density housing occur in one square. Comparison of this map with that of major roads (Fig. 3.8) reveals the importance of Q_{FV} because the general grid nature of the streets is evident in the Q_F map.

The effect of changing the area used to determine the surface parameters can be seen from Figure 4.4. In this example the influence of changing the radius of a circle or a quadrant is considered. In Figure 4.4 the radius was increased from 100 m to 4.9 km in 100 m increments. Surface parameters are determined for the area of the quadrant or circle from the tower out to that radius. If increasing the radius had no effect one would see the same temporal

Figure 4.2 Anthropogenic heat flux for JD 22, 1987. Plots shows the three components of the flux and the total hourly flux.

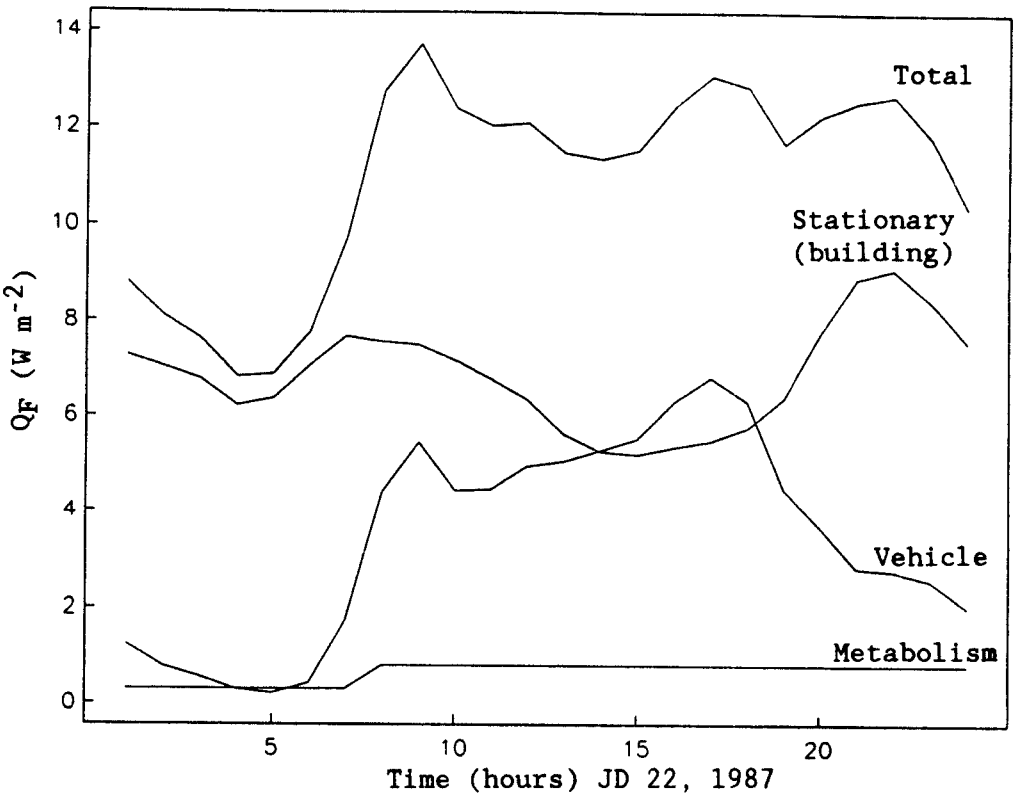

Figure 4.3 Map of anthropogenic heat flux for 900 LAT, JD 22, 1987 centred on the Sunset site. Inner circle has a radius of 2 km.

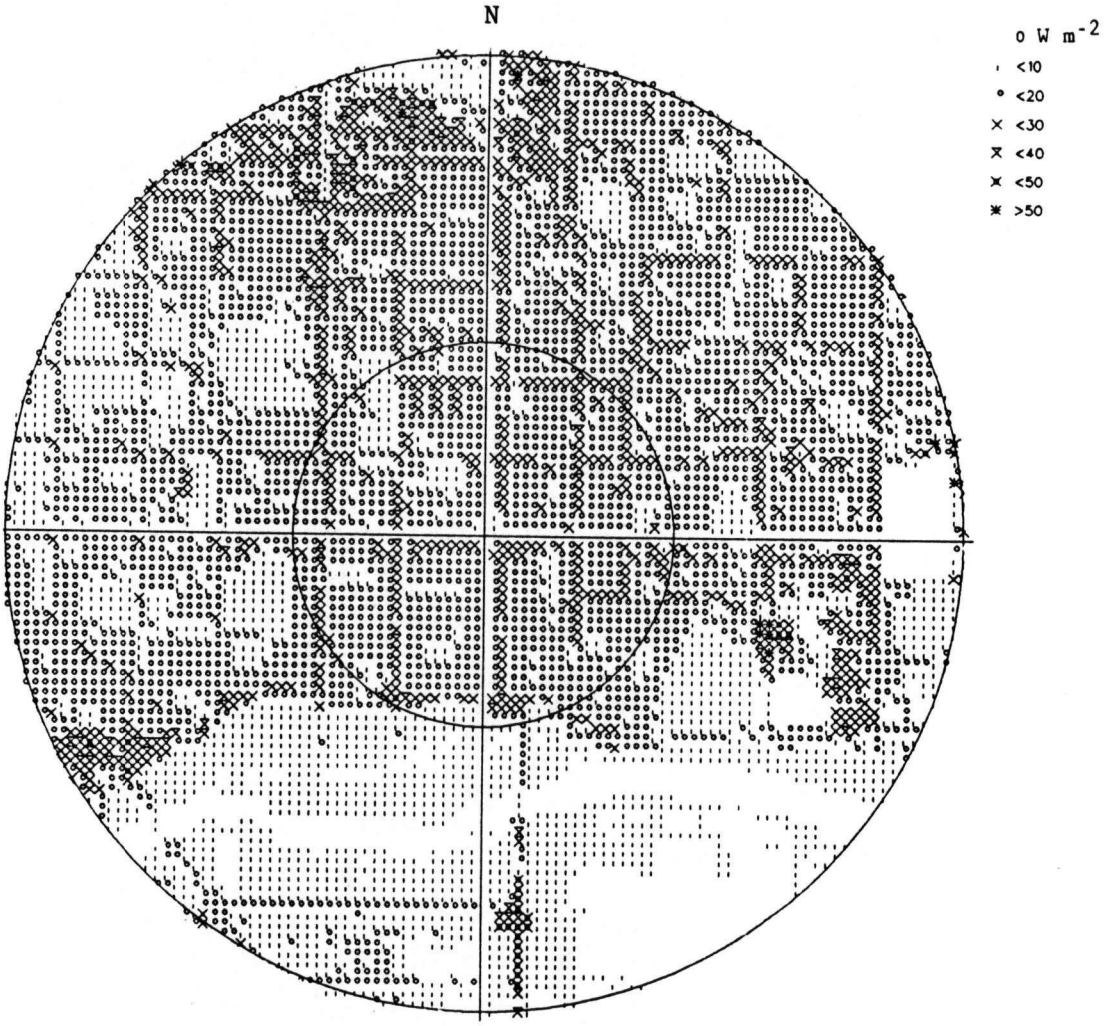

Figure 4.4 Anthropogenic heat flux (W m^{-2}) with increasing radius from the tower for JD 22, 1987:
(a) circle
(b) NW quadrant
(c) NE quadrant
(d) SW quadrant
(e) SE quadrant.

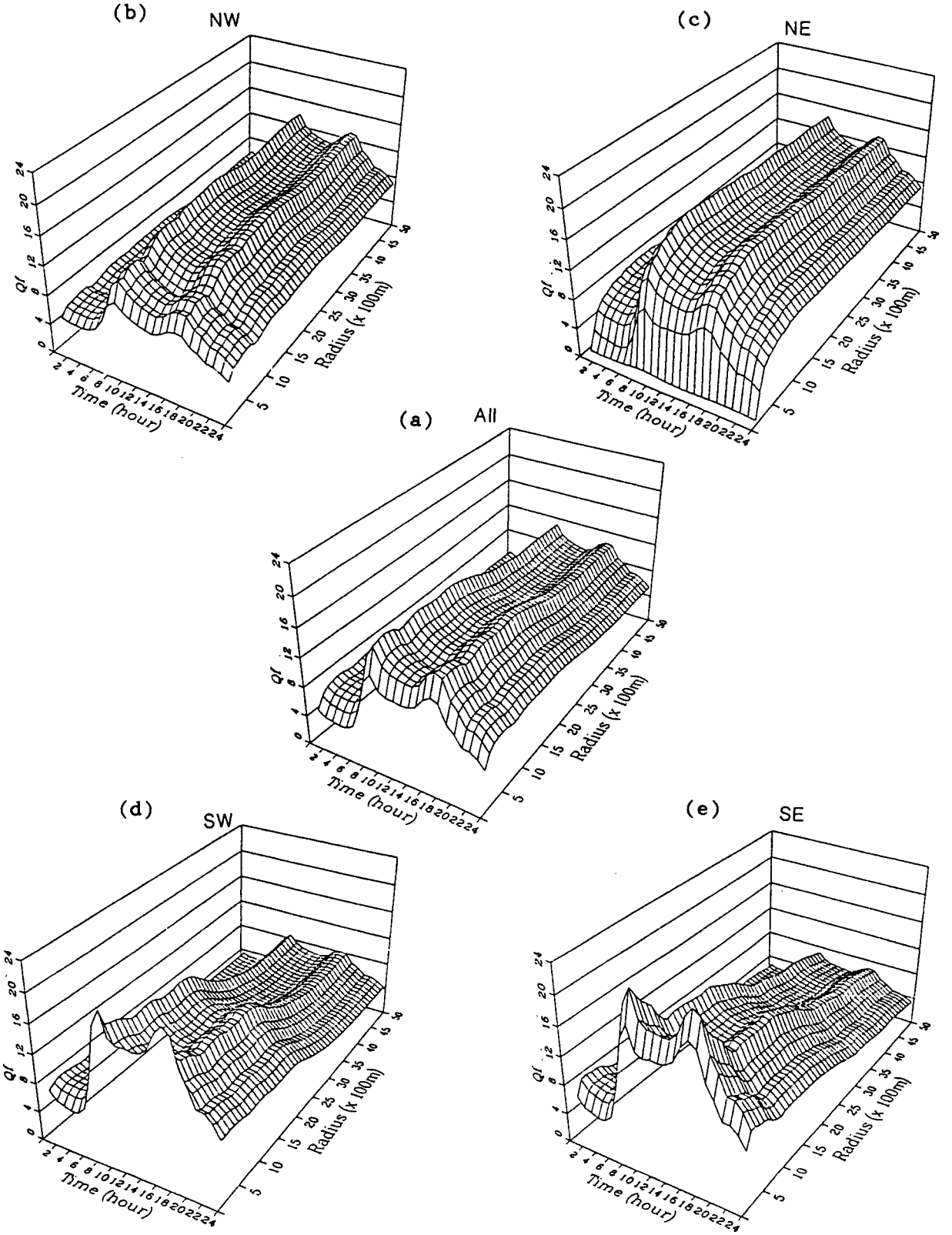

trend through the day extending along the radius axis (y-axis). As can be seen there is considerable variability. The greatest variability occurs close to the tower. This is in part a consequence of the fact that as the radius is extended the surface characteristics are averaged over a larger area and therefore any small change is less significant.

Further, if the area used to assign values to surface parameters exerts no influence it would be expected that hourly Q_F fluxes, calculated using different source areas schemes, would plot on a one-to-one line. Figure 4.5 is a plot of Q_F modelled for 1708 hours using two different schemes: (i) plumes as calculated from the Schmid (1988) model (here assumed to be the best method to describe the source area for a turbulent flux, see section 3.2); and (ii) 2 km radius circle. The surface parameterisation is static with the circle, but with the plumes it changes with the changing meteorological conditions. It can be seen that the two Q_F values do not plot along a one-to-one line. The mean for the plume values was 9.51 W m^{-2} (s.d.=3.08 W m^{-2}), and that for the 2 km circle was 8.63 W m^{-2} (s.d.=2.34 W m^{-2}). The RMSE for the relation was 2.35 W m^{-2}. This can be explained by the location of the source areas. Figure 4.6 shows the wind direction frequencies for the 1708 hours that have been compared. Figure 4.6a shows the wind direction for all 1708 hours; Figure 4.6b shows the wind direction for those hours when the plumes were greater than the 2 km radius circle; and, Figure 4.6c when the circle Q_F were greater. The plumes are generally greater when the wind direction is from the two southerly quadrants and generally less when from the two northerly quadrants. This can be explained by the surface types and therefore anthropogenic energy sources found within the area (see Fig. 3.9).

As stated in Chapter 3 since the plumes require Q_H data, which is not always available the simpler 'sectors' which incorporate some of the dynamic

Figure 4.5 Hourly anthropogenic heat flux modelled using plumes and 2 km radius circle as the basis for assigning values to surface parameters.

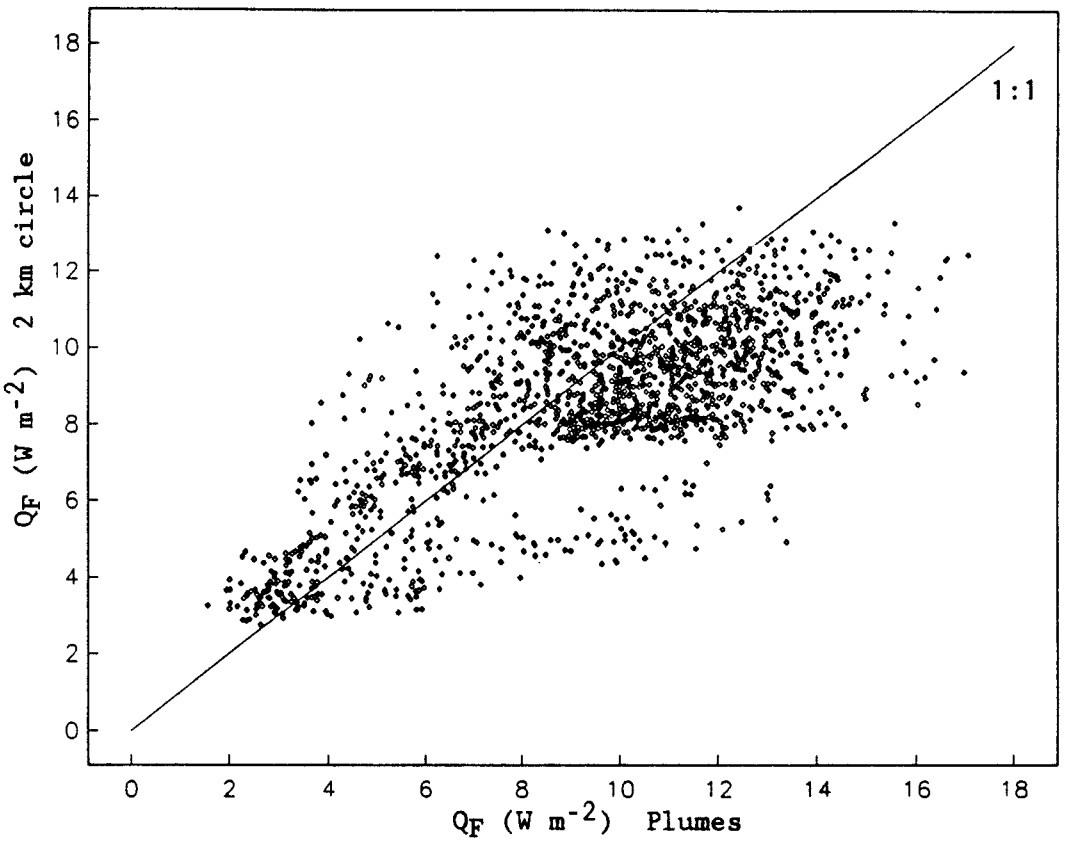

Figure 4.6 Wind direction frequency plot for:
(a) all hours
(b) hours when Q_F plumes greater then 2 km radius circle
(c) hours when Q_F plumes less than 2 km radius circle.

(a)

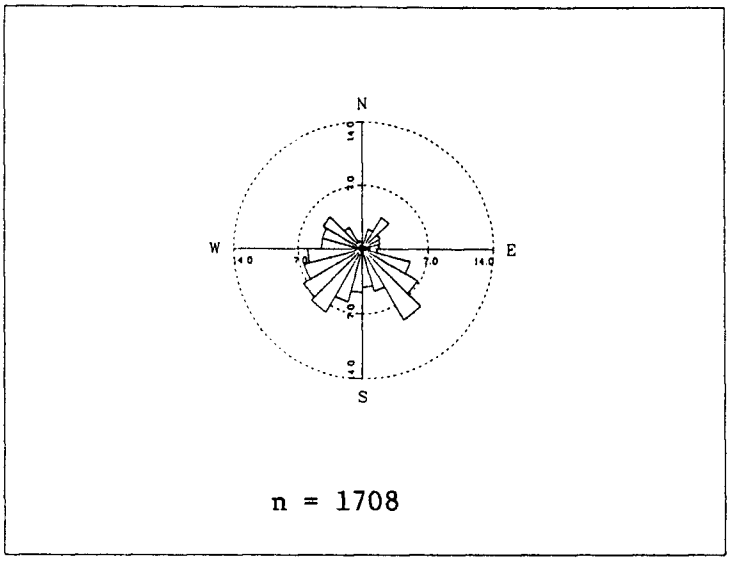

(b)

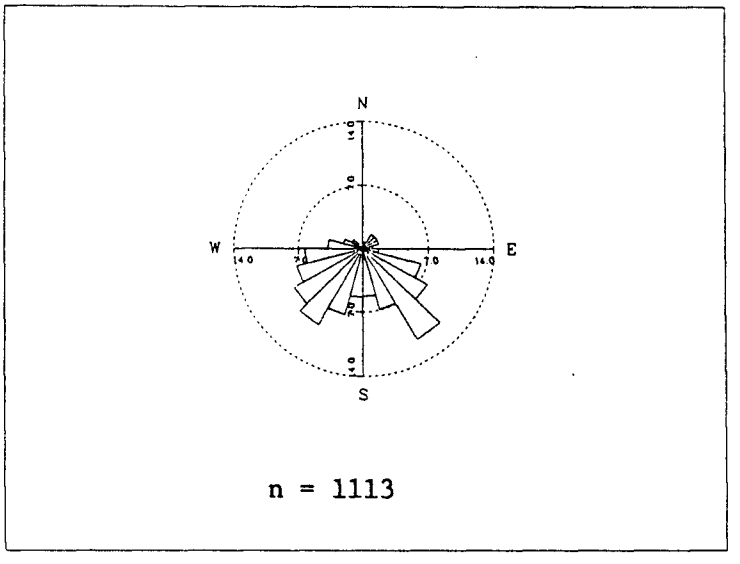

(c)

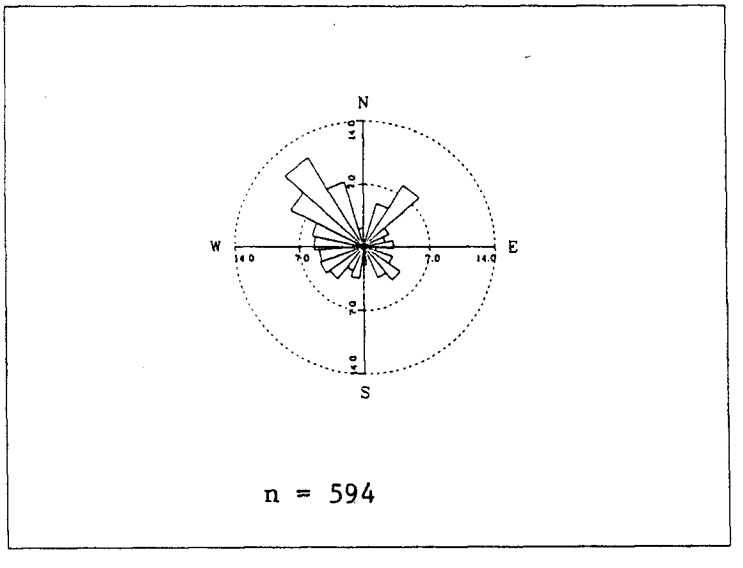

nature of source areas are proposed (section 3.2.2). Figure 4.7 is a plot of 1708 hourly Q_F values modelled using plumes and sectors as the basis for assigning values to surface parameters. The mean for the sectors is 9.08 W m^{-2} (s.d.=3.17 W m^{-2})(see above for plumes), and the RMSE is 1.18 W m^{-2}. The sectors simulate the source area of the plumes reasonably well. Therefore it is proposed that in the absence of Q_H, sectors be used for assigning surface parameter values. This allows for continuous calculation of Q_F.

4.4 Incorporation of anthropogenic heat flux into the energy balance

Consideration needs to be given to the inclusion of the Q_F term in the energy balance. It is dependent upon how the other terms of the energy balance have been assessed. In this study some portion of Q_F is already incorporated in measurements of the output fluxes: Q_H (using the SAT) and RTDMS temperatures. Measurements of Q*, also, partially include Q_F because it affects the long-wave exchange portion of Q* via the surface temperature (T_S):

$$L\uparrow = \epsilon\sigma T_S^4 \qquad (4.7)$$

$$Q^* = K^* + (L\downarrow - L\uparrow) \qquad (4.8)$$

where $L\uparrow$ - long-wave radiation emitted from the surface (W m^{-2});
ϵ - emissivity of the surface materials; and
σ - Stefan-Boltzmann constant (W m^{-2} K^{-4});
K* - net shortwave radiation (W m^{-2}); and
$L\downarrow$ - long-wave radiation received at the surface (W m^{-2}).

Q_F causes an increase in T_S which leads to an increase in $L\uparrow$. Within a 0 - 40°C range a one degree rise in T_S results in a 5 to 6 W m^{-2} increase in $L\uparrow$. Therefore the measured Q* flux includes a reduction due to the Q_F flux.

The increase in T_S, and therefore the effect on Q*, is a function of the heat capacity of the building fabric, the 3-D surface area of the building and the amount of energy released within the building. The effect on the temperature can be calculated approximately through the following steps:

Figure 4.7 Plot of hourly Q_F calculated using plumes and sectors for assigning values for surface parameters.

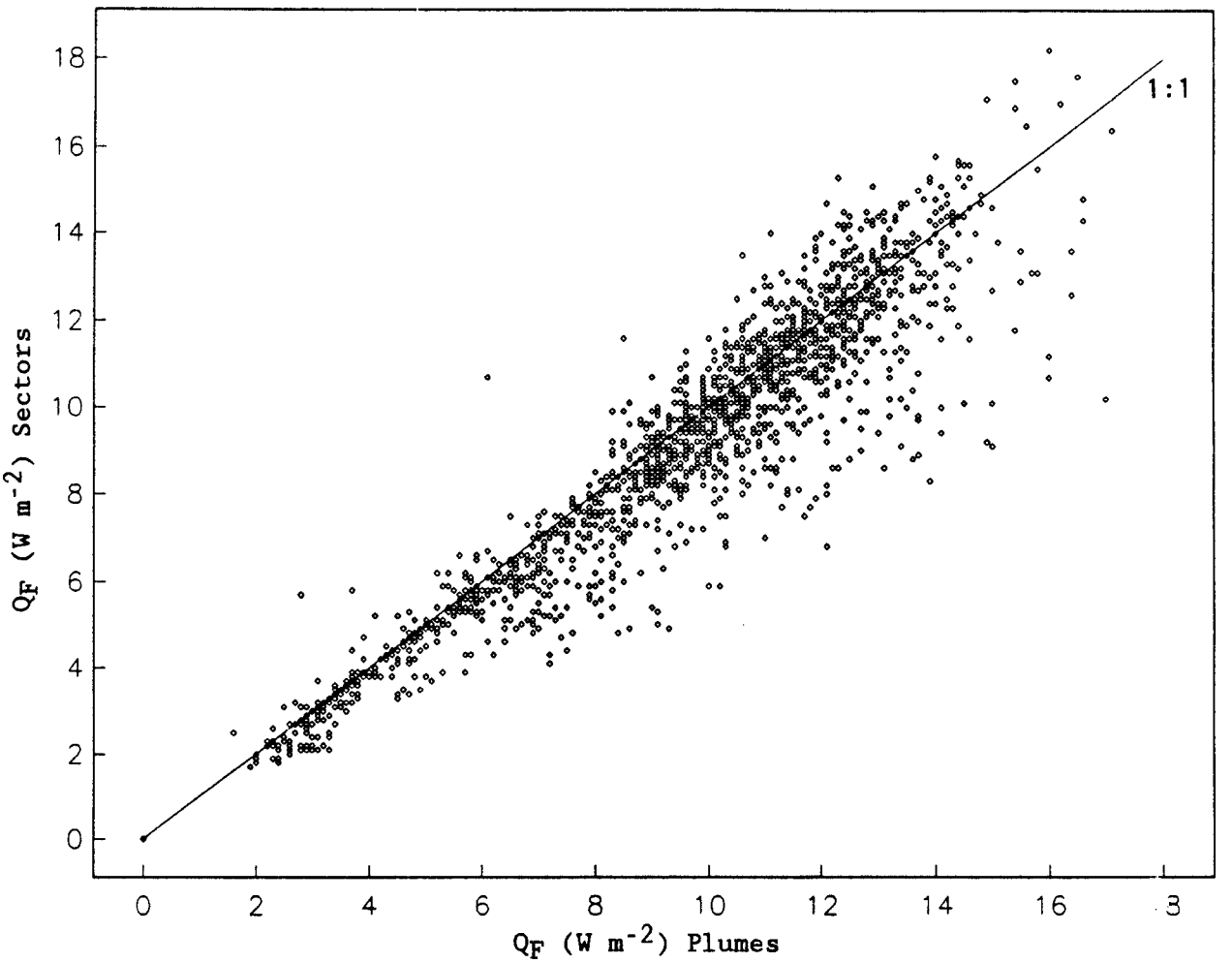

1) The average maximum hourly Q_{FM} and Q_{FH} are calculated for a time period (units of Joules) for an individual 'average' premise.

2) The summed Q_{FM} and Q_{FH} are reduced by 30% because of air leakage heat losses from buildings (Canadian General Standards Board, 1980).

3) The surface area of the buildings is calculated and used to determine a mean flux density (W m^{-2}) loss from within the buildings.

4) Using values assigned for the heat capacity of the building fabrics and building thicknesses the change in external surface temperature can be calculated.

5) The effect on $L\uparrow$ is calculated and the net effect on Q* determined. Such calculations indicate that the increase in T_S will be less than one Celsius degree. The effect on Q* is very small under most conditions. Therefore in this study Q_F was directly added to the energy balance.

The significance of Q_F in the seasonal energy balance is discussed in Chapter 6.

CHAPTER 5: STORAGE HEAT FLUX

5.1 Introduction

In urban areas, the sub-surface or storage heat flux (ΔQ_S) is the net uptake or release of energy from the urban system. It includes latent and sensible heat changes in the air, buildings, vegetation, and ground extending from above roof-level to a depth in the ground where net heat exchange over the period of study is negligible (Oke & Cleugh, 1987). One reason to determine the size of this flux is to ascertain the amount of available energy ($Q^*+Q_F-\Delta Q_S$) for the turbulent sensible (Q_H) and latent (Q_E) heat fluxes. It is not possible to directly measure the integrated heat storage of the urban system. There are two indirect methods to obtain 'measured' values of ΔQ_S. Firstly, one could measure ΔQ_S for all the component surfaces within the study area and combine them with an appropriate weighting scheme. In an urban area this requires a large sampling effort because of the multi-facetted surface with its wide range of surface materials. There have been studies for individual surface types, for example concrete by Doll et al. (1985); and roofs by Yap (1972) and Taesler (1978).

Secondly, if all other terms of the energy balance are measured ΔQ_S can be determined as the residual:

$$\Delta Q_S = Q^* + Q_F - Q_H - Q_E \qquad (5.1)$$

This method has the disadvantages that: (1) all the other fluxes have to be measured and by methods not requiring the storage heat flux to be determined; and (2) because ΔQ_S is a residual the calculated flux contains the net cumulative errors of the other measurements.

In this study ΔQ_S is needed, not only to model Q_E, but also to determine the 'measured' Q_E for the evaluation of model performance. This chapter outlines the methods used to determine ΔQ_S on an hourly basis and compares the

values obtained with those 'measured' by the residual method.

5.2 Methods of Calculation

There are currently two types of models to calculate urban ΔQ_S. Firstly, there are those that use heat conduction equations incorporated in surface energy balance models. Most boundary layer models use values of thermal properties for building materials and a one-dimensional heat conduction equation based at some assumed urban 'surface' plane (Oke and Cleugh, 1987). Some come close to portraying 3-dimensional urban surface geometry (e.g. Terjung and O'Rourke, 1980; Sievers and Zdunkowski, 1986). Unfortunately none have been verified using measured heat flux densities (Oke and Cleugh, 1987). Peikorz (1987) attempted to measure and model this flux for individual surfaces and to combine them into an urban model. Unfortunately he did not have ΔQ_S residuals against which to compare the fluxes. He was forced to rely on measurements in a concrete path and a lawn. Full determination requires an extensive array of temperature measurements which sample all facets and surface types.

Secondly, there are models which estimate storage as a function of Q* and the surface cover types present in the study area. This is the type of model used here. This kind of model has the advantage of not requiring extensive temperature measurements and requires relatively little computational resources. Three such models are outlined below and their performance assessed.

5.2.1 Objective linear regression model (Oke, Kalanda and Steyn, 1981)

The model proposed by Oke et al. (1981), to estimate spatially averaged urban heat storage, combines empirical linear regression equations between net

radiation (Q*) and ΔQ_S, for a number of urban surfaces and weights their role in proportion to the plan area of greenspace and built surface present in the study area:

$$\Delta Q_S = \sum_{i=1}^{n} \alpha_i (a_i Q^* + b_i) \qquad (5.2)$$

where α_i - the fraction of the area covered by the ith surface type; and
a_i, b_i - coefficients in the parameterization for the ith surface type.

Oke et al. (1981) present equations determined from measured data for a roof, an urban canyon, and pavement. These are combined to assign the coefficients for the daytime (Q*>0) built surface type. The daytime and nocturnal (Q*<0) greenspace coefficients are based on data collected from sites with short grass. At night the built coefficients are based on data for an urban canyon. Oke et al. (1981) present the following equations for Sunset:

$$\Delta Q_S = (Q^*-27) \times 0.25 \qquad Q^*>0 \qquad (5.3)$$

$$\Delta Q_S = Q^* \times 0.67 \qquad Q^*<0 \qquad (5.4)$$

The fractions of greenspace and built covers were based on a 2 km radius circle.

5.2.2 Hysteresis model (Camuffo and Bernardi, 1982; Oke and Cleugh, 1987)

Observations in bare soil have shown that there is a different relationship between the rising and falling limb of the daily cycle between Q* and ΔQ_S, and that ΔQ_S peaks one to two hours before Q*. Camuffo and Bernardi (1982) suggested a relationship between ΔQ_S and Q* which takes into account this hysteresis pattern. The general form of the equation has three terms:

$$Q_S = a_1 Q^* + a_2 \frac{dQ^*}{dt} + a_3 \qquad (5.5)$$

where a_1, a_2, a_3 - empirical coefficients; and

$$\frac{dQ^*}{dt} = Q^*(t) - [Q^*(t+1) + Q^*(t-1)]/2 \qquad (5.6)$$

The second term gives the hysteresis loop departures from the linear relationship .

Oke and Cleugh (1987) observed this hysteresis pattern in measurements of Q* and ΔQ_S (determined by residual) conducted in July/August 1978 at Sunset, Vancouver. They used the hourly ensemble averages to determine the following coefficients for all hours: a_1=0.35, a_2=0.28 and a_3=-40; and, when Q* is positive: a_1=0.30, a_2=0.25 and a_3=-22. The hysteresis form seems capable of representing most features of the storage regime: the magnitude by day and by night, the daytime phase shift relative to the net radiation, and the times of transition between heat release and uptake (Oke and Cleugh, 1987).

5.2.3 Objective hysteresis model (Cleugh, 1988)

The disadvantage of the Oke and Cleugh (1987) models are, as they note, that the coefficients only relate to the specific site and weather conditions of the 1978 study. Further developing the hysteresis idea for urban areas Cleugh (1988) combines Camuffo and Bernardi (1982) type hysteresis equations derived from data for individual surface types with an Oke et al. (1981) type of areal weighting scheme to create an objective method applicable to any urban site.

The surface description required involves determination of the plan area of greenspace, the 3-dimensional area of roofs, the plan area of paved surfaces, and the 3-dimensional area of walls (Table 5.1). The four areas are determined as a percentage of the plan area plus the area of walls and roof (i.e. the total is greater than the plan area). These percentage values are used with coefficients for each of the surface types (see Table 5.2).

Table 5.1 Percentage of surface type in the Sunset study area for use with the objective hysteresis model for storage heat flux density. Total area = 2D greenspace + 3D roof + 2D impervious + 3D walls

	Surface Type (%)			
	Greenspace	Roof	Impervious	Walls
2 km radius				
Circle	31	23	20	26
Quadrant NE	28	24	20	28
SE	27	25	21	27
SW	32	21	23	24
NW	36	21	18	25
Cleugh (1988)[a]: circle	43	13	11	33
Plumes				
Mean (n=1715)	30	23	20	27
sd	5	2	2	2
max	66	27	34	30
min	23	9	14	10
Error in ß ≤20%				
All hours: mean	31	23	20	27
Q^*+Q_F positive: mean	31	23	20	28
Sectors				
Mean (n=3779)	32	22	20	26
sd	6	2	2	3
max	52	26	25	30
min	24	16	14	19
Error in ß ≤20%				
All hours: mean	32	22	20	25
Q^*+Q_F positive: mean	29	23	20	28
Mean when model applied to all hours in study period when Q^*+Q_F positive				
Plumes & Sectors	30	23	20	27

a Cleugh (1988) calculated the proportion of each surface type using a different method to that used in this study. She used the data for a 2 km radius circle presented by Kalanda (1979) and Steyn (1980) which was based on samples from aerial photographs. She used the two-dimensional percent landuse, the number of buildings and their mean dimensions to calculate the proportions. She assumed that the roofs were flat, which is probably reasonable in this case as the average 3D area is not much greater than the 2D area. The major difference between the two studies is in the vegetation percentages.

Table 5.2 Individual surface coefficients for the objective hysteresis storage heat flux model and the mean coefficients arising from its application to Sunset, Vancouver.

	a_1	a_2	a_3	
(a) **Surface Type** (Cleugh, 1988)				**Surfaces, No. of data sets**
Greenspace	0.34	0.38	-21.9	Short grass, bare soil (3)
Rooftop	0.30	0.34	-23.0	Vancouver, Uppsala (2)
Impervious	0.59	0.36	-49.6	Concrete, asphalt (2)
Canyon	0.32	0.01	-27.7	Vancouver (1)
(b) **Application of objective hysteresis model: Sunset, Vancouver**				
2 km radius circle				
Cleugh (1988)	0.35	0.25	-29.4	
Present study	0.38	0.27	-29.3	
Source areas - mean coefficients for hours when 'measured' ΔQ_S[b] available				
All hours Plumes	0.37	0.27	-29.1	
Sectors	0.37	0.27	-29.1	
Q^*+Q_F positive:				
Plumes	0.37	0.26	-29.4	
Sectors	0.37	0.26	-29.2	
- application to whole study period 1987 when Q^*+Q_F is positive:				
Plumes & Sectors	0.38	0.27	-29.3	

b 'Measured' as a residual in the energy balance

5.3 'Measured' storage heat flux 1987

Most tests of urban ΔQ_S models have been conducted with summertime data. For this study and to help establish their generality it was necessary to test these models under other conditions to assess their performance in non-summertime conditions.

In this study it is possible to determine ΔQ_S as a residual (ΔQ_{SR}) when:

1) Q* is measured directly;

2) Q_F is calculated as outlined in Chapter 4;

3) Q_H is measured directly using the SAT system (Q_{HS}); and

4) ß is measured using the RTDMS system.

Q_E is calculated using:

$$Q_{ES} = Q_{HS} / ß \qquad (5.7)$$

ΔQ_{SR} can be calculated using equation 5.1. As was noted above, this method incorporates the net errors from the other fluxes in the ΔQ_S term. In order to obtain the best estimate of ΔQ_{SR} it is necessary to pay attention to the errors in the measurements that contribute to the 'measured' values. The error in Q* was taken to be ±5% (Latimer, 1972), and in Q_{HS} to be ±10% (Tanner, pers. comm.). The errors in ß vary with the size of the absolute temperature gradients and the temperature (see Appendix III). The rejection of data with large errors in ß mean that the data set is reduced considerably. There were 1586 hours when all terms were measured and the resulting fluxes (Q_{ES}, ΔQ_{SR}) were reasonable. Of these hours, 23% (362 hours) had an error in ß of <10%. The majority of these hours (97%) were when Q^*+Q_F was less than zero (see Table 5.3). Of the 1586 hours, 66% had an error in ß of <60%.

Plots of the ensemble averages of ΔQ_S and Q* show that the hysteresis pattern reported by Oke and Cleugh (1987) in urban areas during summer also occurs in winter and spring (Fig. 5.1). The coefficients for the Camuffo and

Figure 5.1 Plots of hourly ensemble averages of storage heat flux residual and net radiation for hours when error in Bowen Ratio is:
(a) < 20% (21-59 n=101, 60-120 n=250, 151-179 n=243)
(b) < 30% (21-59 n=122, 60-120 n=313, 151-179 n=362)
(c) < 40% (21-59 n=138, 60-120 n=313, 151-179 n=369)

(a)

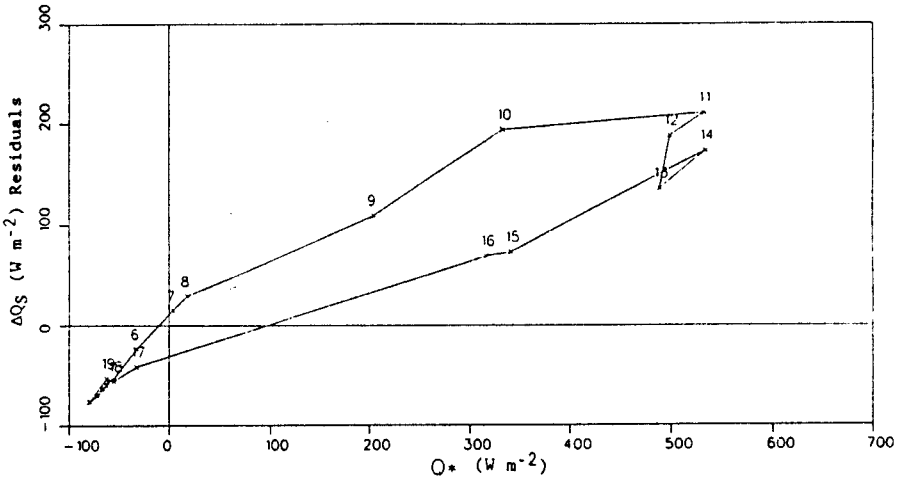

(b)

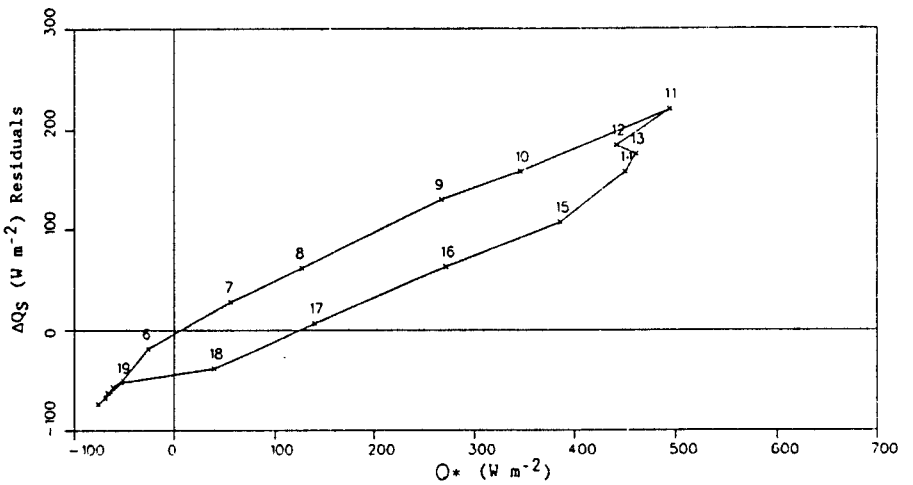

(c)

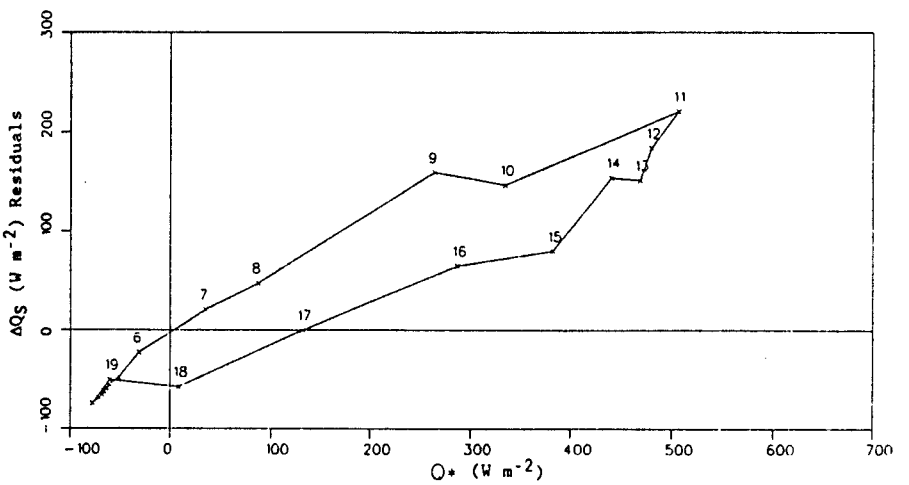

Numbers on plots indicate time (LAT)

Bernardi (1982) type of equation were determined for different sizes of errors in ß for: all hours; when Q^*+Q_F was ≤ 0; and when Q^*+Q_F was positive (Table 5.3). It should be noted that these fitted coefficients were used only for descriptive purposes. The model used for calculating ΔQ_S in the energy balance in this study uses the objectively determined coefficients (see sections 5.4, 5.5).

The parameters obtained when Q^*+Q_F is negative suggest that virtually all the energy is being removed from storage, and the hysteresis term (a_2) is not significant. Since there is a bias in the data towards hours when Q^*+Q_F is ≤ 0, the parameters for the complete set (all hours) are biased towards these hours. Therefore, when hours with Q^*+Q_F positive are fitted as a separate set, the values assigned to a_1 and a_3 are reduced, and a_2 is increased (see Table 5.3). There is more scatter (r^2 is smaller) and a larger standard error for the hours when Q^*+Q_F is positive. Hours with <10% error in ß have a high value of a_1 because Q^*+Q_F for these hours is only just greater than zero.

From the foregoing it appears that the appropriate type of equation to model ΔQ_S should allow for ΔQ_S to equal Q^*+Q_F when the latter is negative, and when Q^*+Q_F is positive the values of the parameters be similar to those determined when the error in ß is between <12% and <20% (see Table 5.3). It should be noted that if it is necessary during calculations to subtract ΔQ_S from Q^*+Q_F the result will always be zero if ΔQ_S equals Q^*+Q_F when the latter is negative. For example, this occurs when calculating the sensible heat ($Q_{H\beta}$) and latent heat ($Q_{E\beta}$) fluxes from ß. This results in all nocturnal $Q_{H\beta}$ and $Q_{E\beta}$ being equal to zero. Therefore for some purposes the equality $\Delta Q_S = Q^*+Q_F$ is inappropriate. In this study for the hours when Q^*+Q_F is negative the following were used: a_1=0.98, a_2=0.004 and a_3=2.5 (Table 5.3 ß errors <16% and <17%).

Table 5.5 Statistical results of comparison between 'measured' and modelled ΔQ_S. The 'measured' ΔQ_S uses ß values with errors of ≤20%.

Equation	m_f	r^2	RMSE W m^{-2}	MAE W m^{-2}	d	N&S	n
All hours							
Objective linear[f]	0.64	0.87	36.6	25.1	0.91	0.77	595
Hysteresis[g]	0.76	0.87	30.4	18.3	0.95	0.84	595
Objective hysteresis[h]:							
Cleugh coeff.	0.76	0.87	30.7	21.7	0.95	0.84	595
Plumes	0.83	0.87	36.8	25.1	0.96	0.86	285
Sectors	0.81	0.87	29.3	20.5	0.95	0.85	595
Q^*+Q_F (positive)							
Objective linear[f]	0.54	0.48	88.0	66.8	0.69	0.25	72
Hysteresis[g]: Q* positive	0.62	0.61	76.1	57.2	0.78	0.44	72
Objective hysteresis[h]:							
Cleugh coeff.	0.72	0.60	70.2	53.2	0.83	0.52	72
Plumes	0.69	0.50	69.9	52.8	0.80	0.47	61
Sectors	0.77	0.59	66.8	50.3	0.56	0.56	72
All hours: If Q^*+Q_F negative ΔQ_S modelled = Q^*+Q_F							
Objective hysteresis[h]:							
Cleugh coeff.	0.85	0.90	26.3	11.0	0.96	0.88	595
2 km circle	0.90	0.90	25.2	10.8	0.97	0.89	595
Plumes	0.85	0.89	35.4	25.1	0.96	0.87	285
Sectors	0.85	0.90	26.4	11.1	0.96	0.88	595
All hours: If $Q^*+Q_F \leq 0$ ΔQ_S modelled $-0.98(Q^*+Q_F)+ 0.004\ dQ^*+Q_F/dt + 2.5$							
Objective hysteresis[h]:							
Cleugh coeff.	0.83	0.90	26.0	10.9	0.96	0.88	595
2 km circle	0.89	0.90	24.9	10.6	0.97	0.89	595
Plumes	0.88	0.89	33.8	15.9	0.97	0.88	285
Sectors	0.87	0.90	25.1	10.8	0.97	0.89	595

m slope of linear functional relationship between 'measured' & modelled ΔQ_S
RMSE - root mean square error
MAE - mean absolute error
d - index of agreement Wilmott and Wicks (1980)
N&S - goodness of fit Nash and Sutcliffe (1970)
f - Oke *et al.* (1981)
g - Camuffo and Bernardi - type using Oke & Cleugh (1987) coefficients
h - Cleugh (1988)

To obtain enough data to look at the monthly variation in the hysteresis equation coefficients it is necessary to use data with <30% and <40% error in ß (Table 5.4). This means that the values of individual coefficients are greater than if data with less error had been used. The coefficients for Q^*+Q_F negative are very consistent between months and for most purposes ΔQ_S could be set equal to Q^*+Q_F under all conditions.

The coefficients for the hours when Q^*+Q_F is positive are less consistent. For the January-February period (JD 21-59) there are so few data points that the three points added when the threshold is relaxed to <40% error change the equation quite substantially. The a_1 coefficients for April (91-120) and June (152-179) are larger than for the other months. There is no clear trend towards a greater percentage of Q^*+Q_F going into ΔQ_S as the seasons proceed towards summer.

5.4 Comparison of Storage heat flux models with 'measured' ΔQ_S

5.4.1 The different models

ΔQ_S was calculated using the models outlined in section 5.2 (objective linear; hysteresis; objective hysteresis). The modelled fluxes were compared with 'measured' ΔQ_S (see 5.3) when the error in ß was ≤20%. Table 5.5 summarises the statistics for the various methods when compared against the 'measured' ΔQ_S. As was noted above, the data set is biased towards the hours when Q^*+Q_F is negative.

As was expected the performance of the objective linear model was the poorest. Measures of goodness of fit such as the slope of the linear functional relationship (m_f) between the residuals and the modelled flux (Mark and Church, 1977), the correlation coefficient (r^2), Wilmott and Wicks' (1980) index of agreement (d), and Nash and Sutcliffe's (1970) "goodness of fit"

Table 5.4 Monthly variation in hysteresis equation coefficents.

	a_1	a_2	a_3	r^2	S.E.[b]	n[c]
Error in ß <30%						
Q^*+Q_F negative (linear)						
JD 21-59	0.81		-2.9	0.72	16.1	107
60-90	1.00		5.6	0.84	10.2	107
91-120	0.98		1.7	0.93	5.4	141
121-151	1.09		8.6	0.85	6.4	136
152-179	1.06		5.4	0.95	3.2	89
Q^*+Q_F negative						
JD 21-59	0.80	0.26	-3.8	0.74	15.6	107
60-90	0.97	0.17	3.2	0.86	9.7	107
91-120						141
121-151	1.15	-0.14	13.7	0.88	5.7	136
152-179						89
Q^*+Q_F positive						
JD 21-59	0.39	0.76	-20.2	0.58	60.1	15
60-90	0.31	0.31	-7.7	0.51	47.6	19
91-120	0.45	0.34	-44.0	0.52	76.6	46
121-151	0.39	0.33	-23.2	0.55	68.5	47
152-179	0.54	0.46	-43.0	0.84	51.6	41
Error in ß <40%						
Q^*+Q_F (all hours)						
JD 21-59	0.42	0.59	-22.9	0.73	27.5	138
60-90	0.41	0.39	-30.6	0.87	25.4	147
91-120	0.46	0.33	-33.2	0.47	41.4	215
121-151	0.44	0.18	-39.7	0.88	38.8	208
152-179	0.55	0.43	-34.2	0.55	32.6	161
Q^*+Q_F (negative)						
JD 21-59	0.81	0.27	-3.7	0.76	14.8	120
60-90	1.00	0.18	5.2	0.85	10.7	119
91-120	0.98	-0.01	1.7	0.93	5.3	146
121-151	1.14	-0.13	12.7	0.88	5.6	142
152-179	0.86	0.16	-10.1	0.94	3.4	96
Q^*+Q_F (positive)						
JD 21-59	0.32	0.65	-5.2	0.60	56.7	18
60-90	0.34	0.37	-7.8	0.58	46.3	28
91-120	0.48	0.35	-40.7	0.57	72.2	69
121-151	0.41	0.19	-25.9	0.54	67.5	66
152-179	0.56	0.44	-38.4	0.85	51.3	65

b S.E. - standard error ($W\ m^{-2}$)
c n - number of data points

Table 5.5 Statistical results of comparison between 'measured' and modelled ΔQ_S. The 'measured' ΔQ_S uses ß values with errors of ≤20%.

Equation	m_f	r^2	RMSE W m^{-2}	MAE W m^{-2}	d	N&S	n
All hours							
Objective linear[f]	0.64	0.87	36.6	25.1	0.91	0.77	595
Hysteresis[g]	0.76	0.87	30.4	18.3	0.95	0.84	595
Objective hysteresis[h]:							
Cleugh coeff.	0.76	0.87	30.7	21.7	0.95	0.84	595
Plumes	0.83	0.87	36.8	25.1	0.96	0.86	285
Sectors	0.81	0.87	29.3	20.5	0.95	0.85	595
Q^*+Q_F (positive)							
Objective linear[f]	0.54	0.48	88.0	66.8	0.69	0.25	72
Hysteresis[g]: Q* positive	0.62	0.61	76.1	57.2	0.78	0.44	72
Objective hysteresis[h]:							
Cleugh coeff.	0.72	0.60	70.2	53.2	0.83	0.52	72
Plumes	0.69	0.50	69.9	52.8	0.80	0.47	61
Sectors	0.77	0.59	66.8	50.3	0.56	0.56	72
All hours: If Q^*+Q_F negative ΔQ_S modelled = Q^*+Q_F							
Objective hysteresis[h]:							
Cleugh coeff.	0.85	0.90	26.3	11.0	0.96	0.88	595
2 km circle	0.90	0.90	25.2	10.8	0.97	0.89	595
Plumes	0.85	0.89	35.4	25.1	0.96	0.87	285
Sectors	0.85	0.90	26.4	11.1	0.96	0.88	595
All hours: If $Q^*+Q_F \leq 0$ ΔQ_S modelled $-0.98(Q^*+Q_F)+ 0.004\ dQ^*+Q_F/dt + 2.5$							
Objective hysteresis[h]:							
Cleugh coeff.	0.83	0.90	26.0	10.9	0.96	0.88	595
2 km circle	0.89	0.90	24.9	10.6	0.97	0.89	595
Plumes	0.88	0.89	33.8	15.9	0.97	0.88	285
Sectors	0.87	0.90	25.1	10.8	0.97	0.89	595

m slope of linear functional relationship between 'measured' & modelled ΔQ_S
RMSE - root mean square error
MAE - mean absolute error
d - index of agreement Wilmott and Wicks (1980)
N&S - goodness of fit Nash and Sutcliffe (1970)
f - Oke et al. (1981)
g - Camuffo and Bernardi - type using Oke & Cleugh (1987) coefficients
h - Cleugh (1988)

(N&S) are furthest from 1.0 of all three models. Also the root mean square error (RMSE) and the mean absolute error (MAE) are the largest. The hysteresis-type models performed better. Of the two hysteresis models, the objective one, where coefficients are determined by the proportions of surface types present, performed better than the empirical fits to the July/August 1978 data of Oke and Cleugh (1987).

The inclusion of a separate equation for the hours when Q^*+Q_F is negative leads to an even better performance of the objective hysteresis model (Table 5.5) (Fig. 5.2a,b). The equality $\Delta Q_S = Q^*+Q_F$ is satisfactory but, as expected, the use of a best fit equation to the 1987 data leads to the best performance. For the reasons outlined in the preceding section this form of equation was utilised for calculating the hourly ΔQ_S, when Q^*+Q_F is less than zero, used in the remainder of this research. For the hours when Q^*+Q_F was greater than zero the objective coefficients (Table 5.2a, note coefficients in Table 5.2b are the mean coefficients, see section 5.4.2) with changing land use proportions were used.

The largest ΔQ_S flux densities are underestimated by all of the models (Fig. 5.2a,b, 5.3a,b). There appears to be a 'capping' on the modelled ΔQ_S. The maximum 'measured' $\Delta Q_S \approx 370$ W m^{-2}, whereas the maximum modelled $\Delta Q_S \approx 290$ W m^{-2} (Fig. 5.2b, Fig. 5.3b). Even when the flux density is modelled with the two equations fitted to the 1987 data (i.e. coefficients for when Q^*+Q_F positive and Q^*+Q_F is negative see Table 5.3) the modelled values are relatively low (Fig. 5.3b). This was also seen in the results reported by Cleugh (1988) for July-September 1986 (see her Fig. A3.3). Her maximum 'measured' flux is ≈ 290 W m^{-2}, whereas the maximum modelled flux ≈ 190 W m^{-2}.

Figure 5.2 Residuals versus modelled storage heat flux densities using the objective hysteresis model and including changing source areas for hours when plumes could be identified:
(a) all hours equation
(b) equation using $\Delta Q_S = Q^* + Q_F$ when $Q^* + Q_F$ is negative.

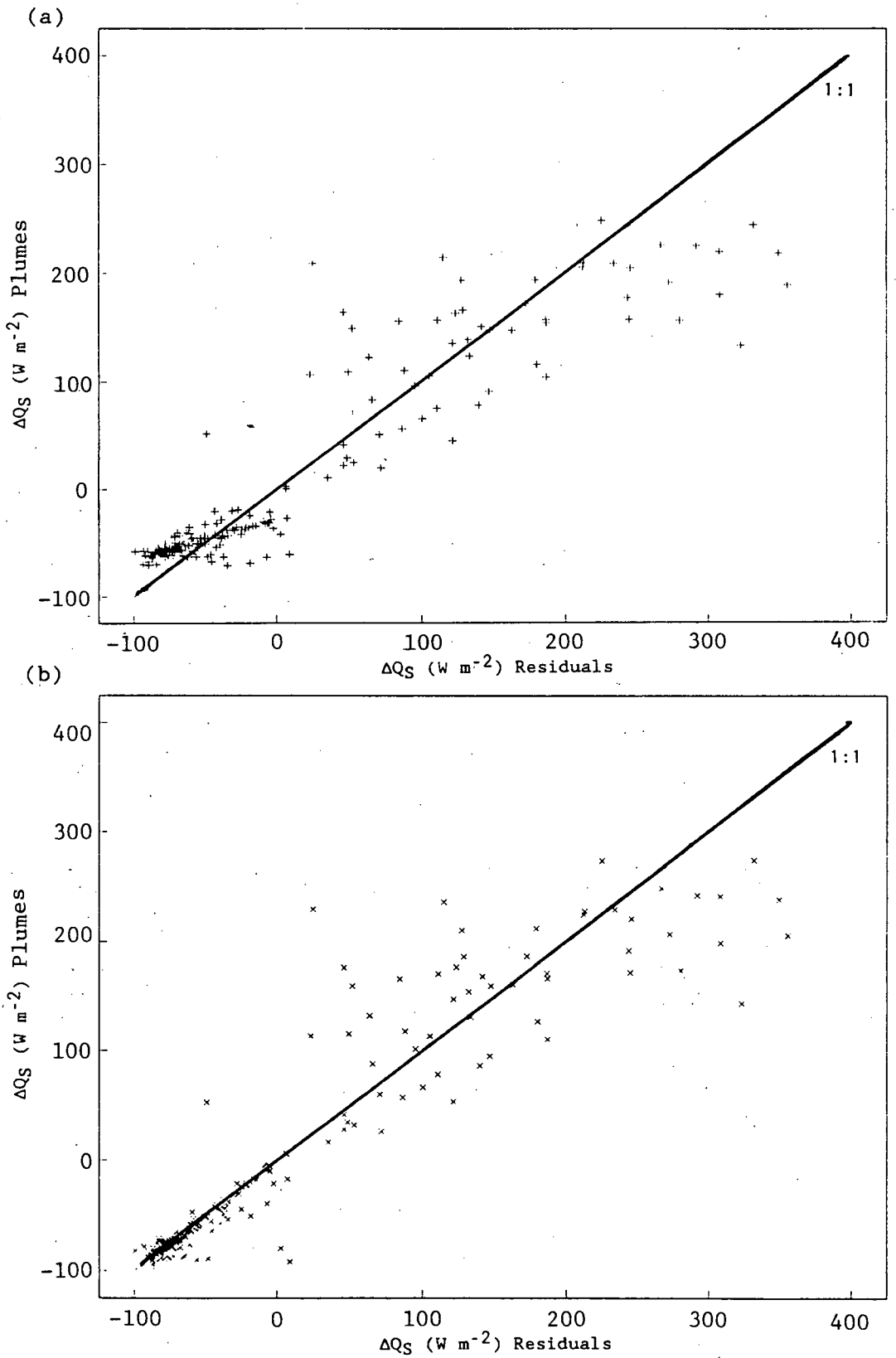

Figure 5.3 Modelled versus 'measured' storage heat flux density with ß < 20% error:
(a) using Cleugh (1988) coefficients
(b) using best-fit coefficients for 1987 data and separate equations for $Q^* + Q_F$ negative or positive.

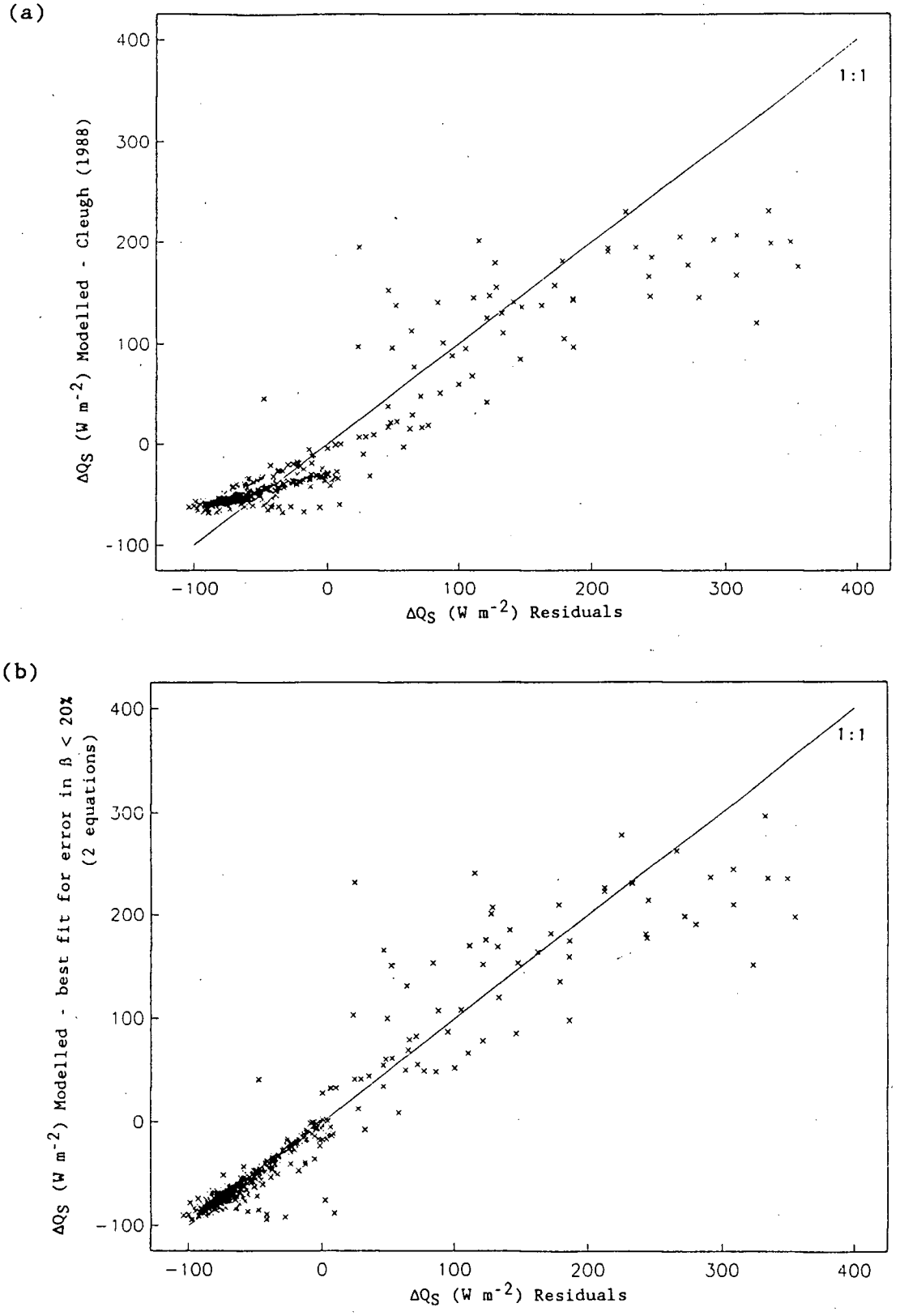

5.4.2 Influence of land use description

In this section the influence of using a static or dynamic surface description in the objective hysteresis model is discussed.

Table 5.1 gives the mean and range of the land use proportions during the study period. The 'measured' ΔQ_S hours have similar mean proportions to the whole study period. The proportions of the surface land use which are present in the 2 km radius circle are also very similar to the mean when the source areas are taken into account. The maximum percentage difference between the mean of the various techniques is 2% for any particular land use type. Table 5.2 also includes the maximum and minimum for all the hours in the study period for each surface type. The maximum variability occurs in the greenspace surface type, with a range $\approx$ 40% (plumes)(see Fig. 3.10). The range of the other three surface types is approximately 20% (plumes). The maximum and minimum values of the coefficients of the ΔQ_S model are associated with the extremes in land uses, as would be expected (see Table 5.2). The a_1 and a_3 coefficients are similar for greenspace, roofs, and canyon. The a_2 are similar for greenspace, roofs and impervious surface types. The maximum (0.41) and minimum (0.36) values of a_1 occur when the pavement proportion is at its maximum and minimum respectively. The maximum a_2 (0.33) and the minimum absolute value of a_3 (26.9) are associated with the maximum vegetation and minimum wall area. The minimum a_2 (0.25) is associated with the maximum wall area. The maximum absolute value of a_3 (32.1) occurs when the pavement is at the maximum.

The objective model is conservative with respect to changes in proportions of surfaces present. Table 5.2 presents the mean equations when the turbulent source areas are used to determine the surface proportions for the models. The equations vary very little, and as was noted above, the extremes are also not

very large when the varying source areas are taken into account. The mean equations for the source areas and the equation for the fixed 2 km radius circle are all virtually the same. The coefficients are very similar to those determined as the best fit when Q^*+Q_F is positive and ß has an error of 12-20% (Table 5.3). When the surface described by the mean for the 2 km circle (this study) and description is allowed to vary due to change in source area there is some variability but on the whole very close agreement between the modelled fluxes. The variation is probably smaller than the deviation from the 'true' ΔQ_S. Therefore if one is not interested in hour-to-hour variability the use of a mean surface description should be satisfactory.

Using the database it is possible to calculate the size of the storage heat flux density for each grid square for any hour or any energy conditions. Figures 5.4a,b are maps of ΔQ_S when the error in ß <16 % for the ensemble hours 0800 (Q^*+Q_F=30 W m^{-2}, $d(Q^*+Q_F)/dt$=107 W m^{-2}) and 1200 LAT (Q^*+Q_F=550 W m^{-2}, $d(Q^*+Q_F)/dt$=55 W m^{-2}), respectively. ΔQ_S ranged from -9 W m^{-2} to 29 W m^{-2} at 0800 LAT and from 151 to 292 W m^{-2} at 1200 LAT. The parks have the highest ΔQ_S (compare Fig. 5.4a with Fig. 3.9) at 0800 LAT. At midday the road pattern is evident (compare Fig. 5.4b with Fig. 3.8). This figure demonstrates the influence of both the land use and the three coefficients. The grid squares which have the largest flux are not the same at both times, although those with the smallest fluxes are similar. This indicates that consideration of the source area for some sites may be more critical than would appear to be the case at the present study site. Changing the surface types influences the calculated ΔQ_S in a different manner through the day because of the changing weighting of the a_1 and a_2 coefficients.

Figure 5.4 Map of storage heat flux for:
(a) ensemble 800 LAT
(b) ensemble 1200 LAT
(see text for full details)

(a)

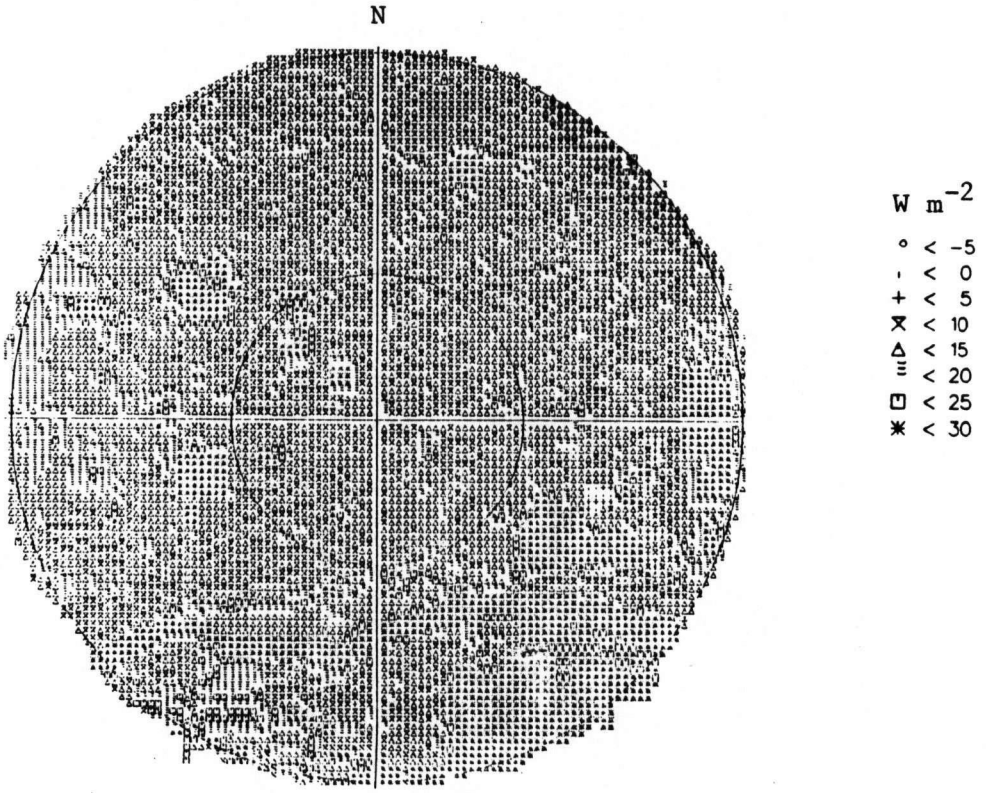

(b)

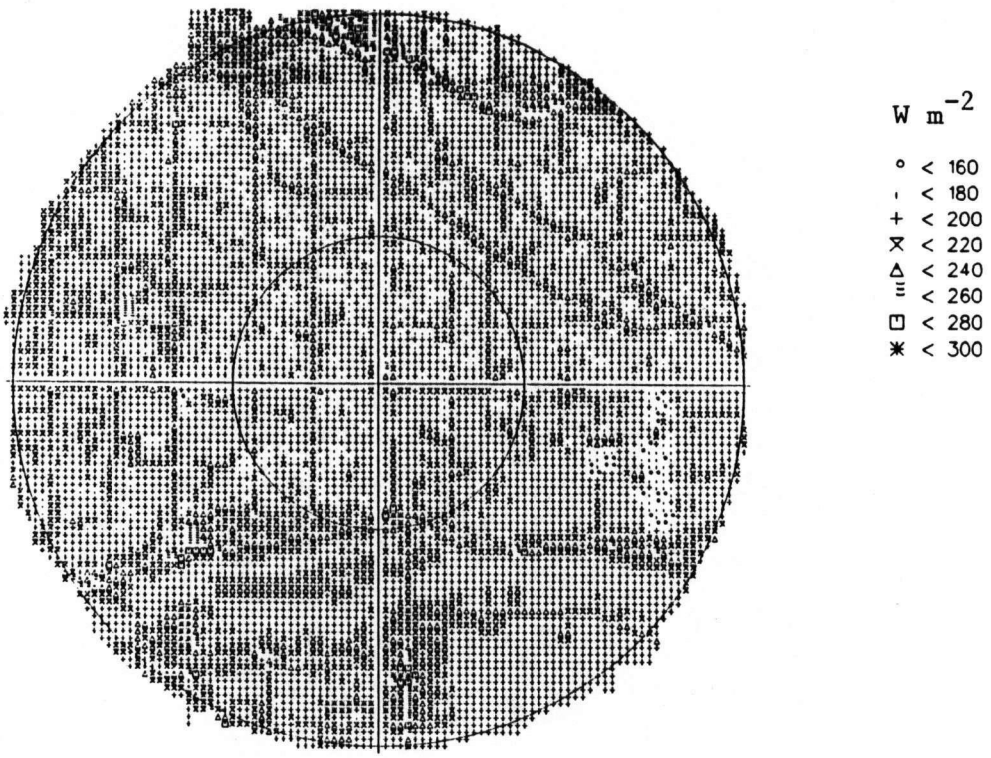

5.4 Discussion

This study is one of the first to consider storage heat flux during non summertime conditions. It is encouraging that the objective hysteresis ΔQ_S model, previously only used in the summer, performs so well. Application of the model taking into account the varying source areas suggests that (unless the surrounding site is extremely heterogeneous) the model can be applied using only a mean areal determination of the surface description. The parameterization is conservative with respect to changes in the proportions of land use. In this study the changing source areas were taken into account.

The objective hysteresis model does not include the 3-dimensional character of vegetation. Since the model is performing satisfactorily it seems that this can continued to be ignored. The area of vegetation, excluding grass, is small compared to the proportions of other surface types in the Sunset study area (Chapter 3). There have been detailed studies of the storage heat flux for a young eucalyptus forest (Aston, 1985), mixed forest (McCaughey, 1985) and Amazonian tropical forest (Moore and Fisch, 1986) but there are no data available for the storage heat flux of individual trees and bushes. Determination of the hysteresis equation coefficients from the data presented in these publications suggest extremely small proportions of net radiation going into storage. From the Aston (1985) data a_1=0.0004, a_2=0.18 and a_3=3.9; for the McCaughey (1985) data a_1=0.11, a_2=0.11 and a_3=-12.3 (it is not possible to use the Moore and Fisch (1986) data). These equations are probably not appropriate for inclusion in the objective model because in an urban area individual trees/bushes have a greater solar radiation load over the whole plant; in particular the trunk, stem and branches rather than just the crown.

The significance of heat storage in the seasonal energy balance is discussed in Chapter 6.

CHAPTER 6 URBAN ENERGY BALANCE

6.1 Introduction

The surface energy balance of an extensive urbanised surface may be written:

$$Q^* + Q_F = Q_H + Q_E + \Delta Q_S + \Delta Q_A \quad (6.1)$$

where Q^* - net all-wave radiation flux density (W m^{-2});
Q_F - anthropogenic heat flux density (W m^{-2});
Q_H - sensible heat flux density (W m^{-2});
Q_E - latent heat flux density (W m^{-2});
ΔQ_S - net heat storage (W m^{-2}); and
ΔQ_A - net heat advection (W m^{-2}).

The preceding chapters have outlined the measurement programme and the methods to calculate individual fluxes, excluding latent heat. In this chapter the results of the previous chapters are used to obtain hourly latent heat fluxes and energy balances. These results are the first extended (more than one or two days) measured urban balances for winter and spring conditions.

6.2 Determination of hourly energy balances

When models, rather than measurements, were used to determine a flux the source area of the associated turbulent fluxes were taken into account, using the method outlined in Chapter 3, to ensure that the energy balance was consistent for the hour. As was noted in Chapter 3, it was not possible to calculate the source area using the Schmid model for all hours of the study period, due to the absence of Q_H measurements. On those occasions 'sectors' rather than 'plumes' were used to describe the source area locations and to access the surface database to obtain the appropriate surface description.

The methods used to determine each of the fluxes are as follows:

1) Q^* - directly measured as described in Chapter 2.

2) Q_F - calculated using the method described in Chapter 4.

3) ΔQ_S - calculated using the objective hysteresis model outlined in Chapter

5. The model used was the version with a separate equation for the hours when Q^*+Q_F is less than zero (a_1=0.98, a_2=0.004, a_3=2.5), and which took into account varying source areas.

4) Q_H - determined using one of two methods. If Q_{HS} was available from the eddy correlation measurement (see Chapter 2) it was used. Otherwise, the measured Bowen ratio (ß) was used to calculate $Q_{H\beta}$:

$$Q_{H\beta} = \frac{\beta\ (Q^* + Q_F - \Delta Q_S)}{1 + \beta} \qquad (6.2)$$

If the resulting $Q_{H\beta}$ and latent heat fluxes ($Q_{E\beta}$) were realistic and the error in $Q_{H\beta}$ and $Q_{E\beta}$ were less than 30%; or if the absolute size of both fluxes were less than 20 W m^{-2}, then the calculated fluxes were used.

5) Q_E - this was dependent on the method used to determine Q_H. If Q_{HS} was available then Q_E was determined as a residual (Q_{ER}):

$$Q_{ER} = Q^* + Q_F - \Delta Q_S - Q_{HS} \qquad (6.3)$$

When Q_{HS} was not available then $Q_{E\beta}$ was calculated:

$$Q_{E\beta} = \frac{(Q^* + Q_F - \Delta Q_S)}{1 + \beta} \qquad (6.4)$$

The hours when this was used are the same as those for $Q_{H\beta}$.

6) ΔQ_A - omitted on the basis of Steyn's (1985) analysis of data from the same tower. He showed that energy residuals from over-determined balances are zero in the mean, and are unrelated to wind speed or direction. This strongly suggests that the site is not characterised by systematic local scale advection. This conclusion is further supported by the small spatial variability found by Schmid (1988) when comparing eddy correlation measurements of Q_H measured on the Sunset tower with those from a mobile tower operated at several sites within a 2 km radius.

The reason for choosing to accept Q_{HS} first rather than following a procedure of determining an optimum energy balance, such as that suggested by

Steyn (1985), is based on the expectation that this procedure will produce the smallest error in the turbulent fluxes (see Chapter 2 and Appendix III).

A comparison was conducted between the turbulent sensible heat flux densities determined from the SAT (Q_{HS}) and the RTDMS ($Q_{H\beta}$). There were only 8 hours when Q_{HS} was measured and the error in $Q_{H\beta}$ was less than 10% (Table 6.1, Fig. 6.1) but these, except for one point, plot on the one-to-one line. Figures 6.1b-d show that as the error in $Q_{H\beta}$ increases the number of extreme outliers does not increase; i.e. they are present at <20% error. At <100% error there is noticeable inclusion of values close to zero; in particular $Q_{H\beta}$ are calculated as almost equal to zero, whereas for the same hours Q_{HS} have a greater range. These results are similar to those reported by Cleugh and Oke (1986) for a rural site. They find a best fit line of $Q_{H\beta} = 0.96Q_{HS} + 24.8$ with an r^2 of 0.74 and a RMSE of 34.1 W m^{-2} (n=69).

There were 2324 hours with Q_{HS} data and an additional 788 hours when ß was measured and the fluxes met the conditions outlined above. Therefore it was possible to determine the energy balance for 3112 of the 3795 hours during the period JD 21-179, 1987. ΔQ_S was calculated for most of the 3779 hours with Q* data. For these hours it is possible to calculate the total turbulent energy (Q_H+Q_E) by difference.

6.3 Measured hourly energy balance, 1987

The ensemble hourly energy balances were calculated for each month and for the entire measurement period (Table 6.2, 6.3, Figure 6.2). The hours included are only those for which all fluxes of the budget were determined. For practical reasons this means the data set is biased slightly towards conditions with high radiative input (drier weather). This can be seen by comparing Table 6.2a (energy balance hours only) with Table 6.2c (all hours

Table 6.1 Comparison of Q_{HS} and $Q_{H\beta}$ (W m^{-2}) with varying errors in ß.

% error in ß	n	$Q_{H\beta}$ Mean	sd	Q_{HS} Mean	sd	RMSE	MAE	m_f	r^2
<10%	8	32.2	35.9	35.4	52.6	23.4	13.7	0.69	0.87
<20%	499	170.2	93.7	139.9	88.9	68.1	52.0	1.34	0.58
<30%	683	149.3	94.8	122.9	72.1	67.0	72.1	1.31	0.58
<40%	777	136.8	96.5	114.2	74.0	64.9	47.5	1.30	0.60
<50%	846	128.8	97.4	107.6	75.2	63.1	45.7	1.30	0.63
<60%	890	123.5	98.2	103.7	76.0	62.2	44.6	1.29	0.64
<70%	948	117.2	99.3	98.5	76.8	61.0	43.2	1.29	0.66
<80%	991	112.8	99.5	95.2	77.1	60.0	42.2	1.28	0.67
<90%	1033	108.6	99.7	92.3	77.5	59.6	41.7	1.28	0.67
<100%	1079	104.1	99.9	88.9	77.9	59.0	40.9	1.27	0.68

n - number of hours
sd - standard deviation
RMSE - root mean square error
MAE - mean absolute error
m_f - slope of linear functional relationship (Mark and Church, 1977)

Figure 6.1 Comparison of Q_H determined using eddy correlation (SAT) and Bowen Ratio - energy balance methods:
(a) < 10% error in ß
(b) < 20% error in ß
(c) < 30% error in ß
(d) < 100% error in ß

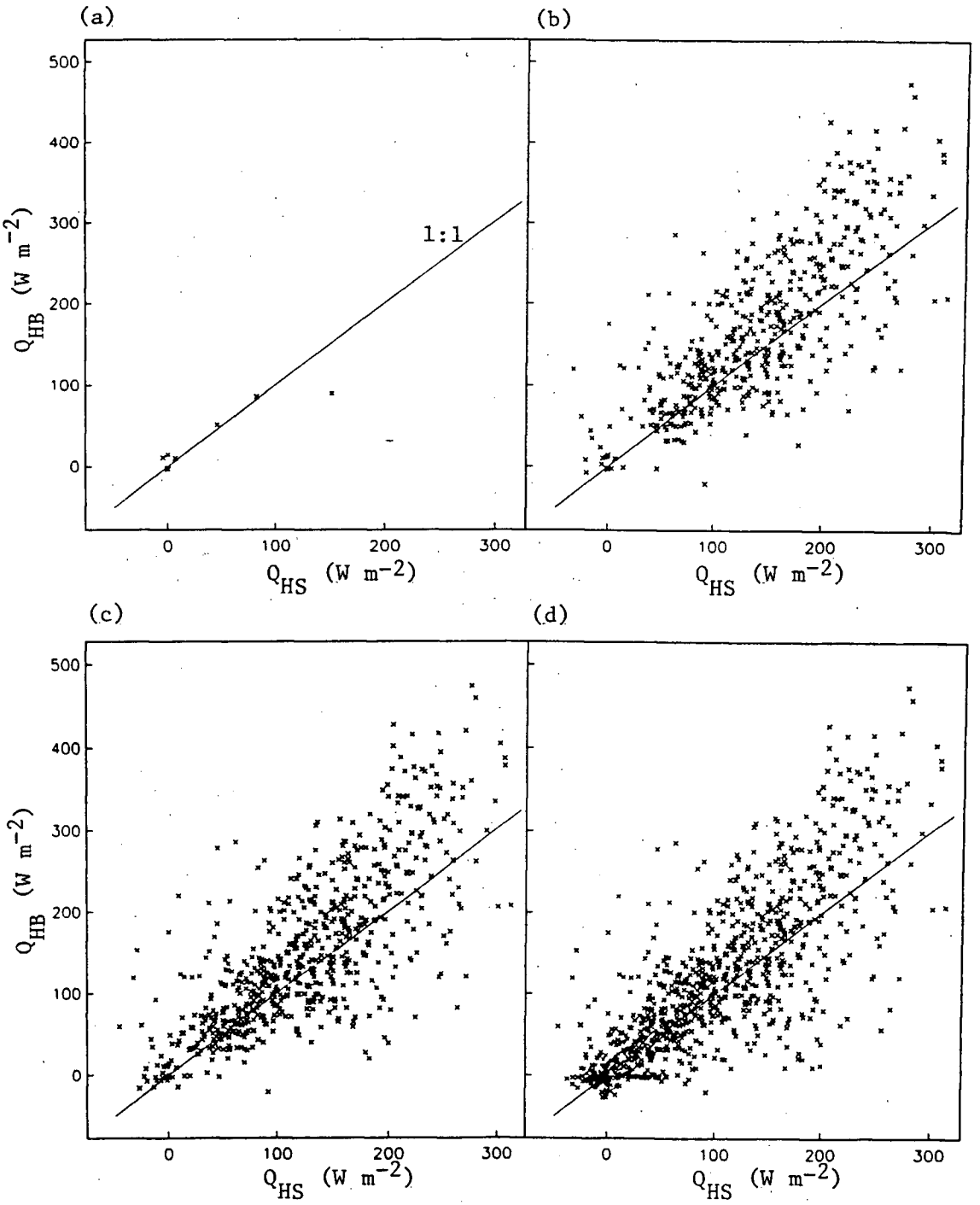

Table 6.2 Mean daily (24 hours) energy balance components for the whole measurement period and by month, 1987. Ensemble averages for:
(a) mean fluxes (W m^{-2}) for energy balance hours
(b) ratios of flux to available energy for energy balance hours
(c) mean fluxes (W m^{-2}) and ratios for all hours with net radiation data.

(a)	Q^*	Q_F	ΔQ_S	Q_H	Q_E	% of hours usable
JD 21-179	94.3	8.3	12.4	48.1	42.2	82.0
21-59	22.1	9.0	-9.6	15.9	24.8	75.5
60-90	77.0	8.9	7.1	42.5	36.4	74.1
91-120	89.0	8.3	9.8	40.6	46.9	91.5
121-151	133.3	7.6	23.8	66.7	50.4	82.8
152-179	139.6	7.6	25.7	72.3	49.2	92.9

(b)	$\frac{Q^*}{Q^*+Q_F}$	$\frac{Q_F}{Q^*+Q_F}$	$\frac{\Delta Q_S}{Q^*+Q_F}$	$\frac{Q_H}{Q^*+Q_F}$	$\frac{Q_E}{Q^*+Q_F}$	ß
JD 21-179	.92	.08	.12	.47	.41	1.14
21-59	.71	.29	-.31	.51	.80	0.64
60-90	.90	.10	.08	.49	.42	1.17
91-120	.91	.09	.11	.42	.48	0.87
121-151	.95	.05	.17	.47	.36	1.32
152-179	.95	.05	.17	.49	.33	1.47

(c)	Q^*	Q_F	ΔQ_S	$\frac{Q^*}{Q^*+Q_F}$	$\frac{Q_F}{Q^*+Q_F}$	$\frac{\Delta Q_S}{Q^*+Q_F}$
JD 21-179	76.0	8.4	6.0	0.90	0.10	0.07
21-31	1.3	9.4	-13.2	0.12	0.88	-1.23
32-59	14.8	9.1	-13.4	0.62	0.38	-0.56
21-59	10.9	9.2	-13.5	0.54	0.46	-0.67
60-90	51.0	8.9	-2.1	0.85	0.15	-0.04
90-120	86.4	8.3	8.8	0.91	0.09	0.09
121-151	121.3	7.7	20.2	0.94	0.06	0.16
152-179	134.3	7.6	24.0	0.95	0.05	0.17

Figure 6.2 Ensemble average energy balance plots.

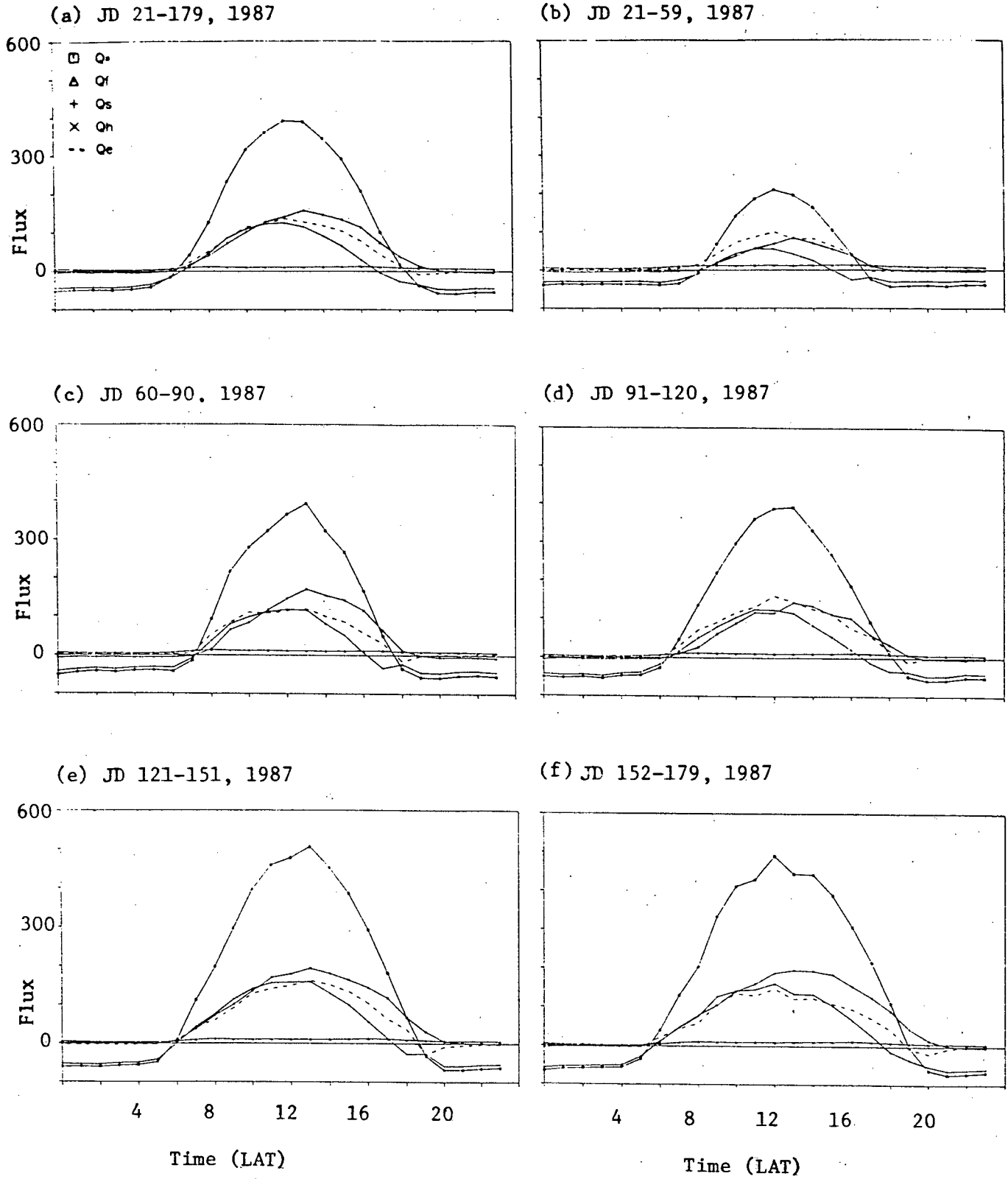

Table 6.3 Daytime (Q*>0) energy balance fluxes and ratios of fluxes to available energy for the whole measurement period and by month, 1987. The fluxes are calculated from hourly ensemble averages for each time period. (a) Energy balance fluxes (MJ m^{-2} d^{-1}) (b) ratios Also included are results from the same site for two summer periods in 1980 and 1983 (see text).

(a)	Q^*	Q_F	ΔQ_S	Q_H	Q_E	n
JD 21-179	10.18	0.48	2.79	4.19	3.68	12
21-59	3.98	0.52	1.14	2.29	3.07	8
60-90	8.91	0.43	2.39	3.86	3.10	10
91-120	9.84	0.48	2.61	3.62	4.10	12
121-151	13.81	0.47	4.04	5.65	4.59	13
152-179	14.25	0.48	4.24	6.09	4.40	13
1983[a] 199-265	13.81		3.04	6.04	4.73	13
1980[b] July-mid Aug.	13.86		1.99	1.23	3.86	

(b)	$\frac{Q^*}{Q^*+Q_F}$	$\frac{Q_F}{Q^*+Q_F}$	$\frac{\Delta Q_S}{Q^*+Q_F}$	$\frac{Q_H}{Q^*+Q_F}$	$\frac{Q_E}{Q^*+Q_F}$	ß
JD 21-179	.96	.04	.26	.39	.34	1.14
21-59	.92	.08	.17	.35	.47	0.74
60-90	.95	.05	.26	.41	.33	1.24
91-120	.95	.05	.25	.35	.40	0.88
121-151	.97	.03	.28	.40	.32	1.23
152-179	.97	.03	.29	.41	.30	1.38
1983[a] 199-265			.22	.44	.34	1.28
1980[b] July-mid Aug.			.23	.11	.67	0.16

a Cleugh and Oke (1986) - 30 days during this time period
- Q_F not included in energy budget
- daytime hours assumed to be 13

b Oke and McCaughey (1983) - 19 days during this time period
- Q_F not included in energy budget

n - number of daytime hours

with radiation data).

The ratios reported in Table 6.2b (daily - 24 hours) and Table 6.3b (daytime - Q*>0) allow a comparison of the relative importance of individual fluxes in the energy balance between months. Included in Table 6.3 are the results of measurements conducted at the same site as this study by Oke and McCaughey (1983), and Cleugh and Oke (1986) in the summers of 1980 and 1983, respectively. In both studies Q* was measured in the same manner as here but Q_F was not included in the energy balance. (Note therefore that ratios include only Q*). Oke and McCaughey (1983) measured ß using a reversing differential psychrometer system different to that used in this study, see Kalanda et al. (1980) for full details. They used the objective linear storage heat flux parameterization (see section 5.2.1) to obtain ΔQ_S together with ß to calculate Q_H and Q_E. Cleugh and Oke (1986) also used the objective linear storage scheme and Q_H was measured using a SAT leaving Q_E as a residual in the energy balance. The difference in methods, especially considering their dependence on ΔQ_S and the results in Chapter 5, suggest that the results should be compared with caution. The only fluxes directly comparable with the present results are Q*, and Q_H for 1983.

As expected, Q_F decreases in significance and size as Q* increases from winter to summer (Table 6.2, 6.3). The relative importance is greater for the whole day (Table 6.2) than for the daytime hours (Table 6.3). In the daytime hours it is less than 10% of the energy input (Q^*+Q_F) for all months. When the whole day is considered Q_F makes a larger than 10% contribution to the energy balance up until April. Therefore it probably can be considered negligible or can be ignored only if research is being conducted for daytime hours, or if the whole day is under consideration in a non-wintertime study. It is probably only necessary to pay close attention to the diurnal variability if a winter-

time study is being conducted.

The 1987 daytime $\Delta Q_S/(Q^*+Q_F)$ ratio increases from 0.17 to 0.29 as Q* increases (Table 6.3). The 1987 ratios are higher than for the two summertime studies, except for January/February, but of course a different method was used in 1987. There is a net gain in ΔQ_S for each month except January-February. It is relevant to enquire whether this pattern makes sense in relation to the annual storage input/output regime. This was checked using Q* data collected at a suburban site (Kerrisdale) 8 km to the west of the Sunset site in 1982 (Grimmond, 1983) and the objective hysteresis storage heat flux model (with separate equations for daytime and nighttime). Table 6.4 shows that at Kerrisdale there are 5 months of net storage heat loss; March and October are the transition months between net gain and net loss; and the peak gain occurs in June. Using this model it is calculated that in 1982 there was a small net gain in ΔQ_S. Ideally there should be zero net heat storage over the annual period, but the result is considered satisfactory.

The daily (Table 6.2) and daytime (Table 6.3) Q_H flux increases with increasing Q*. The monthly mean daily ratio varies between 0.42 and 0.51 but does not show a distinct seasonal trend. The daytime ratios vary between 0.35 and 0.41. When Q_F is excluded from the ratio the June ratio of 0.43 is very similar to the 1983 summertime ratio of 0.44. The May 1987 data had the same mean daytime Q* as the 1983 data. The Q_H/Q^* ratio for 1983 was 0.44 and for May 1987 was 0.41. The 1987 data seem to be more like the 1983 data set than that for 1980.

Q_E, generally, increases with increasing Q*. However, the daytime and daily Q_E in June 1987 was less than for May. This resulted in a slightly lower proportion of Q^*+Q_F going into Q_E. The trend of the mean monthly daily $Q_E/(Q^*+Q_F)$ ratio shows a decrease from 0.80 in January/February to 0.33 in

Table 6.4 Mean daily Q* and ΔQ_S by month for Kerrisdale, Vancouver 1982

	Q* W m^{-2}	Q_F[a] W m^{-2}	ΔQ_S W m^{-2}
1982			
JD 22-31+[b]	-0.7	9.4	-18.9
31-59	20.2	9.1	-12.2
60-90	54.2	8.9	0.9
91-120	102.9	8.3	18.1
121-151	134.1	7.7	28.7
152-181	144.3	7.6	32.7
182-212	123.6	7.6	26.2
213-243	103.6	7.7	17.7
244-273	66.6	8.3	4.4
274-304	30.6	8.9	-5.2
305-334	3.7	9.1	-18.2
335-365	-7.3	9.4	-20.2
Year	64.9	8.5	4.6

a Q_F mean values from 1987 data (see Table 6.3). Assuming that the flux is similar for the two areas and years; and that the flux is symmetrical in the year around June.

b The January period was measured in two parts: JD 22-31, 1982 and 1-21, 1983.

June. In the wintertime this may be due to the combination of frequent rain events and small radiation input. Under such conditions the energy goes into drying the surface first. The daytime Q_E/Q^* ratios do not show as pronounced a trend. The 1983 ratio was 0.34 and those for May and June 1987 are 0.33 and 0.31 respectively. June 1987 had low rainfall (see Table 2.2), with rain being recorded on only 6 days.

The mean daily ß (calculated from ensemble Q_H and Q_E fluxes) varies between 0.64 and 1.47 with a mean for the measurement period of 1.14. The daytime mean for the measurement period is the same with a range of 0.74 to 1.38. There is no distinct trend with season. January/February and April ß values are less than 1.00. The 1983 summertime ß falls between the May and June 1987 data. The 1987 mean of 1.14 is close to the typical value of 1.00 given by Oke (1982) for suburban areas.

The daily trends for the mean monthly fluxes are shown in Figure 6.2. The data for the whole measurement period (Fig. 6.2a) show that Q_H, Q_E, and ΔQ_S follow a very similar path until about 1200 LAT. In the afternoon Q_H is greater than Q_E which in turn is greater than ΔQ_S. Q_H goes through zero after Q^*, Q_E at approximately the same time as Q^*, and ΔQ_S about an hour earlier.

From Figure 6.2 it can be seen that Q_E is an important term in the energy balance in all months. In particular, it is the dominant output flux in the January/February period. The diurnal trend of the ensemble energy balances for March to June are remarkably similar in form. The three output fluxes are very similar before solar noon. This is different than the summertime energy balances reported by Cleugh and Oke (1986) and is probably in large part due to the inclusion of the hysteresis type storage heat flux function compared to the linear one they used. This demonstrates the importance of the storage parameterization, as it influences the apparent size of Q_E unless Q_E is

determined independently. The ensemble plots, except for January/February, are generally similar to those of the Cleugh and Oke study in the afternoon with Q_H the largest flux, then Q_E and then ΔQ_S. This suggests that the relative importance of the fluxes remains similar through the spring and summer. However, the winter may show the greatest difference as noted above. Further winter measurements are needed to document this.

The evaporative fluxes calculated here are used in Chapter 8 for comparison with modelled fluxes.

CHAPTER 7 RESISTANCES, DRAINAGE AND STORAGE CAPACITY

7.1 Introduction

In this chapter the three remaining sub-models of the modified Penman-Monteith-Rutter-Shuttleworth evapotranspiration-interception model are presented. The models are for aerodynamic resistance (r_a), surface resistance (r_S), and drainage (D). The first two are used with the Penman-Monteith evapotranspiration equation, and the third is used in the calculation of the running water balance of the surface water store (see Chapter 1).

7.2 Aerodynamic resistance

After the input of energy, the most important factor governing the rate of evaporation is the efficiency of removal of water vapour from the surface (Stewart, 1984). For a given wind speed and vapour pressure the rate of removal of water vapour depends on the atmospheric turbulence created by the wind blowing over the surface roughness elements. The integrated transfer coefficient for water vapour between the evaporating surface and some reference height in the free atmosphere is termed the aerodynamic resistance (r_a), or its reciprocal the aerodynamic conductance (g_a). It can be estimated using the following equations.

Under neutral atmospheric conditions r_a can be determined using the logarithmic wind profile (Monteith, 1965):

$$r_a = (1/g_a) = \{\ln[(z - d)/z_0]\}^2/(k^2u) \qquad (7.1)$$

where z - wind speed measurement height (m);
d - displacement length (m);
z_0 - momentum roughness length (m);
k - von Kármán's constant; and
u - horizontal wind speed (m s^{-1}).

In non-neutral conditions, and for water vapour exchange, the following expression applies (Thom, 1972):

$$r_a = \{\ln[(z - d)/z_0] - \psi\}\{\ln[(z - d)/z_{0v}] - \psi_v\}/(k^2u) \qquad (7.2)$$

where ψ - stability function for momentum exchange;
ψ_v - stability function for water vapour exchange; and
z_{0v} - water vapour roughness length.

In this study, for unstable conditions the stability functions are those of Dyer (1974) based on a comparison with measured z/L (see Appendix IV). For stable conditions the relations of Dyer (1974) and van Ulden and Holtslag (1985) are used (see Appendix IV). The water vapour roughness length was taken to be 10% of the momentum roughness length (Brutsaert, 1983).

Thom & Oliver (1977) proposed a semi-empirical formula based on Penman's (1948) original formula for r_a for crops:

$$r_a = 4.72 \{\ln[(z - d)/z_0]\}/(1 + 0.5u) \qquad (7.3)$$

Calculation of r_a using equations 7.1 or 7.3 only requires hourly wind speed whereas the non-neutral version requires stability data (see Appendix IV). It is assumed that the r_a obtained when the boundary layer stability is taken into account is closest to the 'true' value, but in many forest evaporation-interception studies the neutral method has been used alone and found to be satisfactory (Shuttleworth, 1988a). Figure 7.1 is a comparison between the results from the three equations using those hours when stability could be estimated from a directly measured sensible heat flux ('sonic' method, Appendix IV). It shows r_a calculated by each method plotted against the measured wind speed. The effective height (z-d) of the anemometer was 19 m and z_0=0.52 m (Chapter 2). Under certain conditions the stability corrected r_a becomes extremely large: firstly, when the atmosphere is unstable ($-0.4 < z/L < 0$) and wind speed is less than 0.5 m s^{-1}; and secondly, when the atmosphere is slightly stable ($z/L > 0$) with low wind speed. In this study under these conditions r_a was set to 175 s m^{-1}, the maximum value obtained by the neutral method. When the atmosphere is more stable there is a wider range of r_a for

Figure 7.1 Aerodynamic resistance calculated for hours when it was possible to determine stability with direct measurements of Q_H: neutral atmosphere equation (—); Thom & Oliver (1977) equation (--); and, non-neutral equation (x).

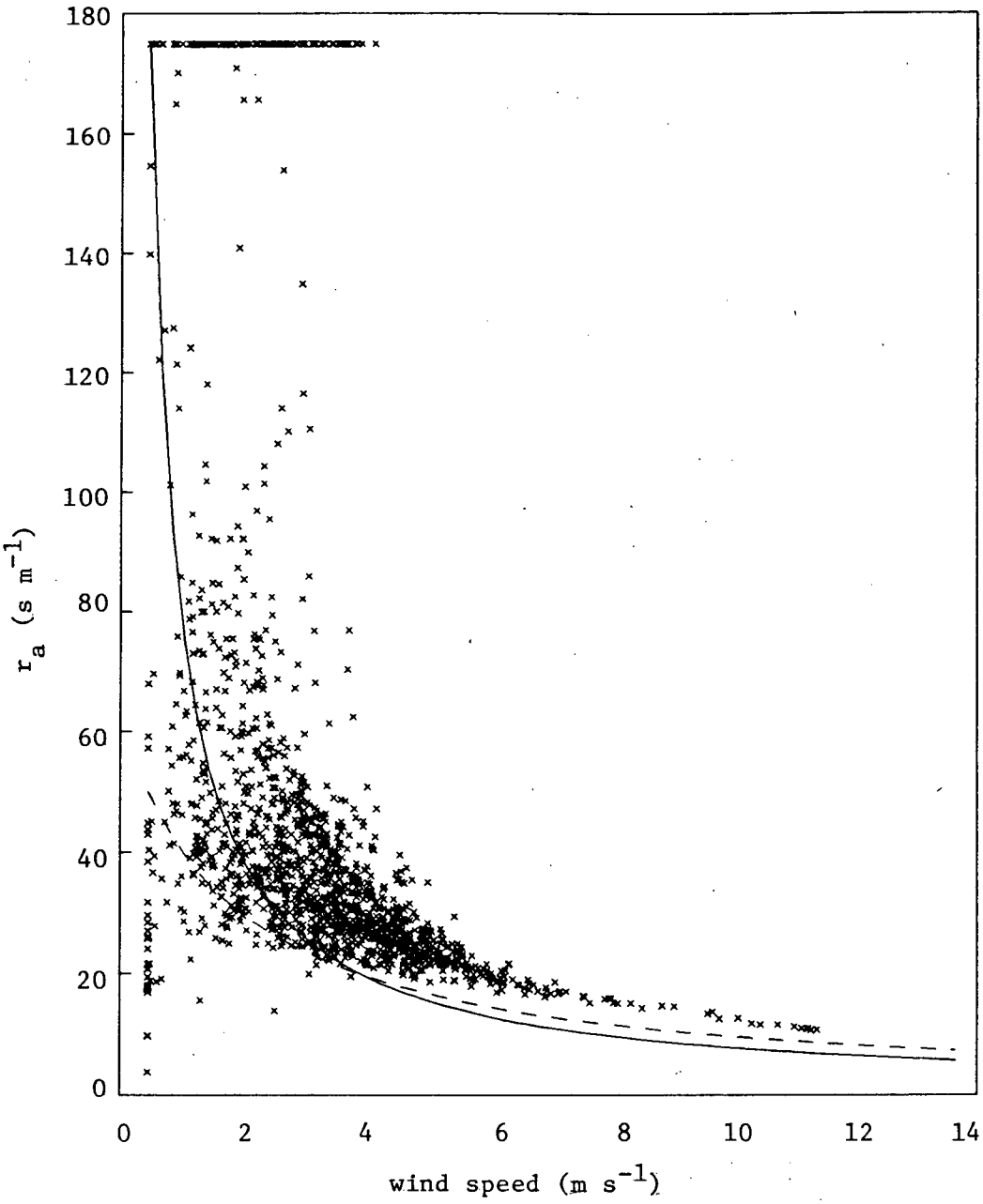

low wind speeds.

The neutral results plot approximately in the middle of the stability corrected r_a. The Thom and Oliver equation does not show as much variability. It would appear that in urban areas, as in forested environments, that the neutral formula is a reasonable approximation. Stewart (1984), for a forest, using the neutral equation calculated r_a to be 5 s m^{-1} (z_0=1.3 m, z-d=5 m, u= 2 m s^{-1}). This value is obviously influenced not only by z_0 and d, characteristics of the surface, but also by z. When z-d is increased to 19 m (the same as for this study) r_a=21.4 s m^{-1}. For a crop he calculated r_a to be 29 s m^{-1} (z_0=0.13 m, z-d=3 m, u=2 m s^{-1}). If z-d is changed to 19 m, r_a=74 s m^{-1}. When z-d is standardized it can be seen that the urban value (r_a=38.5 s m^{-1}) is approximately half that above a crop and twice that above a forest.

The implications associated with the use of the individual r_a models are discussed in conjunction with the sensitivity analyses of the whole evapotranspiration-interception model in Chapter 8.

7.3 Surface resistance

When there is no rain or dew on vegetation, water loss occurs through the foliage stomata. This process is biologically controlled and changes with micrometeorological conditions. The biophysical and biochemical mechanisms of stomatal resistance (r_{ST}) are poorly understood (Shuttleworth, 1988a). The form of stomatal response often is qualitatively similar from one species to the next, but it exhibits marked variations in quantitative terms both between and within species (Jarvis et al., 1976). At the whole canopy scale Shuttleworth (1976, 1978, 1979) has shown that the bulk stomatal resistance is closely related to the surface resistance (r_S) as defined by Monteith (1965). In this approach the complex array of r_{ST} for the individual leaves is

replaced by an equivalent system containing a single hypothetical leaf with a single r_S. Thom (1972) showed that if the source of water vapour evaporated is the canopy of a forest, and the aerodynamic resistance used correctly describes the transfer of water, then r_S is equivalent to the bulk r_{ST}. In the more general case where some of the water vapour comes from other layers (e.g. litter layer and understorey), changes in r_S also reflect changes in their rates of evaporation as well as changes in the canopy (Stewart, 1988). In urban areas the diversity of vegetation makes the determination of a bulk stomatal resistance virtually impossible due to sampling problems and the added complication posed by the non-vegetated areas. Therefore it is necessary to model r_S as a single integrated resistance for the whole system.

At present there is insufficient knowledge to interpret the effects of environmental variables on r_{ST} using a mechanistic model (Stewart, 1988). However, as proposed by Jarvis (1976) a physically-based model to predict r_{ST} can be determined from empirical relationships between r_{ST} and controlling environmental variables. Results from plant physiological studies have shown that r_{ST}, or its inverse conductance (g_{ST}), depends primarily on the following environmental variables: photon flux density, ambient carbon dioxide concentration, leaf-air specific humidity difference, leaf temperature and leaf water status (Jarvis, 1976).

In an attempt to develop a model of r_S for the whole canopy for use with the Penman-Monteith model researchers have utilised the results of plant physiological studies of r_{ST}. Empirical formulae that describe whole-canopy r_S of forests in terms of the same or similar variables identified to control r_{ST}, have been calibrated against micrometeorological data (Gash et al., 1988; Lindroth, 1985; Sellers et al., 1986/Shuttleworth, 1988a; Shuttleworth, 1988b; Stewart, 1988). The general form for the canopy model is expressed in similar

mathematical form to that proposed by Jarvis (1976) for stomatal response of individual leaves to the environmental variables identified above. In addition r_S has been shown to be dependent on seasonal changes in leaf area index (LAI) (Calder, 1977).

The general form of these models (expressed as a conductance (g_S) is:

$$g_S = P_1 \, L \, g(\text{variables}) \qquad (7.4)$$

where P_1 - maximum value of the surface conductance (m s^{-1});
L - leaf area index (LAI); and
g(variables) - functions of the environmental variables which have values between zero and unity.

This general form was used to develop a model for the Sunset study site. It assumes that surface conductance is a function of the non-synergistic interaction between stomatal aperture, leaf area index and environmental variables. It operates on an hourly time scale. The environmental variables identified by Jarvis (1976) as directly influencing stomatal resistance were not available but were replaced by closely related ones. Stewart (1988) replaced quantum flux density with measurements of total solar radiation. In this study it was replaced by net radiation (Q*). Following Stewart (1988) leaf-air specific humidity was replaced with specific humidity deficit (δq); leaf temperature by air temperature (T); and leaf water status by soil moisture deficit ($\delta\theta$). The form of the model is:

$$g_S = P_1 g(Q^*) g(\delta q) g(T) g(\delta\theta) g(L) \qquad (7.5)$$

The dependence on Q* is expressed using the same mathematical form of equation as has been used for solar radiation (see e.g. Shuttleworth, 1988a):

$$g(Q^*) = (Qm/(P_2 + Q^*)/[Qm/(Qm + P_2)] \qquad (7.6)$$

where Qm - maximum hourly net radiation annually (W m^{-2}); and
P_2 - fitted parameter (W m^{-2}).

The dependence on δq is expressed as (Gash et al., 1988; Stewart, 1988):

$$g(\delta q) = 1 - P_3 \, \delta q \qquad 0 < \delta q < P_4 \qquad (7.7)$$

$$= 1 - P_3 P_4 \qquad \delta q \geq P_4 \tag{7.8}$$

The dependence on T is defined by (Stewart, 1988):

$$g(T) = (T - T_L)(T_H - T)^{Tc}/[(T - T_L)(T_H - T)^{Tc}] \tag{7.9}$$

where:

$$T_c = (T_H - P_5)/(P_5 - T_L) \tag{7.10}$$

where T_L, T_H - minimum and maximum temperature limits (°C).

The dependence on $\delta\theta$ is described by (Stewart, 1988):

$$g(\delta\theta) = 1 - \exp(P_6 (\delta\theta - (S_1/P_6 + S_2))) \tag{7.11}$$

where S_1, S_2 - fitted parameters which relate to the maximum $\delta\theta$.

The dependence on LAI follows Dolman et al. (1988), but allows for the greater diversity of vegetation found in the suburban area compared to a temperate forest:

$$g(L) = [(L\ A_U) / Lm) + A_I]/(A_U + A_I) \tag{7.12}$$

where A_U - area unirrigated (m^2);
Lm - maximum LAI in A_U; and
A_I - area irrigated (m^2).

To optimise the values of the parameters ($P_1,\ldots,P_6$) for the study area non-linear least squares regression (Denis et al., 1981; Gay, 1983; Moore, 1986) was used with 'measured' values of r_S and the environmental variables identified above. When the surface is dry it is possible to determine a 'measured' surface resistance (r_S) by rearranging the Penman-Monteith equation, and with measured latent heat flux (Q_E) (Monteith, 1965) to give:

$$r_S = \left(\frac{s\ ß}{\gamma} - 1\right) r_a + \frac{\rho\ c_p}{\gamma} \frac{V}{Q_E} \tag{7.13}$$

The hours used to develop and test the model were those daylight hours for which aerodynamic resistance could be calculated with the stability correction that was determined using directly measured Q_H (see eqn. 7.2), and when the surface was dry. For the surface to be classed as dry it had to meet the following criteria: rain was not recorded in the current or previous three

hours; three hours with positive Q* had occurred since rainfall; the hour preceding recorded rain was regarded as not dry; to account for dew the surface was not dry until two hours after Q* was greater than zero; the wetness sensors record the surface as dry; and that the surface was observed not to have puddles or received traces of rain. These latter times were based on visual observations of the surface wetness. The criteria are similar to those used by Shuttleworth (1988b). 543 hours of measured r_S met these criteria. Figure 7.2 shows the ensemble mean and standard deviation of g_S for these hours. The diurnal trend is similar to that reported for forests (e.g. Shuttleworth, 1988b). The values tend to be smaller than those reported for forests (approximately 75%) and to have a greater hourly standard deviation (approximately double)(see e.g. Stewart and de Bruin, 1984; Shuttleworth, 1988b; Stewart, 1988).

The data were split in two by putting alternate available days into two data sets: one of 300 and the other of 243 hours. This was done because no independent data set exists for a suburban area which covers as wide a range of conditions as collected in this study. The two data sets were used independently to develop and test the model.

The data used to develop and test the model were 'measured' at the Sunset tower (see Chapter 2). Q* and T were measured directly, δq was calculated from the measured T, and pressure, p. Soil moisture deficit was determined for unirrigated areas using profiles of gravimetric soil moisture and the dry bulk density of the soil. Irrigated areas were found to have no soil moisture deficit at any time. The surface description database and the source area model (see Chapter 3) enabled the area with coniferous, deciduous and grass vegetation, and the area irrigated and unirrigated to be identified for each hour. Thus an areally-weighted $\delta\theta$ was determined for each hour. It was assumed

Figure 7.2 Diurnal trend of ensemble mean and standard deviation of measured surface conductance for hours which met the criteria outlined in the text.

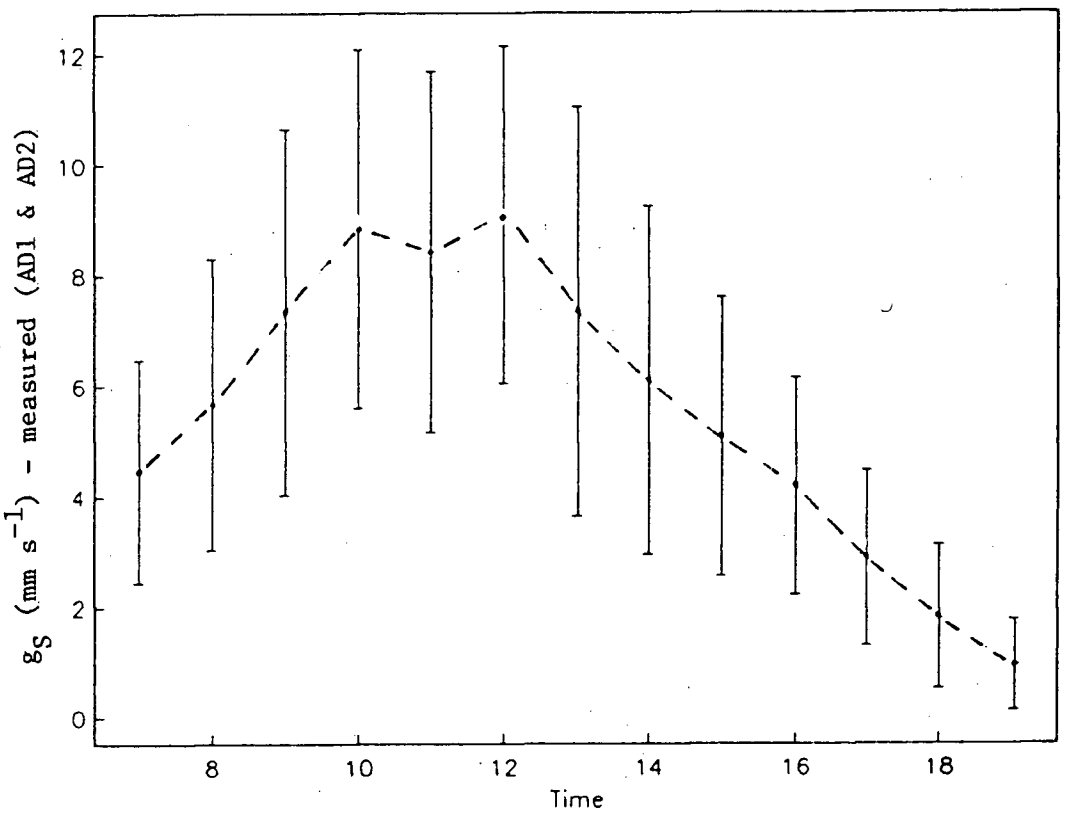

that the area irrigated is grass and that because of lawn-mowing the LAI of the grass remains constant seasonally at 1.6 (Ripley and Redmann, 1975). LAI for the unirrigated area was determined as an areally weighted average of the coniferous LAI, deciduous LAI and the grass value of 1.6 for the source area for each hour. LAI for coniferous and deciduous vegetation was set to a maxima of 6 and 4 respectively and minima of 4 and 0 respectively (Kramer and Kozlowski, 1979). 360° panorama photographs were taken from the tower approximately weekly to identify the stages of the growing season. They were used to model LAI for each day of the study period for the two vegetation types using (Street and Opik, 1984):

$$\log \frac{L + 1}{a - (L + 1)} = k[(d-d_0)-(d_1-d_0)] \qquad (7.14)$$

where a - maximum LAI minus the winter minimum (1);
k - fitted parameter (0.05);
d - Julian day of interest;
d_0 - starting day of curve from winter minimum of LAI (JD 45); and
d_1 - day of inflection of S curve (JD 95).

Therefore it was possible to assign a daily value of LAI for each vegetation type and, depending on the source area being sampled determine the weighted average of LAI for each hour. The area irrigated was determined based on visual surveys and water use data (Chapter 2) in conjunction with the data base and the source area model to determine the surface types sampled each hour.

The model parameters Lm, Qm, T_H, T_L, S_1 and S_2 must be assigned before the model can be fitted to the measured data. From the calculated LAI, the maximum-areally weighted Lm is 3.1. From measured Q* during June (which has the highest values for the year) Qm was set to 725 W m^{-2}. Following Stewart (1988) and Gash et al. (1988) T_H was set to 40°C and T_L to 0°C. S_1 and S_2 were determined by trial and error (Dolman et al., 1988) to be 0.45 mm and 15 mm respectively.

Table 7.1 lists the fitted parameters and the test statistics. The values of the model parameters (Table 7.1a) P_3 to P_6 are similar to those reported by Stewart (1988) and Gash et al. (1988) for temperate forests (Thetford, U.K. and Les Landes, France respectively). The first two parameters (P_1, P_2) are somewhat dissimilar from those of Stewart (1988) and Gash et al. (1988). This is expected due to two reasons. Firstly the land use of this study is different. The canopy vegetation is more heterogeneous and there are areas that are non-vegetated. This will influence P_1. Secondly, P_2 is associated with net all-wave radiation in this study rather than net solar radiation as in the other two studies. Several different forms of the model were tried taking into account features that are distinctly urban. The model presented gave the best explanation of variance.

The statistics pertaining to model development and performance tests are presented in Tables 7.1b and 7.1c respectively. The model was first developed using data set AD2 and tested against AD1. Independently the process was reversed and the AD1 data set was used to develop the model and AD2 to test. The r^2 of 0.71 for model AD2 is similar to that reported by Stewart (1988). The lower degree of explanation with data set AD1 is consistent regardless whether the data were used to develop or test the model. This may be attributed to the greater number of outliers in this data set as evident in Figure 7.3a. Inspection reveals these to be hours characterised by cloudy and partly cloudy conditions, suggesting that the net radiation function is inadequate for these conditions. All three models show larger unsystematic than systematic errors, which indicates there is only a small consistent bias in the model estimates. The slope of the best fit line indicates an under-prediction for low g_S (high r_S) and an under-prediction for high g_S (low r_S). The slopes forced through the origin for the tests (Table 7.1c) are similar to

Table 7.1 Surface resistance model fitted parameters and test statistics

(a) Model parameters

Model	n	P_1 mm s^{-1}	P_2 W m^{-2}	P_3 kg g^{-1}	P_4 g kg^{-1}	P_5 °C	P_6 mm^{-1}
Alternate Days 1 (AD1)	300	56.35	694.9	0.0857	9.44	20.07	0.0105
Alternate Days 2 (AD2)	243	53.95	634.0	0.0821	8.91	18.88	0.0107
All days (All)	543	55.20	669.6	0.0840	9.02	19.56	0.0106

(b) Model development statistics

Data set used for Model	Test	r^2	m_0	m_f	c_f mm s^{-1}	RMSE mm s^{-1}	$RMSE_S$ mm s^{-1}	$RMSE_U$ mm s^{-1}	d	
AD 1	AD 1	0.61	0.90	0.79	1.29	2.35	1.45	1.85	0.87	
AD 2	AD 2	0.71	0.93	0.87	0.69	1.75	0.88	1.52	0.91	
All	All	0.65	0.91	0.82	1.05	2.11	1.21	1.73	0.89	
(c) Model test statistics										
AD 1	AD 2	0.71	0.89	0.87	0.44	1.79	0.91	1.54	0.91	
AD 2	AD 1	0.61	0.92	0.78	1.57	2.36	1.47	1.85	0.87	
May-June										
AD 1	AD 2	0.72	0.89	0.74	1.14	1.75	0.89	1.50	0.91	n=184
AD 2	AD 1	0.65	0.92	0.65	2.49	2.26	1.38	1.79	0.88	n=202

n - number of hours
m_0 - slope forced through the origin
m_f & c_f - slope (principal axis) and intercept for linear functional relation (Mark and Church, 1977)
RMSE - root mean square error
$RMSE_S$ - systematic error
$RMSE_U$ - unsystematic error
d -index of agreement (Wilmott and Wicks, 1980)

Figure 7.3 Comparison between hourly measured and modelled surface conductance:
(a) model AD1 data AD2
(b) model AD2 data AD1

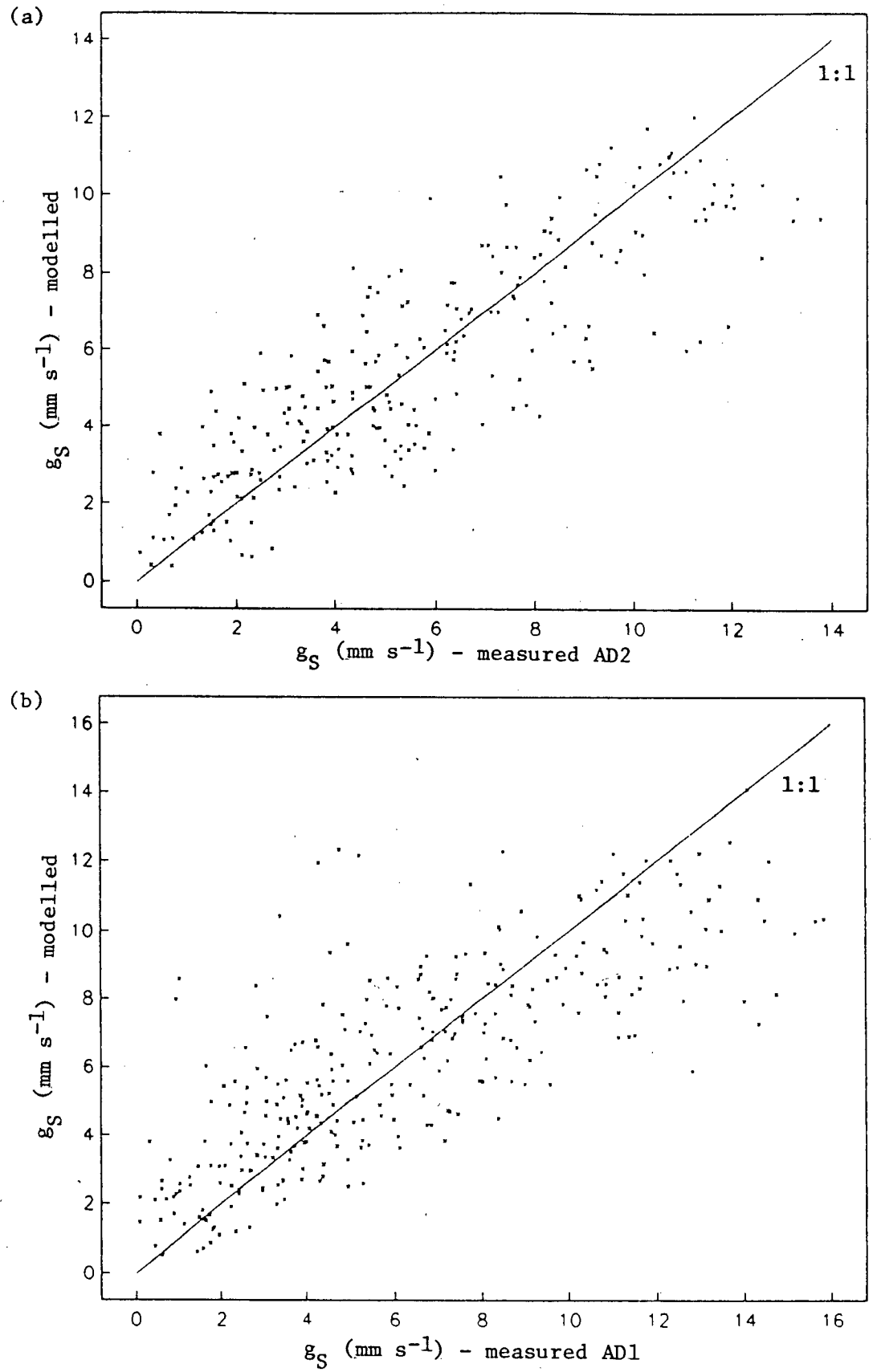

those obtained by Stewart (1988). Figure 7.4a,b show the diurnal trend of the ensemble mean measured and modelled (using the opposite model) g_S. The modelled and measured data exhibit the same trend using either model. In both cases the model under-predicts in the morning.

The AD1 model was selected for calculation of r_S in the evapotranspiration-interception model. This model, when tested, has the lowest RMSE and the slope of the line (m_f), derived from functional analysis (Mark and Church, 1977) is the closest to unity. The other two models are used in the sensitivity analyses (see Chapter 8). The results suggest that this form of model is promising for use in urban areas. It has the advantage of being dynamically responsive to both meteorological and seasonal conditions.

7.4 Drainage

Most of the thesis to this point has been concerned with the evapotranspiration portion of the Penman-Monteith-Rutter evapotranspiration-interception model. As noted in Chapter 1 the model calculates a running water balance (eqn 1.14). The determination of the drainage rate for urban areas is problematic. This term does not correlate directly with urban runoff. It has to be envisaged as that loss from the 'storage layer' which is no longer available for evaporation; e.g. the water may enter a pipe system or infiltrate into the soil. Given the range of vegetation and other surfaces in urban areas the measurement of the drainage rate involves a vast sampling problem. Added to this is the difficulty of making actual observations. Even in forest areas, there is always a significant error involved in the measurement of this term (Shuttleworth, 1988a).

To overcome these difficulties with the urban environment it was decided to use values for the parameters of the drainage functions taken from the

Figure 7.4 Ensemble mean of measured and modelled surface conductance:
(a) data AD2 (-) modelled AD1 (▲)
(b) data AD1 (-) modelled AD2 (▲)

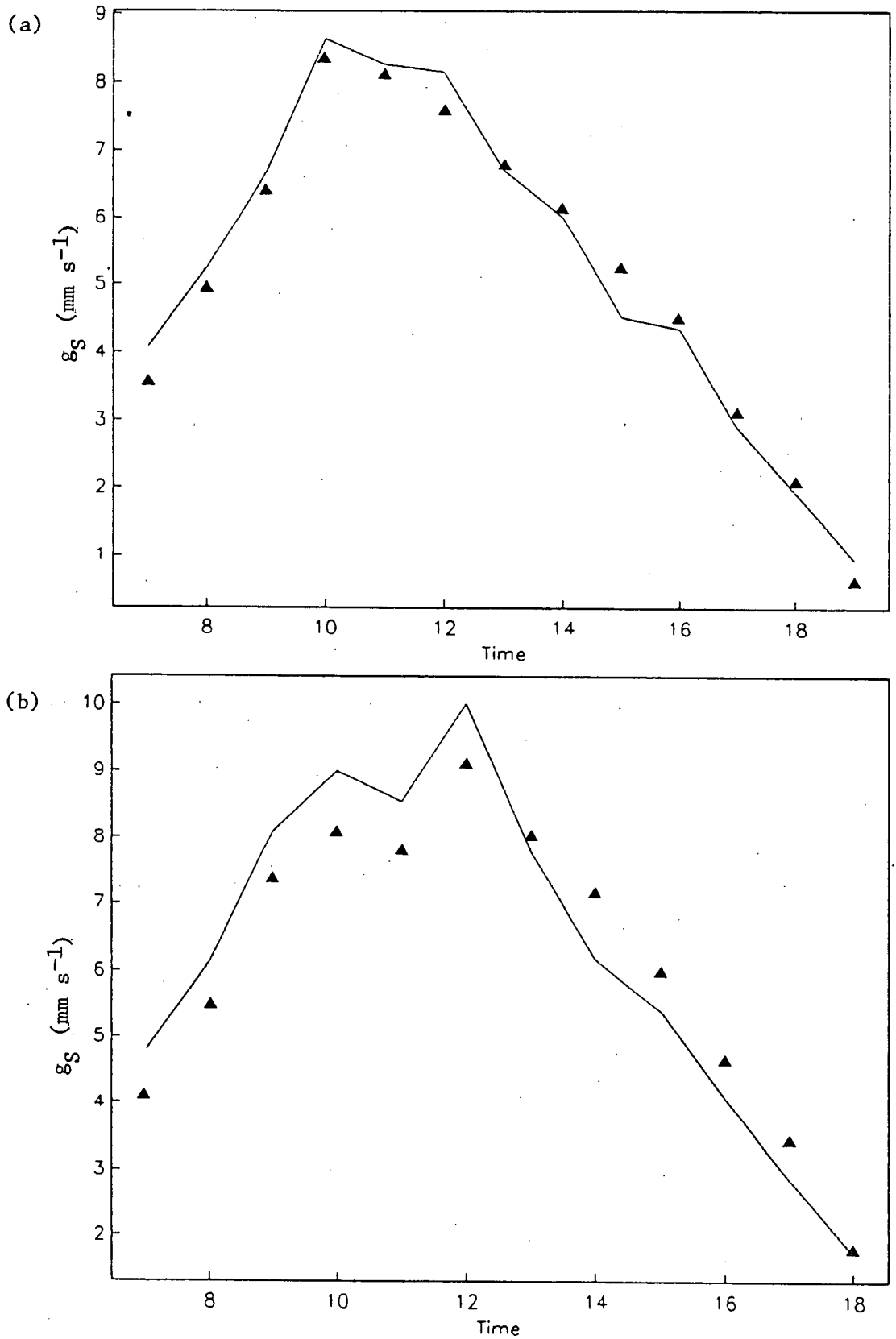

literature. The approach for calculating the drainage rate is outlined below.

The model developed in this study, for urban areas, has a single layer moisture store (Fig. 1.2). The drainage function describes the rate at which water drains from this moisture store. It is set proportional to the current water status of this store. In the original papers of Rutter et al. (1971, 1975) they proposed:

$$D = D_0 \exp\{b(C-S)\} \qquad (7.15)$$

where D_0 - drainage rate when C=S;
b - empirical coefficient; and
S - amount of water the canopy stores/retains after the rainfall and throughfall cease.

However, this formulation has an inherent difficulty in predicting a finite drainage when the canopy is dry (Calder, 1977). It has been rewritten (e.g. Halldin et al., 1979) to rectify this so that it reads:

$$D = D_0 \exp[(bC)-1] \qquad (7.16)$$

This drainage function has been used by Halldin et al. (1979), Calder et al. (1984), Calder and Wright (1985) and Hall (1985). Other proposals include Calder's (1977) linear threshold model, and Massman's (1983) model which explicitly includes the rainfall rate in addition to the stored water. Thus far Massman's (1983) model has only been tested in old growth Douglas fir forests and one of the drip parameters in his dynamic model varies from storm to storm. Calder and Wright (1985) compared the Calder (1977) threshold model and equation 7.16 both of which had been optimised at a different site in the same forest. Equation 7.16 which has been widely used, gave slightly better performance.

Here equation 7.16 is used for the proportion of the source area which is vegetated but not irrigated. Table 7.2 lists values for the equation parameters which have been taken from the literature.

For the area which is impervious the urban runoff literature is used. There

Table 7.2 Values of drainage function parameters (see text for explanation) All equations mm h^{-1} except Shuttleworth (1988b) mm min^{-1}. Note that when calculation is conducted within the evapotranspiration-interception model the resulting drainage is adjusted for the time step of the calculation.

Author	Surface	Equation	D_0	b	T[a]
Calder (1977)	Norway & Sitka spruce	$D_0 \exp(bC)$	0.18	1.76	-
		D_0C C<T	0.21	-	1.9
		D_0C -b C>T	3.2	5.6	1.9
Calder & Wright (1985)	Norway & Sitka spruce	7.16	0.013	1.71	-
		D_0C C<T	0.21	-	2.5
		D_0C -b C>T	3.4	7.9	2.5
Hall (1985)	Heather	7.16	0.00085	5.13	-
	Wax base & tray	7.16	0.21	27.09	-
Shuttleworth (1988b)	Tropical forest (Amazonian)	7.15	0.0014	5.25	-
Falk & Niemczynowicz (1978)	Car park	7.17	32.0	1.5	-
	Car park, road	7.17	5.7	1.5	-
	Bicycle park	7.17	28.0	1.5	-
		7.18	10.0	3.0	-
	Car park	7.17	15.0	1.5	-
	Car park	7.17	12.0	1.5	-
	Car park, road	7.17	17.0	1.5	-
	Bicycle park	7.17	27.0	1.5	-
	Car park	7.17	22.0	1.5	-
	Bar park	7.17	21.7	1.5	-

a T - threshold value

have been a small number of studies which have determined the runoff from a single surface type rather than for a land use area. Falk and Niemczynowicz (1978) proposed the following equations for the relationship between drainage and storage (using the same notation as above):

$$D = D_0 (C_{t-1}-S)^b \quad (7.17)$$

$$D = D_0 (C_{t-1})^b \quad (7.18)$$

They report values of the optimised coefficients from measurements conducted in nine small (78 - 413 m^2) completely paved catchments (Table 7.2). Equation 7.17 allows for no drainage when $C < S$. This assumption has also been used by researchers in forested areas, for example Gash and Morton (1978) and Mulder (1985). Pratt et al. (1984) suggest that the rate of drainage from flat roofs can be assumed to be the same as paved surfaces of 1% slope. Equation 7.18 was used for the paved, built surfaces and for irrigated grass.

In this study it was not possible to directly test the performance of any individual drainage equation. They can be assessed by the performance of the whole evapotranspiration-interception model against the measured latent heat flux and by comparing the modelled surface state (C) with the wetness sensors (see Chapter 8). The effect of the choice of equation and parameters is compared in the sensitivity analysis of the whole evapotranspiration-interception model in Chapter 8.

7.5 Storage capacity

The values of the surface storage capacity, like the drainage functions, were based on values taken from the literature. The capacity for a surface type is assumed to be constant through time for all types except deciduous vegetation, where allowance is made for the change between winter and summer. This is done by the addition to the winter storage capacity (S_{dW}) of an

increment (S_dst):

$$S_dst = (S_{dS} - S_{dW})/(t_e - t_b) \quad (7.19)$$

where S_{dS} - summer deciduous storage capacity (mm);
t_e - Julian day on which the transition ends; and
t_b - Julian day on which the transition begins

for each day of the transition period.

Tables 7.3 and 7.4 list values taken from the literature for anthropogenic and vegetated surface types. The values used in this study area are: for paved surfaces 0.48 mm (Falk and Niemczynowicz, 1978); for roofs 0.25 mm (Davies and Hollis, 1982); for coniferous trees 1.2 mm (Shuttleworth, 1988a); for deciduous trees when leafless 0.3 mm and when in leaf 0.8 mm (Shuttleworth, 1988a); and for grass 1.3 mm (Zinke, 1967). The influence of changing the values assigned to surface types are discussed in the sensitivity analysis of the model in Chapter 8.

Table 7.3 Values of storage capacity for paved surfaces/roofs taken from the literature

Source	Surface Type	Storage capacity (mm)
Brater (1968)	Pavement	1.6
	Small paved area	1.0-2.5
Wright - McLaughlin Engineers (1969)	Large paved areas	1.3-3.8 (2.5)
	Roof - flat	2.5-7.6 (2.5)
	- sloped	1.3-2.5 (1.3)
Marsalek (1977)	Impervious	1.57 SWMM default
Mechler & Riecken (1977)	Impervious	1.6
Falk & Niemczynowicz (1978)	Parking lot	0.13
	Parking lot & road	1.05
	Bicy. & parking	0.48, 0.33
	Parking	0.52, 0.56, 0.56, 0.57
	Parking & road	0.51
Kidd (1978)	Urban	0.67 S.E. 0.11
		0.53 0.10
		0.49 0.12
		0.50 0.18
		0.45 0.10
		0.50 0.29
		0.32 0.12
		0.41 0.29
Davies & Hollis (1982)	Roof (pitched)	0.25
	Road	1.00
Pratt et al. (1984)	Roof (pitched)	1.08
Bulfill (1984)	Highway	1.30
		1.38
Niemczynomicz (1986)	Urban	0.7
Nouh(1986)	Residential-imperv	1.5

Table 7.4 Values of storage capacity for vegetation taken from literature

Source	Surface type	Storage capacity (mm)
Brater (1968)	Grassland	6.4
Wright-McLaughlin Engineers (1969)	Lawn grass	5.1-12.7 (7.6)
	Wooded areas & grass fields	5.1-15.2 (10.2)
Rutter et al. (1985)	Corsican pine	1.05
	Douglas fir	1.2
	Norway spruce	1.5
	Hornbeam - leafy	1.0
	- leafless	0.65
	Oak - leafy	0.875
	- leafless	0.275
	- defoliated	0.175
Marsalek (1977)	Urban - pervious	4.67
Mechler & Riecken (1977)	Pervious	6.4
Nouh (1986)	Residential-perv.	6.4
Shuttleworth (1988a)	Coniferous trees	1.2 ±0.3
	Deciduous - in leaf	0.8
	- leafless	0.3
Zinke (1967)	Grass	1.3

PART III MODEL PERFORMANCE AND CONCLUSIONS

CHAPTER 8 PERFORMANCE OF THE EVAPOTRANSPIRATION-INTERCEPTION MODEL

8.1 Introduction

The Penman-Monteith-Rutter-Shuttleworth evapotranspiration-interception model and modifications for its use in the urban environment were described in Chapter 1. In subsequent chapters sub-models required for the model have been developed and where possible tested. In this chapter the performance of the complete model is evaluated by comparison with measured latent heat flux densities at the Sunset suburban site. The results of sensitivity analyses of the model are also presented.

8.2 Structure of the model

The computer version of the model was written in FORTRAN-77 and run on an Amdahl 5860 mainframe computer at UBC. The code has also been run on an IBM-compatible personal computer using the WATFOR-77 compiler.

The complete model consists of the following components:

1) a modified version of the Schmid (1988) source area model (Chapter 3);
2) the surface database and acquisition subroutines (Chapter 3, Appendix V);
3) the anthropogenic heat flux model (Chapter 4);
4) the storage heat flux model (Chapter 5); and
5) the evapotranspiration model (Chapters 1, 7, 8).

The sub-models can be run together as one model or each of the sub-model components can be run as stand-alone models. The model is described here assuming that results of the source area model and database acquisition sub-models have already been obtained and are read in as hourly data.

The basic structure of the evapotranspiration-interception model is presented in Figure 8.1. The first step in a model run is to read the initial

Figure 8.1 Basic structure of evapotranspiration-interception model for urbanized areas.

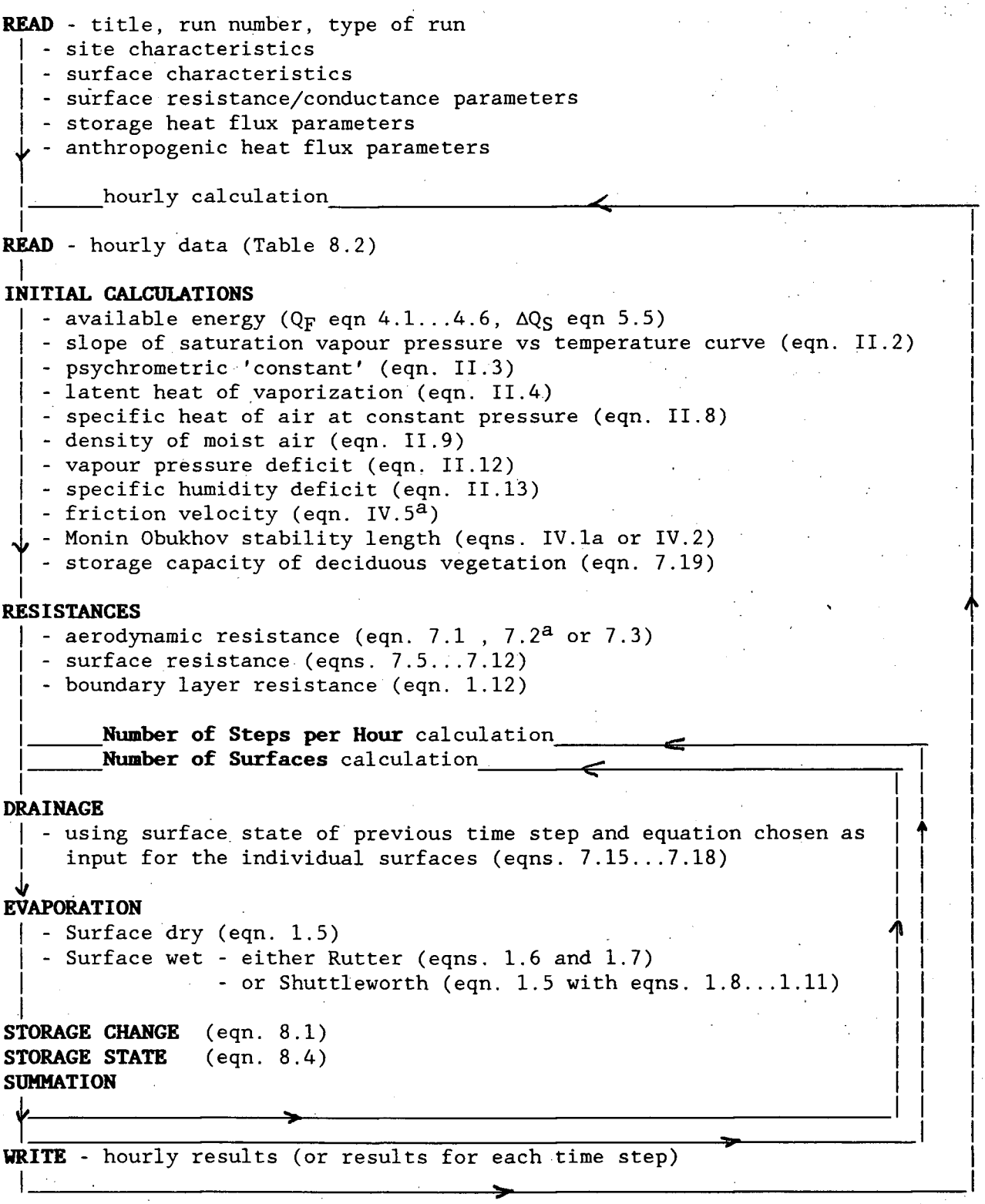

a calculated with eqns IV.6, IV.7, IV.9, IV.13, IV.14

data requirements. These are listed in Table 8.1. At this stage a number of choices are made about the type of run to be conducted:

1) The equation to be used for the calculation of evaporation during the transition between wet and dry surfaces has to be specified. The original Rutter et al. (1971) model uses a ratio of the amount of water on the canopy to the storage capacity (eqn. 1.7) with the Penman-Monteith equation when the surface is wet (eqn. 1.6). This means there is a change to equation 1.5 when the surface is dry. Shuttleworth (1978) proposed a physically continuous treatment of the transition between the wet and dry canopies (eqns. 1.8...1.11 with 1.5). This second form is the 'base' method of calculation in this study.

2) The method used to calculate the aerodynamic resistance has to be identified. The 'base' method is the non-neutral equation (7.2) which takes into account changing atmospheric stability. It should be noted that when all the data requirements are not met for this method (see section 7.2) the calculation defaults to the neutral method (eqn. 7.1). A comment is written into the output when this occurs.

3) The length of the sub-hour time step for the calculations, and therefore the number of steps per hour, is stated. When this type of model has been used in forest environments time steps of 120 (Shuttleworth, 1988b), 300 (Rutter et al., 1971) and 720 seconds (Sellers and Lockwood, 1981) have been used. The sub-hour time step allows for changes in the drainage rate, surface state (amount of water on the surface at any time) and therefore evapotranspiration rate within an hour. The 'base' time step used in this study is 300 seconds, i.e. 12 steps per hour (Fig. 8.1).

4) The form in which the hourly data are to be read has to be selected. Since many of the calculations are identical for repeated runs of the model, and require large amounts of input data it is possible to do some of the initial

Table 8.1 Initial data requirements for the model.

Title	Title or comment Run number
Type of run	Transition between wet and dry surface - Rutter (eqn. 1.7) or Shuttleworth (eqn. 1.8) Aerodynamic resistance type - neutral (eqn. 7.1), non-neutral (eqn. 7.2) or Thom & Oliver (1977) (eqn. 7.3) Time step in seconds Form in which hourly data to be read in i.e. if some of the initial calculations have been done or not
Site characteristics	Height of wind speed measurements Zero-plane displacement length Roughness length for momentum Number of surface types
Surface characteristics	Surface which is irrigated for each surface: - storage capacity - drainage function type - Falk & Niemczynowicz (eqn. 7.17) - Falk & Niemczynowicz (eqn. 7.18) - Rutter corrected (eqn. 7.16) - Rutter uncorrected (eqn. 7.15) - drainage coefficients (section 7.4): D_0, b - initial surface storage status Storage capacity transition deciduous winter-summer - day transition begins, ends - summer storage capacity
Surface resistance/ conductance parameters	Maximum leaf area index Maximum air temperature Minimum air temperature S_1, S_2 related to soil moisture deficit (eqn 7.11) Maximum net radiation $P_1 \ldots P_6$ parameters (eqns 7.5...7.12) Maximum/night-time surface resistance
Anthropogenic heat flux parameters	Energy used by a vehicle (eqn. 4.3) Total mean consumption by an individual consumer for the time period of study - by premise class for electricity & gas Gas efficiency (eqn. 4.5) Metabolic rate for people and animals by time of day
Storage heat flux parameters	a_1, a_2, a_3 parameters by surface type: Table 5.2

calculations before-hand and read these results in. An example of this is the calculation of available energy ($AE=Q^*+Q_F-\Delta Q_S$). To calculate all the components from scratch (i.e. to calculate both Q_F and ΔQ_S and then AE) for each hour requires a large amount of additional initial (Table 8.1) and hourly input (Table 8.2).

5) The number of surface types needed to characterize the study area has to be specified. In this study the 'base' number was six, namely: paved, built, coniferous, deciduous, grass unirrigated and grass irrigated. Note that this specifically refers to the evaporation calculation whereas other calculations require different aspects of the surface to be identified (e.g. Chapter 4). In addition to these choices values are assigned to the site and surface characteristics (Table 8.1) including values for the parameters for calculation of surface resistance, storage and anthropogenic heat fluxes and for determination of the source area of the flux.

The remainder of the model is in a loop involving reading in the data (Table 8.2) and performing the calculations for each hour. The initial calculations are listed in Figure 8.1 together with the appropriate equation numbers. Allowance is made for change in the storage capacity of deciduous vegetation as the leaves grow between winter and summer (eqn. 7.19).

The next step is the calculation for the hour of the aerodynamic (eqn. 7.1, 7.2 or 7.3), boundary layer (eqn. 1.12) and surface resistances (eqns. 7.5 ... 7.12). The remaining steps of the model are conducted for the number of steps per hour for the number of surface types (Fig. 8.1). After drainage and evapotranspiration have been calculated the surface storage change (ΔC) is calculated for each surface:

$$\Delta C = PX - D - E \qquad (8.1)$$

where PX - water arriving at the surface (mm);
D - drainage (mm); and

Table 8.2 Hourly data requirements for the model

	Units	Symbol	Comments
Day			
Hour			
Rainfall	mm	P	
Net radiation	W m^{-2}	Q*	
Wind speed	m s^{-1}	u	
Wind direction	°, rad	φ	
Standard deviation of φ	°, rad	σ_φ	
Air temperature	°C	T_d	
Wet bulb temperature	°C	T_W	
or relative humidity	%	RH	
Pressure	Pa	p	
Sensible heat flux or	W m^{-2}	Q_H	optional
temperature difference	°C	ΔT_d	optional
External water use	mm	wu	
Leaf area index	-	LAI	
Soil moisture deficit	mm	$\delta\theta$	
2-D fraction of:			
pavement	-		
built	-		
grass	-		
deciduous	-		
coniferous	-		
irrigated	-		
unirrigated	-		
Anthropogenic heat flux	W m^{-2}	Q_F	
or			
Length of road			
- major	m		
- minor	m		
Number of vehicles			
- major road	-		
- minor road	-		
Grid consumption			
- electricity	W		
- gas	J		
Number of consumers			
by premise type	-		
Number of people	-		
Number of animals	-		
Storage heat flux	W m^{-2}	ΔQ_S	
or			
Proportion of			Note: total area equals the sum
- 2D greenspace	-		of these four (see Table 5.1)
- 3D walls	-		
- 3D roof	-		
- 2D impervious	-		

E - evapotranspiration (mm).

For a non-irrigated surface:

$$PX = P \tag{8.2}$$

where P - rain (mm); and for an irrigated surface:

$$PX = P + wu \tag{8.3}$$

where wu - external water use (mm).

The state of each surface store (C) is then updated:

$$C_t = C_{t-1} - \Delta C \tag{8.4}$$

if $C_t \leq 0$ then for calculation purposes $C_t = 0$

where t - time.

When C_t is set to zero vegetation can continue to transpire as the plants have access to soil water. A running water balance is maintained for each surface type. The flux calculated for an individual hour is weighted for the surface types occurring in the source area of the measurements (Chapter 3). At the end of each hour these fluxes are written out (Table 8.3).

8.3 Performance of the Model

8.3.1 Methods used to compare the performance of the model

The performance of the model was compared with the measured latent heat flux densities collected at the Sunset site, Vancouver (see Chapters 2 & 6). The model was initialized with the surface dry, on JD 33 at 0000 LAT, and terminated on JD 179 at 0800 LAT, when field measurements ceased. In this 3513 hour period, when Q_E was modelled continuously, there are 2944 hours of measured Q_E (see Chapter 6) available for comparison.

The model's performance is evaluated at a number of temporal scales:

1) Hourly - each hour with measured flux data are compared to the corresponding modelled value.

Table 8.3 Output from the evapotranspiration-interception model

	Units	Comments
Day		
Hour		
Latent heat flux	W m^{-2}	
Evapotranspiration	mm	
Cumulative evapotranspiration	mm	
Drainage	mm	
Surface state	mm	whole & each surface type
Change	mm	
Comment	-	if not possible to calculate stability
Aerodynamic resistance	s m^{-1}	
Surface resistance	s m^{-1}	

2) Daily - fluxes for all measured hours available on a day are averaged and compared with the average modelled flux for those hours. Because of missing data this may mean that a 'day' does not necessarily consist of 24 hours.
3) Cumulative hourly - hours for which there are measurements are accumulated and compared with the cumulated modelled flux for the same hours. Again because of missing data the values are less than the 'true' total E for the time period (JD 33-179).
4) Ensemble hourly - for each month and for the whole time period (JD 33-179) the values for a particular hour are averaged.

The performance of the model, in particular the surface water state, was also compared with the wetness sensors (Chapter 2). The two wetness sensors, which were situated on unirrigated grass and on a coniferous tree/hedge, gave an indication of when these parts of the surface were wet or dry. They were not installed until JD 38.

8.3.2 'Base' run of the model

For the 'base' run of the model the values assigned to the various parameters were chosen from experience to be those considered to be the most physically realistic (Table 8.4) and are not a best-fit to the model. Drainage coefficients (Table 7.2) and surface storage capacities (Table 7.3, 7.4) were chosen from values given in the literature. The transition between summer and winter values for the deciduous vegetation storage capacity were based on panorama photographs taken approximately weekly from the tower. The model was run with the available energy already calculated using the models described in Chapter 4 and Chapter 5. The value of r_S max was set to 9999 s m^{-1} (following Shuttleworth, 1988b) when the calculated values of g_S approached zero or were negative.

Table 8.4 Values assigned to parameters for the 'base' run of the model

Parameter	Value assigned					
Title	Sunset, Vancouver, 1987					
Run number	1					
Type of run						
transition wet/dry	Shuttleworth (eqn. 1.8)					
r_a type	Non-neutral (eqn. 7.2)					
Time step of calculations (s)	300					
Site characteristics						
z_U (m)	22.50					
d (m)	3.50					
z_0 (m)	0.52					
Number of surface types	6					
Surface characteristics						
Surface	1 Pavement	2 Building	3 Coniferous	4 Deciduous	5 Grass unirrig	6 Grass irrig
S (mm)	0.48	0.25	1.2	0.3	1.3	1.3
D function (eqn. #)	7.18	7.18	7.17	7.17	7.17	7.18
coefficient - D_0	10	10	0.013	0.013	0.013	10
- b	3	3	1.71	1.71	1.71	3
C(t=0)	0.0	0.0	0.0	0.0	0.0	0.0
Deciduous transition						
T_b (JD)	65					
T_e (JD)	115					
S_{ds} (mm)	0.80					
Surface irrigated (surface #)	6					
Surface conductance						
Lm	3.10					
T_H (°C)	40.00					
T_L (°C)	0.00					
S1 (mm)	0.45					
S2 (mm)	15.00					
Qmax (W m^{-2})	725.00					
P_1 (mm s^{-1})	53.95					
P_2 (W m^{-2})	633.95					
P_3 (kg g^{-1})	0.0821					
P_4 (g kg^{-1})	8.91					
P_5 (°C)	18.88					
P_6 (m m^{-1})	0.0107					
r_S max (s m^{-1})	9999.00					

The statistics for the model's performance as compared to the measured Q_E are presented on an hourly and daily basis in Table 8.5. The statistics for the model are better on an hourly than a daily basis primarily because of the large number of hourly data points. Figures 8.2 and 8.3 are scatter plots of the hourly and daily measured versus modelled data points, respectively. In both figures the data are distributed around the one to one line. The hourly RMSE of 27.7 W m^{-2} can be considered to be of the same order as the error of the measurements. Figure 8.4 shows the cumulative E for the measurement period. From this it can be seen that the model generally under-predicts until JD 130. Towards the end of the study period the cumulative totals are almost identical.

Figure 8.5 shows the time series of measured and modelled Q_E. In the early part of the year the model under-predicts during the middle of the day. From mid-March onwards the model mimics the measured data extremely well under all conditions except for dewfall.

Plots of ensemble mean values of Q_E for the whole study period and for each month (Fig. 8.6a-f) illustrate model performance at the diurnal time scale, and changes in this seasonally. Figure 8.6a, for the entire study period, suggests that on average the model under-predicts in mid- to late-morning and slightly over-predicts in the late afternoon. The maximum ensemble mean difference of 17.6 W m^{-2} occurs at 1200 LAT when the measured flux is 137.7 W m^{-2}. From the monthly plots it can be seen that in the earlier months on average the model under-predicts (Fig. 8.6b,c,d) and later in the year over-predicts in the afternoons (Fig. 8.6e,f). In February (Fig. 8.6b) the model under-predicts all day. At 1200 LAT the mean modelled Q_E (50 W m^{-2}) is approximately half the mean measured value (99 W m^{-2}). In March and April (Fig. 8.6c,d) the model performs very well in the afternoon but under-predicts

Table 8.5 Statistics for the 'base' model values of Q_E

Statistic	Hourly	Daily
Number of points (n)	2944	125
Mean		
Measured ($W\ m^{-2}$)	40.10	40.49
Modelled ($W\ m^{-2}$)	40.38	41.87
Standard deviation (sd)		
Measured ($W\ m^{-2}$)	63.03	21.80
Modelled ($W\ m^{-2}$)	58.20	23.87
Slope - functional analysis (m_f)[a]	0.92	1.10
Coefficient of determination (r^2)	0.81	0.71
Root mean square error (RMSE)($W\ m^{-2}$)	27.65	13.00
RMSE systematic ($RMSE_S$)($W\ m^{-2}$)	10.72	2.17
RMSE unsystematic ($RMSE_U$)($W\ m^{-2}$)	25.49	12.82
Index of agreement (d)[b]	0.95	0.91
Goodness of fit (N&S)[c]	0.81	0.64

a Mark and Church (1977)
b Wilmott and Wicks (1980)
c Nash and Sutcliffe (1970)

Figure 8.2 Comparison of hourly measured and modelled Q_E for the 'base' model run

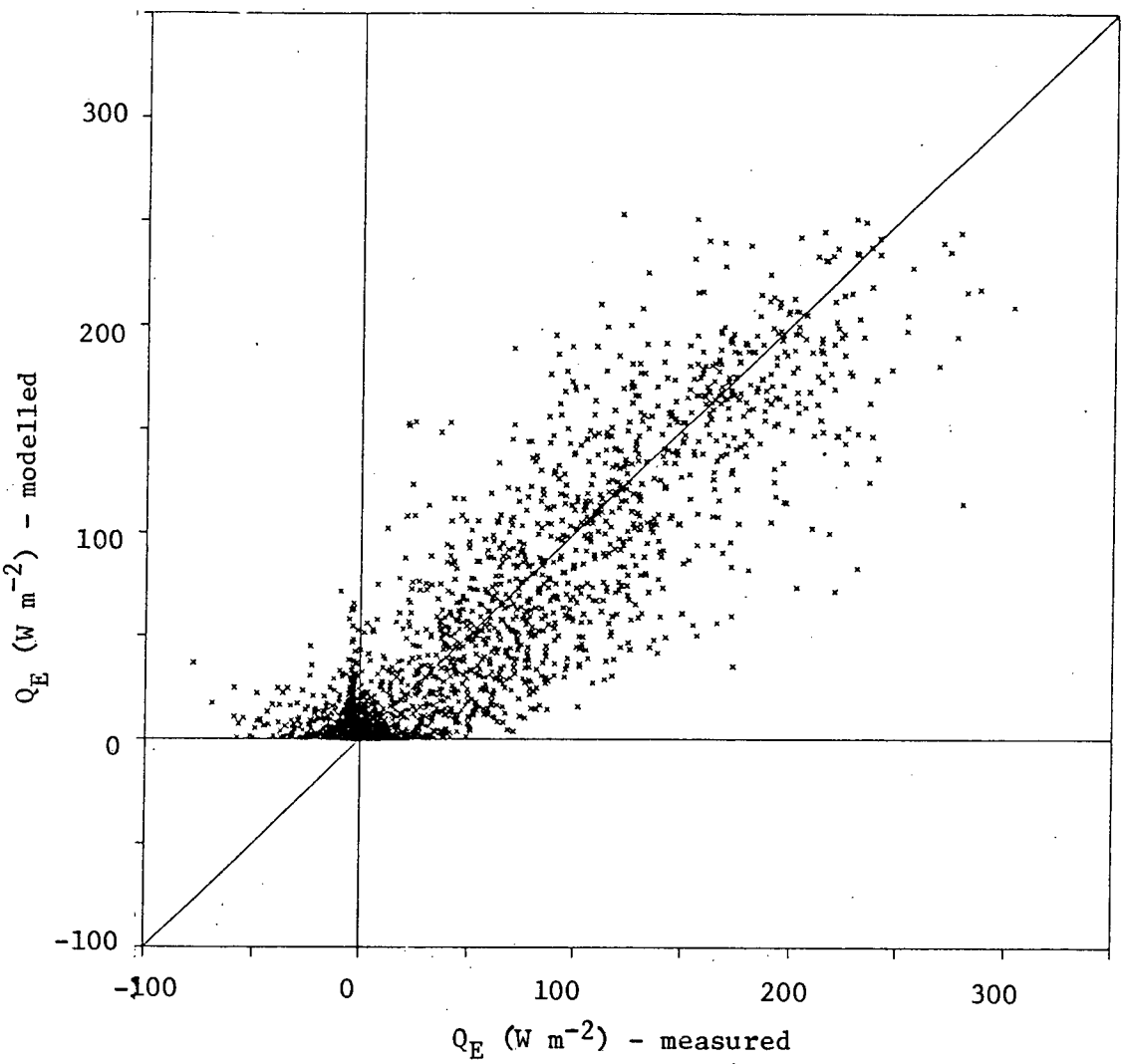

Figure 8.3 Comparison of daily measured and modelled Q_E for the 'base' model run

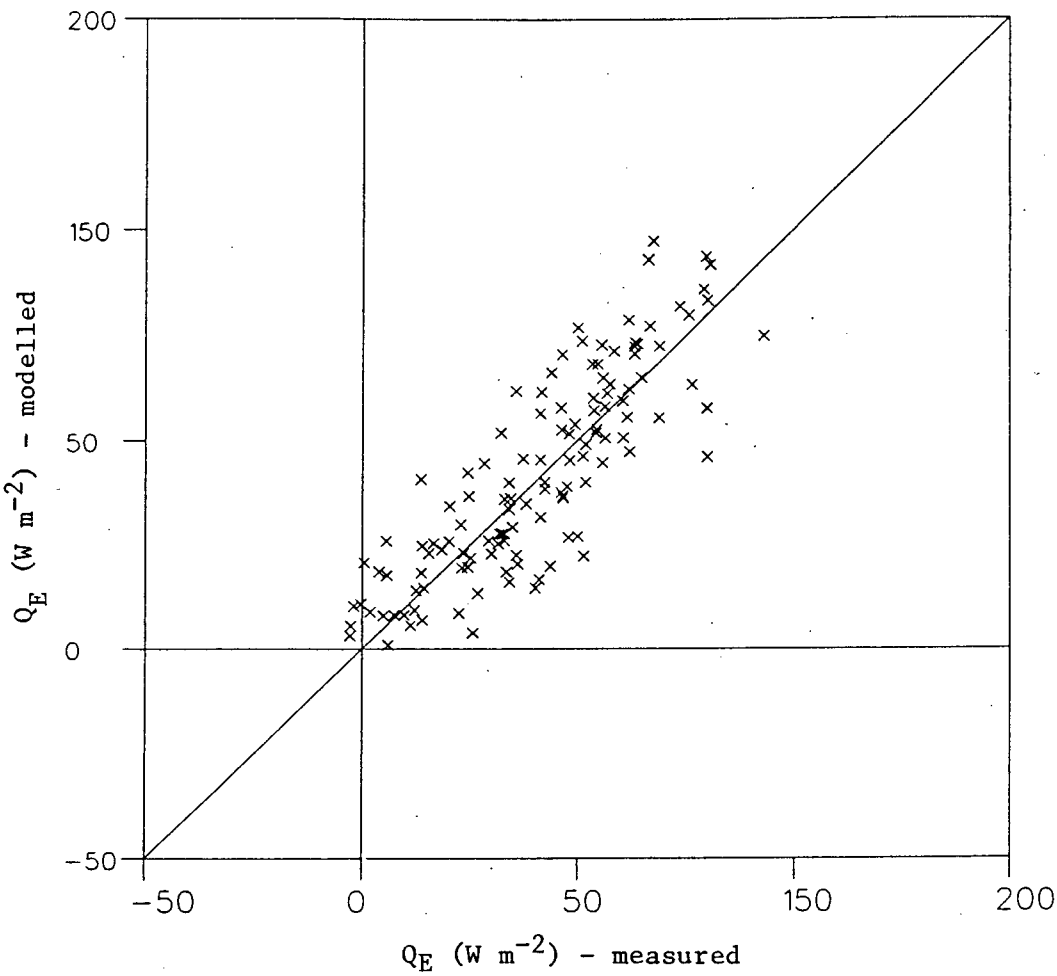

Figure 8.4 Cumulative plot of measured and modelled ('base' run) evaporation (see text for details).

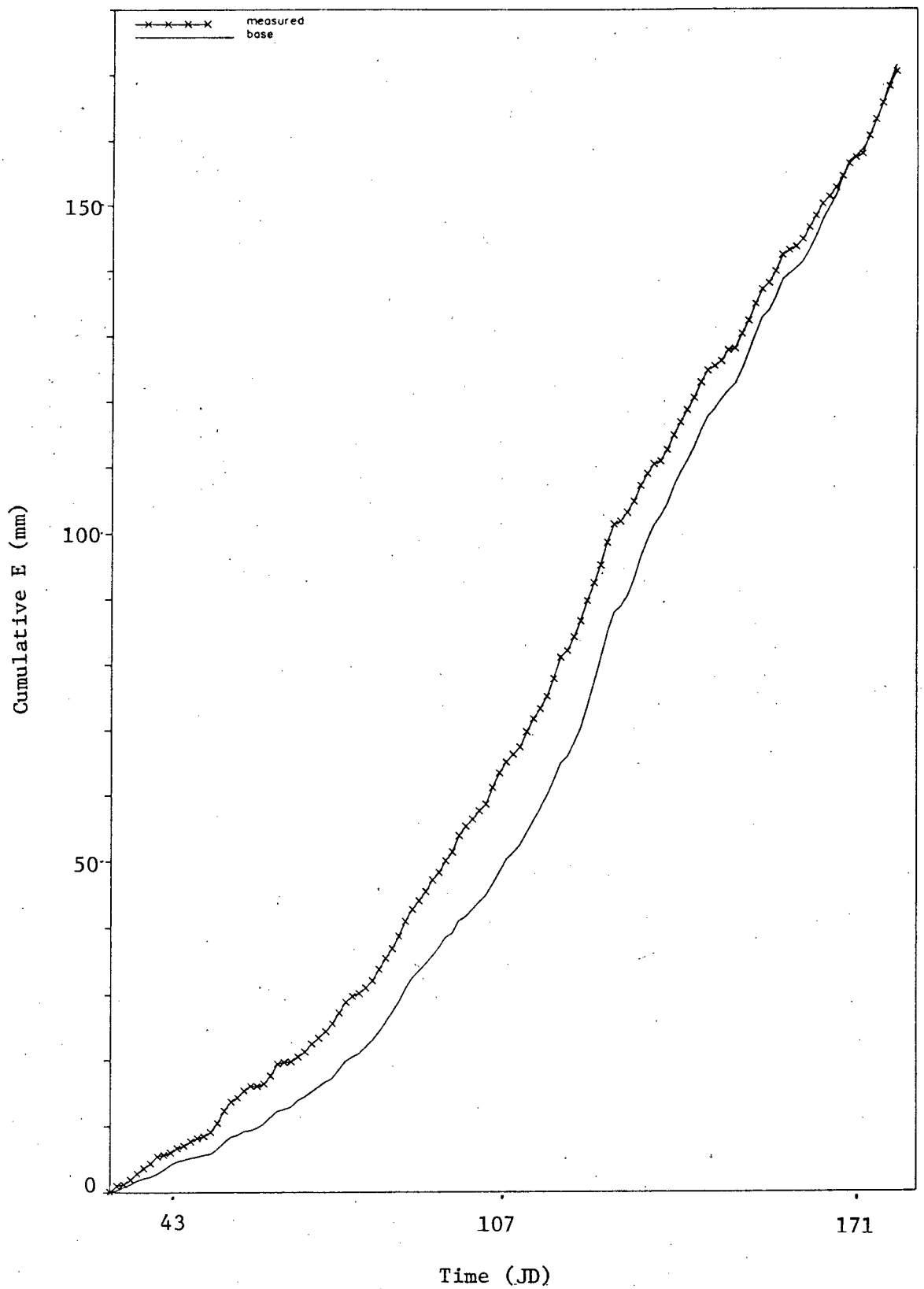

Figure 8.5 Time series of hourly measured (—) and modelled (--) Q_E (base). Note that the measured data are not continuous.

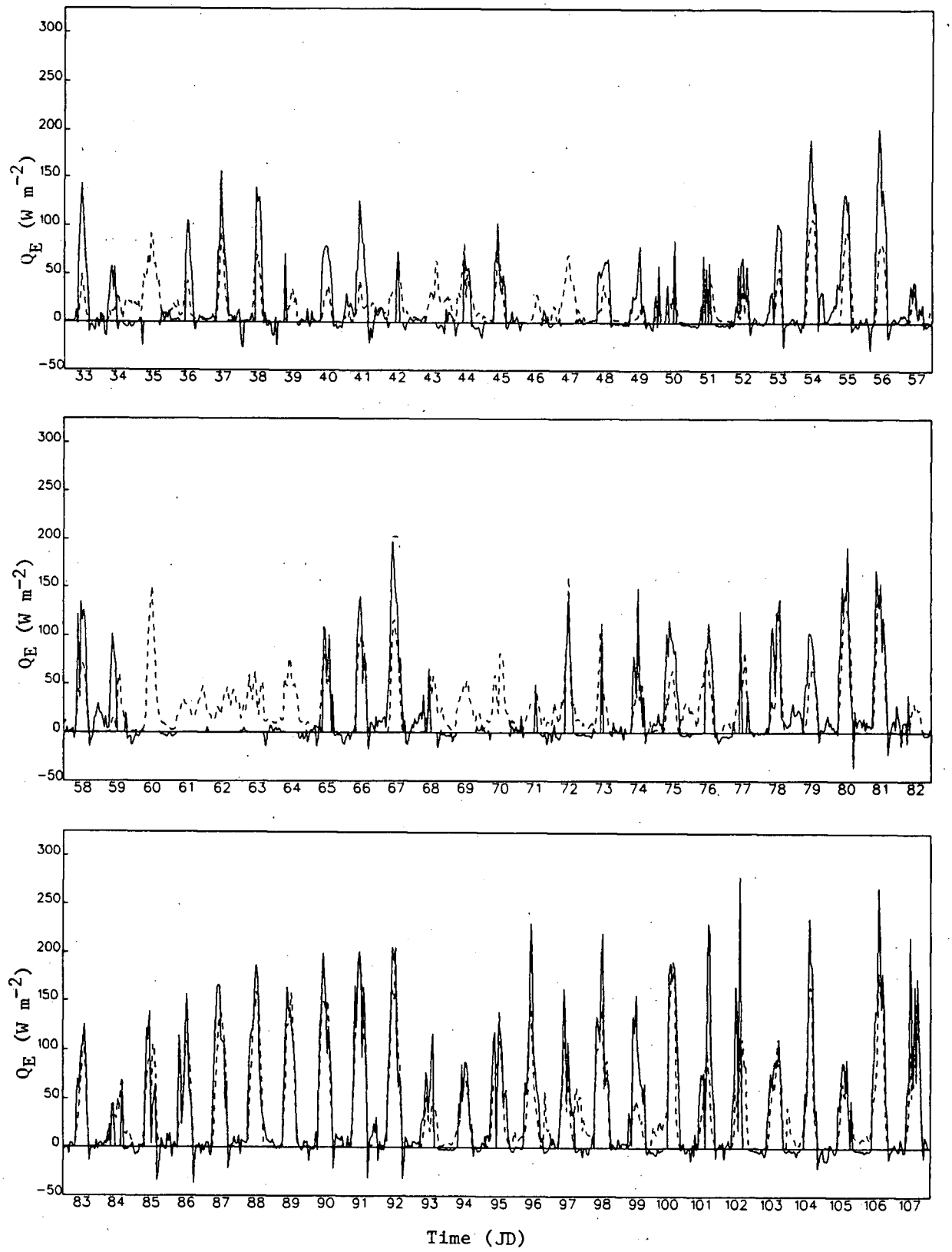

Figure 8.5 (cont.)

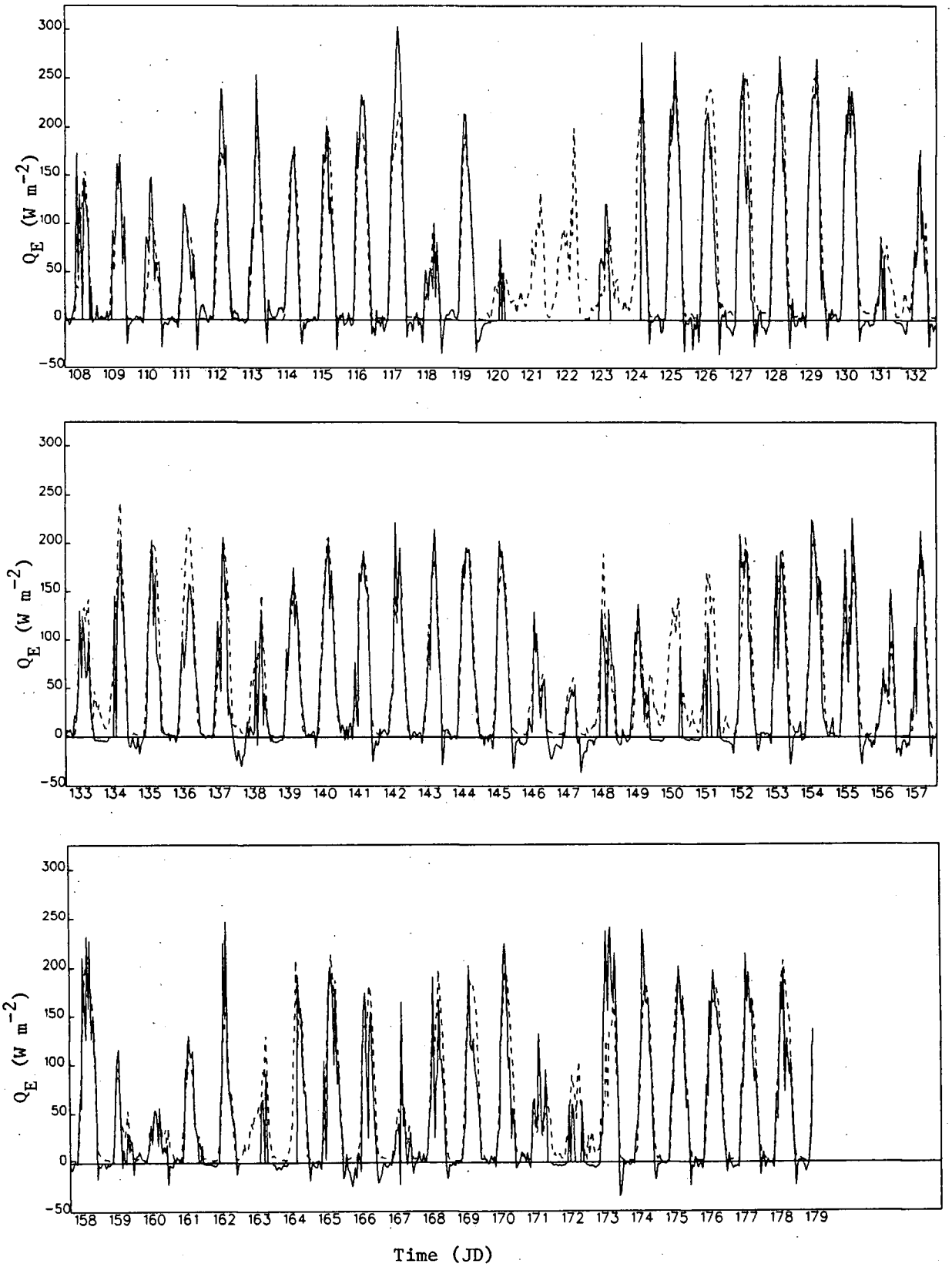

Figure 8.6 Ensemble plots of measured and modelled ('base' run) Q_E

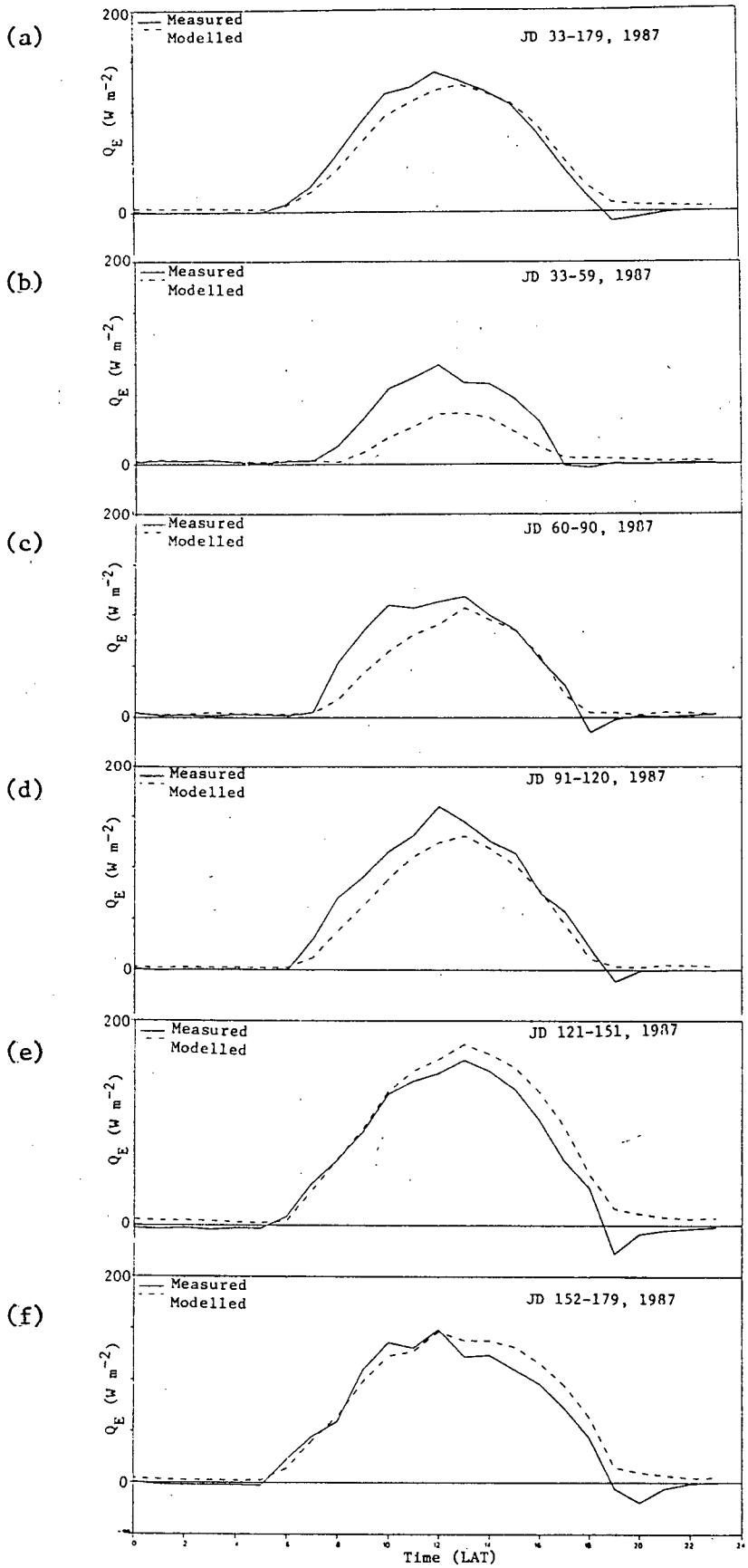

in the morning. In May and June (Fig. 8.6e,f) the opposite occurs; that is the model performs extremely well in the morning but over-predicts in the afternoon. From this it is concluded that the model does well on the average but for individual time periods the performance is not so good.

Figure 8.7 provides a means to compare the modelled surface state with that recorded by the wetness sensors. In each box of five traces the upper two plots show the water arriving at the surface; at the top is the rainfall received by all surfaces, and the second is the external water use (wu) which is only received by the irrigated grass portion of the surface. External water use did not begin until JD 121 (Chapter 2). The third plot shows the status of the wetness sensors (i.e. whether wet or dry). The sensor located on the grass (dashed line) has a smaller range than that located on the coniferous vegetation (solid line). The grass sensor range is from half way between wet and dry and the wet end. The fourth trace is the modelled surface water status of the whole surface and the fifth or lowest plot shows the modelled wetness status of the individual surface types. The six individual surfaces are not separately labelled but the vegetated surfaces are those which hold more water on the surface and the lesser values are the built and paved surfaces. Once irrigation begins the state of the irrigated grass surface (Fig. 8.7c,d the dashed line in the lowest plot) becomes distinguishable from the other surfaces. Looking at this set of figures (8.7a,b,c,d) it can be seen that the model does an extremely good job of indicating when the surface is dry. The modelled surface state follows a very similar path to the sensors. Visual observations of drying indicate that the paved and built surfaces dry more quickly than the vegetated surfaces and it can be seen in Figure 8.7 that the modelled paved and built surfaces mimic this pattern. This suggests that the drainage functions in the evaporation model are simulating the surface water

Figure 8.7 Plots of precipitation, water use, surface wetness and modelled surface water state (see text for details).

(a) JD 34-74

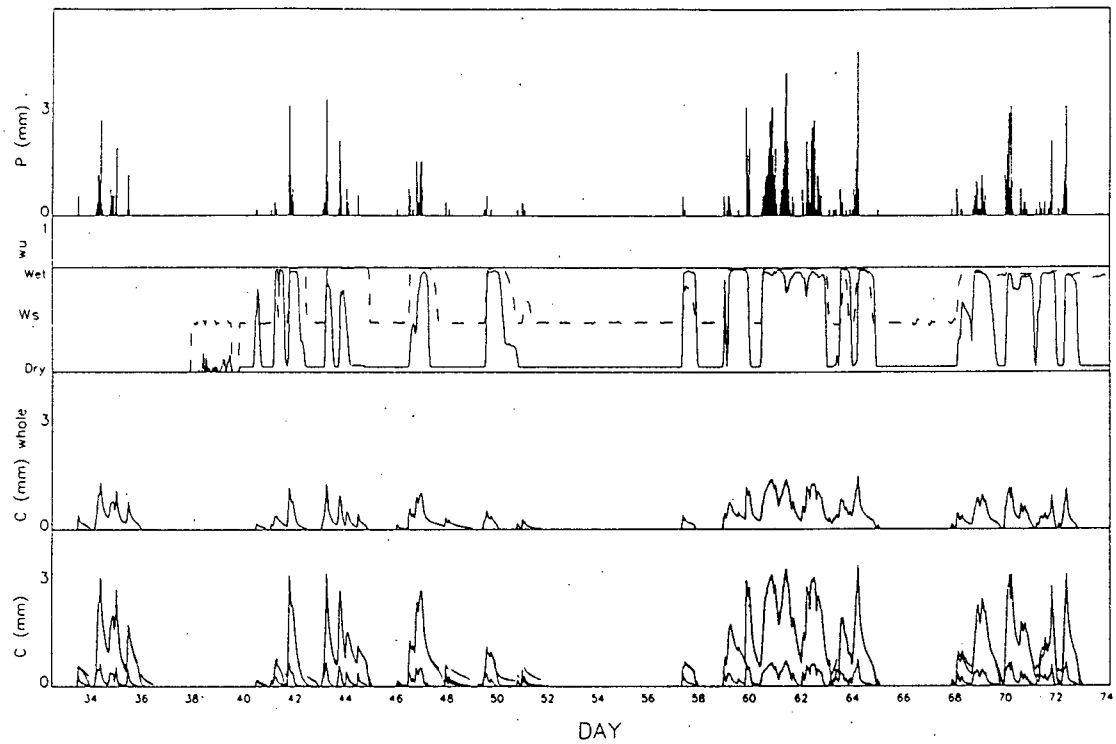

(b) JD 75-116

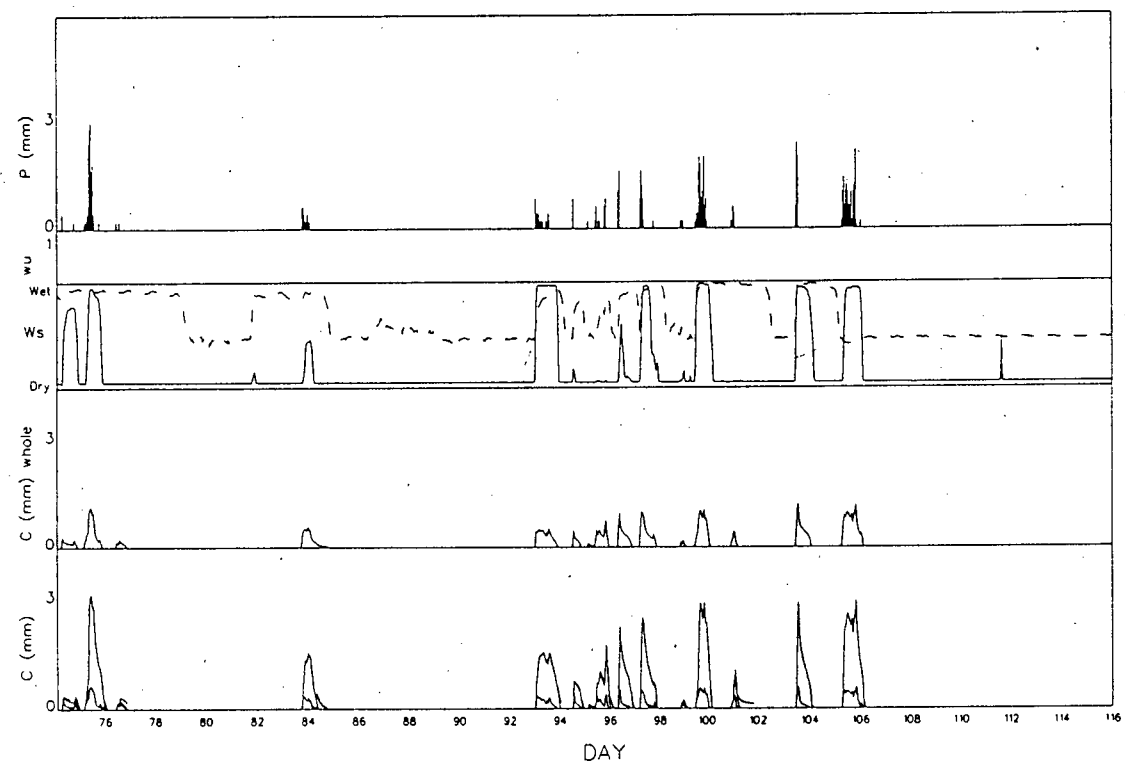

Figure 8.7 (cont.)

(c) JD 117-157

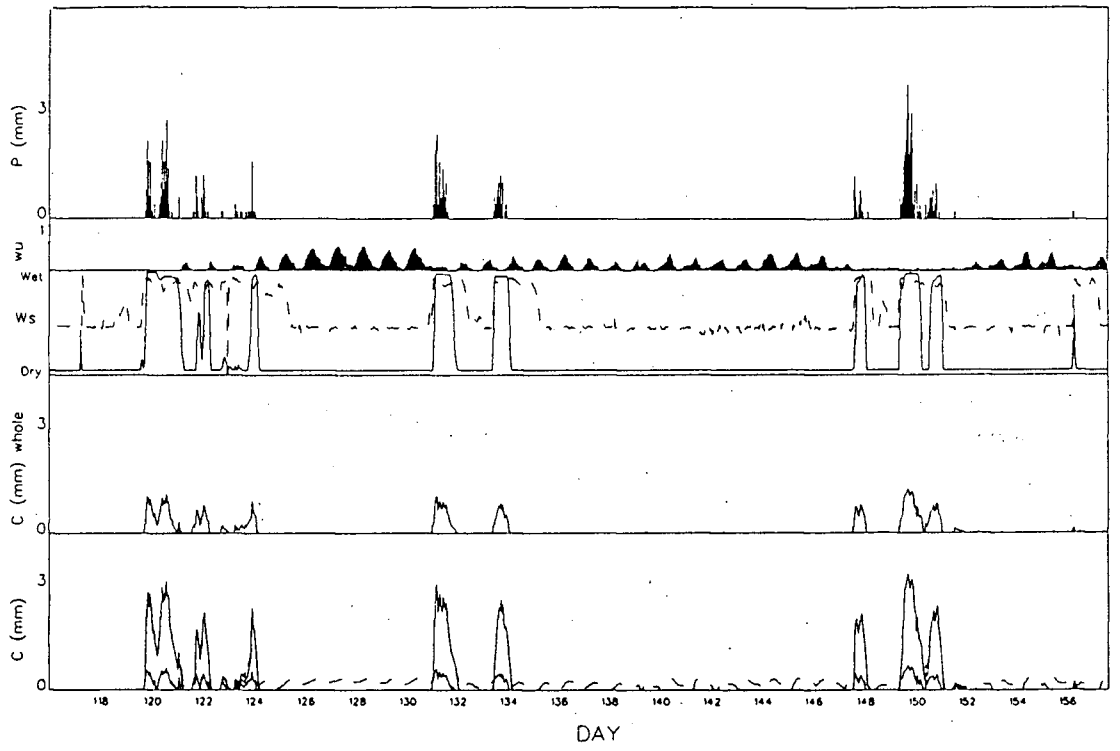

(d) JD 158-179

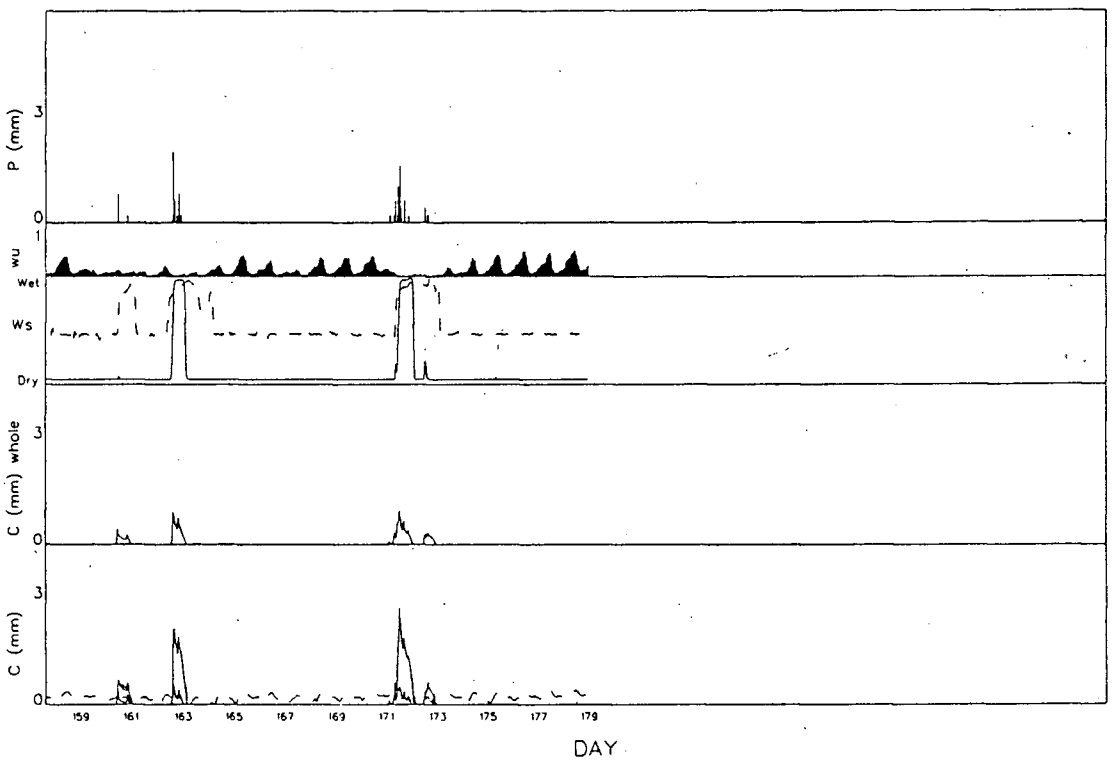

state appropriately. The only feature not well represented is the occurrence of dewfall. This was visually evident on the grass but not simulated.

In summary it appears that although the model does well on average it generally under-predicts in the early part of the year and performs better in the spring/early summer, although it may tend to over-predict. The modelled Q_E is always greater than zero. Dewfall is not predicted but was observed to occur on grass on some nights. Dewfall is thought to be one of the reasons why the model under predicts in the morning. The evaporation of dew and the drying of the surface in the morning will result in a larger measured evaporation rate. The over prediction of the model appears to coincide with the beginning of external water use. The over prediction may in part be due to the water use input being too large. The water use data used as hourly input were collected in another more affluent area of Vancouver (Chapter 2) and pro-rated for the area in the present study area.

8.4 Sensitivity analysis of the model

In order to assess the robustness of the model and its sensitivity to various input parameters and equations the performance of the model was investigated when various of the initial inputs (Table 8.1) were changed over a range of values. The effect of making such changes is reported in comparison to both the measured results and the 'base' run. In each case only the variable of interest was changed from the 'base' run (Table 8.4), unless otherwise specified. Cumulative plots are used to show the influence of the changes on the modelled evaporation (E) because they allow the seasonal effects to be gauged.

8.4.1 Rutter

The model was run after changing the way in which the transition between wet and dry was represented from the Shuttleworth approach (1.5 with 1.8, 1.9, 1.10, 1.11) to the two-step Rutter equations (1.5, 1.6, 1.7). The performance of the model using the Rutter instead of the Shuttleworth equations is significantly poorer (Table 8.6, Fig. 8.8). The model was run using three different conditions: firstly, (termed Rutter in Table 8.6) the only thing changed was the set of transition equations; secondly, (termed Rutter - drain 1) the model was run with a change of the drainage coefficient b for surfaces 1, 2,and 6 from 3 to 1.5 (see Table 8.4); and thirdly, (termed Rutter - drain 2) the drainage functions for all surfaces were set to equation 7.17 with D_0=0.0014 and b=5.25 (Shuttleworth, 1988b). For the first two runs, the model under-predicts consistently for all months which means the cumulative total E is considerably less than that measured (Fig. 8.8). Part of the problem is that the evaporation rates do not appear to be large enough to dry the surface completely. This may be overcome by using steeper drainage functions (i.e. more drainage per time step). The Rutter model appears to be very sensitive to the drainage functions. In view of this result and the relatively good performance of the Shuttleworth unified approach no further sensitivity runs were made with this form of the model.

8.4.2 Time step of calculations

As noted above this type of model has been run with 120, 300, and 720 s time steps. In the sensitivity analysis the model is run with a 3600 s interval in addition to these 3 time steps (Fig. 8.9, Table 8.7). Apart from the obvious increase in computational time, the effect of decreasing the

Table 8.6 Statistics of model performance for Q_E when the Rutter transition equations are used (see text for further explanation).

Statistic[a]	'Base'	Rutter	Rutter drain 1	Rutter drain 2
(a) Hourly				
Mean (W m^{-2})	40.38	10.07	5.80	43.82
sd (W m^{-2})	58.20	19.36	14.64	59.18
m_f	0.92	0.31	0.23	0.94
r^2	0.81	0.19	0.13	0.71
RMSE (W m^{-2})	27.65	64.78	68.62	34.56
$RMSE_S$ (W m^{-2})	10.72	62.38	67.24	13.61
$RMSE_U$ (W m^{-2})	25.49	17.46	13.69	31.76
d	0.95	0.51	0.48	0.91
N&S	0.81	-0.06	-0.19	0.70
(b) Daily				
Mean (W m^{-2})	41.87	10.56	6.05	45.15
sd (W m^{-2})	23.87	11.61	9.03	28.60
m_f	1.10	0.53	0.41	1.31
r^2	0.71	0.07	0.04	0.57
RMSE (W m^{-2})	13.00	37.06	40.85	19.32
$RMSE_S$ (W m^{-2})	2.17	35.33	39.88	4.66
$RMSE_U$ (W m^{-2})	12.82	11.21	8.86	18.75
d	0.91	0.47	0.43	0.84
N&S	0.64	-1.89	-2.51	0.21

a see Table 8.5 for explanation of statistics

Figure 8.8 Influence of using the Rutter and Shuttleworth transition equations on the cumulated E.

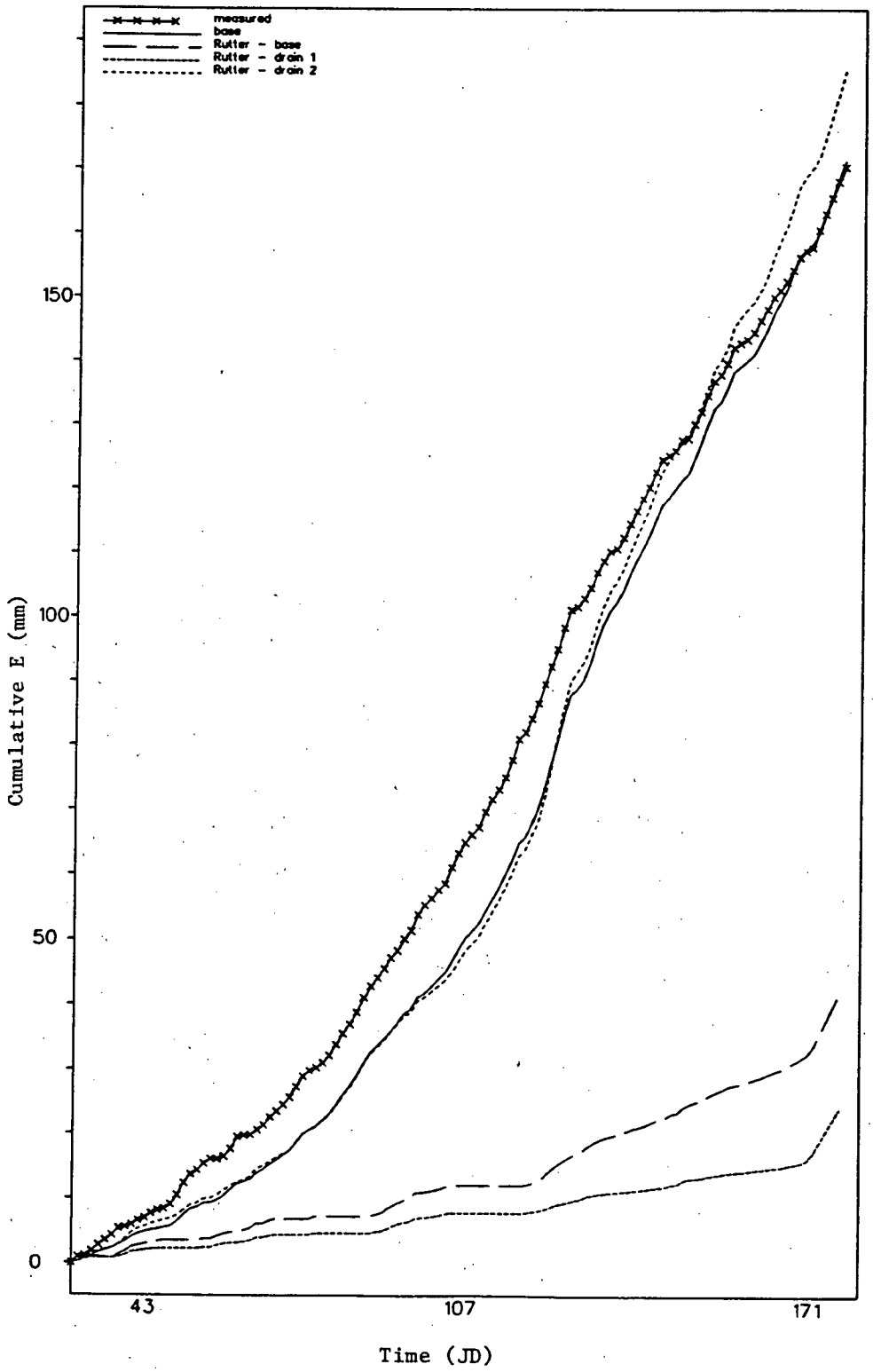

Figure 8.9 Influence of changing the time step of the calculation on the cumulated E.

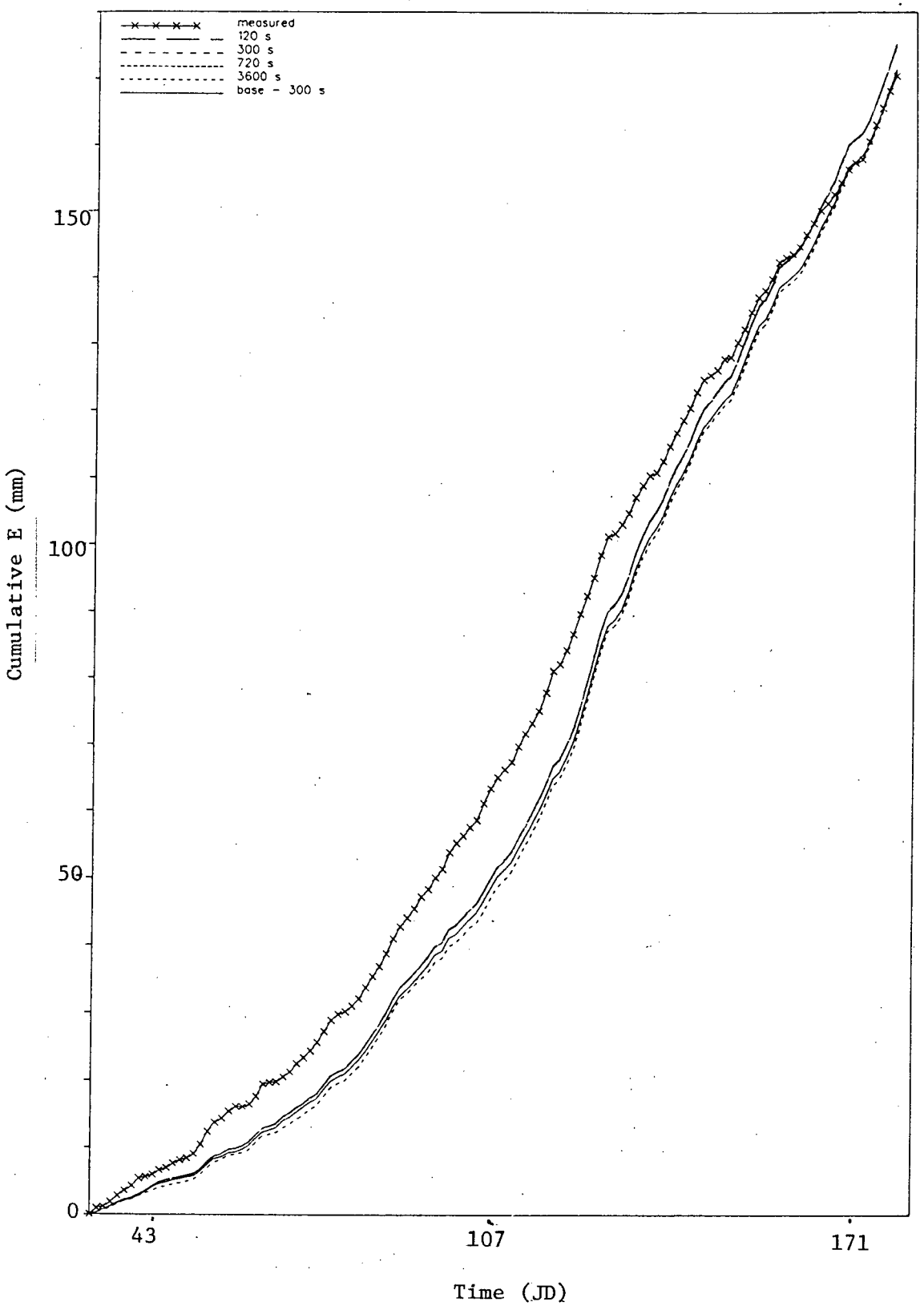

Table 8.7 Statistics of model performance for Q_E when the computational time step changed. Note base calculations have a 300 s time step but a different method of calculating r_S max (see section 8.4.4).

Statistic[a]	Computational time step (s) 'Base '	120	300	720	3600
(a) Hourly					
Mean (W m^{-2})	40.38	41.26	41.24	41.20	40.26
sd (W m^{-2})	58.20	57.67	57.67	57.68	57.86
m_f	0.92	0.91	0.91	0.92	0.92
r^2	0.81	0.80	0.80	0.80	0.81
RMSE (W m^{-2})	27.65	27.96	27.95	27.90	27.80
$RMSE_S$ (W m^{-2})	10.72	11.39	11.38	11.35	11.09
$RMSE_U$ (W m^{-2})	25.49	25.54	25.53	25.49	25.49
d	0.95	0.94	0.94	0.94	0.94
N&S	0.81	0.80	0.80	0.80	0.81
(b) Daily					
Mean (W m^{-2})	41.87	42.72	42.71	42.65	41.66
sd (W m^{-2})	23.87	24.19	24.19	24.23	24.60
m_f	1.10	1.11	1.11	1.11	1.13
r^2	0.71	0.71	0.71	0.71	0.72
RMSE (W m^{-2})	13.00	13.21	13.20	13.18	12.99
$RMSE_S$ (W m^{-2})	2.17	2.62	2.60	2.53	1.45
$RMSE_U$ (W m^{-2})	12.82	12.95	12.95	12.94	12.91
d	0.91	0.91	0.91	0.91	0.92
N&S	0.64	0.63	0.63	0.63	0.65

a See Table 8.5 for explanation of statistics

computational interval to 120 s (number of steps per hour=30) is not to improve the performance of the model (Table 8.7). Extending the interval to 720 s (number of steps per hour=5) shows slight improvement in the statistical performance of the model but otherwise no significant change in the results.

The effect of changing to 3600 s is to have the surface dry too quickly. Plots of the state of the surface show a series of spikes (Fig. 8.10) rather than the more realistic gradual drying (Fig. 8.7). There is slight improvement in the statistics for the performance of the model compared to the 720 s time step. The ensemble plots for each month do not change appreciably.

It would appear from these results that the model can be run at the longer 720 s time step rather than 300 s, and maintain a realistic surface state. Extending the time step to one hour, however, results in less realistic surface state predictions.

8.4.3 Aerodynamic resistance

The 'base' version of the model used the non-neutral r_a equation (7.2). Runs were made using the neutral and the Thom and Oliver (1977) equations for calculating r_a (eqns 7.1, 7.3 respectively). These lead to a slightly poorer set of statistics for model performance but the model does work slightly better in the earlier months (Table 8.8, Fig. 8.11). The model is not particularly sensitive to which equation is used and therefore it is not essential to have the input necessary to calculate the stability functions for the determination of r_a. There is very little difference between the modelled Q_E using the neutral and Thom and Oliver equations. The neutral equation generates slightly higher values for Q_E (Fig. 8.11).

Figure 8.10 Influence of using a 3600 s time step on the modelled water surface state. Note the spikes in the lower portion of the plot compared to Fig. 8.6.

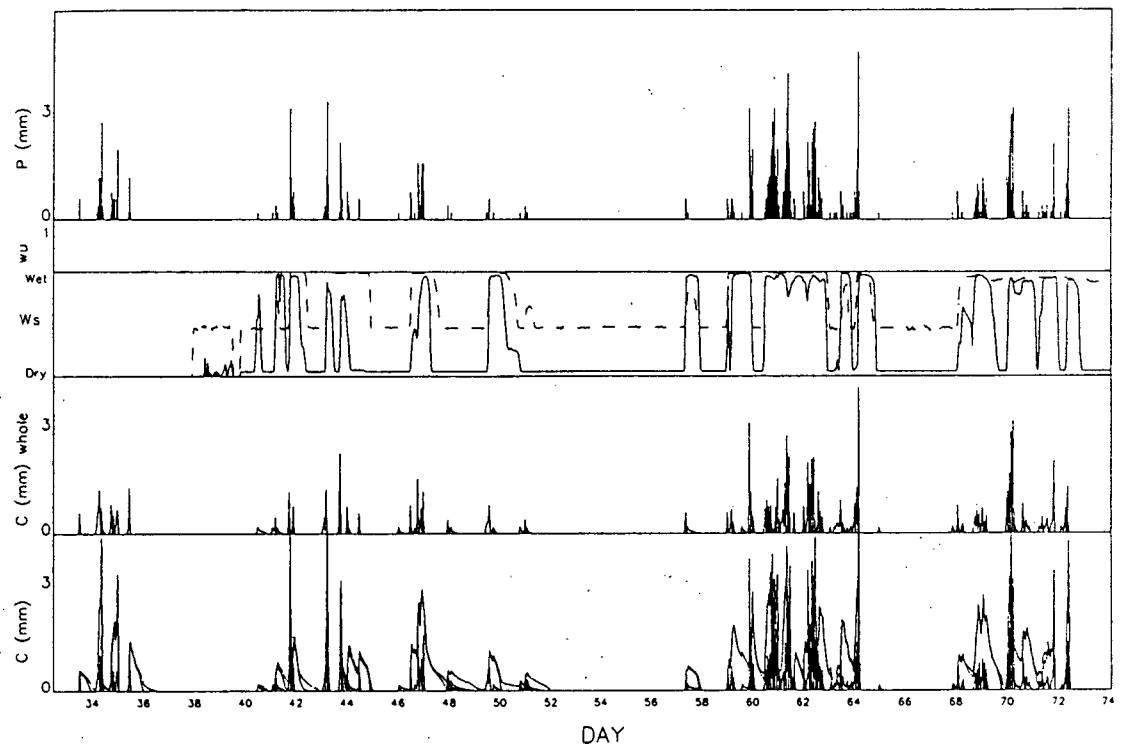

Table 8.8 Statistics of model performance for Q_E when the r_a equation is changed

Statistic[a]	r_a equation: Non-neutral[b]	Neutral	Thom & Oliver
(a) Hourly			
Mean (W m^{-2})	40.38	42.13	41.64
sd (W m^{-2})	58.20	59.74	58.14
m_f	0.92	0.95	0.92
r^2	0.81	0.79	0.79
RMSE (W m^{-2})	27.65	29.07	29.00
$RMSE_S$ (W m^{-2})	10.72	10.09	11.47
$RMSE_U$ (W m^{-2})	25.49	27.26	26.64
d	0.95	0.94	0.94
N&S	0.81	0.79	0.78
(b) Daily			
Mean (W m^{-2})	41.87	43.71	43.25
sd (W m^{-2})	23.87	24.54	24.13
m_f	1.10	1.13	1.11
r^2	0.71	0.68	0.67
RMSE (W m^{-2})	13.00	14.39	14.27
$RMSE_S$ (W m^{-2})	2.17	3.59	3.43
$RMSE_U$ (W m^{-2})	12.82	13.94	13.85
d	0.91	0.90	0.90
N&S	0.64	0.56	0.57

a See Table 8.5 for explanation of statistics
b Base equation

Figure 8.11 Influence of equation used to calculate aerodynamic resistance on cumulated E.

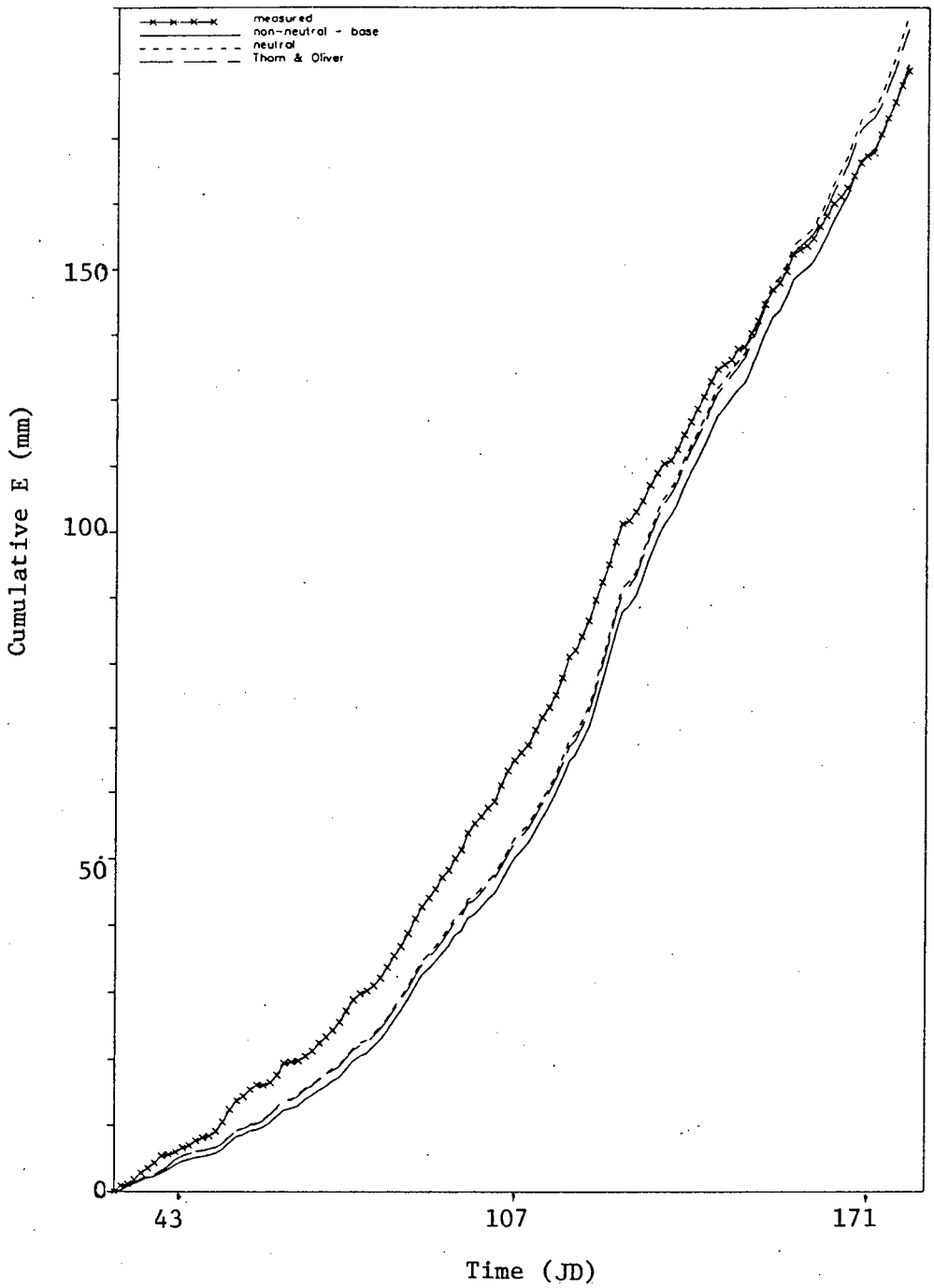

8.4.4 Surface resistance

The changes made to the model relating to r_S can be split into two types: firstly those concerning the r_S maximum; and, secondly those changing the values of the parameters used within the r_S sub-model (see section 7.3).

The model was run with five different methods to deal with large r_S (or g_S approaching zero) and when Q* is negative. In the 'base' run when g_S approaches zero or becomes negative r_S is set to 9999 s m^{-1}. In the other four cases r_S was set to 9999, 2500, 1250 or 750 s m^{-1} when Q* is negative. Table 8.9 contains the hourly and daily statistics for the comparison with these changes. It can be seen that there is very little difference between the 'base' run and those when r_S max was set to 9999 s m^{-1}. As the value of r_S max is decreased the performance deteriorates slightly. Figure 8.12 shows a systematic influence on the cumulative plots. This is primarily due to the fact that as r_S max is reduced night-time values of Q_E increase, and therefore accumulated Q_E becomes larger. However, the daytime performance is not improved.

The values of the r_S parameters ($P_1 \ldots P_6$) were changed between the three sets of model parameters presented in Table 7.1 (AD2 were the 'base' parameters). Table 8.10 presents the statistics for the hourly and daily comparisons. The 'base' results are generally slightly better than when the other two sets of parameters were used. Figure 8.13 shows the cumulative plot for the three sets of r_S parameters and the measured values. Using AD1 and All parameters the calculated day-time fluxes are slightly less than for the 'base' case. The values obtained using AD1 are smaller than those using the All parameters. The AD1 and All versions of the runs remain closer to parallel with the measured cumulative E during the later months, suggesting that they are better at predicting Q_E than the AD2 ('base') parameters which are over-

Table 8.9 Statistics of model performance for Q_E when r_S max is changed

Statistic[a]	r_S max (s m^{-1}) 9999	2500	1250	750	'Base'
(a) Hourly					
Mean (W m^{-2})	40.38	41.24	42.28	43.51	40.38
sd (W m^{-2})	58.20	57.67	57.07	56.42	58.20
m_f	0.92	0.91	0.91	0.90	0.92
r^2	0.81	0.80	0.80	0.79	0.81
RMSE (W m^{-2})	27.65	27.95	28.43	29.16	27.65
$RMSE_S$ (W m^{-2})	10.72	11.38	12.24	13.37	10.72
$RMSE_U$ (W m^{-2})	25.49	25.53	25.65	25.91	25.49
d	0.95	0.94	0.94	0.94	0.95
N&S	0.81	0.80	0.80	0.79	0.81
(b) Daily					
Mean (W m^{-2})	41.88	42.71	43.71	44.91	41.87
sd (W m^{-2})	23.87	24.19	24.56	24.99	23.87
m_f	1.10	1.11	1.13	1.15	1.10
r^2	0.71	0.71	0.72	0.72	0.71
RMSE (W m^{-2})	13.01	13.20	13.52	14.01	13.00
$RMSE_S$ (W m^{-2})	2.17	2.60	3.38	4.47	2.17
$RMSE_U$ (W m^{-2})	12.83	12.95	13.09	13.28	12.82
d	0.91	0.91	0.91	0.91	0.91
N&S	0.64	0.63	0.62	0.59	0.64

a See Table 8.5 for explanation of statistics

Figure 8.12 Influence of the maximum value assigned to r_s on cumulated E.

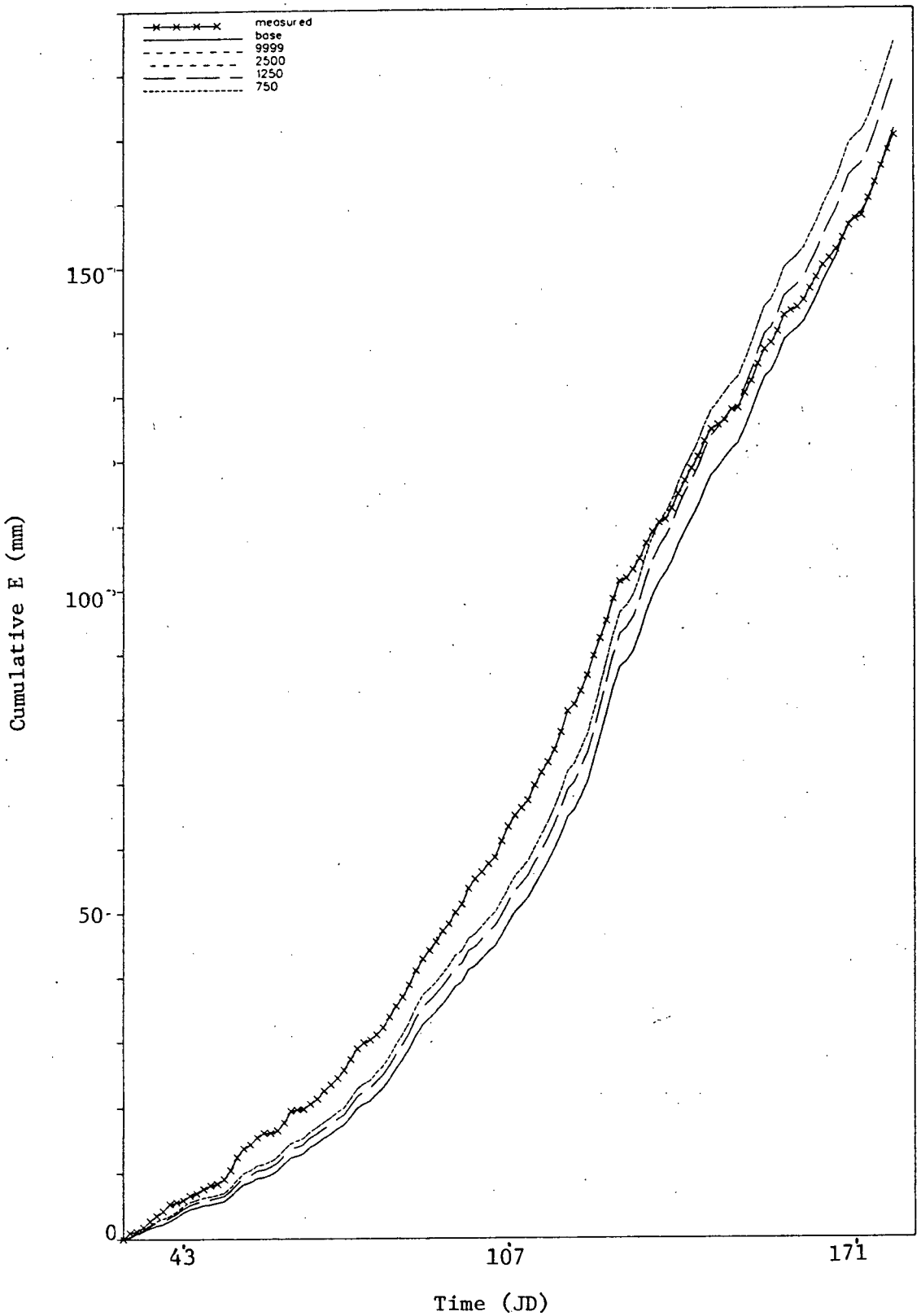

Table 8.10 Statistics of model performance for Q_E when r_S parameters are changed

Statistic[a]	r_S parameters ADl	All	'base'
(a) Hourly			
Mean (W m^{-2})	39.20	39.84	40.38
sd (W m^{-2})	56.31	57.43	58.20
m_f	0.89	0.91	0.92
r^2	0.81	0.81	0.81
RMSE (W m^{-2})	27.64	27.65	27.65
$RMSE_S$ (W m^{-2})	12.45	11.42	10.72
$RMSE_U$ (W m^{-2})	24.68	25.53	25.49
d	0.94	0.95	0.95
N&S	0.81	0.81	0.81
(b) Daily			
Mean (W m^{-2})	40.68	41.32	41.87
sd (W m^{-2})	22.85	23.52	23.87
m_f	1.05	1.08	1.10
r^2	0.70	0.71	0.71
RMSE (W m^{-2})	12.81	12.93	13.00
$RMSE_S$ (W m^{-2})	2.70	2.20	2.17
$RMSE_U$ (W m^{-2})	12.52	12.74	12.82
d	0.91	0.91	0.91
N&S	0.65	0.65	0.64

a See Table 8.5 for explanation of statistics

Figure 8.13 Influence of the parameters used for calculating r_s on cumulated E.

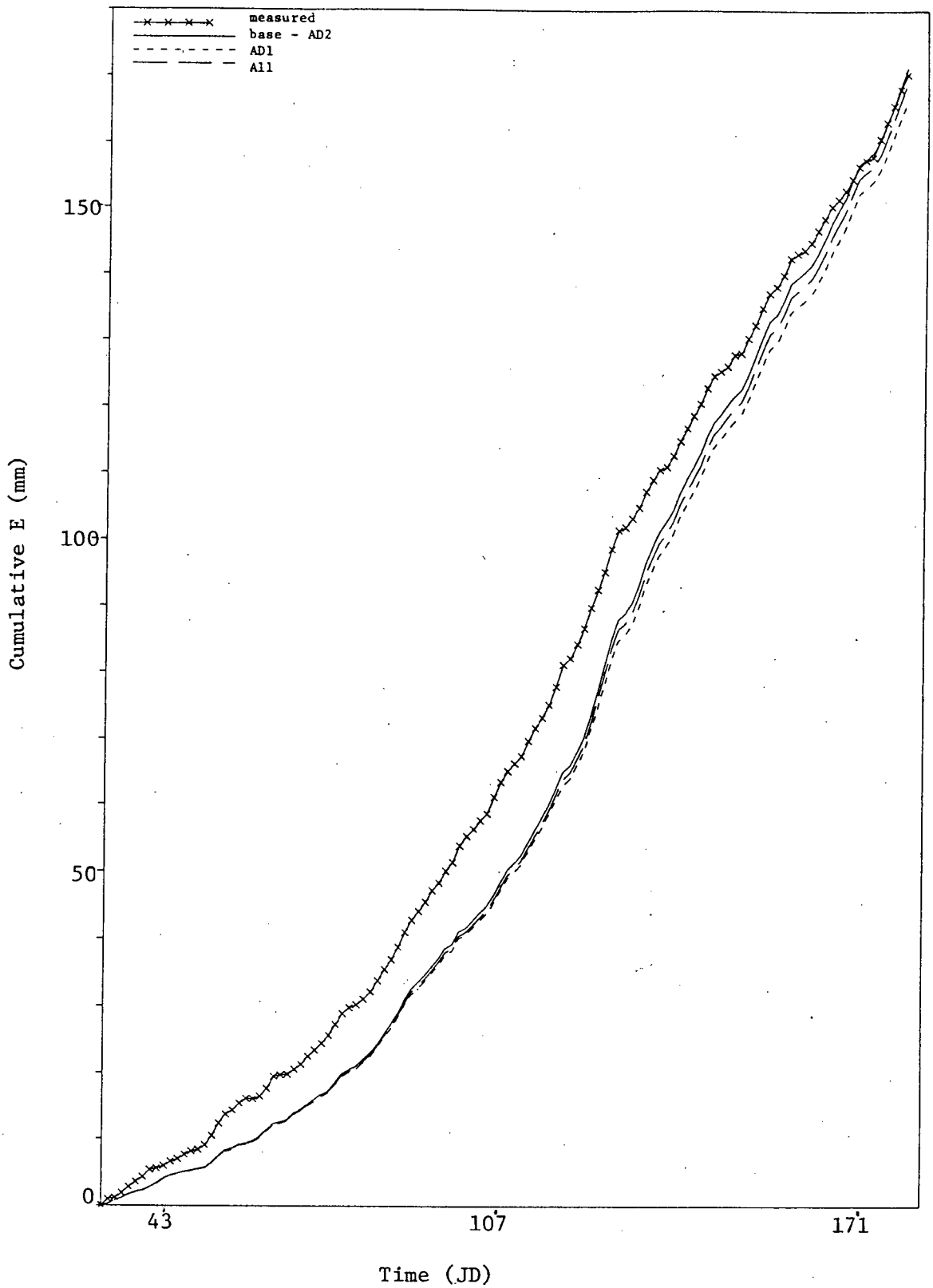

predicting.

The model responds to reasonably small changes in r_S (as will be produced by changing r_S model parameters) but it is not so sensitive as to make the use of any of the models in section 7.3 unwise.

8.4.5 Storage capacities

Three types of changes were made to the model relating to the storage capacity (S): firstly, changing the value of S for an individual surface and keeping the remainder of the surfaces at the base value; secondly changing all surface values on a single run; and thirdly, changing the storage capacity in conjunction with the drainage functions. The results of the latter alterations are discussed in the drainage section which follows.

The storage capacity of each of the surface types was changed over a range of values determined from previous studies (Tables 7.3, 7.4). It should be appreciated that the magnitude of the response of the model depends not only on the change in the value of S but also on the relative abundance of the surface type within the study area (see Chapter 3). A priori it is to be expected that changes to the deciduous and coniferous vegetation have the least effect because they occupy the two smallest areas within the current study site, whereas changes in the grass capacity will have the most effect.

For paved surfaces S was changed from 0.30 to 2.50 mm (Table 8.11). The effect of this is to decrease the mean modelled value of Q_E and the RMSE, $RMSE_S$ and $RMSE_U$. The systematic error for the MSE of the daily Q_E shows an improvement from 3.4% to 1.6%. This suggests that model performance would be improved by increasing the size of S for the paved surfaces, although there is less than 1 W m^{-2} change in the ensemble values for each of the months. However, the overall results show that the model is not particularly sensitive

Table 8.11 Statistics of model performance for Q_E when S the value of S is changed for the pavement

Statistic[a]	S capacity (mm) - pavement 0.3	0.48[b]	0.56	1.00	2.50
(a) Hourly					
Mean (W m^{-2})	40.55	40.38	40.32	40.13	39.96
sd (W m^{-2})	58.19	58.20	58.21	58.23	58.25
m_f	0.92	0.92	0.92	0.92	0.92
r^2	0.81	0.81	0.81	0.81	0.81
RMSE (W m^{-2})	27.72	27.65	27.63	27.56	27.52
$RMSE_S$ (W m^{-2})	10.76	10.72	10.70	10.64	10.60
$RMSE_U$ (W m^{-2})	25.54	25.49	25.47	25.42	25.40
d	0.95	0.95	0.95	0.95	0.95
N&S	0.81	0.81	0.81	0.81	0.81
(b) Daily					
Mean (W m^{-2})	42.07	41.87	41.81	41.57	41.39
sd (W m^{-2})	23.76	23.87	23.90	24.03	24.14
m_f	1.09	1.10	1.10	1.10	1.11
r^2	0.71	0.71	0.71	0.72	0.72
RMSE (W m^{-2})	13.04	13.00	12.99	12.94	12.91
$RMSE_S$ (W m^{-2})	2.40	2.17	2.09	1.83	1.62
$RMSE_U$ (W m^{-2})	12.82	12.82	12.82	12.81	12.81
d	0.91	0.91	0.91	0.92	0.92
N&S	0.64	0.64	0.65	0.65	0.65

a See Table 8.5 for explanation of statistics
b 'Base' value

to changes in the size of S within the range of values reported in the literature.

The influence of changing S for buildings from 0.25 to 2.50 mm (Table 8.12) results in a very similar response in the calculated Q_E as for the changes in S of the pavement. This is quite reassuring given that it is difficult to measure and/or assign absolute values to this parameter (see for example Falk & Niemczynowicz, 1978).

The response to changes in the size of S for coniferous vegetation from 0.75 to 2.5 mm (Table 8.13), the size of the winter and summer values of S for deciduous vegetation, and the timing of the transition between these (Table 8.14) are virtually undetectable. This is in large part due to their relative insignificance in the Sunset study area in terms of proportions of surface cover (Fig. 3.9).

The values assigned to S for grass were varied over the large range quoted in the literature (Table 7.4) from 0.5 to 10.2 mm (Table 8.15, Fig. 8.14). The irrigated and unirrigated grass were assigned the same value except for the one case where the unirrigated grass was assigned a larger value of 10.2 mm compared to the irrigated value of 7.6 mm. The model showed a distinct response to the increase in the size of S for grass for two reasons. Firstly, the size of the changes to S are much larger than for other surface types because a wider range of values have been reported in the literature (see Tables 7.3, 7.4); and secondly, because grass is the most extensive individual surface type in the study area. Three things are apparent from Figure 8.13: firstly, for grass the smaller the value of S the larger the modelled E; secondly, increasing the size of S beyond a certain point (smaller than 6.4 mm) has no further influence on calculated E; and thirdly, once external water use begins (JD 121), which occurs on a portion of the grass, there is a

Table 8.12 Statistics of model performance for Q_E when the value of S is changed for buildings

Statistic[a]	S capacity (mm) - buildings 0.25[b]	0.48	1.00	2.50
(a) Hourly				
Mean (W m^{-2})	40.38	40.18	39.94	39.77
sd (W m^{-2})	58.20	58.23	58.26	58.29
m_f	0.92	0.92	0.92	0.93
r^2	0.81	0.81	0.81	0.81
RMSE (W m^{-2})	27.65	27.61	27.54	27.52
$RMSE_S$ (W m^{-2})	10.72	10.67	10.61	10.57
$RMSE_U$ (W m^{-2})	25.49	25.46	25.42	25.40
d	0.95	0.95	0.95	0.95
N&S	0.81	0.81	0.81	0.81
(b) Daily				
Mean (W m^{-2})	41.87	41.64	41.37	41.18
sd (W m^{-2})	23.87	24.01	24.17	24.28
m_f	1.10	1.10	1.11	1.11
r^2	0.71	0.71	0.72	0.72
RMSE (W m^{-2})	13.00	12.98	12.93	12.91
$RMSE_S$ (W m^{-2})	2.17	1.91	1.58	1.38
$RMSE_U$ (W m^{-2})	12.82	12.84	12.83	12.84
d	0.91	0.91	0.92	0.92
N&S	0.64	0.65	0.65	0.65

a See Table 8.5 for explanation of statistics
b 'Base' value

Table 8.13 Statistics of model performance for Q_E when the value of S is changed for coniferous vegetation

Statistic[a]	S capacity (mm) - coniferous vegetation 0.75	0.90	1.20[b]	1.50	2.0	2.5
(a) Hourly						
Mean (W m^{-2})	40.39	40.39	40.38	40.37	40.36	40.35
sd (W m^{-2})	58.20	58.20	58.20	58.20	58.20	58.19
m_f	0.92	0.92	0.92	0.92	0.92	0.92
r^2	0.81	0.81	0.81	0.81	0.81	0.81
RMSE (W m^{-2})	27.65	27.65	27.65	27.65	27.65	27.65
RMSES (W m^{-2})	10.72	10.72	10.72	10.72	10.72	10.72
$RMSE_U$ (W m^{-2})	25.49	25.49	25.49	25.49	25.49	25.49
d	0.95	0.95	0.95	0.95	0.95	0.95
N&S	0.81	0.81	0.81	0.81	0.81	0.81
(b) Daily						
Mean (W m^{-2})	41.88	41.88	41.87	41.86	41.85	41.84
sd (W m^{-2})	23.86	23.86	23.87	23.88	23.88	23.88
m_f	1.09	1.09	1.10	1.09	1.09	1.10
r^2	0.71	0.71	0.71	0.71	0.71	0.71
RMSE (W m^{-2})	13.00	13.00	13.00	13.00	13.00	13.00
$RMSE_S$ (W m^{-2})	2.18	2.18	2.17	2.16	2.15	2.13
$RMSE_U$ (W m^{-2})	12.82	12.82	12.82	12.82	12.82	12.82
d	0.91	0.91	0.91	0.91	0.91	0.91
N&S	0.65	0.64	0.64	0.64	0.64	0.64

a See Table 8.5 for explanation of statistics
b 'Base' value

Table 8.14 Statistics of model performance for Q_E when the value of S and the timing of the transition period is changed for deciduous vegetation

	S capacity (mm) - deciduous vegetation								
Winter:	0.20	0.30[b]	0.40	0.30	0.20	0.30	0.40	0.30	0.30
Summer:	0.80	0.80	0.80	0.60	0.60	0.90	0.90	0.80	0.80
T_b (JD):	65	65	65	65	65	65	65	85	45
T_e (JD):	115	115	115	115	115	115	115	95	135
Statistic[a]									
(a) Hourly									
Mean (W m^{-2})	40.38	40.38	40.39	40.40	40.40	40.38	40.39	40.38	40.39
sd (W m^{-2})	58.20	58.20	58.21	58.21	58.21	58.20	58.20	58.20	58.21
m_f	0.92	0.92	0.92	0.92	0.92	0.92	0.92	0.92	0.92
r^2	0.81	0.81	0.81	0.81	0.81	0.81	0.81	0.81	0.81
RMSE (W m^{-2})	27.65	27.65	27.66	27.66	27.65	27.65	27.66	27.66	27.64
$RMSE_S$ (W m^{-2})	10.72	10.72	10.71	10.71	10.71	10.72	10.72	10.72	10.71
$RMSE_U$ (W m^{-2})	25.48	25.49	25.50	25.50	25.50	25.49	25.50	25.50	25.49
d	0.95	0.95	0.95	0.95	0.95	0.95	0.95	0.95	0.95
N&S	0.81	0.81	0.81	0.81	0.81	0.81	0.81	0.81	0.81
(b) Daily									
Mean (W m^{-2})	41.87	41.87	41.89	41.90	41.89	41.87	41.88	41.87	41.88
sd (W m^{-2})	23.87	23.87	23.86	23.86	23.86	23.87	23.86	23.87	23.86
m_f	1.09	1.10	1.09	1.09	1.09	1.09	1.09	1.09	1.09
r^2	0.71	0.71	0.71	0.71	0.71	0.71	0.71	0.71	0.71
RMSE (W m^{-2})	13.00	13.00	13.01	13.01	13.01	13.00	13.00	13.01	13.00
$RMSE_S$ (W m^{-2})	2.17	2.17	2.19	2.20	2.19	2.17	2.18	2.17	2.18
$RMSE_U$ (W m^{-2})	12.82	12.82	12.82	12.82	12.82	12.82	12.82	12.83	12.82
d	0.91	0.91	0.91	0.91	0.91	0.91	0.91	0.91	0.91
N&S	0.64	0.64	0.64	0.64	0.64	0.64	0.64	0.64	0.64

a See Table 8.5 for explanation of statistics
b 'Base' value

Table 8.15 Statistics of model performance for Q_E when the value of S is changed for irrigated and unirrigated grass

	S capacity (mm) grass				
Irrigated	0.5	1.3[b]	6.4	7.6	7.6
Unirrigated	0.5	1.3	6.4	7.6	10.2
Statistic[a]					
(a) Hourly					
Mean (W m^{-2})	43.08	40.38	38.03	37.91	37.87
sd (W m^{-2})	59.91	58.20	56.72	56.65	56.65
m_f	0.95	0.92	0.90	0.90	0.90
r^2	0.78	0.81	0.83	0.83	0.83
RMSE (W m^{-2})	30.07	27.65	26.42	26.39	26.40
$RMSE_S$ (W m^{-2})	10.58	10.72	11.69	11.75	11.76
$RMSE_U$ (W m^{-2})	28.15	25.49	23.70	23.63	23.63
d	0.94	0.95	0.95	0.95	0.95
N&S	0.77	0.81	0.82	0.82	0.82
(b) Daily					
Mean (W m^{-2})	44.66	41.87	39.44	39.31	39.25
sd (W m^{-2})	26.09	23.87	22.45	22.39	22.42
m_f	1.20	1.10	1.13	1.03	1.03
r^2	0.67	0.71	0.75	0.75	0.75
RMSE (W m^{-2})	15.60	13.00	11.58	11.53	11.52
$RMSE_S$ (W m^{-2})	4.20	2.17	2.61	2.69	2.68
$RMSE_U$ (W m^{-2})	15.02	12.82	11.28	11.21	11.21
d	0.89	0.91	0.93	0.93	0.93
N&S	0.49	0.64	0.72	0.72	0.72

a See Table 8.5 for explanation of statistics
b 'Base' value

Figure 8.14 Influence of the value assigned to the surface storage capacity of grass on cumulated E.

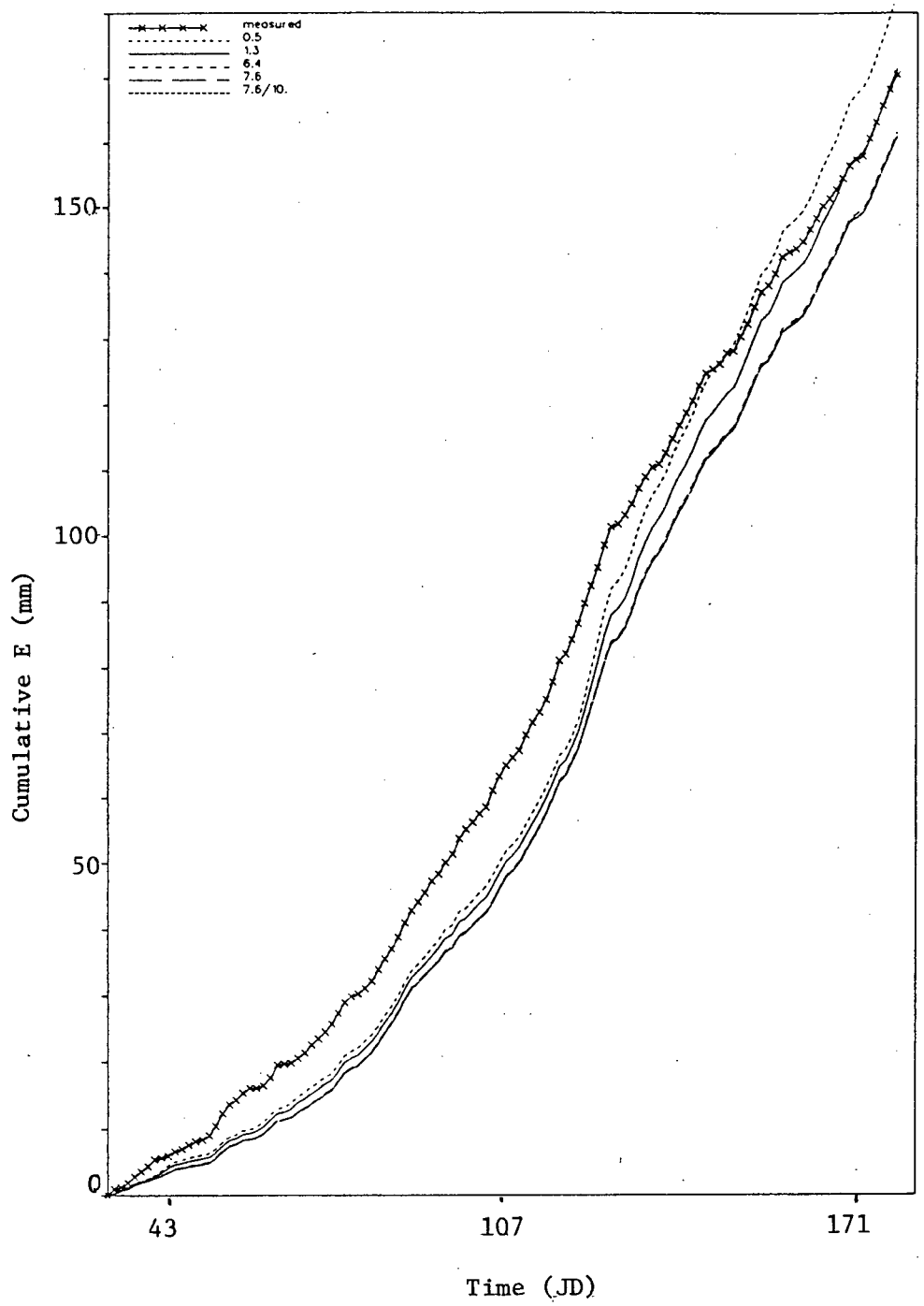

distinct increase in the modelled values of E (i.e. a steeper slope in Fig. 8.14). The statistics show slightly contradicting effects of changing the size of S at the hourly and daily scales. With increasing S the hourly statistics show a decreased m_f, an increased r^2, a decreased RMSE and $RMSE_U$ but an increased $RMSE_S$. On a daily basis however increasing S is associated with a decrease in RMSE, and in both the $RMSE_S$ and $RMSE_U$. The hourly ensemble data show that the largest difference from the 'base' results occurs at 1800 hours LAT. In the winter the difference at this time was ≤ 7 W m^{-2} for S=0.5 mm. During June the difference was ≤ 20 W m^{-2}. With large values of S the modelled Q_E was reduced by 2-3 W m^{-2} during the winter, and in June the maximum difference in the morning is approximately 6 W m^{-2} and in the late afternoon approximately 15 W m^{-2}. It would appear from this sensitivity analysis the size which influences the modelled Q_E is around the value of 1.3 mm suggested by Zinke (1967). The larger values although called depression storage capacity in the literature (see section 7.4) may represent a 'lumped fit' to other parts of larger runoff models rather than physically realistic values.

The second type of changes to the storage capacities involved altering all the values of S for the different surfaces at one time. Four runs of this type were conducted (see Table 8.16 for details): firstly, all values of S were decreased to small values for each of the respective surface types (see Tables 7.3, 7.4); secondly, all surfaces were assigned large values; thirdly, all storage capacities were set to 0.5 mm; and fourthly, all were set to 1.0 mm. Figure 8.15 shows the effect of these changes on cumulated E. All of the runs under-predict Q_E until the onset of irrigation, as does the base run. After that time the slope of the cumulative curve steepens considerably for all runs except for the curve for the case where S was assigned a large value for each surface. For all curves, except for the base run, after about JD 145 the

Table 8.16 Statistics of model performance for Q_E when S capacity changed for all surface types

	S capacity (mm) - all surfaces				
	small	base	large	all	all
S pavement	0.30	0.48	2.50	0.5	1.0
S building	0.25	0.25	2.50	0.5	1.0
S coniferous	0.75	1.20	2.50	0.5	1.0
S deciduous[b]	0.20	0.30	0.40	0.495	0.995
S grass	0.50	1.30	7.60	0.5	1.0
Statistic[a]					
(a) Hourly					
Mean (W m^{-2})	43.26	40.38	36.85	47.39	45.72
sd (W m^{-2})	59.92	58.20	56.92	63.03	62.33
m_f	0.95	0.92	0.90	1.00	0.99
r^2	0.78	0.81	0.83	0.75	0.77
RMSE (W m^{-2})	30.16	27.65	26.48	33.40	31.71
$RMSE_S$ (W m^{-2})	10.66	10.72	11.75	11.15	10.13
$RMSE_U$ (W m^{-2})	28.21	25.49	23.73	31.49	30.05
d	0.94	0.95	0.95	0.93	0.93
N&S	0.77	0.81	0.82	0.72	0.75
(b) Daily					
Mean (W m^{-2})	44.87	41.87	38.09	49.20	47.39
sd (W m^{-2})	25.99	23.87	23.21	29.27	28.77
m_f	1.19	1.10	1.06	1.34	1.32
r^2	0.66	0.71	0.76	0.60	0.63
RMSE (W m^{-2})	15.66	13.00	11.76	20.46	18.90
$RMSE_S$ (W m^{-2})	4.42	2.17	2.87	8.76	6.97
$RMSE_U$ (W m^{-2})	15.03	12.82	11.40	18.49	17.57
d	0.88	0.91	0.93	0.83	0.85
N&S	0.48	0.64	0.71	0.12	0.25

a See Table 8.5 for explanation of statistics
b Deciduous value for winter
Deciduous values for summer using the same headings as above
for summer 0.60 0.80 0.90 0.5 1.0

Figure 8.15 Influence of changing all the surface storage capacities on the cumulated E (see text and Table 8.16 for further details).

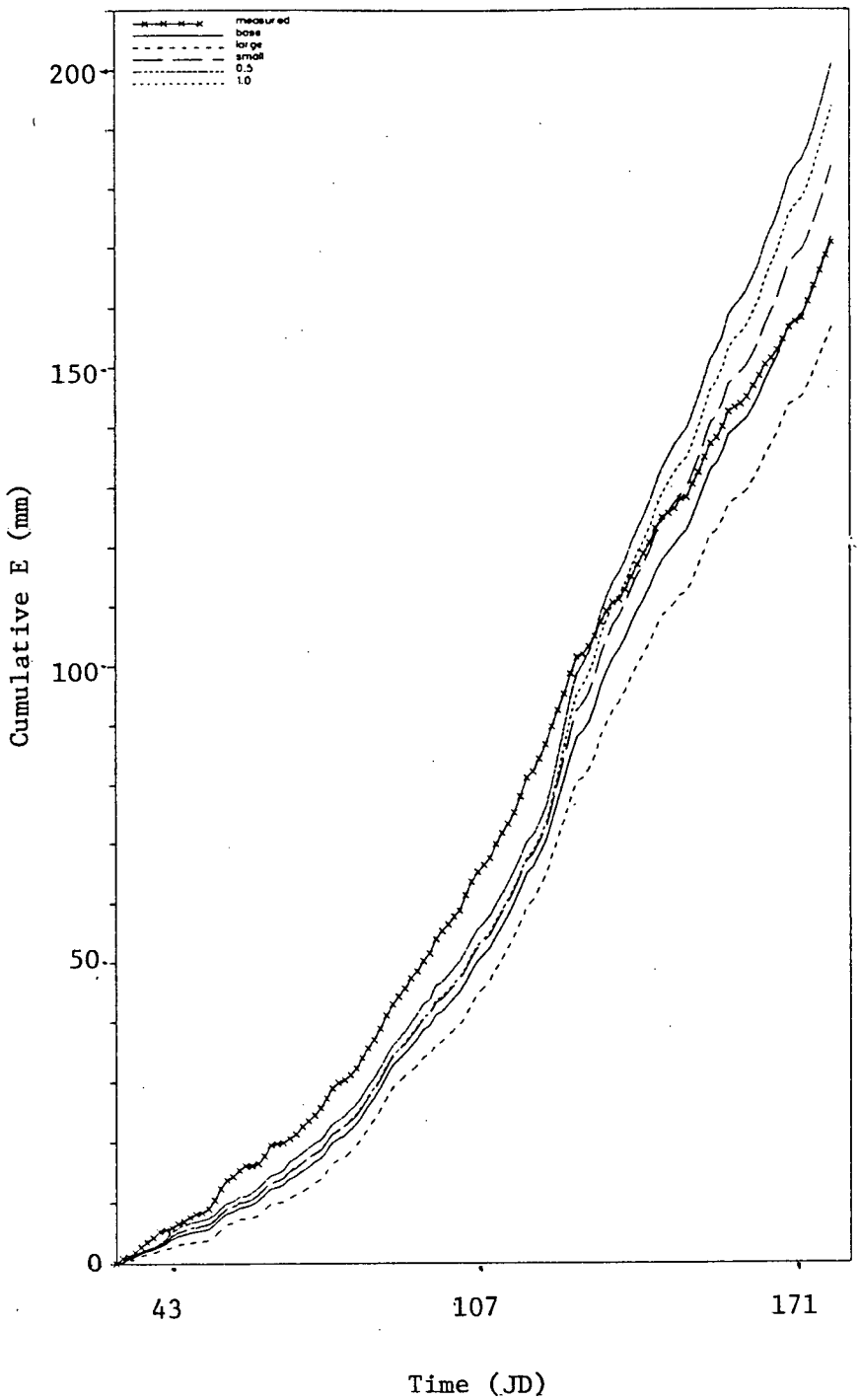

performing well on a hour to hour basis. The statistics for the runs compared with the measured data suggest that when the surface storage capacities are set to larger values the model performs better (Table 8.16).

8.4.6 Drainage functions

The drainage functions were varied over a range of coefficients and equation types (see Table 8.17 for details) with the storage capacities for all surfaces being set to one value then changed to 0.5 mm (Table 8.17), 1.0 mm (Table 8.18), and 2.0 mm (Table 8.19). The effects of changing the drainage functions can be seen more clearly from the cumulative plots (Figs. 8.16, 8.17, 8.18). The largest values are obtained when S=0.5 mm.

With all of the models the beginning of external water use is associated with a steep rise in the slope of the cumulative curves. When S=0.5 mm all of the cumulative curves cross the measured E curve (Fig. 8.16). When S=1.0 mm and equation 7.20 is used the cumulative E is less than the measured E, but by the end of the study period they are converging, indicating over-prediction in the latter period. The same equation under predicts the cumulative E when S=2.0 mm (Fig. 8.18) but maintains a more similar slope to that of the measured E.

These runs show the Shuttleworth form of transition is sensitive to the drainage functions used, but not to the same extent as when the Rutter transition is used. This indicates care must be taken in assigning drainage functions and coefficients. It appears that those selected in this study for the Sunset site simulate the drainage and surface water state well (see Fig.

Table 8.17 Statistics of model performance for Q_E when the drainage functions are changed and S = 0.5 mm

			Drainage functions - S = 0.5 mm all surfaces					
Eqn no.:	v[b]	v[c]	7.20	7.18	7.18	7.20	7.20	7.17
Coeff D_0:	v	v	10	0.013	0.018	32	12	0.0014
Coeff b:	v	v	3	1.71	1.76	1.5	1.5	5.25
Statistic[a]								
(a) Hourly								
Mean (W m^{-2})	40.38	47.39	41.88	49.92	48.82	46.77	46.90	45.11
sd (W m^{-2})	58.20	63.03	59.77	65.65	64.09	61.26	61.32	60.67
m_f	0.92	1.00	0.95	1.04	1.02	0.97	0.97	0.96
r^2	0.81	0.75	0.77	0.72	0.73	0.75	0.75	0.76
RMSE (W m^{-2})	27.65	33.40	30.26	36.78	35.32	32.83	32.88	32.13
$RMSE_S$ (W m^{-2})	10.72	11.15	10.58	12.23	11.99	11.98	12.01	11.47
$RMSE_U$ (W m^{-2})	25.49	31.49	28.35	34.69	33.22	30.57	30.61	30.02
d	0.95	0.93	0.94	0.91	0.92	0.93	0.93	0.93
N&S	0.81	0.72	0.77	0.66	0.69	0.73	0.73	0.74
(b) Daily								
Mean (W m^{-2})	41.87	49.20	43.41	51.94	50.71	48.31	48.44	46.75
sd (W m^{-2})	23.87	29.27	26.77	28.96	28.49	28.56	28.54	27.95
m_f	1.10	1.34	1.23	1.32	1.31	1.31	1.31	1.28
r^2	0.71	0.60	0.68	0.54	0.57	0.62	0.62	0.64
RMSE (W m^{-2})	13.00	20.46	15.37	22.72	21.35	19.24	19.30	17.99
$RMSE_S$ (W m^{-2})	2.17	8.76	2.93	11.46	10.23	7.85	7.98	6.28
$RMSE_U$ (W m^{-2})	12.82	18.49	15.09	19.61	18.74	17.56	17.57	16.86
d	0.91	0.83	0.89	0.79	0.81	0.84	0.84	0.86
N&S	0.64	0.12	0.50	-0.09	0.04	0.22	0.22	0.32

a See Table 8.5 for explanation of statistics
b 'Base' equations with base S capacities
c 'Base' equations but S = 0.5 for all surfaces

Table 8.18 Statistics of model performance for Q_E when the drainage functions are changed and S = 1.0 mm

	Drainage functions - S = 1.0 mm all surfaces							
Eqn no.:	v[b]	v[c]	7.20	7.18	7.18	7.20	7.20	7.17
Coeff D_0:	v	v	10	0.013	0.018	32	12	0.0014
Coeff b:	v	v	3	1.71	1.76	1.5	1.5	5.25
Statistic[a]								
(a) Hourly								
Mean (W m^{-2})	40.38	45.72	39.34	48.20	46.97	48.24	48.35	47.26
sd (W m^{-2})	58.20	62.33	58.64	64.20	62.89	53.23	63.31	62.57
m_f	0.92	0.99	0.93	1.02	1.00	1.00	1.00	0.99
r^2	0.81	0.77	0.80	0.75	0.76	0.76	0.76	0.76
RMSE (W m^{-2})	27.65	31.71	28.33	34.17	32.85	32.90	32.97	32.35
$RMSE_S$ (W m^{-2})	10.72	10.13	10.63	11.08	10.80	11.32	11.36	11.01
$RMSE_U$ (W m^{-2})	25.49	30.05	26.26	32.32	31.02	30.89	30.96	30.42
d	0.95	0.93	0.94	0.92	0.93	0.93	0.93	0.93
N&S	0.81	0.75	0.80	0.71	0.73	0.73	0.73	0.74
(b) Daily								
Mean (W m^{-2})	41.87	47.39	40.71	50.12	48.82	49.81	49.91	48.89
sd (W m^{-2})	23.87	18.77	25.44	28.22	27.79	28.49	28.48	28.13
m_f	1.10	1.32	1.17	1.29	1.27	1.31	1.31	1.29
r^2	0.71	0.63	0.72	0.57	0.60	0.61	0.60	0.61
RMSE (W m^{-2})	13.00	18.90	13.44	20.79	19.49	20.22	20.30	19.39
$RMSE_S$ (W m^{-2})	2.17	6.97	0.29	9.64	8.34	9.32	9.43	8.41
$RMSE_U$ (W m^{-2})	12.82	17.57	13.43	18.42	17.62	17.95	17.98	17.47
d	0.91	0.85	0.91	0.82	0.84	0.83	0.83	0.84
N&S	0.64	0.25	0.62	0.09	0.20	0.14	0.13	0.21

a See Table 8.5 for explanation of statistics
b 'Base' equations with base S capacities
c 'Base' equations but S = 1.0 for all surfaces

Table 8.19 Statistics of model performance for Q_E when the drainage functions are changed and S = 2.0 mm

	Drainage functions - S = 2.0 mm all surfaces						
Eqn no.:	v[b]	7.20	7.18	7.18	7.20	7.20	7.17
Coeff D_0:	v	10	0.013	0.018	32	12	0.0014
Coeff b:	v	3	1.71	1.76	1.5	1.5	5.25
Statistic[a]							
(a) Hourly							
Mean (W m^{-2})	40.38	37.64	45.28	44.01	50.94	51.02	50.38
sd (W m^{-2})	58.20	57.74	62.52	61.41	67.60	67.69	67.16
m_f	0.92	0.92	0.99	0.97	1.07	1.07	1.07
r^2	0.81	0.81	0.78	0.79	0.75	0.75	0.75
RMSE (W m^{-2})	27.65	27.41	30.86	29.93	35.64	35.75	35.24
$RMSE_S$ (W m^{-2})	10.72	11.25	9.41	9.44	11.70	11.76	11.33
$RMSE_U$ (W m^{-2})	25.49	24.99	29.39	28.40	33.67	33.76	33.37
d	0.95	0.95	0.94	0.97	0.92	0.92	0.92
N&S	0.81	0.81	0.76	0.79	0.68	0.68	0.69
(b) Daily							
Mean (W m^{-2})	41.87	38.92	47.18	45.83	52.68	52.77	52.19
sd (W m^{-2})	23.87	24.51	26.98	26.51	29.47	29.49	29.27
m_f	1.10	1.12	1.24	1.22	1.35	1.35	1.34
r2	0.71	0.74	0.63	0.65	0.54	0.54	0.55
RMSE (W m^{-2})	13.00	12.52	17.81	16.61	23.32	23.42	22.81
$RMSE_S$ (W m^{-2})	2.17	1.71	6.70	5.36	12.19	12.28	11.70
$RMSE_U$ (W m^{-2})	12.82	12.41	16.50	15.72	19.88	19.94	19.58
d	0.91	0.92	0.86	0.87	0.79	0.79	0.79
N&S	0.64	0.67	0.33	0.42	-0.15	-0.15	-0.09

a See Table 8.5 for explanation of statistics
b 'Base' equations with base S capacities

Figure 8.16 Influence of changing drainage functions and coefficients on the cumulated E when S = 0.5 mm for all surfaces.

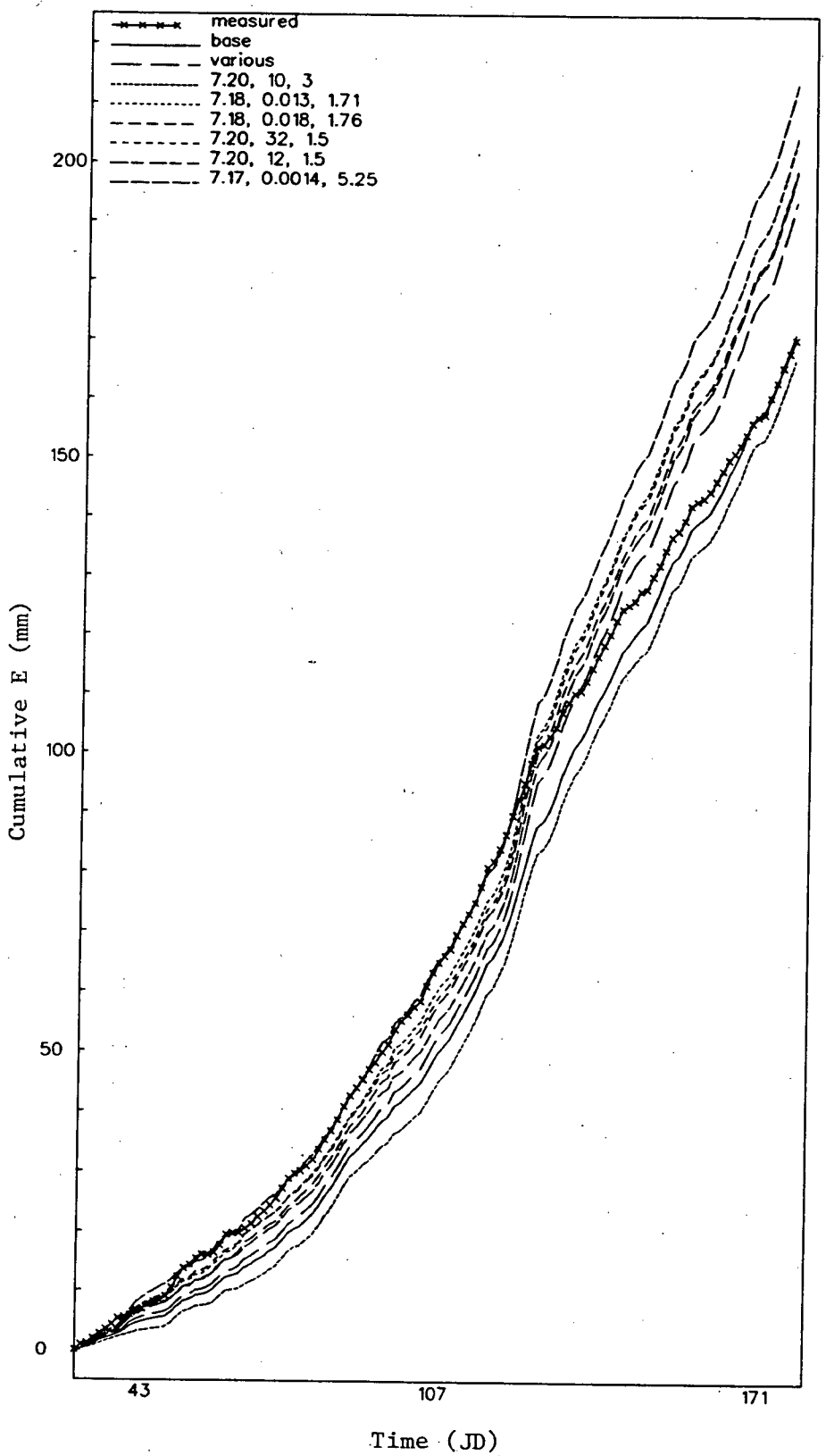

Figure 8.17 Influence of changing drainage functions and coefficients on the cumulated E when S = 1.0 mm for all surfaces.

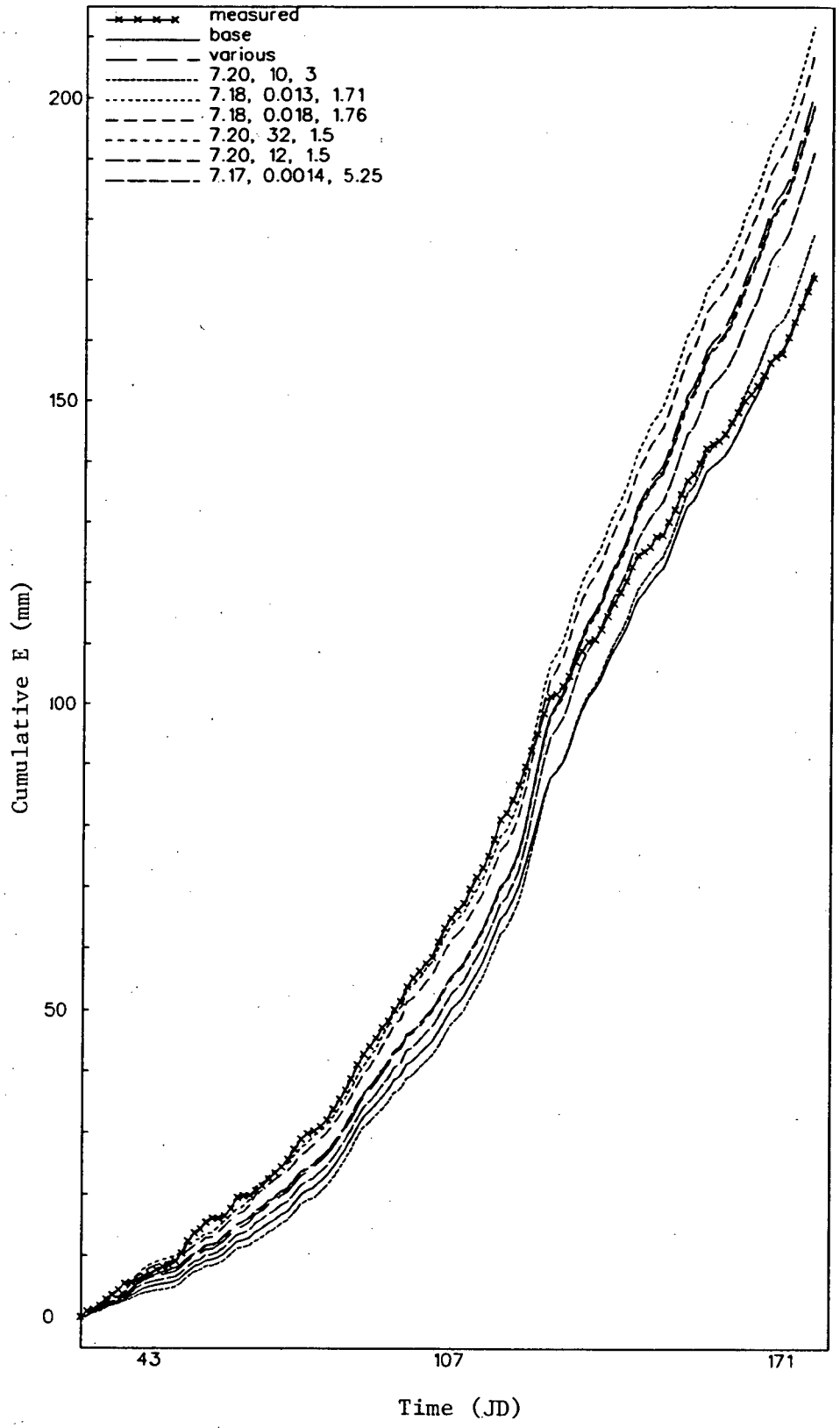

Figure 8.18 Influence of changing drainage functions and coefficients on the cumulated E when S = 2.0 mm for all surfaces.

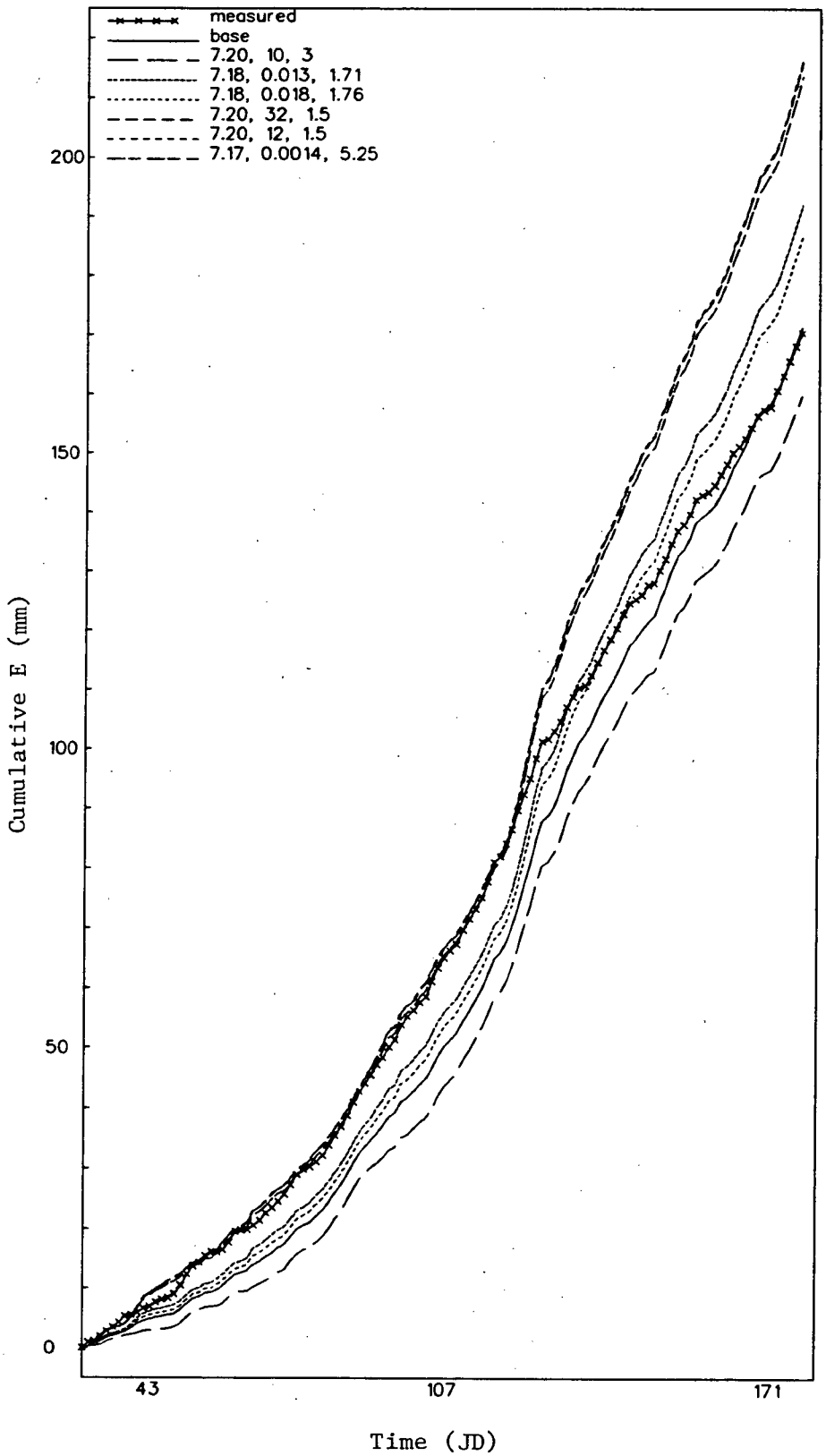

8.7).

8.5 Discussion

One portion of the model requiring more attention in the future is the under prediction in the earlier part of the year. The measured Q_E suggest that it is an important part of the urban energy and water balances (see Chapter 6) in these months and should not be ignored. The first line of pursuit should be with regard to the surface resistance. The model developed in Chapter 7 is based on very little winter data with a dry surface and therefore may not be fully representative. Further, for the summer months careful thought needs to be given to the hourly input of external water use. It is probable that the water use calculated for input in this study was too large. For the reasons stated below this hourly input was not adjusted to fit the measured data.

From the sensitivity analyses it can be concluded that if the model is to be applied to other areas close attention needs to be paid to the drainage and storage capacities of the dominant surface types and the results of these sensitivity analyses be kept in mind with regards to the effects of setting appropriate values. Wetness sensors, located on a number of representative surfaces, appear to be a simple of way of assessing the performance of the model if measurements of Q_E are not available (as is frequently the case).

The model developed in this thesis, the performance of which is discussed in this chapter, shows definite promise for use in urban areas. The objective of this thesis was not to model the evapotranspiration for a particular time and place but to consider a methodology for modelling evapotranspiration continuously over a range of meteorological conditions in urbanized terrain. Therefore there has been no explicit attempt to fit/calibrate the model to the measured data. The performance of the model, using physically realistic values

obtained from the literature for the drainage functions and storage capacities with the other sub-models developed earlier in the thesis, suggests that this type of approach to modelling is definitely useful for predicting urban evapotranspiration and state of the surface.

If this model is to be applied at other locations the changes required for application of the model primarily relate to the assignment of parameter values. For example if a tropical city is under consideration it would be advisable to conduct Q_E measurements so that the surface resistance sub-model had appropriate parameters. For the tropical case, and other locations where intense rainfall events occur further investigation of the Massman (1985) drainage functions, which allow for the inclusion of the intensity of rainfall, may be worthwhile. In this study the case of snow has been explicitly ignored. The incorporation of this as an additional sub-model should be reasonably easy with the appropriate melt equations. The model would have to keep a record not only of the depth of water within a store but also whether it was in a liquid or a solid state.

Discussion of simplifications to the model which would allow its more ready application have already been mentioned (e.g. the use of sectors instead of plumes, and the use of the neutral equation for r_S instead of the non-neutral version). There is merit in further research into the influence of simplifications, in particular to adapt the model so that it requires only routinely-collected meteorological data.

Prior to this work there is no other model to compute hourly evapotranspiration for urban terrain. However, there are models at the daily time scale (e.g. Grimmond et al., 1986; Cleugh, 1988). The Cleugh (1988) model, which uses a coupled surface and mixed layer approach, was not available at the time of writing but in any case requires atmospheric

soundings that were not available. The Grimmond et al. (1986) model is a combination advection-aridity model developed from that of Brutsaert and Stricker (1979). It has been applied elsewhere in Vancouver (Grimmond and Oke, 1986) as part of an urban water balance study. Here this model was run using the 'base' data so that its performance could be compared with the evapotranspiration-interception model (Table 8.20, Fig. 8.19). In the comparison the Grimmond et al. (1986) evaporation sub-model was run independently using the empirical coefficients reported in their study. The surface database and source area sub-models were used to determine the available energy and the sizes of the irrigated and unirrigated areas. Comparison of these results with those obtained for the 'base' run of the evapotranspiration-interception model at the daily time scale (Table 8.5, Fig. 8.3) shows that whilst both perform acceptably the model developed in this study performs better; with a better slope, less scatter around the one to one line and improved statistics. In particular the RMSE is halved and the r^2 and d are considerably improved.

Table 8.20 Comparison of the performance of two models to calculate daily evapotranspiration in urbanized terrain

Statistic	Grimmond et al. (1986)	Present Study
Number of points (n)	125	125
Mean		
Measured ($W\ m^{-2}$)	40.49	40.49
Modelled ($W\ m^{-2}$)	37.49	41.87
Standard deviation (sd)		
Measured ($W\ m^{-2}$)	21.80	21.80
Modelled ($W\ m^{-2}$)	34.36	23.87
Slope - functional analysis (m_f)[a]	1.56	1.10
Coefficient of determination (r^2)	0.41	0.71
Root mean square error (RMSE)($W\ m^{-2}$)	26.53	13.00
RMSE systematic ($RMSE_S$)($W\ m^{-2}$)	2.94	2.17
RMSE unsystematic ($RMSE_U$)($W\ m^{-2}$)	26.37	12.82
Index of agreement (d)[b]	0.75	0.91
Goodness of fit (N&S)[c]	-0.50	0.64

a Mark and Church (1977)
b Wilmott and Wicks (1980)
c Nash and Sutcliffe (1970)

Figure 8.19 Comparison of daily measured and modelled evaporation using the Grimmond et al. (1986) advection-aridity model and the 1987 Sunset data set

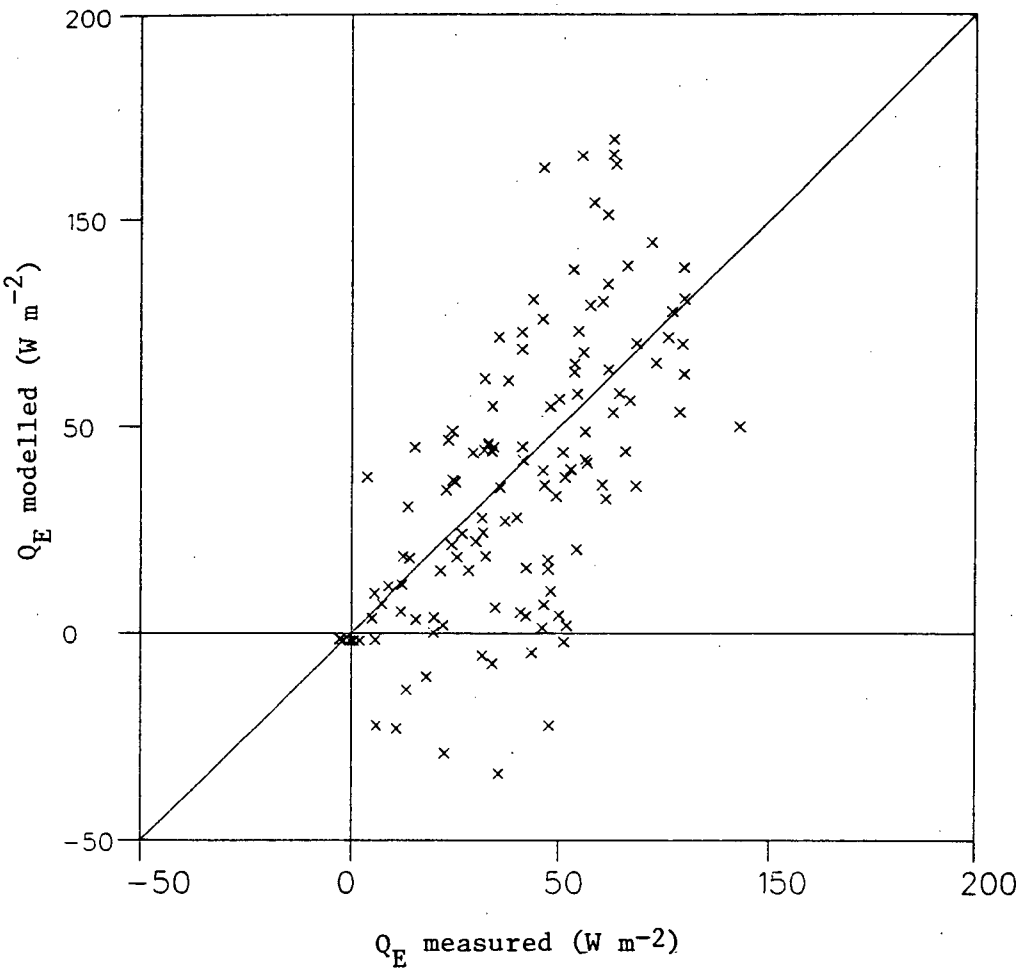

CHAPTER 9 CONCLUSIONS

9.1 Summary of conclusions

The objective of this thesis was to develop a model to calculate evapotranspiration from urban areas for use over a wide range of meteorological conditions. This dictates the need for a model which can cope with changing water availability at the surface both during and following rainfall. Considering this it was deemed appropriate to adopt an evapotranspiration-interception approach.

Development of the evapotranspiration-interception model created the need for sub-models to calculate anthropogenic heat flux, storage heat flux, aerodynamic resistance, surface resistance and drainage. Knowledge of the nature of the 'surface' is a common requirement of these sub-models and the overall model, so a scheme to archive surface information was also developed.

The main conclusions which can be drawn from this study are:

- To determine the value for a surface parameter (e.g. amount of greenspace) it is necessary to locate the area which is to be described. The location of the boundaries for this area may affect the value assigned to the surface parameters and therefore any subsequent flux calculations. In an area, such as suburban terrain, it is possible at the local scale to identify an area which is homogeneous (e.g. a residential area) but within this homogeneous unit there is a large degree of sub-scale heterogeneity (e.g. vegetation, buildings, roads). The influence of this sub-scale heterogeneity is demonstrated through the calculation of anthropogenic heat flux, storage heat flux, and latent heat flux with the aid of a database which stores surface characteristics (e.g. greenspace, building type etc.).
- An objective means for locating the boundaries of the source area contributing to turbulent and radiant heat flux measurements at a point is

presented. It uses a modified version of the source area model developed by Schmid (1988). A simplified version, termed 'sectors', was developed. It requires more easily obtained input data than the full source area model and less computation time yet it maintains most of the physics. Combining the source area calculations with the surface description database it is possible to obtain a spatially consistent energy balance even when some terms are measured and others are calculated. This method also has applications when comparing modelled and measured fluxes to ensure their spatial consistency.

- The anthropogenic heat flux is spatially very variable therefore the location of the boundaries of the area used to calculate the anthropogenic heat flux contributing to the energy balance at a point strongly influences the size of the flux obtained. Seasonally the anthropogenic heat flux is not so variable. For the Sunset site it only varies from a mean daily value of 9.5 W m^{-2} (winter) to 7.5 W m^{-2} (summer).
- The objective hysteresis model proposed by Cleugh (1988) to calculate urban heat storage performs well in all seasons during the daytime. At night the storage heat flux is approximately equal to the sum of the net radiation and anthropogenic heat flux. At the Sunset site the influence of the changing surface type (due to changing source area locations) on the storage heat flux was minimal. Nevertheless there is evidence to suggest that in areas where the surface is less homogeneous this may not be the case.
- The winter/spring urban energy balances observed in this study are different to those reported for summertime conditions at the same site. The fluxes are not symmetrical about solar noon. This is primarily due to the storage heat flux being determined by the more realistic objective hysteresis equation rather than the objective linear equation. Hence earlier interpretations should be modified. Apart from this feature the spring season balances are

similar to those reported for the summertime in terms of the relative importance of the individual fluxes.

- The wintertime energy balance appears to be different to that in spring and summer. The most noticeable feature is the increased importance of the latent heat flux. On average it is the largest output flux in the balance. A secondary, more expected feature, is the increased importance of anthropogenic heat flux as an input.
- The aerodynamic resistance of an urban area can be reasonably approximated by a simple neutral stability wind equation. Such simplification has the limitation of showing no variability for a given wind speed.
- The use of modified Jarvis (1976) functions to calculate surface resistance for urban areas proved encouraging. The statistics for the performance of the optimised suburban surface resistance sub-model are similar to those obtained for forested areas (e.g. Stewart, 1988).
- The Penman-Monteith-Rutter-Shuttleworth evapotranspiration interception model developed in this thesis for urban areas performed very well. It is an improvement over available methods. Inclusion of the Shuttleworth (1978) unified transition between wet and dry surfaces was found to be superior to the Rutter et al. (1971, 1975) transition scheme. This is in large part due to the increased sensitivity of the evaporation to the drainage functions when the Rutter transition is used.
- It is possible to use the evaporation-interception model with values of storage capacity, drainage function and other hydrologic parameters taken from the literature to obtain realistic hourly and daily estimates of latent heat flux and surface water state.

9.2 Future research

Throughout the thesis, where appropriate, specific recommendations for future research have been made and are not repeated here. The overall conclusion is that the Penman-Monteith-Rutter-Shuttleworth model is very useful in the urban environment but so far it has only been tested at one suburban site. Further fieldwork in other cities and climates to test the model would be helpful in demonstrating its robustness. There is also need for further winter time measurements to determine whether the results obtained here are typical. Ideally it would be of great value to have a means of directly measuring the latent heat flux (e.g. by eddy correlation using fast response hygrometry) and thereby overcome some of the problems of accumulated errors in other fluxes. The surface resistance model would also benefit from being optimised from a wider range of field data to investigate further the effects of surface cover and seasonality.

REFERENCES CITED

Aldrich R. 1976: The measurement of rainfall at the ground level. J. Hydrol. (N.Z.), 15, 35-40.

Alley W.M., D.R. Dawdy & J.C. Schaake Jr. 1980: Parametric-deterministic urban watershed model. J. Hydraul. Div. Amer. Soc. Civ. Eng., 106 (HY5), 679-690.

Arnfield A.J. 1982: An approach to the estimation of the surface radiative properties and radiation budgets of cities. Phys. Geog., 3, 97-122.

Aston A.R. 1985: Heat storage in a young Eucalypt forest. Agr. For. Meteorol., 35, 281-297.

Atkinson B.W. 1985: The urban atmosphere. Cambridge University Press, Cambridge, Great Britain, 89p.

Bach W. 1970: An urban circulation model. Arch. Met. Geoph. Biokl. Ser B., 18, 155-168.

Brutsaert W. 1982: Evaporation into the atmosphere. Reidel, Dordrecht, Holland, 299p.

Brutsaert W. & H. Stricker 1979: An advection-aridity approach to estimate actual regional evapotranspiration. Water Resour. Res., 15, 443-350.

Bulfill M.C. 1984: Hydrological aspects of the study of non-point pollution on a motorway catchment. In Urban storm drainage, Proc. 3rd Int. Conf., Goteborg, Sweden, June 4-8, 1984, 275-283.

Calder I.R. 1977: A model of transpiration and interception loss from a Spruce forest in Plynlimon, Central Wales. J. Hydrol., 33, 247-265.

Calder I.R., R.L. Hall, R.J. Harding & I.R. Wright 1984: The use of wet-surface weighing lysimeter system in rainfall interception studies of Heather. J. Clim. Appl. Meteorol., 23, 461-473.

Calder I.R. & I.R. Wright 1985: Gamma ray attenuation studies of interception from Sitka Spruce: some evidence for a traditional transport mechanism. Water Resour. Res., 22, 409-417.

Camuffo D. & A. Bernardi 1982: An observational study of heat fluxes and the relationship with net radiation. Bound. Lay. Meteorol., 23, 359-368.

Canada, Environment, Atmospheric Environment Service 1987: Monthly Meteorol. Summary, January-June, 1987, Vancouver International Airport.

Canada General Standards Board 1980: Handbook on insulating homes for energy conservation. Canadian Government Publishing Centre, Ottawa, 51-GP-42 MP.

Canada, Statistics, Census Division, 1987. Census of Canada 1986, Enumeration data, Ottawa, Canada.

Chandler, T.J. 1976: Urban climatology and its relevance to urban design. WMO Tech. Note No. 149, 61p.

Ching J.K.S., J.F. Clarke & J.M. Godowitch 1983: Modulation of heat flux by different scales of advection in an urban environment. Bound. Lay. Meteorol., 25, 171-191.

Cleugh H.A 1988: Development and evaluation of a regional evaporation model: A study of surface and atmospheric controls on the suburban evaporation regime. Unpubl. Ph.D. Thesis, Department of Geography, Univ of British Columbia (in preparation).

Cleugh H.A. & T.R. Oke, 1986: Suburban-rural energy balance comparisons in summer for Vancouver, B.C. Bound. Lay. Meteorol. 36, 351-369.

Cook N.H. & E. Rabinowicz 1963: Physical measurement and analysis. Addison-Wesley, Reading, Mass., 312p.

Davies H. & T. Hollis 1982: Measurements of rainfall-runoff volume relationships and water balance for roofs and roads. In Urban storm drainage, Proc. 2nd Int. Conf., Urbana, Illinois, 1981, 434-443.

Dennis J.E. Jr, D.M. Gray & R.E. Welch 1981: Algorithm 573 NL2SOL an adaptive non-linear least squares algorithm. Assoc. Computing Machinery Trans. on Math. Softw., 7, 369-383.

Doll D., J.K.S. Ching & J. Kaneshiro, 1985: Parameterisation of subsurface heating for soil and concrete using net radiation data. Bound. Lay. Meteorol., 32, 351-372.

Dolman A.J., J.B. Stewart & J.D. Cooper 1988: Predicting forest transpiration from climatological data. Agr. For. Meteorol., 42, 339-353.

Draper J.E. & J.S. Klingman 1972: Mathematical analysis. (2nd edn.) Harper & Row, New York, 691p.

Dyer A.J. 1974: A review of flux-profile relationships. Bound. Lay. Meteorol., 7, 363-372.

Dyer A.J. & C.F. Bradley 1982: An alternative analysis of flux-gradient relationships at the 1976 ITCE. Bound. Lay. Meteorol., 22, 3-19.

Falk J. & J. Niemczynowicz 1978: Characteristics of the above ground runoff in sewered catchments. In Urban storm drainage, Helliwell, P.R. (ed.) Pentech Press, London, 159-171.

Finkelstein J. 1971: Comparisons between 4" plastic and 5" copper raingauges. J. Hydrol. (N.Z.), 10, 100-103.

Fritschen L.J. & L.W. Gay 1979: Environmental instrumentation. Springer Verlag, New York, 216p.

Gardner W.H. 1965: Water content. In Methods of soil analysis Part 1: Physical

and mineralogical properties, Black C.A. (ed.), Adv. Agron. 92-93.

Garratt J.R. 1980: Surface influence upon vertical profiles in the atmospheric near-surface layer. Quart. J. Roy. Meteorol. Soc., 106, 803-820.

Gash, J.H.C. 1979: An analytical model of rainfall interception by forests. Quart. J. Roy. Meteorol. Soc., 105, 43-55.

Gash J.H.C. 1986: A note on estimating the effect of limited fetch on micro-meteorological evaporation measurements. Bound. Lay. Meteorol., 35, 409-413.

Gash J.H. & A.J. Morton 1978: An application of the Rutter model to the estimation of the interception loss from Thetford forest. J. Hydrol., 38, 49-58.

Gash J.H., W.J. Shuttleworth, C.R. Lloyd, J.C. Andre, J.P. Goutorbe, & J. Gelpe 1988: Micrometeorological measurements in Les Landes forest during HAPEX-MOBILHY. Agric. For. Meteorol., (in press)

Gay D.M. 1983: Remark on algorithm 573. Assoc. Computing Machinery Trans. on Math. Softw., 9, 139.

Greater Vancouver Regional District 1980: Landuse maps for Burnaby. Scale 1:2500.

Greater Vancouver Regional District 1980: Landuse maps for Richmond. Scale 1:2500.

Greater Vancouver Regional District 1983: Landuse maps for Vancouver. Scale 1:2500.

Grimmond C.S.B. 1983: The suburban water balance: Daily, monthly and annual results from Vancouver, B.C., Unpubl. M.Sc. Thesis, The University of British Columbia, Vancouver, 172p.

Grimmond C.S.B. & T.R. Oke 1986: Urban Water Balance 2: Results from a suburb of Vancouver, B.C. Water Resour. Res., 22, 1397-1403.

Grimmond C.S.B., T.R. Oke & D.G. Steyn, 1986: Urban Water Balance 1: A model for daily totals. Water Resour. Res., 22, 1404-1412.

Grynning S.E., A.A.M. Holtslag, J.S. Irwin & B. Siverstsen 1987: Applied dispersion modelling based on scaling meteorological scaling parameters. Atmos. Env., 21 79-89.

Hall M.J. 1984: Urban hydrology. Elsevier, London, 299p.

Hall R.L. 1985: Further interception studies of Heather using a wet surface weighing lysimeter system. J. Hydrol., 81, 193-210.

Halldin S., H. Grip & K. Perttu 1979: Model for energy exchange of a pine forest canopy. In Comparison of Forest Water and Energy Exchange Models, Halldin, S. (ed.), Int. Soc. Ecological Modelling, Copenhagen, 1979, 59-75.

Hay J.E. & T.R. Oke 1976: The climate of Vancouver. Tantalus Research Limited, Vancouver, 49p.

Henderson-Sellers B. 1984: A new formula for latent heat of vaporisation of water as a function of temperature. Quart. J. Royal Meteorol. Soc., 110, 1186-1190.

Hickok R. 1977: New encyclopedia of sports. McGraw-Hill Book Co., New York, 544p.

Hillel D. 1971: Soil and water: Physical principles and processes. Academic Press, New York, 288p.

Horton R.E. 1919: Rainfall interception. Mon. Weather Rev., 47, 603-623.

Hutchinson P. 1969: A note on random raingauge errors. J. Hydrol. (N.Z.), 8, 8-10.

Jarvis P.G. 1976: The interpretation of the variations in leaf water potential and stomatal conductance found in canopies in the field. Phil. Trans. Roy. Soc. Lond. B., 273, 593-610.

Jarvis P.G., G.B. James & J.J. Landsberg 1976: Coniferous forest. In Vegetation and atmosphere vol. 2, Case studies, Monteith, J.L. (ed.) Academic Press, New York, 171-240.

Kalanda B.D. 1979: Suburban evaporation estimates in Vancouver. Unpubl. M.Sc. Thesis, The University of British Columbia, Vancouver, 123p.

Kalanda B.D., T.R. Oke & D.L. Spittlehouse 1980: Suburban energy balance estimates for Vancouver, B.C. using Bowen Ratio energy-balance approach. J. Appl. Meteorol., 19, 791-802.

Kerschgens M.J. & R.L. Drauschke 1986: On the energy budget of a wintry mid-latitude city atmosphere. Contrib. Atmos. Phys., 59, 115-125.

Kidd C.H.R. 1978: A calibrated model for the simulation of the inlet hydrograph for fully sewered catchments. In Urban storm drainage, Helliwell P.R. (ed.), Pentech Press, London, 172-186.

Kramer P.J. & T.T. Kozlowski 1979: Physiology of woody plants. Academic Press, New York, p. 64.

Kutzbach J.E. 1961: Investigations of the modification of wind profiles from artificially controlled surface roughness. Annual Report, Dept. of Meteorology, Univ. of Wisconsin.

Lacy R.E. 1977: Climate and building. Building Research Establishment Report, Dept. Of Env., B.R.E., London, HMSO, 185p.

Landsberg H.E. 1981: The urban climate. Academic Press, London, 275p.

Latimer J.R. 1972: Radiation measurement. Int. Field Year for the Great

Lakes Tech. Manual Ser. 2, NRC/USNAS/IHD, Ottawa, 53p.

Lazaro T.R. 1979: Urban hydrology: A multidiscipline approach. Ann Arbor Science, Michigan, 249p.

Lettau H.H. 1969: Note on aerodynamic roughness-element description. J. Appl. Meteorol., 8, 828-832.

Leyton L., E.R.C. Reynolds & F.B. Thompson 1967: Rainfall interception in forest and moorland. In Forest Hydrology, Sopper W.E. & H.W. Lull (eds.), Pergamon, Oxford, 163-178.

Lindroth A. 1985: Canopy conductance of coniferous forests related to climate. Water Resour. Res., 21, 297-304.

List R.J. 1966: Smithsonian Meteorological Tables, (6th edn.) Smithsonian Institute, Washington, D.C., 527p.

Lowe P.R. 1977: An approximating polynomial for the computation of saturation water vapour pressure. J. Appl. Meteorol., 16, 100-103.

Mandeville A.N. & J.C. Rodda 1970: A contribution to the objective assessment or areal rainfall amounts. J. Hydrol. (N.Z.), 9, 281-291.

Marsalek J. 1977: Data collection, instrumentation and verification of models. Modern concepts in urban drainage, Conf. Proc. 5, Canada-Ontario agreement on Great Lakes water quality, 173-200.

Massman W.J. 1983: The derivation and validation of a new model for the interception of rainfall by forests. Agr. Meteorol., 28, 261-286.

McCaughey J.H. 1985: Energy balance storage terms in a mature mixed forest at Petawawa Ontario - A case study. Bound. Lay. Meteorol., 31, 89-101.

McCaughey J.H., D.W. Mullins & M. Publicover 1987: Comparative performance of two reversing Bowen Ratio measurement systems. J. Atmos. Oceanic Technol., 4, 724-730.

McIntosh D.H. & A.S. Thom 1972: Essentials of meteorology. Wykeham, London, 239p.

Moore C. 1986: Double-precision routines NL2SOL NL2SNO. Univ. British Columbia Computing Centre Technical Note 214, 17p.

Moore C.J. & G. Fisch 1986: Estimating heat storage in Amazonian tropical forest. Agr. For. Meteorol., 38, 147-169.

Monteith, J.L. 1965: Evaporation and environment. Symp. Soc. Exp. Biol., 19, 205-224.

Mulder J.P.M. 1985: Simulating interception loss using standard meteorological data. In The forest-atmosphere interaction, Hutchinson B.A. & B.B. Hicks (ed.), Reidel, 177-196.

Munro D.S. & T.R. Oke 1975: Aerodynamic boundary-layer adjustment over a crop in neutral stability. Bound. Lay. Meteorol., 9, 53-61.

Nash J.E. & J.V. Sutcliffe 1970: River flow forecasting through conceptual models. Part I - A discussion of principles. J. Hydrol., 10, 282-290.

Nicholson S.E. 1975: A pollution model for street-level air. Atmos. Env., 9, 19-31.

Niemcynomicz J. 1986: A non-linear rainfall-runoff simulation model applicable to a desk calculator. In Urban drainage modelling, Maksimovic C. & Radojkovic (ed.), Proc. Int. Symp. on comparison of urban drainage models with real catchment data, '86, Dubrovnik, Yugoslavia, 74-84.

Nouh M. 1986: Effect of model calibration on the least-cost design of storm-water drainage systems.In Urban drainage modelling, Maksimovic C. & Radojkovic (ed.), Proc. Int. Symp. on comparison of urban drainage models with real catchment data, '86, Dubrovnik, Yugoslavia, 61-73.

Oke T.R. 1976: The distinction between canopy and boundary layer urban heat islands. Atmos., 14, 268-277.

Oke T.R. 1978: Boundary layer climates. Methuen, London, 372p.

Oke T.R. 1982: The energetic basis of the urban heat island. Quart. J. Roy. Meteorol. Soc., 108, 1-24.

Oke T.R. 1984: Methods in urban climatology. In Applied climatology, Kirchhofer W., A. Ohmura & W. Wanner (eds.), Zurcher Geog. Schriften 14, ETH, Zurich, 19-29.

Oke T.R. 1987: The surface energy budgets of urban areas. Modelling the Urban Boundary Layer. Amer. Meteorol. Soc., Boston, 1-52.

Oke T.R. 1988: The urban energy balance. Prog. Phys. Geog., 12, 471-508.

Oke T.R. 1989: The micrometeorology of the urban forest. Phil. Trans. Roy. Soc. Lond. (in press)

Oke T.R. & H.A. Cleugh 1987: Urban heat storage derived as energy budget residuals. Bound. Lay. Meteorol., 39, 233-245.

Oke T.R., H.A. Cleugh & S. Grimmond 1988: Evapotranspiration in urban areas. In Int. Symp. Hydrological processes and water management in urban areas, UNESCO, 24-29 April, 1988, Duisburg, 107-112.

Oke T.R., B.D. Kalanda & D.G. Steyn 1981: Parameterisation of heat storage in urban areas. Urban Ecol., 5, 45-54.

Oke T.R. & J.H. McCaughey 1983: Suburban-rural energy balance comparisons for Vancouver, B.C.: An extreme case? Bound. Lay. Meteorol., 26, 337-354.

Pasquill F. 1972: Some aspects of boundary layer description. Quart. J. Roy. Meteorol. Soc., 98,469-494.

Peikorz G. 1987: Die energiebilanz einer stadtischen struktur, Dipl. Meteorologie, Rheinische Friedrich-Wilhelm-Universitat, Bonn, 99p.

Penman H.L. 1948: Natural evaporation from open water, bare soil and grass. Proc. Roy. Soc. Lond. Ser. A, 193, 120-145.

Pratt C.J., J.J. Harrison & J.R.W. Adams 1984: Storm runoff simulation in runoff quality investigations. Urban storm drainage, Proc. 3rd Int. Conf., Goteborg, Sweden, June 4-8, 1984, 285-294.

Randerson D. 1984: Atmospheric science and power production. U.S. Dept. Energy, Office of Science and Tech. Information, 850p.

Rapier D.A. & P.J. Grant 1971: Comparison of wetting losses on two types of raingauge. J. Hydrol. (N.Z.), 10, 104-108.

Raupach M.R. 1979: Anomalies in flux-gradient relationships over forest. Bound. Lay. Meteorol., 16, 467-486.

Reifsnyder W.E. 1967: Radiation geometry in the measurement and interpretation of radiation balance. Computer program for the determination of view factors. Agric. Meteorol., 4, 255-280.

Ripley E.A. & R.E. Redmann 1975: Grassland. In Vegetation and the atmosphere, vol. 2, Case studies, Monteith J.L. (ed.), Academic Press, London, 351-398.

Ross S.L. & T.R. Oke 1988: Tests of three urban energy balance models. Bound. Lay. Meteorol., 44, 73-96.

Roth M. 1988: Spectral analysis of turbulence in an unstable suburban atmosphere. Unpubl. M.Sc. Thesis, The University of British Columbia, Vancouver, 80p.

Rutter A.J., K.A. Kershaw P.C. Robins & A.J. Morton 1971: A predictive model of rainfall interception in forests I. Derivation of the model from observations in a plantation of Corsican pine. Agric. Meteorol., 9, 367-384.

Rutter A.J., A.J. Morton & P.C. Robins 1975: A predictive model of rainfall interception in forests II: Generalisation of the model and comparison with observations in some coniferous and hardwood stands. J. Appl. Ecol., 12, 367-380.

Schmid HP.E. 1988: Spatial scales of sensible heat flux variability: Representativeness of flux measurements and surface layer structure over suburban terrain. Unpubl. Ph.D. Thesis, The University of British Columbia, Vancouver, 299p.

Sellers P.J. & J.G. Lockwood 1981: A computer simulation of the effects of differing crop types on the water balance of small catchments over long time periods. Quart. J. Roy. Meteorol. Soc., 107, 395-414.

Sellers P.J., Y. Minz & A. Dalchen 1986: The design of the simple biosphere model (SiB) for use in general circulation models. J. Atmos. Sci., 43, 505-531.

Shuttleworth W.J. 1976: Experimental evidence for failure of the Penman-Monteith equation in partially wet conditions. Bound. Lay. Meteorol., 10, 91-94.

Shuttleworth W.J. 1978: A simplified one-dimensional theoretical description of the vegetation-atmosphere interaction. Bound. Lay. Meteorol., 14, 3-27.

Shuttleworth W.J. 1979: Evaporation. Institute of Hydrology Report 56, Wallingford, UK, 61p.

Shuttleworth W.J. 1983: Evaporation models in the global water budget. In Variations in the global water budget, Street-Perrott A., M. Beran & R. Radeliffe (eds.), Reidel, Dordrecht, 147-171.

Shuttleworth W.J. 1988a: Micrometeorology of temperate and tropical forests. Phil. Trans. Roy. Soc. Lond. (in press)

Shuttleworth W.J. 1988b: Evaporation from Amazonian rainforest. Proc. Roy. Soc. Lond. B, 233, 321-346.

Sievers U. & W.G. Zdunkowski 1986. A microscale urban climate model. Contr. Atmos. Physics, 59, 13-40.

Sman H.T., C.C.D.F. van Ree & M. Loxham 1988: Water balance techniques applied to industrial complexes. In Int. Symp. Hydrological processes and water management in urban areas, UNESCO, 24-29 April, 1988, Duisburg, 121-132.

Smith F.B. 1957: The diffusion of smoke from a continuous elevated point source into a turbulent atmosphere. J. Fluid Mech., 2, 49.

Stewart J.B. 1984: Measurement and prediction of evaporation from forested and agricultural catchments. Agr. For. Manag., 8, 1-28.

Stewart J.B. 1988: Modelling surface conductance of pine forest. Agr. Forest Meteorol., 43, 19-35.

Stewart J.B. & H.A.R. de Bruin 1984: Preliminary studies of the dependence of surface conductance of Thetford forest on environmental conditions. In The forest-atmosphere interaction, Hutchinson B.A. & B.B. Hicks (ed.) Reidel, 91-104.

Steyn D.G. 1980: Turbulence, diffusion and daytime mixed layer depth over a coastal city. Unpubl. Ph.D. Thesis, The University of British Columbia, Vancouver, 161p.

Steyn D.G. 1985: An objective method to achieve closure of overdetermined surface energy budgets. Bound. Lay. Meteorol., 33, 303-310.

Steyn D.G. & D.A. Faulkner 1986: The climatology of sea-breezes in the Lower Fraser Valley, B.C. Clim. Bull., 20, 21-39.

Steyn D.G. & I. McKendry 1988: Quantitative and qualitative evaluation of a 3 dimensional mesoscale numerical model simulation of a sea breeze in complex terrain. Mon. Weather Rev., (in press)

Steyn D.G. & T.R. Oke 1982: The depth of the daytime mixed layer at two coastal sites: a model and its validation. Bound. Lay. Meteorol., 24, 161-180.

Taesler R. 1978: Observational studies on 3 dimensional temperature and wind fields in Uppsala. Proc. WMO Symp. Bound. layer physics applied to specific problems air pollution, WMO #510, Geneva, 23- 30.

Terjung W.H. & P.A. O'Rourke 1980: Simulating the causal elements of urban heat islands. Bound. Lay. Meteorol., 19, 93-118.

Thom A.S. 1972: Momentum, mass and heat exchange of vegetation. Quart. J. Roy. Meteorol. Soc., 99, 154-170.

Thom A.S. & H.R. Oliver 1977: On Penman's equation for estimating regional evaporation. Quart. J. Roy. Meteorol. Soc., 103, 345-357.

van den Ven F.M.H. 1988: Urban Hydrological cycle. In Int. Symp. Hydrological processes and water management in urban areas, UNESCO, 24-29 April, 1988, Duisburg, A-1-15.

van Ulden A.P. & A.A.M. Holtslag 1985: Estimation of atmospheric boundary layer parameters for diffusion applications. J. Clim. Appl. Meteorol., 24, 1196-1207.

Vancouver Board of Parks and Recreation 1986: Parks and facilities chart. General Information, 16p.

Vancouver City 1987: Zoning and development By-Law No.3573.

Vancouver Planning Department 1985: Aerial Photographs. Scale 1;2500.

Vancouver School Board 1982: Facilities Services. 2p.

Waugh J.R. 1971: Evaluation of rainfall data from plastic and copper rain-gauges. J. Hydrol. (N.Z.), 10, 109-112.

Weil J.C. 1985: Updating applied diffusion models. J. Clim. Appl Meteorol., 24, 1111-1130.

Weiss A. & D.L. Lukens 1981: An electronic circuit for the detection of leaf wetness and a comparison of 2 sensors under field conditions. Plant Dis. 65, 41-43.

Wenzell H.G. & M.L. Voorhees 1980: Adaptation of ILLUDAS for continuous simulation. J. Hydraul. Div. Amer. Soc. Civ. Eng., 106 (HY 11), 1795-1812.

Whitford R.K. 1984: Energy efficient autos: Progress and prognosis. In Annual Review of Energy, vol. 9, Hollander J.M. & Brooks M. (eds.), 375-408.

Wilmott C.J. & D.E. Wicks 1980: An empirical method for the spatial interpolation of monthly precipitation within California. Phys. Geog., 1, 59-73.

Wright-McLaughlin Engineers Ltd. 1969: Urban storm drainage criteria manual. 2 vols. Denver Regional Council of Governments.

Wyngaard J.C. 1973: On surface-layer turbulence. In Workshop on micrometeorolgy, Haugen D.A. (ed.), Amer. Meteorol. Soc., 101-149.

Yap D.H. 1973: Sensible heat fluxes in and near Vancouver, B.C. Unpubl. Ph.D. Thesis, The University of British Columbia, Vancouver, 177p.

Yersel M. & R. Gobel 1986: Roughness effects on urban turbulence measurements. Bound. Lay. Meteorol., 37, 271-284.

Zinke P. 1967: Forest interception studies in the U.S. In Forest Hydrology, Sopper W.E. & H.W. Lull (eds.), Pergamon, Oxford, 137-161.

APPENDIX I JULIAN DAY CALENDAR FOR MEASUREMENT PERIOD 1987

Day	JAN	FEB	MAR	APRIL	MAY	JUNE
1		32	60	91	121	152
2		33	61	92	122	153
3		34	62	93	123	154
4		35	63	94	124	155
5		36	64	95	125	156
6		37	65	96	126	157
7		38	66	97	127	158
8		39	67	98	128	159
9		40	68	99	129	160
10		41	69	100	130	161
11		42	70	101	131	162
12		43	71	102	132	163
13		44	72	103	133	164
14		45	73	104	134	165
15		46	74	105	135	166
16		47	75	106	136	167
17		48	76	107	137	168
18		49	77	108	138	169
19		50	78	109	139	170
20		51	79	110	140	171
21	21	52	80	111	141	172
22	22	53	81	112	142	173
23	23	54	82	113	143	174
24	24	55	83	114	144	175
25	25	56	84	115	145	176
26	26	57	85	116	146	177
27	27	58	86	117	147	178
28	28	59	87	118	148	179
29	29		88	119	149	
30	30		89	120	150	
31	31		90		151	

APPENDIX II EQUATIONS USED IN CALCULATIONS

II.1 Temperature Difference (ΔT)

The same method is used for both the dry bulb and the wet bulb temperature differences from the RTDMS:

$$\Delta T = (\Delta T_1 - \Delta T_2)/2 \qquad \text{(II.1)}$$

where ΔT_1 - mean of the temperature difference for the two 10 minute periods which during the daytime are negative ($^\circ$C); and
ΔT_2 - mean of the two 10 minute temperature differences when the carts are reversed ($^\circ$C).

II.2 Slope of the saturation vapour pressure curve (s)

From Lowe (1977):

$$s = a_0 + T(a_1 + T(a_2 + T(a_3 + T(a_4 + T(a_5 + a_6 T))))) \qquad \text{(II.2)}$$

where a_0 - a_6 - coefficients (Table II.1); and
T - temperature ($^\circ$C).

Table II.1: Coefficients for use with Lowe (1977) polynomials (temperature $^\circ$C)

a	$e_S(> 0^\circ)$ (Pa)	$e_S(< 0^\circ)$ (Pa)	$s(>0^\circ)$ (Pa $^\circ C^{-1}$)	$s(<0^\circ)$ (Pa $^\circ C^{-1}$)
0	6.10779961	6.109177959	$4.438099984 \times 10^{-1}$	$5.030305237 \times 10^{-1}$
1	$4.436518521 \times 10^{-1}$	$5.03469897 \times 10^{-1}$	$2.857002636 \times 10^{-2}$	$3.773255020 \times 10^{-2}$
2	$1.428945805 \times 10^{-2}$	$1.886013408 \times 10^{-2}$	$7.938054040 \times 10^{-4}$	$1.267995369 \times 10^{-3}$
3	$2.650648471 \times 10^{-4}$	$4.176223716 \times 10^{-4}$	$1.215215065 \times 10^{-5}$	$2.477563108 \times 10^{-5}$
4	$3.031240396 \times 10^{-6}$	$5.824720280 \times 10^{-6}$	$1.036561403 \times 10^{-7}$	$3.005693132 \times 10^{-7}$
5	$2.034080948 \times 10^{-8}$	$4.838803174 \times 10^{-8}$	$3.532421810 \times 10^{-10}$	$2.158542548 \times 10^{-9}$
6	$6.136820929 \times 10^{-11}$	$1.838826904 \times 10^{-10}$	$-7.090244804 \times 10^{-13}$	$7.131097725 \times 10^{-12}$

II.3 Psychrometric constant (γ)

From Fritschen and Gay (1979):

$$\gamma = (c_p\ p)/(\epsilon L_V) \qquad \text{(II.3)}$$

where c_p - specific heat of air at constant pressure (J kg^{-1} K^{-1}), see below;
p - atmospheric pressure (Pa);
ϵ - ratio of the molecular weight of water vapour to that of dry air (0.62197 List, 1966); and
L_V - latent heat of vaporization calculated using the wet bulb

temperature T_W (J kg^{-1}).

II.4 Latent Heat of Vaporization (L_V)

From Henderson-Sellers (1984):

$$L_V = 1.91846 \times 10^6 \ (T/\ (T-33.91))^2 \qquad (II.4)$$

where T - temperature (K).

II.5 Mixing Ratio (r)

From Fritschen and Gay (1979):

$$r = \ (\epsilon\ e_a)/(p - e_a) \qquad (II.5)$$

where e_a - vapour pressure (Pa).

II.6 Vapour Pressure (e_a)

From Fritschen and Gay (1979):

$$e_a = e_S - \frac{m_1}{m_2}\frac{c_P}{\epsilon L_V}\ p\ (T_d - T_W) \qquad (II.6)$$

where e_S - saturation vapour pressure (Pa) at T_W;
L_V - determined at T_W;
T_d - dry bulb temperature (°C); and
T_W - wet bulb temperature (°C).

The ratio m_1/m_2 approaches unity when ventilation velocities exceed about 3 m s^{-1}. For this study the ratio was assumed to be unity.

II.7 Saturation Vapour Pressure (e_S)

From Lowe (1977):

$$e_S = a_0 + T(a_1 + T(a_2 + T(a_3 + T(a_4 + T(a_5 + a_6T))))) \qquad (II.7)$$

where a_0 - a_6 - coefficients (Table II.1).

II.8 Specific Heat of Air at Constant Pressure (c_P)

From List (1966):

$$c_P = (0.2403 + 0.4409\ r) \times 4186.7456 \qquad (II.8)$$

Note that c_P is dependent on r, which is dependent on e_a, which is dependent on c_P. Therefore it is necessary to calculate these iteratively. In this study c_P was initially set to 1010 J kg^{-1} K^{-1} then equations II.5, II.8 and II.6

were solved until the difference between the old and new c_p was acceptable (<0.0001 difference).

II.9 Density of moist air (ρ)

From List (1966) ρ in kg m^{-3} is:

$$\rho = \frac{p}{T'_V} 0.34838 \qquad (II.9)$$

where T'_V - adjusted virtual temperature, see below.

II.10 Adjusted virtual temperature (T'_V)

From List (1966):

$$T'_V = c_A T_d (1 + r/\epsilon)/(1 + r) \qquad (II.10)$$

where c_A - compressibility factor of moist air (0.9995).

II.11 Relative Humidity (RH)

RH was calculated from the RTDMS data using (McIntosh & Thom, 1972):

$$RH = 100 \ e_a/e_S \qquad (II.11)$$

where e_S - calculated using T_d.

II.12 Vapour pressure deficit (V)

V (Pa) is calculated using the dry bulb temperature to calculate both e_a and e_S:

$$V = e_S(T_d) - e_a(T_d) \qquad (II.12)$$

II.13 Specific humidity deficit (δq)

δq (g kg^{-1}) is calculated from V using (Dolman et al., 1988):

$$\delta q = \epsilon V/p \qquad (II.13)$$

APPENDIX III: ERROR ANALYSIS FOR THE RTDMS AND FLUXES CALCULATED FROM IT

This discussion of errors follows Kalanda (1979), who used the method of Cook and Rabinowicz (1963). The probable absolute error in a given result Y, where $Y = F(x_1, x_2)$, may be expressed as:

$$\delta Y = [(\partial Y/\partial x_1 \ \delta x_1)^2 + (\partial Y/\partial x_2 \ \delta x_2)^2]^{0.5} \qquad \text{(III.1)}$$

The wet- (ΔT_W) and dry-bulb (ΔT_d) temperatures differences are determined from a calibration equation of the form:

$$\Delta T = mx + c \qquad \text{(III.2)}$$

where m - slope;
x - signal (mV); and
c - intercept.

The probable error ($\delta\Delta T$) is:

$$\delta\Delta T = [(\partial\Delta T/\partial c \ \delta c)^2 + (\partial\Delta T/\partial m \ \delta m)^2 + (\partial\Delta T/\partial x \ \delta x)^2 \ ]^{0.5} \qquad \text{(III.3)}$$

Since $\partial\Delta T/\partial c=1$, $\partial\Delta T/\partial m=x$ and $\partial\Delta T/\partial x=m$ III.3 becomes:

$$\delta T = [(\delta c)^2 + (x\delta m)^2 + (m\delta x)^2 \ ]^{0.5} \qquad \text{(III.4)}$$

The calibration equations for the thermopiles and their errors are listed in Table III.1. δx is determined from the data logger (CR21X). The full scale range (FSR) error is 0.05% of the 5.0 mV FSR used; i.e. 2.5×10^{-3} mV. The error in ΔT_W is approximately 0.007°C (Cleugh, 1988). This leads to a 5-15% error in the range of temperature differences measured.

Table III.1 RTDMS thermopile calibration values
(McCaughey, pers. comm., 1986)

Sensor	m	δm	c	δc
ΔT_W	0.00248	0.000003	-0.003617	0.003478
ΔTd	0.00249	0.000002	-0.013774	0.002310

The error in ß is computed from:

$$\delta ß = [(\partial ß/\partial\Delta T_W \ \delta\Delta T_W)^2 + (\partial ß/\partial\Delta T_d \ \delta\Delta T_d)^2 + (\partial ß/\partial s \ \delta s)^2]^{0.5} \qquad \text{(III.5)}$$

where s - slope of the saturation vapour pressure curve versus temperature

curve (Pa $^{\circ}C^{-1}$)

Kalanda (1979) solved the partial differential equations for III.5:

$$\partial ß/\partial \Delta T_d = [(s+\gamma)/\gamma\ \Delta T_W) - 2\Delta T_d + \gamma/(s+\gamma)(\Delta T_d^2/\Delta T_W)]^{-1} \quad \text{(III.6)}$$

$$\partial ß/\partial \Delta T_W = [(s+\gamma/\gamma\ \Delta T_W^2/\Delta T_d - 2\Delta T_W + \gamma/(s+\gamma)\Delta T_d]^{-1} \quad \text{(III.7)}$$

$$\partial ß/\partial s = [-(s+\gamma)^2/\gamma\ \Delta T_W/\Delta T_d - 2(s+\gamma) + \Delta T_d/\Delta T_W]^{-1} \quad \text{(III.8)}$$

The error in the latent heat flux ($Q_{Eß}$) can be computed:

$$\delta Q_E = [(\partial Q_E/\partial Q^*\ \delta Q^*)^2 + (\partial Q_E/\partial \Delta Q_S\ \delta \Delta Q_S)^2 + (\partial Q_E/\partial ß\ \delta ß)^2]^{0.5} \quad \text{(III.9)}$$

where the solution of the partials are:

$$\partial Q_E/\partial Q^* = 1/(1+ß) \quad \text{(III.10)}$$

$$\partial Q_E/\partial \Delta Q_S = -1/(1+ß) \quad \text{(III.11)}$$

$$\partial Q_E/\partial ß = (Q^* - \Delta Q_S)/(1+ß)^2 \quad \text{(III.12)}$$

The error in the sensible heat flux ($QH_ß$) can be computed:

$$\delta Q_H = [(\partial Q_H/\partial Q^*\ \delta Q^*)^2 + (\partial Q_H/\partial \Delta Q_S\ \delta \Delta Q_S)^2 + (\partial Q_H/\partial ß\ \delta ß)^2]^{0.5} \quad \text{(III.13)}$$

where the solution of the partials are:

$$\partial Q_H/\partial Q^* = ß/(1+ß) \quad \text{(III.14)}$$

$$\partial Q_H/\partial \Delta Q_S = -ß/(1+ß) \quad \text{(III.15)}$$

$$\partial Q_H/\partial ß = (Q^* - \Delta Q_S)/(1+ß)^2 \quad \text{(III.16)}$$

For $Q_{Hß}$ and $Q_{Eß}$ errors, for both Q^* and ΔQ_S an error equal to 5% of Q^* was assumed.

APPENDIX IV CALCULATION OF STABILITY AND FRICTION VELOCITY

Monin Obukhov stability length (L) and friction velocity (u_*) were calculated for each hour during the study period, using the iterative procedure of van Ulden and Holtslag (1985). It was possible to calculate L using two different methods. The first, here termed 'sonic', uses sensible heat flux (Q_H) data (Randerson, 1984):

$$L = -(u_*^3 \rho c_p T_d)/(k g Q_H) \quad (IV.1)$$

where u_* - friction velocity (see below)(m s^{-1});
k - von Kármán's constant (0.41);
g - acceleration due to gravity (9.81 m s^{-2});
c_p - specific heat capacity of air at constant pressure (J kg^{-1} K^{-1});
ρ - density (kg m^{-3}); and
T_d - dry bulb temperature (°C).

The second method, termed here 'Bowen', uses the temperature differences measured by the RTDMS (van Ulden and Holtslag, 1985):

$$L = (T_d u_*^2)/(k g \theta_*) \quad (IV.2)$$

where θ_* - temperature scale for turbulent heat transfer:

$$\theta_* = (k \Delta\theta)/[\ln((z_2-d)/z_1) - \psi_H((z_2-d)/L) + \psi_H((z_1-d)/L)] \quad (IV.3)$$

where z_2, z_1 - heights of the RTDMS sensors (m);
d - displacement length (m);
$\psi_H(z/L)$ - corresponding stability functions (see below); and
$\Delta\theta$ - potential temperature difference (McIntosh and Thom, 1972):

$$\Delta\theta = \Delta T\ (100.0/p)^K \quad (IV.4)$$

where $K = R/c_p$;
R - gas constant of dry air (287.04 J kg^{-1} K^{-1}) (List,1966); and
p - pressure (Pa).

u_* was calculated iteratively with L using (Van Ulden and Holtslag, 1985):

$$u_* = (k u(z_3-d))/[\ln((z_3-d)/z_o) - \psi_M((z_3-d)/L) + \psi_M(z_o/L)] \quad (IV.5)$$

where $u(z_3)$ - wind speed at the height of the anemometer (m s^{-1});
z_o - roughness length (m); and
$\psi_M(z/L)$ - stability functions (see below).

A comparison between measured u_* and L and the corresponding modelled values while varying the stability functions was conducted for unstable

conditions. The stability function used for heat when L<0 (unstable) (van Ulden and Holtslag, 1985) is:

$$\psi_H = 2 \ln [(1 + y^2)/2] \quad \text{(IV.6)}$$

where y was defined by Dyer (1974) as:

$$y = (1 - 16\ z/L)^{0.25} \quad \text{(IV.7)}$$

and alternatively by Dyer and Bradley (1982) as:

$$y = (1 - 14\ z/L)^{0.25} \quad \text{(IV.8)}$$

The stability function for momentum when L<0 (unstable) (van Ulden and Holtslag, 1985) is:

$$\psi_M = 2 \ln[(1 + X)/2] + \ln[(1 + X^2)/2] - 2 \tan^{-1}(X) + \pi/2 \quad \text{(IV.9)}$$

where X was defined by Dyer (1974) as:

$$X = (1 - 16\ z/L)^{0.25} \quad \text{(IV.10)}$$

and alternatively by Dyer and Bradley (1982) as:

$$X = (1 - 28\ z/L)^{0.25} \quad \text{(IV.11)}$$

A comparison was also conducted with values of u_* calculated without taking stability into account. These 'neutral' values are calculated from:

$$u_* = k\ u(z_3\text{-}d)/\ln((z_3\text{-}d)/z_0) \quad \text{(IV.12)}$$

The data used are those collected by Roth (1988) at the Sunset site in August-September 1986. 28 hours of turbulence data were available. The stability functions calculated using either Dyer (1974) or Dyer and Bradley (1982) forms are compared with the measured data in Figures IV.1 and IV.2 and Table IV.1 summarises the statistical results. The index of agreement (d) has a range between 0 and 1, where 1 indicates perfect agreement between the observed and predicted values (Wilmott and Wicks, 1980). The highest d value and lowest RMSE (root mean square error) was obtained from the sonic method using the Dyer (1974) stability function for both u_* and z/L. It should be noted that the ability to predict z/L is not as good as for u_*. The 'neutral'

Figure IV.1 Measured versus modelled u*. (Modelled (+) Bowen (Δ) Sonic (*) Neutral methods).

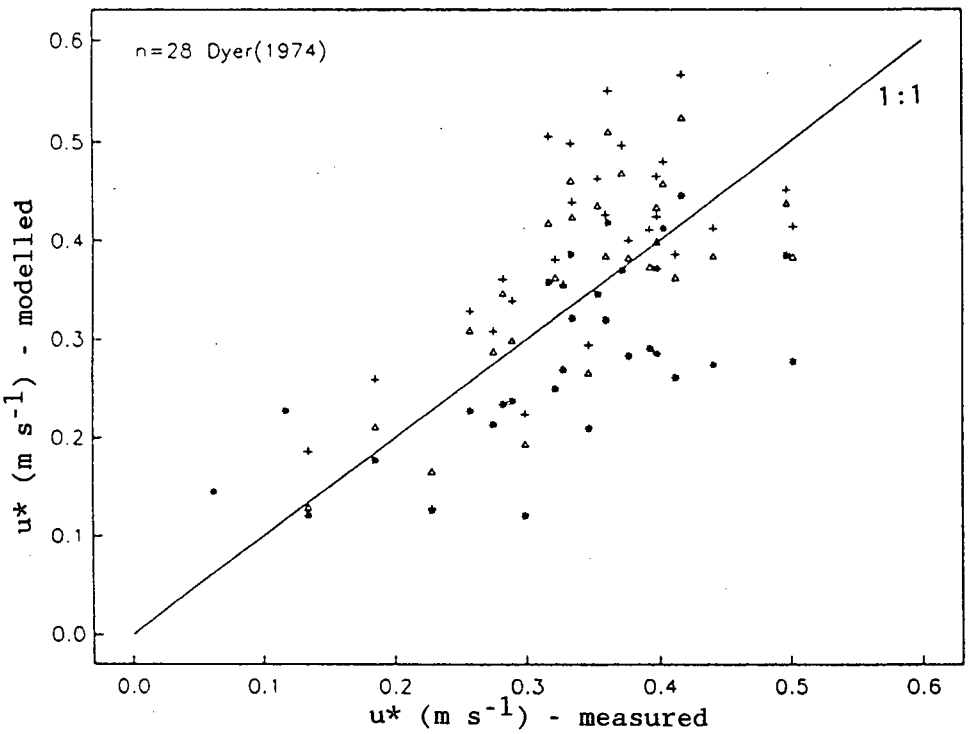

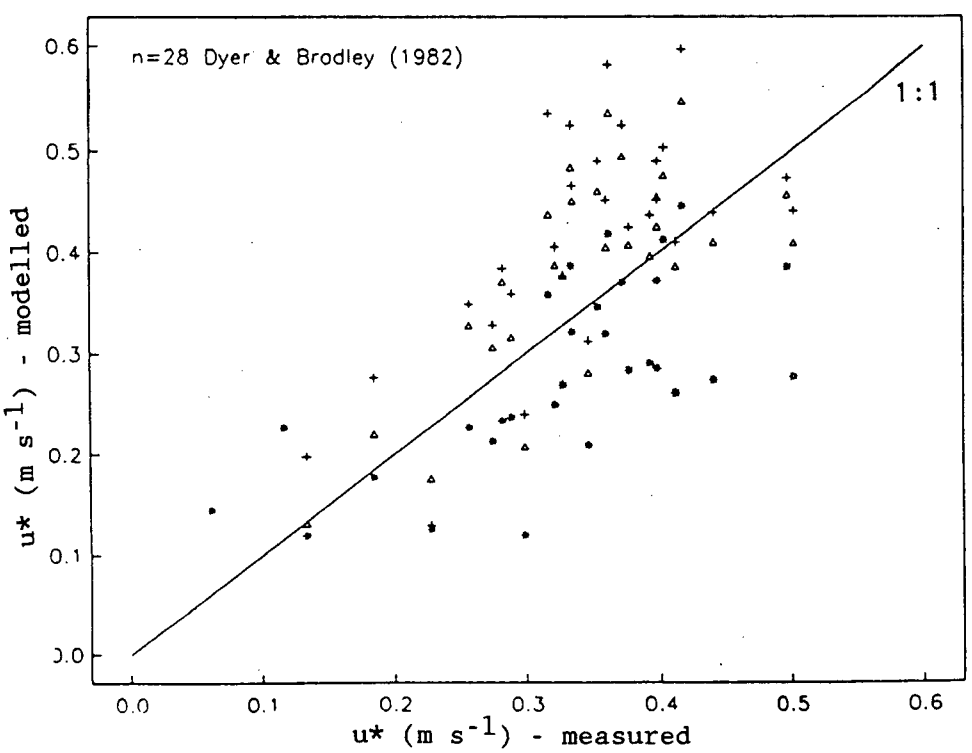

Figure IV.2 Measured versus modelled z/L. (Modelled (+) Bowen (Δ) Sonic (*) Neutral methods).

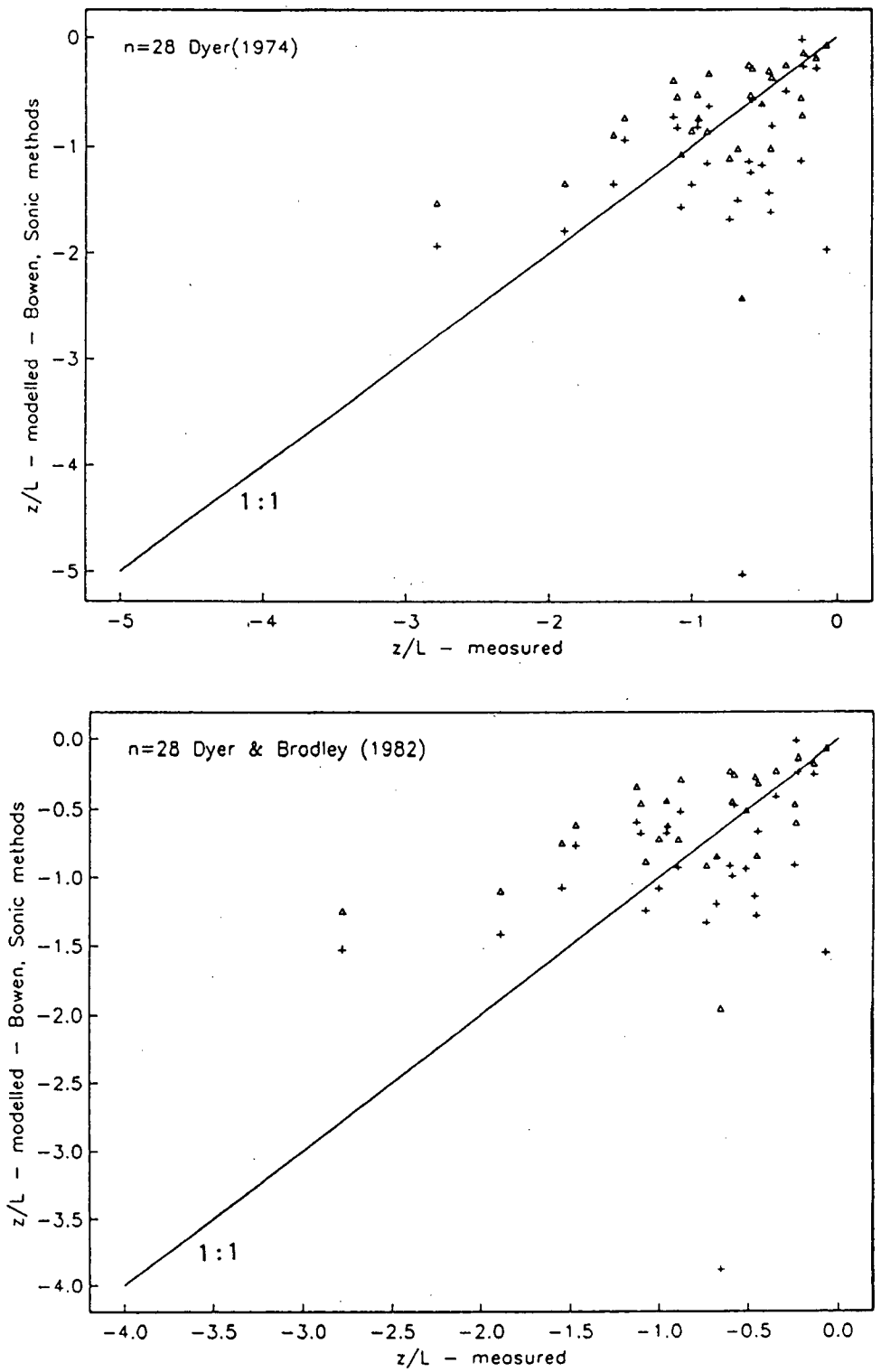

method in most cases under-predicts u_* relative to the measured values (Fig. IV.1) and in all cases predicts lower u_* values than any of the Bowen or sonic methods with the Dyer (1974).

No data were available to test stability formulations for the stable (L>0) case at the Sunset site. Considering the unstable results it was decided to adopt the Dyer (1974) result for heat:

$$\psi_H = -5\ (z-d)/L \qquad \text{(IV.13)}$$

and for momentum that of van Ulden and Holtslag (1985):

$$\psi_M = -17(1 - \exp(-0.29(z-d)/L) \qquad \text{(IV.14)}$$

Table IV.1 Comparison between measured and modelled values of (a) u_* and (b) z/L with different stability functions: Dyer (1974) and Dyer and Bradley (1982) and different methods: Bowen and Sonic (see text)

		Dyer (1974)		Dyer and Bradley (1982)	
	Measured	Bowen	Sonic	Bowen	Sonic
(a) u_* (m s^{-1})					
Mean	0.34350	0.39107	0.36232	0.41411	0.38254
S.D.	0.08188	0.10374	0.09837	0.10946	0.10308
RMSE	-	0.09089	0.07140	0.10768	0.08114
d[a]	-	0.74551	0.82451	0.69240	0.79592
(b) (z-d)/L					
Mean	-0.80839	-1.22310	-0.70871	-0.97800	-0.59164
S.D.	0.57445	0.88792	0.49203	0.68211	0.39726
RMSE	-	1.04623	0.55160	0.81862	0.55595
d	-	0.41471	0.68398	0.45604	0.64476

a d - Index of agreement (Wilmott and Wicks, 1980)

APPENDIX V PROCEDURE FOR ACCESSING DIFFERENT SOURCE AREA GEOMETRIES FROM THE DATABASE

To conduct the comparison between different boundary location scenarios different geometric shapes had to be accessed from the database. For all geometric shapes if the location of the boundary included any part of a grid square the square was incorporated.

V.1 Circles and Quadrants

Since a circle is symmetrical around the y- and x-axes the grid squares to be sampled can be determined for one quadrant. For the purposes of this study a quadrant refers to each of the four 90° sectors around the tower (0-89.9°, 90-179.9°, 180-269.9°, 270-359.9°). If the radius (R) of the circle is known then the X and Y co-ordinates can be determined. X is initially set to 0.5, the midpoint of the first grid square. X is incremented by steps of 1.0 after each Y is determined, until $X \geq R$. Smaller steps increase both the fit and the computational time. Y is determined from:

$$Y = (R^2 - X^2)^{0.5} \qquad (V.1)$$

The grid squares for the +X, +Y quadrant are the Y values identified from equation V.1 to Y=1.0 for each X. To determine another quadrant or a circle the sign(s) of X and Y need to be changed as appropriate. To assign a value to a surface parameter the mean for all grid squares identified is calculated.

V.2 Ellipses

The dimensions of the 9 source area ellipses for each hour were calculated using a modified version of the Schmid (1988) source area model (see section 3.2.2). The a, b+c, and d dimensions (Fig. 3.4) plus mean wind direction (φ) are used to identify which grid squares to use for calculating surface parameters.

To calculate the co-ordinates of an elliptical source area it is necessary to first identify the boundaries when it is aligned with the x-axis because, by definition, an ellipse has to have its longest axis parallel to either the x- or y-axis (Draper and Klingman, 1972). The b+c axis is initially assumed to be aligned along the x-axis (90°). The unrotated Y values (Y_{90}) are calculated for X values (X_{90}) from minimum (a) to maximum (a+b+c) in steps of 20 m. The step size can be varied, again the smaller the step the better the fit but the greater the computational time. If b+c is the longest axis then the calculation is conducted as follows:

$$Y_{90} = (d^2 - (d^2((X_{90} - (a+b))^2 / b^2))^{0.5} \quad (V.2)$$

If the d axis is the longest then d is replaced by b and vice-versa in equation V.2.

The located points on the boundaries are then rotated so that the b+c axis is aligned with φ. As the ellipse is symmetrical about the x-axis the rotation can be calculated using the same equations first with a $+Y_{90}$ and second with a $-Y_{90}$ value.

$$X = (\cos(\varphi-90)\ X_{90} + \sin(\varphi-90)\ Y_{90})/SQS \quad (V.3)$$

$$Y = (\cos(\varphi-90)\ Y_{90} - \sin(\varphi-90)\ X_{90})/SQS \quad (V.4)$$

Only the maximum and minimum Y co-ordinates are stored for each X co-ordinate.

Note that the surface parameter value is determined from the mean of the 9 mean band values i.e. a mean value is determined between each ellipse and then for composite ellipse. Thus areas closer to the tower have proportionally a greater influence than those further away.

V.3 Sectors

The area to be identified is determined by φ, the standard deviation of the wind direction (σ_φ) and some indication of stability. In this study net

radiation (Q*) was used as a surrogate for stability. If Q*>0 then the lengths used to define the sector were for unstable conditions otherwise the stable/neutral lengths were used (Table 3.3).

Calculations are performed from one concentration level band (R) to the adjacent band (see Fig. 3.6) in a step-wise fashion at approximately 30 m intervals (r), and then stepped around at approximately 1° intervals (φ_i) from φ-σ_φ to Δ+σ_φ:

$$X = (\cos(90-(\varphi + \sigma_\varphi - \varphi_i))\ (R + r))/SQS \qquad (V.9)$$

$$Y = (\sin(90-(\varphi + \sigma_\varphi - \varphi_i))\ (R + r))/SQS \qquad (V.10)$$

As for the ellipses, only maximum and minimum Y values for each X co-ordinate are stored. The value of a surface parameter, as with the ellipses, is the mean of the 9 mean band values.

V.4 Discussion

For each geometric shape the number of X co-ordinates (or lines of co-ordinate data), and the maximum and minimum value of Y for each X is stored for each hour. These co-ordinates can then be used to calculate a surface parameter from the database. The co-ordinate finding sub-routines can, obviously, also be linked to the process calculation programs. Since the same co-ordinates were used several times they were stored for future use.

Publications

Grimmond, C.S.B., 1981: An evaluation of the contents of some New Zealand Environmental Impact Reports. University of Otago, Geography Discussion Paper No. 27.

Fitzharris, B.B. and C.S.B. Grimmond, 1982: Assessing snow storage and melt in a New Zealand mountain environment. Hydrological Aspects of Alpine and High Mountain Areas, I.A.H.S. Publ. No. 138, 161-168.

Grimmond, C.S.B., 1985: Urban water balance: an integrating framework. World Meteorological Organization Conference on Urban Climatology and its Applications with Regards to Tropical Areas, Mexico City, Mexico. W.M.O Technical Document No. 7.

Grimmond, C.S.B., T.R. Oke and D.G.Steyn, 1986a: Urban water balance I: A model for daily totals. Water Resources Research, 22, 1397-1403.

Grimmond, C.S.B. and T.R. Oke, 1986b: Urban water balance II: Results from a suburb of Vancouver, B.C. Water Resources Research, 22, 1404-1412.

Oke T.R., H.A. Cleugh & S. Grimmond 1988: Evapotranspiration in urban areas. In Intern. Symp. Hydrological processes and water management in urban areas, UNESCO, 24-29 April, 1988, Duisburg, 107-112.

Oke, T.R., H.A. Cleugh, S. Grimmond, HP. Schmid and M. Roth 1988: Evaluation of spatially-averaged fluxes of heat, mass and momentum in the urban boundary layer. In Proc. Symp. on Topoclimatological investigation and mapping, International Geographical Union, Christchurch, August 1988 (in press).